RICE UNIVERSITY

Parameterized Seismic Fragility Assessment and Life-Cycle Analysis of Aging Highway Bridges

by

Jayadipta Ghosh

A THESIS SUBMITTED
IN PARTIAL FULFILLMENT OF THE
REQUIREMENTS FOR THE DEGREE

Doctor of Philosophy

APPROVED, THESIS COMMITTEE

Dr. Jamie E. Padgett, Chair
Assistant Professor, Department of
Civil and Environmental Engineering

Dr. Leonardo Dueñas-Osorio
Associate Professor, Department of
Civil and Environmental Engineering

Dr. Satish Nagarajaiah
Professor, Department of Civil and
Environmental and Mechanical
Engineering and Material Science

Dr. Genevera Allen
Assistant Professor, Department of
Statistics

HOUSTON, TEXAS

April 2013

Abstract

Parameterized Seismic Reliability Assessment and Life-Cycle Analysis of Aging Highway Bridges

by

Jayadipta Ghosh

The highway bridge infrastructure system within the United States is rapidly deteriorating and a significant percentage of these bridges are approaching the end of their useful service life. Deterioration mechanisms affect the load resisting capacity of critical structural components and render aging highway bridges more vulnerable to earthquakes compared to pristine structures. While past literature has traditionally neglected the simultaneous consideration of seismic and aging threats to highway bridges, a joint fragility assessment framework is needed to evaluate the impact of deterioration mechanisms on bridge vulnerability during earthquakes. This research aims to offer an efficient methodology for accurate estimation of the seismic fragility of aging highway bridges. In addition to aging, which is a predominant threat that affects lifetime seismic reliability, other stressors such as repeated seismic events or simultaneous presence of truck traffic are also incorporated in the seismic fragility analysis.

The impact of deterioration mechanisms on bridge component responses are assessed for a range of exposure conditions following the nonlinear dynamic analysis of three-dimensional high-fidelity finite element aging bridge models. Subsequently, time-dependent fragility curves are developed at the bridge component and system level to assess the probability of structural damage given the earthquake intensity. In addition to highlighting the importance of accounting for deterioration mechanisms, these time-evolving fragility curves are used within an improved seismic loss estimation methodology to aid in efficient channeling of monetary resources for structural retrofit or seismic upgrade. Further, statistical learning methods are employed to derive flexible parameterized fragility models conditioned on earthquake hazard intensity, bridge design parameters, and deterioration affected structural parameters to provide significant improvements over traditional fragility models and aid in efficient estimation of aging bridge vulnerabilities. In order to facilitate bridge management decision making, a methodology is presented to demonstrate the applicability of the proposed multi-dimensional fragility models to estimate the in-situ aging bridge reliabilities with field-measurement data across a transportation network. Finally, this research proposes frameworks to offer guidance to risk analysts regarding the importance of accounting for supplementary threats stemming from multiple seismic shocks along

the service life of the bridge structures and the presence of truck traffic atop the bridge deck during earthquake events.

Acknowledgments

When I started to put together my dissertation, I thought that writing the acknowledgements would be the easiest. I was wrong, given the number of wonderful people and instances I have to recall who helped me shape this personal journey. I would like to take this opportunity to thank them.

The person without whose unwavering support, patience, guidance, friendship and mentoring, this work would not have been possible is my advisor Dr. Jamie E. Padgett. Words cannot greatly express the appreciation I have for her. She has given me countless opportunities and experiences which ensured steady intellectual growth and a solid foundation towards the future. She has truly been the finest mentor I have ever worked with in my academic career.

I would like to thank my thesis committee member Dr. Leonardo Dueñas-Osorio who I often felt was the unofficial co-advisor to my thesis given his constant willingness to be disturbed with my plethora of questions on reliability concepts while offering great suggestions. He has always treated me as a member of his own research group and made me feel welcome towards any academically stimulating group activity. I am thankful to my committee member Dr. Satish Nagarajaiah for his suggestions, the courses he offers at Rice and his great teaching abilities which

ensured my strong technical background. He has also been very supportive of the EERI Chapter at Rice, and suggested events and invited distinguished speakers which always helped us improve our chapter activities. I would also like to thank Dr. Genevera Allen for serving on my thesis committee and for her suggestions to improve my thesis. Greatly thankful to her as well for offering the course on Data mining and Statistical learning and making it accessible to students outside the Statistics department to attend and understand.

I am deeply indebted towards the art of music for always providing me a recreational and emotional outlet during my Ph.D., particularly the subgenre Black Metal. The band which comes to my mind first is the ever-elusive atmospheric black metal act, Drudkh. Thanks for consistently delivering great albums. Special thanks to Scott Connor (Malefic) of ex-Xasthur and Nocturnal Poisoning for his personal communications, simplicity, and especially the song "Prison of Mirrors" by Xasthur. Very thankful also towards the true originators of Norwegian Black Metal, bands such as Immortal, Darkthrone, and Emperor who always stuck to the roots and kept Black Metal rightfully away from popular mainstream music.

I have been blessed with the most wonderful officemates one can possibly imagine. Thank you, Navid and Emily for making Ryon 219 always full of fun and frolic. We are probably the happiest and "loudest" office in Ryon Lab! From

outside my office, I am thankful to all my colleagues and friends at Ryon and elsewhere, especially Dharma, Yenny, Vishnu, Citlali, Pradeep, Anish, Keivan, and Isaac. Also, while at Rice I had the wonderful opportunity to meet and become great friends with visiting scholars. Two most wonderful people I met along the way are Fabio and Sara from Italy who always enriched me with their friendship, simplicity, and happiness. Thanks also go to Behzad and Mairead for being such wonderful people and great friends.

Whatever I am today and whatever I have achieved till now would not have been possible without the blessings and constant support of my parents, my brother, and my sister-in-law. Over the years they kept confidence in my abilities and always encouraged me to reach for the stars. Finally, I would like to thank my fiancé, Meera for her love, patience, selflessness, and teaching me how to be happy with the simplest things in life. It is to her and my brother that I dedicate this thesis.

Contents

List of Figures

List of Tables

Chapter 1

INTRODUCTION

1.1. Problem Description

Highway bridges constitute key components of the transportation network across the United States (US) and at present are extensively deteriorating due to adverse environmental conditions, heightened traffic loads and other hazards. The US highway bridge inventory is comprised of nearly 600,000 bridges (FHWA 2011) with a majority built during the Great Depression in the 1930's and in the 1960's and 70's during the establishment of interstate highways (Das 1999). While the former are nearing the end of their service lives and were often constructed following antiquated design standards, the latter are markedly suffering structural deterioration from aging and degradation and are in need of major structural repairs (AASHTO 1993; Estes and Frangopol 2003). Out of the 600,000 bridges within the US inventory, approximately 234,238 bridges are located in states

characterized by moderate to high seismicity (FHWA 2010). A majority of these bridges, particularly in the Central and Southeastern United States (CSUS), are non-seismically designed. Highway bridges with multiple deteriorating structural components and characterized by lack of adequate seismic detailing are likely to be more vulnerable to earthquake hazards compared to pristine structures. Hence, there is a pressing need to estimate the seismic vulnerability of aging bridge structures to assist bridge owners and decision makers in efficient channeling of resources for retrofit decisions and structural upgrades.

In recent decades, seismic fragility curves have emerged as a powerful technique to quantify the probability of meeting or exceeding a certain level of damage given the intensity of seismic shaking. While researchers have focused on the development of these curves for pristine or seismically retrofitted bridge structures (Basoz and Mander 1999; Basoz and Kiremidjian 1999; Gardoni et al. 2003; Nielson and DesRoches 2007a; Padgett and DesRoches 2008; Shinozuka et al. 2000), there has been a historic lack of jointly considering seismic and aging threats within a same framework. The few studies on deteriorating bridge fragility, for instance the recent work by Choe et al. (2009) and Simon et al. (2010), focused only on deterioration of single bridge component, i.e., reinforced concrete bridge

columns. Other researchers, such as Nielson and DesRoches(2007a) have however identified the contribution of multiple bridge components towards seismic vulnerability, of which several are prone to deterioration mechanisms (e.g. steel bridge bearing and elastomeric pad bearings) (Silano and Brinckerhoff 1993; Itoh and Gu 2009). Hence, a more practical aging bridge fragility framework should consider contribution of multiple bridge components towards seismic vulnerability.

Analytical approaches to develop traditional bridge fragility curves conditioned on the ground motion intensity often require significant number of computer simulations to explore the sample space of uncertain input parameters. Such uni-dimensional fragility curves are only suited for vulnerability assessment of pristine bridges or aging bridges with a prescribed level of deterioration and cannot improve from the data available from field monitoring of highway bridges without imposing a substantially high computation burden. This drawback also inhibits the efficient attainment of other objectives such as reliability evaluation and risk ranking of bridges within large aging transportation networks while incorporating sensor monitoring data and in-situ bridge characteristics. Hence flexible parameterized bridge fragility functions are presently needed for enabling efficient

and precise evaluation of deteriorating highway bridges and transportation networks.

In addition to traditionally neglecting the impact of aging mechanisms past research has also disregarded contribution of other critical factors towards seismic vulnerability assessment of highway bridges. One such factor is the exposure of bridge structures to multiple earthquakes in regions characterized by high seismicity. Repeated earthquakes may lead to the reduction in structural strength, thereby rendering the bridge weaker to resist future earthquakes. Another widely prevalent, yet traditionally overlooked phenomenon is the impact assessment of truck and traffic loads on bridge seismic fragility. Since the primary function of highway bridges is the safe passage of vehicles across the nation, it is essential to investigate the influence of live loads on seismic bridge fragility. The relative significance of such threats in the seismic fragility analysis framework has yet to be explored to guide future bridge seismic risk assessment regarding the relative importance of considering repeated events and presence of truck-traffic.

1.2. Objectives and Scope of Research

This research aims to provide an enhanced understanding of the impact of aging and deterioration mechanisms on the seismic vulnerability of highway bridges while also considering other threat scenarios commonly neglected in literature. A primary objective is to develop efficient time-evolving fragility functions to statistically compute the seismic vulnerability of aging highway bridges along their service lives. Such time-dependent reliability functions will aid bridge owners and stakeholders to make practical decisions regarding seismic retrofit and structural upgrades via techniques such as life-cycle cost estimation procedures. Additionally the proposed fragility models will enable reliability estimation of aging transportation systems and promote risk ranking of highway bridges to suit network level objectives.

The specific tasks this research attempts to address are as follows:

1. Characterize the deterioration mechanisms affecting the structural performance of multiple critical bridge components.

2. Develop three dimensional analytical models relative to existing research for aging highway bridge classes which account for the level of structural degradation incurred in different bridge components.
3. Conduct deterministic dynamic analysis to investigate the impact of aging mechanisms on the seismic response of aging bridge structures and provide comparisons with pristine component behavior.
4. Develop time-dependent fragility curves at bridge component and system level to quantify the detrimental effects of aging on bridge seismic fragility and assess the impact of different exposure condition on aging bridge fragility.
5. Extend the traditional single-parameter time-dependent fragility curves and assess different surrogate models rooted in statistical learning techniques to develop multidimensional probabilistic seismic demand models for bridge components conditioned on earthquake intensity, bridge modeling parameters, deterioration affected structural parameters, and bridge geometric parameters.
6. Develop parameterized fragility functions using the multidimensional surrogate models for efficient seismic reliability estimation of aging highway

bridges. Demonstrate the potential of parameterized fragility models in the reliability estimation of bridges in a distributed transportation network after incorporating field instrumentation data following spatial interpolation and statistical updating of deterioration parameters.

7. Develop a framework for seismic vulnerability evaluation of highway bridges subjected to repeated earthquake shocks along their service lives when located in regions characterized by high seismicity.
8. Evaluate the impact of truck-traffic load on the seismic vulnerability of highway bridge structures using realistic truck weigh-in-motion data and propose a joint seismic-live load fragility framework to incorporate site specific truck flow rates and gross vehicle weight.
9. Develop a nonhomogeneous Poisson process framework to estimate seismic losses of aging bridge using a component level approach while accounting for time-dependent bridge failure probabilities and uncertainty in repair procedures.

1.3. Thesis Outline

This thesis is organized into eight chapters with the following content:

Chapter 2 presents an overview of existing literature on seismic fragility assessment of pristine and aging highway bridges while highlighting state-of-the-art methodologies and existing deficiencies which will be addressed in this study. Additionally, existing literature on supplementary threats on highway bridges are also presented which includes damage accumulation in bridges due to repeated earthquake and impact of truck-traffic loads on the seismic vulnerability.

Chapter 3 identifies the different environmental degradation mechanisms affecting the structural characteristics of highway bridge components. Existing models are reviewed and new models are developed in this endeavor. Additionally, statistical distributions of deterioration parameters for different exposure conditions are elaborated. This chapter also details the finite element modeling principles for pristine and aging highway bridge structures.

Chapter 4 presents the mathematical framework for developing component and system level time-dependent bridge fragility curves. Two case study examples are presented corresponding to structurally and materially different bridge types which elaborate the deterministic seismic performance and probabilistic seismic demand model development for aging bridge components. Finally time-evolving

fragility curves are developed at the bridge component and system levels for both bridge types.

Chapter 5 explores a range of surrogate models rooted in statistical learning to develop multidimensional seismic demand models. These models are eventually used along with component capacity estimates to develop flexible parameterized bridge fragility curves which provide significant advantages over the traditional single-parameter time-dependent fragility curves. Dimensionality reduction techniques are explored to ascertain the smoothness of the failure domain and confirm the applicability of surrogate models. Consequently, an application example is presented in which parameterized fragility models are constructed for nine different bridge classes for a part of the transportation network in the state of South Carolina. The parameterized fragility models are used in conjunction with field instrumented or spatially interpolated deterioration parameter data to compute in-situ reliabilities for highway bridges.

Chapter 6 investigates two supplementary threats to highway bridges in addition to the detrimental effects of aging and deterioration mechanisms presented in the previous chapters. Firstly, this chapter presents a probabilistic framework to compute seismic vulnerability of highway bridges that are potentially

subjected to repeated earthquakes along their service lives. Secondly, a joint seismic and live load fragility framework is presented which evaluates the impact of truck-traffic load on the seismic vulnerability of highway bridges. The influence of chemical deterioration mechanisms is not considered in this chapter.

Chapter 7 introduces a nonhomogeneous Poisson process framework which incorporates the time-dependent aging bridge fragility functions developed in the previous chapters to estimate lifetime seismic losses incurred by deteriorating bridge structures using a component level approach. Uncertainty in repair procedures and correlations in component repair costs are also accounted for in this framework.

Finally, Chapter 8 summarizes the research, presents key contributions and highlights future research opportunities.

Chapter 2

OVERVIEW OF SEISMIC FRAGILITY AND SEISMIC LOSS ANALYSIS FOR AGING HIGHWAY BRIDGES

Fragility analysis of highway bridges using probabilistic techniques help to quantify the potential damage of structural components or the overall bridge system during earthquake occurrences. The integration of these fragility models into regional seismic risk assessments provides an opportunity to screen seismically vulnerable bridges for retrofit, project anticipated damage and seismic losses, or support post-event inspection (Taylor et al. 2002; Mackie and Stojadinovic 2006; Nielson and DesRoches 2007a; Padgett and DesRoches 2009). Recognition of the usefulness of bridge fragility functions in managing, assessing and reducing seismic risk has led to the development of several different fragility curve generation methodologies over the past few decades, such as, the early use of expert-opinion based methods

(Rojahn and Sharpe 1985; ATC 1991) and empirically based methods (Basoz and Kiremidjian 1999; Yamazaki et al. 1999; Shinozuka et al. 2000). Addressing certain inherent drawbacks in both expert-based and empirically based fragility methodologies, analytical and simulation based methods have also been extensively studied by several researchers. These methods, differing in the analysis techniques used to simulate the demands on bridge components during the reliability assessment, encompasses elastic spectral analysis (Hwang et al. 2000), nonlinear static analysis (Basoz and Mander 1999; Shinozuka et al. 2000), and nonlinear time-history analysis (Shinozuka et al. 2000; Mackie and Stojadinovic 2001; Choi et al. 2004; Nielson and DesRoches 2007a).

The above mentioned fragility assessment approaches have been prevalently employed for seismic vulnerability assessment of pristine (non-deteriorating) highway bridges structures (Basoz and Mander 1999; Basoz and Kiremidjian 1999; Gardoni et al. 2003; Nielson and DesRoches 2007a), while traditionally ignoring the impact of aging mechanisms affecting the bridge structural performance. The aging and degradation of bridges manifests itself in a number of ways, such as corrosion of steel reinforcement and spalling of cover concrete in reinforced concrete (RC) columns [Figure 2-1(a) and (b)], area loss of steel in bearing anchor bolts and

dowel bars [Figure 2-1(c)], buildup of debris leading to "freezing" of steel bearings [Figure 2-1(d)], and stiffening of elastomeric bearing pads, among others. These components comprise the primary force resisting system of bridges under seismic loading thus having a potentially significant impact on seismic response and fragility estimates. At present nearly half of all the bridges within the US are nearing the end of their service lives and nearly a quarter are in need of significant repairs (ASCE 2013). Given these findings there is an urgent need to investigate and address the following questions: a) Do aging mechanisms have an effect on the seismic response of aging bridge components? b) How significant are the shifts in component and system level seismic fragilities of aging bridges when compared with non-deteriorating pristine structures? c) How can we efficiently compute seismic fragility of aging bridges while potentially benefitting from the data available via field instrumentation and sensor monitoring? and d) Are the projected seismic loss estimates of aging bridges significantly different from pristine bridges? The focus of this thesis is to address these questions from an engineering standpoint after accounting for the probabilistic nature of the problem. The following sections will summarize past research on aging bridge fragility and life-cycle modeling, with an emphasis on seismic loss contributions, while also

highlighting the existing deficiencies which will be extensively addressed in this research.

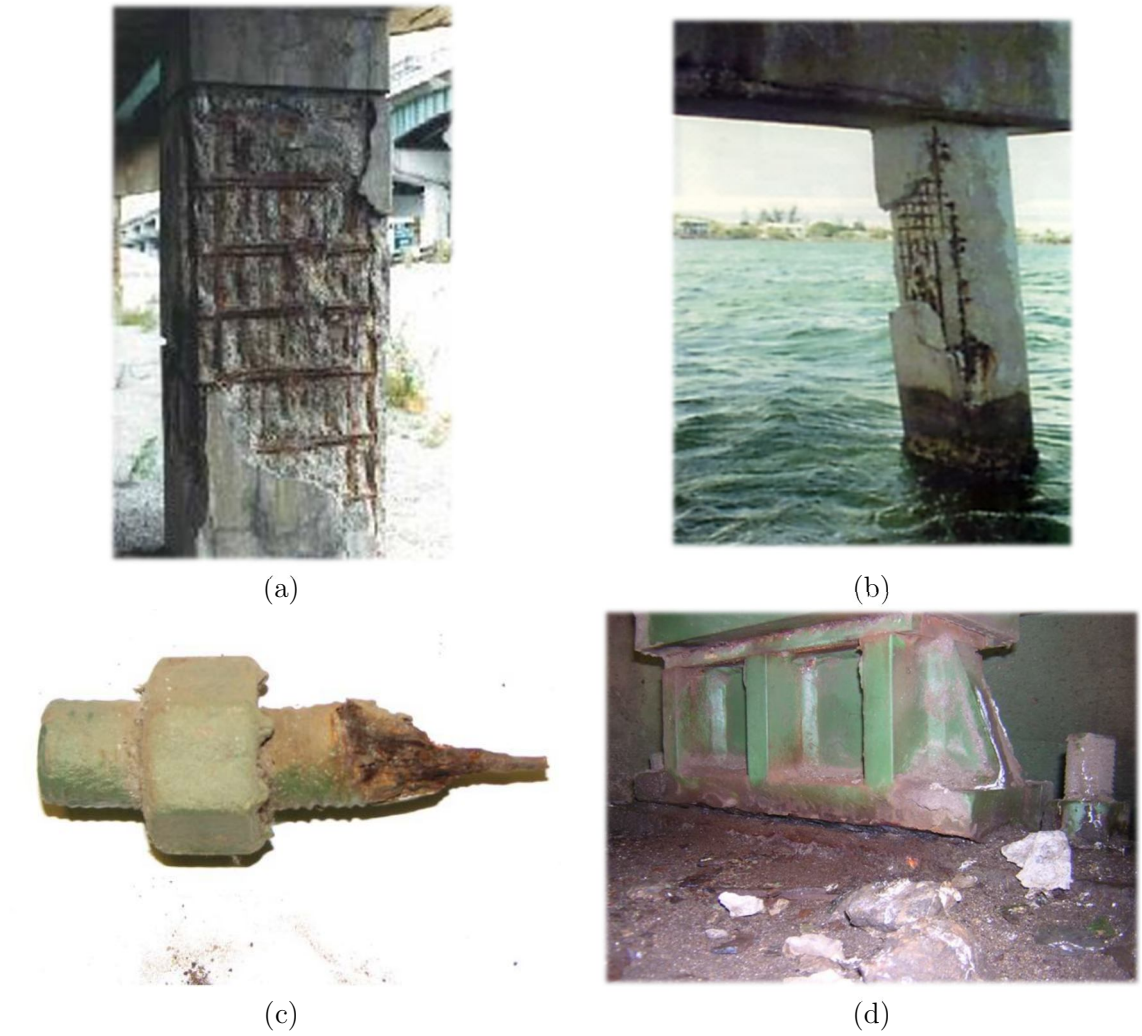

(a) (b)

(c) (d)

Figure 2-1: a) and b) Corrosion deterioration of reinforced concrete highway bridge columns leading to area loss of steel and cracking and spalling of cover concrete [adopted from Lower (2010)], c) complete section loss of anchor bolts in bridge bearings due to corrosion deterioration [adopted from Lindquist (2008)], and d) debris accumulation at bearings marked by formation of corrosion scales which envelop the base plate, anchor bolt, and bottom of the rocker [adopted from Lindquist (2008)]

2.1. Aging Bridge Seismic Fragility Assessment

In contrast to fragility assessment of pristine highway bridges, negligible amount of literature exists on aging highway bridge seismic reliability evaluation. One of the original investigations on this topic can be attributed to the work by Choe et al. (2008, 2009) on the seismic fragility estimates of free standing corroding RC columns and single column box girder bridges when exposed to chlorides stemming from marine exposure zones. Fragility estimates corresponding to column shear and drift demands for both free standing column and the overall bridge system demonstrated a noticeable increase in seismic vulnerability due to aging and deterioration. Although the above study considered deterioration of only a single bridge component (namely, RC columns), it illustrated the importance of capturing the effects of aging on seismic fragility and identified the crucial material and corrosion parameters that most significantly affect the bridge reliability. Alipour et al. (2010) also focused on the fragility assessment of bridges under marine exposure in the California region and underlined the importance of accounting for corrosion deterioration of RC columns. Unlike Choe et al. (2009), their work considered uncertainty in bridge geometric parameters and demonstrated the impact of deteriorating column height on aging bridge fragility. The recent work by

Akiyama et al. (2011) computed the fragility of deteriorating RC columns under marine exposure after calculating displacement ductility capacity based on the buckling of corroding longitudinal reinforcement. Their work however idealized bridge columns as single degree of freedom systems thereby introducing approximations in the subsequent fragility analysis.

While all of the above mentioned studies highlight the importance of accounting for aging and degradation mechanisms when computing aging bridge fragilities, they suffer from some potential drawbacks. Firstly, almost all aging bridge reliability studies focus only on the corrosion deterioration of reinforced concrete columns within the bridge system. Although this maybe sufficient for integral bridges (Choe et al. 2009), for other bridge types, such as multiple span steel or concrete girder bridges without frame action, past studies have illustrated the importance of capturing a number of vulnerable components in the fragility assessment of the bridge system (Nielson and DesRoches 2007b). Therefore, further research is required to evaluate the effect of aging on system response and fragility, considering not only the vulnerability of multiple components but also their simultaneous aging. One such seismically vulnerable critical component traditionally neglected in aging bridge fragility analysis are highway bridge

bearings affected by multiple deterioration mechanisms such as: a) loss of bearing strength due to anchor bolt corrosion when affected by atmospheric chlorides in marine exposure zones or chlorides stemming from leaking of chloride laden water at deck joints after deicing salt application (Silano and Brinckerhoff 1993); b) "freezing" or "locking" of steel bearings due to accumulation of rust products (Mander et al. 1996) restricting their translational and rotational movements during earthquakes; and c) stiffening of elastomeric bearing pads in concrete bridges due to thermal oxidation and aging. The anticipated dynamic behavior of aging highway bridge systems under various time-dependent deterioration mechanisms of multiple bridge components has yet to be characterized to support the development of time-dependent seismic fragility functions, which is one of the main focuses of this research.

In addition to the above deficiency, a majority of past research on aging bridge seismic fragility modeling focused only on chlorides stemming from marine exposure conditions when highway bridges are located within close proximity to the sea coast. A more severe form of chloride induced corrosion stems from the extensive application of deicing salts in bridges across the US, especially in cold regions characterized by moderate to heavy snowfall (Broomfield 1997). Although

past researchers have identified that chloride induced corrosion from deicing salts causes significantly higher degradation than chlorides in a marine environment (Stewart and Rosowsky 1998), there is a lack of literature on the consideration of this exposure condition in seismic reliability analyses and a potential need for comparative assessment of different exposure conditions on aging bridge fragility. Such comparisons will also be investigated in this study after accounting for a diverse range of environmental exposure conditions.

Lastly, most of the past studies on seismic fragility of aging bridges depend on simplified analysis procedures, such as nonlinear static pushover or response spectrum analysis (Choe et al. 2008, 2009), or introduce simplifications such as single degree of freedom idealization of corroding bridge columns (Akiyama et al. 2011). In this study high-fidelity three dimensional finite element aging bridge models will be developed and used to assess the impact of deterioration mechanisms on bridge fragility after conducting nonlinear dynamic time-history analysis of aging bridge models. These three dimensional models are advantageous over existing two dimensional models of highway bridges (Choi 2002, Alam et al. 2012) or single degree of freedom approximations existing in literature Akiyama et al. (2011). The models used in this study results in accurate approximations of

bridge component seismic responses without imposing intractable computational burden. Using these models, in addition to introducing time dependence within the fragility functions, this study will also develop parameterized fragility models for efficient computation of bridge reliability using statistical learning as elaborated in the next section.

2.2. Statistical Learning Techniques for Bridge Reliability Prediction

Seismic fragility assessment of pristine or aging highway bridges involves the computation of failure probabilities in the presence of several basic random variables describing the inherent uncertainties present in the ground motion intensity and the bridge structural modeling parameters. If this vector of basic random variables is represented by $\mathbf{X}$ and characterized by a joint probability density function $f(\mathbf{x})$, then the failure probability or fragility of a bridge component, i.e. exceeding a certain threshold capacity, is given by:

$$P_f = \int_{lsf(\mathbf{x})<0} \dots \int f(\mathbf{x}) d\mathbf{x} \tag{2.1}$$

where, $lsf(\mathbf{x})$ is the limit state function which separates the multi-dimensional probability space into failure and safe domains. The limit state function $lsf(\mathbf{x})$ depends on the structural capacity and demand, which is a function of the basic random variable vector $\mathbf{X}$.

The seismic demand evaluation of critical bridge components involves nonlinear dynamic analysis of complex three dimensional finite element bridge models (Section 2.1) and often requires prohibitively high computation time, even for structure specific analyses. The drawback of high computation cost hinders reliability computation of complex engineering structures such as bridges across the entire parameter space of $\mathbf{X}$ using Monte Carlo simulations, the most versatile, yet infeasible solution technique. Hence, the basic premise of applying statistical learning techniques to provide surrogate models or metamodels is to replace the "true" seismic demand estimates of the bridge components with computationally efficient approximating functions to evaluate the seismic demand, and eventually the failure probability, with significant efficiency.

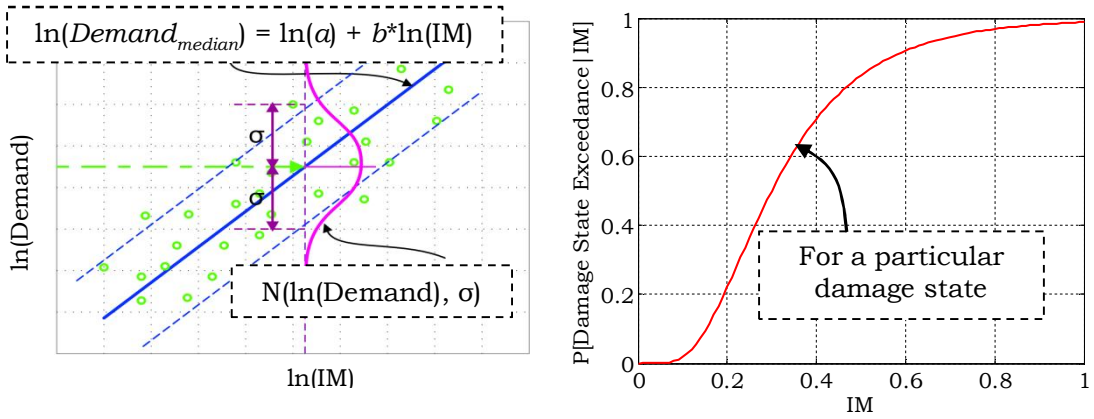

(a) (b)

Figure 2-2: a) Uni-dimensional probabilitic seismic demand model in the lognormal space [adopted from Padgett (2007)], and b) typical example of a highway bridge fragility curve depicting the probability of damage state exceedance given the intensity of ground motion (IM).

Application of metamodels for seismic vulnerability assessment of highway bridges using state-of-the-art methods is rather limited and rudimentary. Traditionally, the seismic fragility of pristine or aging bridges has been developed using first-order polynomial probabilistic seismic demand models conditioned only on a single parameter: the ground motion intensity (Mackie and Stojadinović 2001; Kunnath et al. 2006; Nielson and DesRoches 2007a; Ghosh and Padgett 2010). Figure 2-2(a) shows an example of such demand models in the logarithmic space, wherein the median of the demand is obtained as a linear function of the earthquake intensity measure (IM) following regression analysis of finite element response data (Cornell et al. 2002). Additionally, in such a logarithmic space, the dispersion of the demand is normally distributed. Subsequent comparison of the

single parameter demand model against capacity estimates aids in the development of traditional uni-dimensional bridge fragility curves, which are statements of the conditional probability of meeting or exceeding a particular damage state given the intensity of ground motion (IM) [Figure 2-2(b)].

Although prevalent in the bridge seismic fragility modeling community, single-parameter demand models suffer from two potential drawbacks. Firstly, the single-parameter seismic demand models and subsequent fragility curves are unable to assess the impact of structural or geometric model parameter variation on bridge performance during earthquakes without the costly re-analysis for each set of parameter combination scenario. Therefore the analyst must elect to either conduct fragility modeling for a given structure, which is not practical for a regional inventory of bridges, or derive reliability estimates for overall classes of structures which are not intended for bridge specific inferences. Secondly, these models cannot benefit from new data available following field instrumentation of aging bridges to enable updating of fragility estimates. This is particularly important since a significant percentage of bridges within the United States are rapidly deteriorating (ASCE 2013) and the *Federal Highway Administration's Long-Term Bridge Performance Program* plans to instrument and monitor representative bridges

across the country over the next 20 years (FHWA 2008). Only recently, Seo and Linzell (2012) have developed seismic demand models for horizontally curved steel bridges conditioned on multiple parameters such as concrete strength, steel strength etc. in addition to the ground motion hazard. Their work, however, focused on a single metamodeling strategy, higher order polynomial response surfaces, to approximate bridge response under seismic shaking.

In general, there is a lack of systematic exploration of different surrogate models to determine the best-fitting parameterized probabilistic seismic demand models that aid in efficient approximations of bridge seismic fragility estimates. Addressing this gap, the present study will investigate classical as well as modern surrogate modeling techniques rooted in statistical learning for predicting the seismic response of bridge components given the predictor variable vector. The predictive capabilities of the adopted surrogate demand models will be assessed using standard goodness-of-fit measures their accuracy will be tested against benchmark Monte Carlo simulations. The developed multi-dimensional surrogate models will be eventually used to develop parameterized bridge fragility models using logistic regression procedures. Such vector based fragility models will enable

quick estimation of bridge reliabilities in practice given in-situ bridge conditions and field measurement data.

2.3. Lifetime Seismic Loss Analysis of Aging Bridges

The increase in seismic vulnerability of highway bridges due to aging and deterioration may have significant consequences on the direct and indirect economic losses incurred in earthquake events and pose a challenge for bridge infrastructure owners aiming to invest limited resources in seismic upgrade or risk mitigation efforts. In this regard, seismic loss assessment and life-cycle cost estimation methodologies have emerged as powerful tools to facilitate such decision making processes.

A range of levels of fidelity in loss modeling, uncertainty treatment, and underlying assumptions exist in the literature related to loss assessment of highway bridges under seismic loads. For example, similar to the historic lack of joint consideration of seismic and aging threats, typical seismic loss estimation methodologies of civil infrastructures traditionally ignore the effects of deterioration of structural capacity over their service life (Wen and Kang 2001a; b; Ellingwood and Wen 2005; Furuta et al. 2004). Only recently, the effects of

cumulative seismic vulnerability of corroding columns have been considered in life-cycle cost analysis for bridges (Kumar et al. 2009; Alipour et al. 2010). As mentioned earlier, bridge deterioration mechanisms are however not only restricted to bridge columns but affect other critical bridge components as well (e.g. bridge bearings) (Silano and Brinckerhoff 1993; Hoeke et al. 2009) and should be accounted for in seismic loss estimations.

Additionally, to compute monetary losses incurred to restore bridge functionality following a seismic event, global repair cost ratios have often been adopted [such as those proposed by Basoz and Mander (1999)] to estimate pristine or aging bridge repair cost as a fraction of replacement cost, rather than aggregating the total cost from expenditures to replace or repair its components (Nilsson 2008; Padgett et al. 2010; Mackie et al. 2010; Alipour et al. 2010). However, such approximations in seismic loss estimation do not take into account the risk of seismic damage of each individual structural component or the correlations between component damages (Porter et al. 2001). Such assumptions may lead to potential over- or under-estimation of seismic losses and do not reflect the dissimilar effect of aging and deterioration on various components within a bridge. Recent studies have addressed such pitfalls by investigating component

based seismic loss estimation that also accounts for cost correlations (Goulet et al. 2007; Bradley and Lee 2009). These studies, however, do not explicitly account for time-dependent seismic vulnerability of bridge components due to aging or uncertainty in repair procedures which can have a significant impact on the mean and variance of seismic loss estimates.

The present study addresses such gaps in seismic loss estimation for bridges by providing a seismic loss estimation model that accounts for time varying seismic vulnerability, uncertainty in component repair, and the contribution of multiple correlated components. Deteriorating bridge component fragilities are considered by introducing a new methodology based on a nonhomogeneous Poisson process to estimate the expected value and variance of earthquake losses. Thus the traditionally neglected impact of bridge aging on the lifetime probability of failure and economic losses is explicitly modeled in this approach. In contrasts to other seismic life cycle cost studies of bridges based on degradation of single components or computing loss estimates derived using global repair cost ratios, this framework accounts for the deterioration and cost associated with multiple components that affect the vulnerability, repair approach, and losses incurred.

2.4. Supplementary Threats to the Seismic Vulnerability of Highway Bridges

In addition to neglecting the impact of aging and deterioration, past literature has also overlooked the impact of additional threats affecting the seismic performance of highway bridges. Two such threats this study will explore include: a) the impact of repeated earthquakes in the form of multiple main shocks and main shock – aftershock sequences, and b) the influence of truck-traffic load, present atop the bridge deck, on the seismic vulnerability of highway bridge structures.

2.4.1. Impact of repeated earthquakes on the seismic vulnerability of highway bridges

Multiple earthquakes along the service lives of civil structures, such as buildings, highway bridges, and other lifeline systems, can be expected when located in regions of moderate to high seismicity. Several field investigations have highlighted cases of structural failure as a result of earthquake damage accumulation from repeated shocks. For instance, during the Umbria-Marche earthquake sequence in Central Italy (Amato et al. 1998) on September 26, 1997, several structures withstood a main shock of magnitude 5.9. However, the inherent weakening of

structural capacities following the main shock event led to eventual collapse during the relatively weaker aftershock of magnitude 5.5 on October 14, 1997. The Foligno tower in the Umbria region is a famous structure that collapsed as a result of repeated earthquake shaking during this earthquake sequence (Figure 2-3).

(a) (b)

Figure 2-3: The Folgino tower in the Umbria region which (a) withstood the main shock on September 26, 1997, but (b) collapsed after the aftershock earthquake on October 14, 1997 [**adopted from Prete et al. (1998)**]

In Christchurch, New Zealand, several structures weakened from the magnitude 7.1 Darfield earthquake in September, 2010 suffered partial or complete collapse during a magnitude 6.2 earthquake the following year in February, 2011 (Bradley and Cubrinovski 2011). Similarly, in Turkey, many structures damaged during the Kocaeli earthquake on August 17, 1999 suffered complete collapse during the Duzce earthquake on November 12, 1999. For instance, Figure 2-4

shows a building that was tagged after the Kocaeli earthquake and eventually collapsed during the Duzce earthquake.

Figure 2-4: Collapsed building in Duzce that had already been damaged during the Kocaeli event in Turkey [adopted from Rathje et al. (2006)]

While the aforementioned examples do not focus on bridges, these systems can suffer similar accumulation of seismic damage. In fact numerous bridge structures in moderate to severe seismic zones have been exposed to multiple seismic shocks along their service lives. For instance, the California region alone consisting of 25,354 highway bridges experienced over 500 earthquakes of magnitude 3.0 or larger since the beginning of 2012 (USGS 2013).

The above mentioned real life examples highlight the importance of accounting for repeated seismic shocks and consideration of the history of past earthquake during the lifetime of the existing structures. This has been traditionally ignored when predicting their structural strength or seismic reliability. Moreover, existing studies on seismic life-cycle analysis of pristine or deteriorating structures primarily assume that the structural damages following an earthquake event are always repaired completely to ensure pristine good-as-new conditions before the occurrence of subsequent earthquakes (Wen and Kang 2001; Ghosh and Padgett 2011; Sanchez-Silva et al. 2011). This assumption can often be impractical under conditions such as: a) when the level of damage resulting in structural weakening is visually insignificant to prompt retrofit actions; b) when economic constraints exist which render retrofit or structural upgrades infeasible after every earthquake; and c) when the duration between consecutive earthquakes is too short to initiate retrofit implementations, for instance, during aftershocks. In this regard, a recent study on main shock-aftershock sequence by Yin and Li (2011) revealed that aftershocks and associated downtime costs are critical contributors to the total seismic losses. However, their study did not account for the accumulation of structural damage along the lifetime of the structure while considering the

temporal nature of main shock occurrences. In view of these existing drawbacks, it is of critical importance to develop a framework to predict the probability of structural damage as a result of repeated main shock events along the service life of the structure, or during repeated aftershock occurrences following a main shock.

Some preliminary work on deterministic seismic damage accumulation of structures due to repeated earthquakes can be found in Elnashai et al. (1998) who showed that the ductility demand imposed on a structure following multiple earthquake ground motions is often several times higher than the ductility demand required by a single earthquake occurrence. Studies by Murià-Vila and Jaramillo (1998) revealed a significant reduction in lateral stiffness of a building founded in soft soil under repeated low magnitude earthquake excitations. Recently, Amadio et al. (2003) focused primarily on the behavior of inelastic single degree of freedom system under repeated earthquake ground motion and identified the effects of factors such as structural period, type of earthquake pulse and level of available ductility on damage accretion. However, all of the above mentioned studies are deterministic, without accounting for the inherent probabilistic nature of the hazard or uncertainty in the response of structures under repeated loading conditions. Additionally, these researchers considered a very short duration

between earthquake occurrences which is incapable of capturing the aspect of damage accumulation along the service life of the structure for main shock events. This study will focus on the assessment of damage accumulation of bridges under repeated shocks while accounting for the uncertainty in hazard occurrences.

2.4.2. Influence of truck-traffic load on seismic fragility of highway bridges

The impact of live load on the seismic fragility of highway bridges constitutes the second supplementary threat that this study will address. While a plethora of literature exists solely on live load reliability of bridges under truck-traffic loads (Nowak et al. 2001; Du and Au 2005; Czarnecki and Nowak 2007), or on their vulnerability to seismic hazards alone as described earlier, a negligible amount of research focuses on the simultaneous consideration of live load and earthquake threats. Given the unpredictable nature of earthquakes, truck and traffic loads may be potentially present during the seismic excitation as evidenced by past earthquake events, for instance during the 1994 Northridge, 1995 Kobe, and 2008 Sichuan earthquakes (Basöz and Kiremidjian 1998; Chang 2000) as shown Figure 2-5.

(a) (b)

Figure 2-5: Aerial view of trapped truck-traffic and bridge damage during the a) 1994 Northridge earthquake in California, and b) 2008 Sichuan earthquake in China (Pictures adopted from: http://www.aeronauticpictures.com and http://ocho-onda.blogspot.com respectively)

At present a significant percentage of bridges within the US are characterized by older design features and geometrics (ASCE 2013) rendering them potentially incapable to accommodate current traffic volumes, vehicle sizes and weights. The situation is further exacerbated with half a million overweight trucks being employed in the US to transfer goods (National Safety Commission 2007) and expectations of future truck-traffic that exceeds present standards. In view of the existing deficiencies and lack of adequate literature on the impact of live load on seismic vulnerability of bridges, there is a pressing need for joint fragility assessment and risk modeling to explore the role on traffic loading on the seismic performance of highway bridges.

Multiple critical bridge components contribute to the seismic vulnerability of highway bridges, such as reinforced concrete columns, fixed and expansion bridge bearings, and bridge abutments. While several researchers have thoroughly investigated the impact of earthquake load on the response of these critical components (Choi 2002; Nielson and DesRoches 2007a), the present study will assess if the presence of superimposed truck live loads contributes further to their seismic vulnerability. Additionally, since the position of truck load on the bridge is uncertain, this study assesses the impact of truck location atop the bridge deck on the seismic fragility of the overall bridge system to determine the most detrimental truck position. Further, a general framework will be proposed in which the site-specific traffic characteristics (truck gross vehicle weight histogram and truck flow) can be coupled with conditional reliability estimates to arrive at bridge-specific fragility curves that reflect likelihood of truck presence. This approach is motivated by the increasing availability of Weigh-In-Motion (WIM) data, and the variability of truck flow and the distribution of truck weights across different regions, such as industrial zones and rural areas.

2.5. Closure

Past research on highway bridge fragility analysis has traditionally neglected the impact of aging and deterioration mechanisms on the seismic vulnerability of degrading structural components and overall bridge system. Even the few studies on this topic are marked by potential drawbacks such as consideration of single component deterioration mechanisms under limited environmental exposure conditions, and introduction of overly simplified analysis procedures for aging impact assessment on bridge fragility. In this study aging bridge fragility functions will be assessed after considering the contributions from multiple deteriorating bridge components and using rigorous finite element analysis techniques. Additionally, comparative assessment on the influence of different exposure conditions on bridge fragility will also be presented.

Traditional aging or pristine bridge fragility curves can often result in intractable number of simulations for reliability estimation of highway bridges given the wide range of uncertainty of parameter space. The present study will address this shortcoming by developing flexible parameterized fragility models using statistical learning techniques which will aid in precise and efficient estimation of bridge fragilities after incorporating data available from field instrumentation of highway

bridges. Such multidimensional models offer several advantages over traditional uni-dimensional bridge reliability curves and constitute the next generation of fragility functions towards probabilistic vulnerability of aging highway bridges. These fragility models enable quick estimation of bridge reliabilities in practice given in-situ bridge conditions and field measurement data. The aging bridge fragility functions developed in this study will be used within a nonhomogeneous Poisson process framework for lifetime seismic loss estimation of aging highway bridges. This framework will address several deficiencies in existing loss estimation and seismic life-cycle cost estimation approaches which typically ignore the impact of aging mechanisms and contribution of correlated bridge components towards monetary losses and introduce simplifications such as computing loss estimates using global repair cost ratios.

Finally, this study will focus on two commonly overlooked yet prevalent threats on highway bridge performance. One such threat stems from the exposure of highway bridges to repeated seismic shocks in earthquake prone regions. While field studies in the past have revealed the potential weakening and eventual collapse of structures under multiple earthquakes, existing literature on seismic vulnerability does not explicitly model this phenomenon while considering the

probabilistic nature of the hazard. This study will develop a damage accumulation framework to predict the increase in lifetime seismic vulnerability of highway bridge structures from multiple seismic shock scenarios. The second threat this study will consider is the influence of truck-traffic on bridge seismic fragility. While a significant amount of literature individually exists on live load reliability or seismic fragility, this study will develop a joint seismic-live load fragility framework for the first time in bridge reliability studies.

Chapter 3

AGING HIGHWAY BRIDGE CLASSES: DETERIORATION MECHANISMS AND FINITE ELEMENT MODELING

The strength of highway bridges components, or any structural system, is in general a time-dependent property that may decrease in resistance along the structure's service life. This chapter will introduce the typical highway bridge types considered in this study, different environmental degradation mechanisms, and finite element modeling of deteriorating bridge components in addition to standard modeling principles for pristine bridge components. Additionally, finite element model validation results using experimental test data for several bridge components from the PEER database (PEER 2013) are presented in the Appendix A. Potential reasons for structural strength degradation can be attributed to multiple factors such as corrosion, erosion, other forms of chemical deterioration and fatigue

(Melchers and Frangopol 2008). Highway bridges, often exposed to severe environmental conditions, are particularly vulnerable to strength and resistance loss with time, which may affect the response of the structure under dynamic loading. The present study considers the aging of highway bridges by including probabilistic deterioration models of critical bridge components such as reinforced concrete columns and bridge bearings affected by environmental degradation mechanisms. The extents of degradation suffered by these highway bridge components typically depend on the bridge material and construction type, age of the bridge, and environmental exposure condition.

3.1. Aging Highway Bridge Classes

This study will focus on typical highway bridges located in the region of Central and Southeastern United States (CSUS) encompassing the states of Alabama, Arkansas, Georgia, Illinois, Indiana, Kentucky, Mississippi, Missouri, North Carolina, South Carolina, and Tennessee. The majority of bridges in this region were designed with little or no seismic consideration with typical deficiencies characterized by inadequately detailed columns with limited ductility capacity and

low shear strength, brittle steel bearings, short seat widths, and inadequately reinforced pile caps among others (DesRoches et al. 2004; Nielson 2005).

While the details on the full inventory analysis can be found elsewhere (Nielson and DesRoches 2007a; Nielson 2005), seismic fragility analysis of different bridge classes in this region by Nielson(2005) revealed that Multi-span Continuous (MSC) steel girder bridges and Multi-span Simply Supported (MSSS) concrete girder bridges rank amongst the most popular yet seismically significantly fragile bridges in the region. Additionally, recent work by Ghosh and Padgett (2010, 2012) have revealed that aging and deterioration mechanisms are likely to render these bridge more vulnerable to earthquake hazards. Hence, time-dependent fragility curve development (Chapter 4) and seismic lifetime loss analysis concepts (Chapter 7) will be explored in this thesis primarily focusing on these bridge types. Figure 3-1 shows the typical geometry configuration of these bridge types. The MSC steel girder bridge is characterized by the continuity of steel girders across the bridge bents and presence of high type steel fixed bearings at each girder along the bent beams and expansion bearings at the abutments. The MSSS Concrete girder bridge consists of simply supported bridge girders and elastomeric fixed and expansion bearings at the end of each span. Further modeling details and impact of

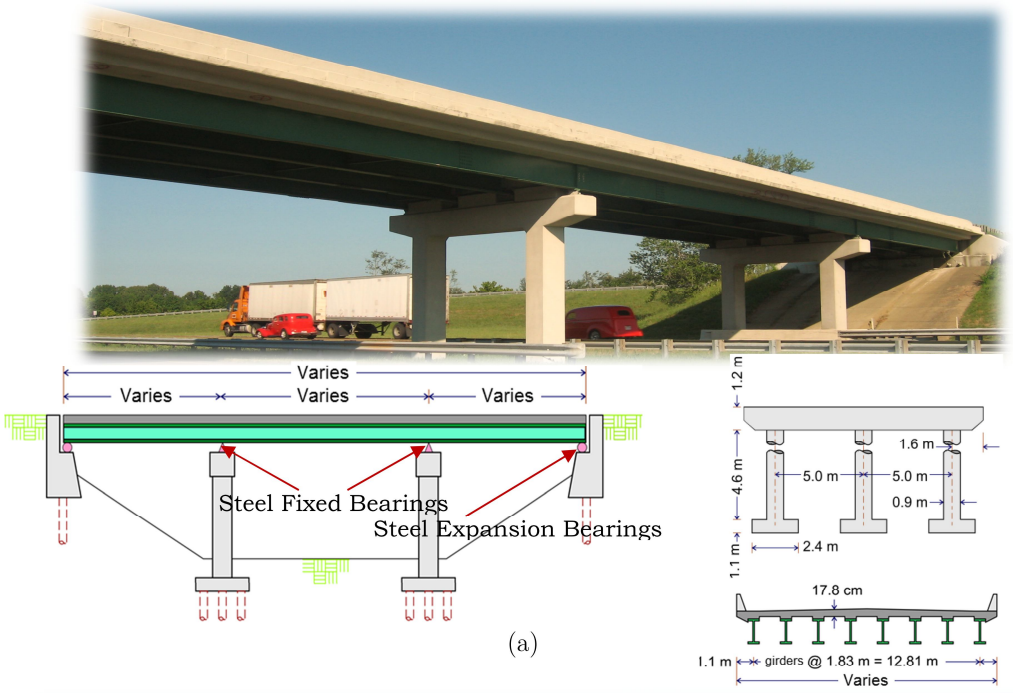

(a)

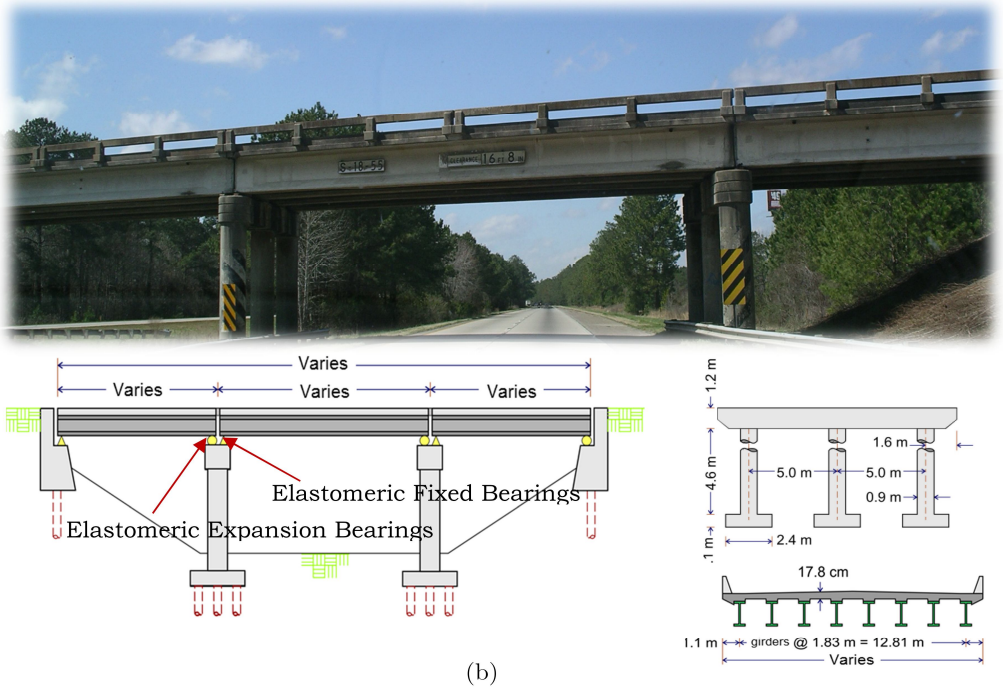

(b)

Figure 3-1: Typical geometry configuration of a) multi-span continuous (MSC) steel girder bridge, and b) multi-span simply supported (MSSS) steel girder bridges in Central and SouthEastern US. Photographs adopted from Padgett (2007).

aging on seismic performance of both bridge types will be presented in subsequent chapters. In addition to the above bridge types, this study will also consider seven other different bridge classes while developing parameterized bridge fragility models for distributed highway bridge networks within the state of South Carolina (Chapter 5). A complete list of all bridge classes considered in this study along with their acronyms and HAZUS (2003) class counterparts are presented in Table 3.1.

Table 3.1: Central and Southeastern US highway bridge classes considered in this study

Bridge Type	Abbreviation	HAZUS Class
Multi-span Continuous Steel Girder	MSC Steel	HWB15, HWB26
Multi-span Simply Supported Concrete Girder	MSSS Concrete	HWB5, HWB17
Multi-span Continuous Concrete Girder	MSC Concrete	HWB10, HWB22
Multi-span Simply Supported Steel Girder	MSSS Steel	HWB12, HWB24
Multi-span Continuous Slab	MSC Slab	HWB10, HWB22
Multi-span Simply Supported Slab	MSSS Slab	HWB5, HWB17
Multi-span Continuous Concrete Box Girder	MSC Concrete Box	HWB10, HWB22
Single Span Concrete Girder	SS Concrete	HWB3
Single Span Steel Girder	SS Steel	HWB3

In general, all the structurally and materially different bridge types considered in this study are prone to the detrimental effects of aging and deterioration mechanisms affecting key critical structural components responsible for lateral load transmissions during earthquakes. Table 3.2 provides an overall synopsis of deterioration mechanisms suffered by these bridge types and the rest of

this chapter will be dedicated to detailing these deterioration mechanisms and subsequent finite element modeling of aging bridge components.

Table 3.2: Deterioration affected structural parameters and forms of degradation corresponding to different bridge types.

Bridge Component	Deterioration Affected Structural Parameter	Mechanism of Degradation
Reinforced concrete bridge deck (common to both steel and concrete girder bridges)	Reinforcing steel	Cross sectional area loss of steel due to corrosion
Steel bridge girders (particular to steel girder bridges)	Steel bridge girders	Girder sectional area loss due to corrosion
Reinforced Concrete (RC) Columns (common to both steel and concrete girder bridges)	Longitudinal and transverse reinforcement	Cross sectional area loss of steel due to corrosion
	Concrete cover	Loss of cover/spalling due to expansive forces from the accumulation of rust products
Elastomeric Bridge Bearings (particular to concrete girder bridges)	Elastomeric bearing pad	Increase in shear modulus due to aging and temperature effects
	Bearing dowel bars	Loss of shear strength due to corrosion deterioration
Steel Bridge Bearings (particular to steel girder bridges)	Bearing anchor bolts	Cross sectional area loss of steel due to corrosion affecting the ultimate lateral strength of the bearings
	Coefficient of friction	Increase in bearing friction due to accumulation of rust products
	Expansion bearing keeper plate	Reduction of keeper plate due to corrosion

3.2. Highway Bridge Deterioration Mechanisms

This section will focus exclusively on the degradation mechanisms of different bridge components depending on their physical conditions (for example, whether embedded in concrete or unprotected) and environmental exposure scenarios.

3.2.1. Corrosion deterioration of reinforced concrete members

Corrosion degradation of reinforced concrete (RC) members primarily results in cross sectional area loss of embedded steel along with secondary effects such as cracking and spalling of cover concrete. This deterioration mechanism is common for critical bridge components with embedded steel members, such as reinforced concrete bridge decks, column longitudinal and transverse reinforcement, steel bearing anchor bolts, and elastomeric bearing dowel bars. Corrosion deterioration of the above mentioned bridge components is investigated in this study under three environmental exposure conditions listed in the decreasing order of corrosivity: a) deicing salt exposure, b) marine splash zone exposure, and c) marine atmospheric exposure.

A wealth of literature exists on the corrosion mechanism of reinforcing steel embedded in concrete, which is typically represented by Fick's second law of

diffusion through a semi-infinite solid (Stewart and Rosowsky 1998). Following the diffusion process, the concentration of chloride ions in concrete must reach a critical threshold to dissolve the protective passive film around the reinforcement, thus initiating reinforcement corrosion. The corrosion initiation time typically depends on the environmental exposure condition. The exposure conditions considered in this research include exposure to chlorides from deicing salts and marine exposure. The impact of different exposure condition on the seismic vulnerability will be assessed in Chapter 4.

It has been shown by researchers that deicing salt exposure results in constant chloride ion concentration near the concrete surface (Hoffman and Weyers 1996; Vu and Stewart 2000) and the corresponding corrosion initiation time is given by (Thoft-Christensen et al. 1996):

$$T_{i_{deicing}} = \frac{x^2}{4D_c}\left[erf^{-1}\left(\frac{C_0 - C_{cr}}{C_0}\right)\right]^{-2} \tag{3.1}$$

where, $T_{i_{deicing}}$ is the corrosion initiation time due to deicing salt exposure, x is the concrete cover depth, D_c is the chloride diffusion coefficient, C_0 is the equilibrium chloride concentration at the concrete surface, and C_{cr} is the critical chloride

concentration that causes dissolution of the protective passive film around the reinforcement and initiates corrosion. Further, *erf* is the Gaussian error function that can be mathematically represented as (Edwards 2006):

$$erf\left(\theta\right) = \frac{2}{\sqrt{\pi}} \int_{0}^{\theta} e^{-t^2} dt \tag{3.2}$$

Table 3.3: Typical lognormal distributions of the random variables affecting the corrosion intitation time under deicing salt exposure conditions from Enright and Frangopol (2008). These estimates are based on data from field instrumentation of bridges in deicing salt exposure zone across the US.The mean estimates indicate the mean of the lognormal distribution and the missing entries for the coefficient of variation (COV) indicates that the uncertainty around the reported mean estimates is unavailable in literature).

Diffusion Coefficient (D_c)		**Surface Chloride Conc. (C_0)**		**Critical Chloride Conc. (C_{cr})**	
Mean (cm^2/year)	COV	Mean (weight % concrete)	COV	Mean (weight % concrete)	COV
0.32	0.05	0.1	0.05	0.030	0.05
0.65	0.1	0.15	0.10	0.035	0.10
1.29	0.15	0.20	0.15	0.040	0.15
1.94	0.20	0.30		0.045	
2.58		0.40			

While the concrete cover depth x is dependent on the geometry of the reinforced concrete structure under consideration, the above mentioned corrosion deterioration parameters D_c, C_0 and C_{cr} are typically found to follow lognormal distributions. The distribution parameters (Table 3.3) are adopted from literature on in-field corrosion related studies of existing bridge components in the United

States exposed to deicing salts (Whiting et al. 1990; Weyers et al. 1994; Enright and Frangopol 1998). Additionally, it is noted that these random variables presented in Table 3.3 are uncorrelated.

Based on a series of laboratory tests by researchers, corrosion initiation time for RC members located in marine zones under the exposure of chlorides can be estimated based on Equation (3.3) (Bertolini et al. 2004; Choe et al. 2009):

$$T_{i_{marine}} = \left\{ \frac{x^2}{4k_c k_e D_0 \left(t_0\right)^{n_{cl}}} \left[erf^{-1}\left(1 - \frac{C_{cr}}{C_s}\right)\right]^{-2} \right\}^{\frac{1}{(1-n_{cl})}} \tag{3.3}$$

where, k_c is the curing factor, k_e is the environmental factor, t_0 is the age of concrete when the compliance test is performed, D_0 is the reference diffusion at t_0 = 28 days, n_{cl} is the age exponent that incorporates the densification of cement paste due to further hydration, and $C_s = A_{cs}(w/b)+\varepsilon_{cs}$ is the chloride concentration at the surface, A_{cs} and ε_{cs} are model parameters, and w/b is the water-binder ratio assumed to be 0.5. Corrosion deterioration under marine exposure conditions is highly dependent on the type of exposure condition: whether located away from the chloride laden sea water; repeatedly subjected cyclic wetting and dry cycles from the sea, or completely submerged under sea water (Figure 3-2). As noted by

researchers in the field of corrosion engineering, the severity of corrosion deterioration under marine exposure is highest during a simultaneous availability of chlorides (from the sea water) and the atmospheric oxygen (Broomfield 1997). Hence, it is evident from Figure 3-2 that structures located in splash and tidal zones will suffer a higher level of deterioration as compared to structures located away from the sea (atmospheric zone) or completely submerged under the sea water resulting in a lack of atmospheric oxygen (submerged zone). The statistical distributions of the variables affecting corrosion initiation time for different marine exposure zones are adopted from Duracrete (2000), Bertolini (2004) and Choe et al. (2008) and presented in Table 3.4.

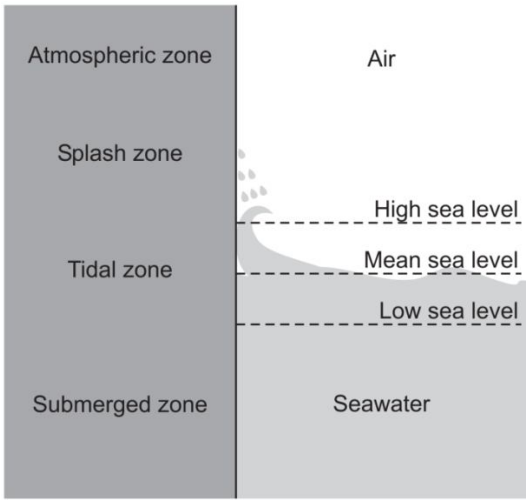

Figure 3-2: Different marine exposure zones with respect to chloride penetration from sea water resulting in eventual corrosion of reinforced concrete members [adopted from Bertolini et al. (2004)]

Table 3.4: Statistical distributions of deterioration parameters variables affecting corrosion initiation time (Duracrete 2000; Bertolini et al. 2004; Choe et al. 2008)

D_o: Reference diffusion coefficient at t_0 = 28 days					
Condition*	Distribution	Mean (mm^2/year)	St. Dev.†† ($10^{-12}m^2$/sec)		
w/c ratio =0.4	Normal	220.9	25.4		
w/c ratio =0.45	Normal	315.6	32.5		
w/c ratio =0.5	Normal	473	43.2		
n_{cl}: Age exponent					
Condition	Distribution	Mean	St. Dev.	A†	B†
All	Beta	0.362	0.245	0	0.98
k_e: Environmental correction factor					
Condition	Distribution	Mean	St. Dev.		
Splash	Gamma	0.265	0.045		
Atmospheric	Gamma	0.676	0.114		
k_c: Curing time correction factor					
Condition	Distribution	Mean	St. Dev.	A	B
curing 1 day	Beta	2.4	0.7	1.0	4.0
curing 3 day	Beta	1.5	0.3	1.0	4.0
curing 7 day	Deterministic	1.0			
curing 28 day	Beta	0.8	0.1	0.4	1.0
A_{cs} and ε_{cs}: Parameters to compute C_s					
Condition	Distribution	A_{cs}		ε_{cs}	
		Mean	St. Dev.	Mean	St. Dev.
Splash	Normal	7.758	1.36	0	1.105
Atmospheric	Normal	2.565	0.356	0	0.405
C_{cr}: Critical chloride concentration					
Condition	w/c ratio	Distribution	Mean	St. Dev.	
Constantly humid or humid-dry cycles (splash and atmospheric zones)	0.3	Normal	0.50	0.10	
	0.4	Normal	0.80	0.10	
	0.5	Normal	0.90	0.15	

* This study adopts a water-cement ratio ($w/c = 0.5$) throughout. ††St. Dev. indicates Standard Deviation, †A and B are the shape parameters of the Beta distribution

Once corrosion initiates by either chloride exposure from deicing salts or marine exposure, the time-dependent loss of reinforcement cross-sectional area can be calculated using the diameter of pristine longitudinal rebar and rate of metal loss due to corrosion (Thoft-Christensen et al. 1996; Enright and Frangopol 1998). In some instances, especially for deicing salt exposure conditions, the corrosion rate r_{corr} has been considered as a constant parameter along the service life primarily due to lack of explicit data for time-dependent corrosion rate modeling (Frangopol et al. 1997; Val et al. 2000; Akgul and Frangopol 2004; Liu 2005). In this thesis a simplified model of a constant rate of corrosion is thereby adopted for this exposure condition. Typical lognormal distributions of time invariant corrosion rate available in literature (Whiting et al. 1990; Weyers et al. 1994; Enright and Frangopol 1998) for structures subjected to corrosion deterioration from deicing salt exposure is presented in Table 3.5 (Enright and Frangopol 1998).

Table 3.5: Main descriptors of lognormally distributed constant corrosion rate for deicing salt exposure reported in literature (Enright and Frangopol 1998)

Corrosion rate (r_{corr})	
Mean (mm/year)	COV
0.013	0.1
0.025	0.2
0.076	0.3
0.127	0.4
0.254	0.5

For marine exposure conditions limited accelerated corrosion tests in the laboratory by researchers have shown the potential time dependence of corrosion current density. For instance, Equation (3.4) shows the commonly adopted form of corrosion current density (in $\mu A / cm^2$) at the beginning of the corrosion propagation phase of RC structures (Yokozaki et al. 1997; Vu and Stewart 2000). Subsequently, based on limited laboratory experiments, Vu and Stewart (2000) observed that this initial corrosion current density reduces with time following Equation (3.5).

$$i_{corr_0} = \frac{37.8\left(1 - w/c\right)^{-1.64}}{x} \tag{3.4}$$

$$i_{corr}\left(t\right) = 0.85 i_{corr_0}\left(t - T_{i_{marine}}\right)^{-0.29} \tag{3.5}$$

In the above equations, i_{corr_0} is the initial corrosion current density, $i_{corr}\left(t\right)$ is corrosion current density at time t in the service life of the aging bridge component, w/c is the water cement ratio of concrete and x is the cover depth in mm. Both corrosion current densities i_{corr_0} and $i_{corr}\left(t\right)$ (in $\mu A / cm^2$) when multiplied with the conversion factor 0.0116, yield the corresponding corrosion rates (for instance, $r_{corr}(t) = 0.0116 i_{corr}(t)$ mm/year).

Once the protective passive film around the reinforcement dissolves due to continued chloride ingress, corrosion initiates and the time-dependent loss of reinforcement cross-sectional area, $A(t)$, can be expressed as (Thoft-Christensen et al. 1996; Enright and Frangopol 1998):

$$A(t) = \begin{cases} nD_i^2 \dfrac{\pi}{4} & for \;\; t \le T_i \\ n\left[D(t)\right]^2 \dfrac{\pi}{4} & for \;\; T_i < t < T_i + D_i / r_{corr}(t) \\ 0 & for \;\; t \ge T_i + D_i / r_{corr}(t) \end{cases} \tag{3.6}$$

where, n is the number of reinforcement bars, D_i is the initial diameter of steel reinforcement, t is the elapsed time in years after corrosion initiation, $r_{corr}(t)$ is the rate of corrosion, and $D(t)$ is the reinforcement diameter t years after corrosion initiation, which can be represented as:

$$D(t) = D_i - r_{corr} \;\; (t) \tag{3.7}$$

Corrosion deterioration and corresponding loss of steel area might also lead to potential secondary effects such as cracking and spalling of cover concrete. This phenomenon is incorporated in this study by adopting the model detailed by Duracrete (2000) which assumes that cover concrete is expected to spall once the

crack width due to accumulation of rust products exceeds a critical limit of 1mm. The cover concrete crack width $w^d(t)$ at any point in the service life of the corroding reinforced concrete member can be computed as (Duracrete 2000):

$$w^d(t) = \begin{cases} w_0 \\ w_0 + b^d \left[p^d(t) - p_0^d \right] \end{cases} \tag{3.8}$$

where, w_0 is the width of initial visible crack (usually assumed to be 0.05mm), b^d is the design value of a parameter depending on the position of the rebar evaluated as:

$$b^d = b^c \gamma_b \tag{3.9}$$

where, the constant parameter b^c equals 0.0086mm/μm for top layer of reinforcement and γ_b is a partial factor which equals 1.00 for chloride induced corrosion. $p^d(t)$ in Equation (3.8) represents the design value of corrosion penetration in micrmeters calculated using Equation (3.10)

$$p^d(t) = \begin{cases} 0 \ \ if \ \ t < T_i \\ V^d w_t (t - T_i) \ \ if \ \ t > T_i \end{cases} \tag{3.10}$$

where, T_i is the corrosion initiation time, that can computed from Equation (3.1) or (3.3) depending on the exposure condition, V^d is the design value of the

corrosion rate, and w_t is the characteristic value of the equivalent period of wetting and equals: 0.5 for corrosion in atmospheric zone, 0.75 for cyclic wet-dry zones (Splash zone), and 1.0 for wet, rarely dry zones (Tidal zone).

The final parameter in Equation (3.8) is p_0^d representing the design value of corrosion penetration necessary to produce a crack in micrometers calculated as:

$$p_0^d = a_1 + a_2 \frac{x}{D_i} + a_3 f_{c,sp}^d \tag{3.11}$$

Where, a_1, a_2, and a_3 are regression parameters with characteristic values of 74.4μm, 7.3 μm, and -17.4 μm/MPa respectively, x is the concrete cover thickness, D_i is the initial rebar diameter, and $f_{c,sp}^d$ is the design value of concrete splitting tensile strength usually taken as 2.61MPa.

This study will investigate the impact of varying environmental exposure conditions on the corrosion deterioration of reinforced concrete members after computing the corrosion initiation time, area loss of steel, and cracking and spalling of concrete using the equations elaborated in this section.

3.2.2. Corrosion deterioration of exposed steel members

Corrosion of steel members is typically expected in bridge components exposed to the open atmosphere such as steel bridge girders and keeper plates of expansion bearings commonly employed in steel bridges. The corrosion of these exposed steel elements is assumed to follow an empirical model following the form of a power law (Komp 1987):

$$y(t) = Pt^{Q} \tag{3.12}$$

where, $y(t)$ is the average corrosion penetration in μm used to compute the extent of corrosion deterioration, t is the time in years, and P and Q are parameters determined from regression analysis of field experimental data. In this study, parameters P and Q are assumed to follow a correlated bivariate lognormal distribution represented as $LN(\lambda_P, \lambda_Q, \zeta_P, \zeta_Q, \rho_{PQ})$, where λ_P, λ_Q and ζ_P, ζ_Q and are means and standard deviations of the equivalent normal distributions for parameters P and Q, and ρ_{PQ} is the correlation coefficient. The lognormal mean values, coefficient of variations, and correlation coefficients determined for steel members exposed to different environments are reported in Table 3.6 based on field tests by Albrecht and Naeemi (1984).

Table 3.6: Statistical parameters for lognormally distributed P and Q to determine the section loss of exposed steel member due to corrosion deterioration (Albrecht and Naeemi 1984). The reported mean values and COV's represent the mean and coefficient of variation of the lognormal distribution.

Exposure Condition	Parameter	Mean	COV	ρ_{PQ}
Rural	P	34.00	0.09	Not available
	Q	0.65	0.10	
Urban	P	80.20	0.42	0.68
	Q	0.59	0.40	
Marine	P	70.60	0.66	-0.31
	Q	0.79	0.49	
Deicing	P	53.5	0.20	-0.55
	Q	0.60	0.40	

While steel bridge girder deterioration has received significant attention pertaining to service load reliability computation of corroded steel bridges (Kayser and Nowak 1989; Czarnecki and Nowak 2008), it has been only recently observed that corrosion of steel keeper plates affect the seismic response of steel bridge expansion bearings (Ghosh and Padgett 2010).

3.2.3. Thermal oxidation of elastomeric bearing pads

Elastomeric bearing pads are prevalently used in concrete girder and slab type bridges and assist in the transfer of forces from the concrete girder superstructure to the substructure. These bearing assemblies consist of two components: an elastomeric rubber pad and steel dowels, both prone to the adverse effects of aging and deterioration. While the steel dowels suffer cross-sectional area loss due to

corrosion deterioration as elaborated earlier, the elastomeric bearing pads undergo a potential increase in shear stiffness due to thermal oxidation.

A key element in the analytical modeling of elastomeric pads lies in the determination of initial shear stiffness of the pad which can be expressed as (Kelly 1997; Choi 2002):

$$k_i = \frac{GA_{pad}}{t_{pad}} \tag{3.13}$$

where, G is the shear modulus of the rubber, A_{pad} is the area of the elastomeric bearing pad and t_{pad} is the thickness. Typically a mean value of the shear modulus based on AASHTO(2012) recommendations is assumed in analytical modeling and seismic fragility analyses of bridges with elastomeric bearings. However, following a series of accelerated exposure tests, Itoh et al. (2006) concluded that the shear modulus of rubber, amongst other properties, is not constant and is highly affected by degradation mechanisms such as thermal oxidation. Consequently, Itoh and Gu (2009) proposed an aging model for natural rubber bearings that reflects the relation among the variation of the different material properties of rubber bearings with temperature, and aging time. For instance they proposed that under

accelerated exposure test conditions the variation in strain energy due to thermal oxidation can be given by:

$$\frac{SE_s}{SE_0} = c_s\sqrt{t_{aging}} + 1 \tag{3.14}$$

where, $\frac{SE_s}{SE_0}$ is the relative strain energy as compared to the initial state at the rubber surface at a specific value of uniaxial strain, SE_0 being the strain energy at the initial state for the same value of uniaxial strain, c_s is the temperature dependent coefficient for strain energy and t_{aging} is the aging time at test temperature in hours under accelerated test conditions.

As evident from Equation (3.14), this formulation is valid only for aging times at the selected test temperature and hence there is a need to correlate the accelerated aging results with deterioration under in-field service conditions at alternate temperatures. This correlation can be achieved using the Arrhenius methodology in the formula proposed by Le Huy and Evrard (1998) as:

$$\ln\left(\frac{t_{test}}{t_{field}}\right) = \frac{E_a}{R}\left(\frac{1}{T_{test}} - \frac{1}{T_{field}}\right) \tag{3.15}$$

where, t_{field} is the time of exposure of the rubber bearing in the field, E_a is the activation energy of rubber (94900J/mol), R is the gaseous constant (8.31J/mol K), T_{test} is the absolute temperature under accelerated thermal oxidation test and T_{field} is the absolute temperature in the field service conditions.

The measure of strain energy change as given by Equation (3.14) can also be used to measure a change in shear modulus (G) to estimate the updated value of initial shear stiffness k_i of the bearing pad for use in fragility modeling of aging bridges. This change can be measured by using a one-parameter *neo-Hookean* material model which provides a simple relation between strain energy and the shear-modulus expressed as (Mase and Mase 1999):

$$SE = G\left(\lambda^2 + \frac{2}{\lambda} - 3\right) \tag{3.16}$$

where, SE is the strain energy, G is the shear modulus and λ is a measure of uniaxial strain for the rubber specimen. Hence a relative change in shear modulus of the rubber bearing due to aging can simply be measured from change in the value of strain energy as follows:

$$\frac{G_{aging}}{G_0} = \frac{SE_s}{SE_o} \tag{3.17}$$

where, G_{aging} is the shear modulus of the aging rubber bearing at time $t = t_{field}$, and G_0 is the initial assumed strain energy at time t_0. The ratio $\frac{SE_s}{SE_o}$ can be conveniently calculated from Equation (3.14) as presented earlier for the accelerated thermal oxidation tests, and shear modulus of the aging bearing derived as:

$$G_{aging} = G_0 \left(c_s \sqrt{t_{aging}} + 1 \right) \tag{3.18}$$

3.2.4. Scope of deterioration modeling and future research opportunities

It is acknowledged that other possible bridge deterioration mechanism such as concrete degradation or fatigue of bridge components and permutations of component aging are feasible, which are outside of the scope of the present study and modeling. Emphasis is placed upon corrosion of steel reinforcement in reinforced concrete columns leading to section loss of steel and cracking of concrete, corrosion of anchor bolts and dowel bars in steel and elastomeric bridge bearings, corrosion of keeper plates in steel expansion bearing assemblies, and increased

coefficient of friction for the steel bearings due to accumulation of rust products. These mechanisms are among the most severe phenomena associated with corrosion of aging bridges exposed to deicing salts and marine environments as identified in a series of past studies (Li et al. 2009; Lindquist 2008; Pantazopoulou et al. 2001; Silano and Brinckerhoff 1993; Itoh and Gu 2009).

Corrosion of reinforcing steel within the concrete columns may lead to secondary effects loss of bond strength, and potential buckling of longitudinal reinforcement during seismic events following the spalling of cover concrete. While previous studies have shown that loss of bond strength is significant for unconfined RC members (Fang et al. 2004; Aquino and Hawkins 2007), it is negligible for members with transverse confinement (Fang et al. 2004). Following the provisions for pre-seismic detailing, bridge columns in Central and Southeastern US are modestly confined and hence fall in between the two above mentioned categories. Deficiencies in experimental data for columns with limited confinement underline the need for future work in this area of research that will lead to viable improvement of analytical models. With respect to buckling of longitudinal reinforcement in corroded columns, a preliminary investigation conducted by Ghosh and Padgett (2012) revealed that even under severe deterioration

conditions, explicit incorporation of rebar buckling phenomena in the bridge models results in less than 1% shift in fragility estimates. Consequently, rebar buckling phenomena is not considered in the finite element aging bridge models. Corrosion of steel girders in the bridge superstructure has, for example, received significant attention in the literature with regards to corrosion process modeling and reliability assessment of bridges under live loading (Kayser and Nowak 1989; Czarnecki and Nowak 2008). However, a preliminary sensitivity study conducted by the author revealed the negligible impact of this process on the bridge's seismic vulnerability. Even in the event that additional girder or superstructure components are added to the system fragility definition, the demands placed on a 100 year corroded bridge girder under seismic loading are not anticipated to exceed the yield capacity of the component and hence remain elastic under seismic loading and negligible in the fragility assessment. Another deterioration mechanism not considered in this study is the fatigue of bridge components, such as bridge girders and bearings due to traffic loads. While contribution of corroding bridge girders is negligible to bridge fragility, future studies should consider the impact of fatigue on bridge bearings. These additional phenomena presented in this section highlight the opportunity for future study, although preliminary analysis conducted as part of

this research indicates that some of these degradation effects can be neglected owing to their limited impact on the bridge fragility.

3.3. Analytical Modeling of Aging Highway Bridges

The deterioration mechanisms discussed in the previous section affect the structural characteristics of critical highway bridge components. In order to investigate the impact of aging on the seismic response and fragility of highway bridges, three-dimensional finite element models characterized by deteriorating structural components are developed in this study using the open source nonlinear finite element package OpenSees (Mazzoni et al. 2009). In this regard, the base modeling assumptions proposed and detailed in Nielson (2005) and Padgett (2007) are used to model pristine bridge components and subsequently enhanced to reflect aging and deterioration mechanisms. The intention of this section is to present the general modeling overview of pristine components and detail how deterioration mechanisms can be incorporated for aging bridge finite element modeling. Model validation using available experimental test data in literature of several bridge components, such and bridge columns and bearings in their pristine state, as well

general validation notes for deteriorating bridge components can be found in Appendix A.

3.3.1. Modeling of deck superstructure

For both concrete and steel girder bridges, the composite slab and girders are modeled using linear elastic beam-column elements since the superstructure is expected to remain elastic during seismic action. As mentioned in Section 3.2.4, a preliminary study indicated that the seismic demands placed on a heavily corroded (100 year old) steel bridge girder is significantly lesser than its yield capacity and hence remains elastic under seismic loading with negligible influence on bridge fragility. The pounding between adjacent bridge decks and bridge deck and abutment is modeled using a bilinear contact element proposed by Muthukumar (2003) which essentially captures the energy dissipation during pounding using a hysteretic model.

3.3.2. Modeling of steel fixed and expansion bearings

Bridge bearings constitute important elements within the bridge system responsible for the transfer of forces from the superstructure to the substructure. In steel bridges, high type steel fixed and expansion bearings are modeled using non-linear

translational springs in the longitudinal and transverse direction, based on the recommendations by Mander et al. (1996) and Nielson(2005). Degraded seismic performance of the bridge bearings have been identified by researchers primarily due to the corrosion debris accumulation resulting in "frozen" or "locked" bearings, as well as the corrosion of anchor bolts and keeper plates used in bearing assemblies. Typically such anchor bolts are used in both fixed and expansion (rocker) bearings, while the keeper plates are typical details in the expansion bearing assemblies. As identified by Mander et al. (1996) bearing anchor bolts often form a "weak-link" in the chain of force transmission from the superstructure to the substructure during seismic events. Corrosion of these elements may potentially result in a shift in performance during seismic loading. The primary reasons for the corrosion of the bearing assembly are the leaking of chloride laden water from the deicing salts through the deck joints (Silano and Brinckerhoff 1993) and the traffic spray scenarios which may further expose these components to airborne chlorides resulting from the passage of vehicles beneath the bridge through chloride laden water (Enright and Frangopol 1998). Recent in-field examples of severe anchor bolt corrosion exist in the literature for typical highway bridges in the state of Georgia, US as shown in Figure 3-3 (Lindquist 2008). In

regions where use of deicing salts on bridge decks is more prevalent, the severity of anchor bolt corrosion may be even more critical. Corrosion of anchor bolts adversely affects bearing performance by reducing the ultimate lateral strength as detailed in the following paragraphs.

(a) (b)

Figure 3-3: a) Steel expansion bearings surrounded by debris due to accumulation of rust products following the corrosion of base plate, anchor bolt, and botoom of rockers, and b) complete section loss of anchor bolt due to corrosion deterioration. [Both figures adopted from Lindquist (2008)].

Figure 3-4(a) shows the arrangement and distribution of forces for a typical fixed bearing along the longitudinal direction. This free body diagram is used to derive the ultimate lateral strength for the fixed bearing in the longitudinal direction, which changes over time due to corrosion. From the equilibrium of horizontal forces, the ultimate lateral strength of the bearing can be obtained as:

$$F_{ult} = \alpha S + \mu V \tag{3.19}$$

and from the equilibrium of vertical forces we have:

$$V = N + \alpha B \tag{3.20}$$

Also, from the equilibrium of moments about the center of the concrete pedestal yields:

$$F_{ult} h = V\left(\frac{w_l - a}{2}\right) \tag{3.21}$$

where, α is the number of anchor bolts, S is the shear force on one anchor bolt, μ is coefficient of friction between masonry plate and bedding material, V is the compression force on the concrete pedestal due to rocking, N is the axial load on the bearing, B is the bond strength of the swedged anchor bolt in the concrete pedestal, h is the height of the bearing from the concrete pedestal to the sole plate rocker interface, w_l is the width of masonry plate in the longitudinal direction and a is depth of pedestal concrete stress block expressed as $a = \frac{V}{0.85 f_c w_t}$, where w_t is the width of masonry plate in the transverse direction and f_c is the concrete compressive strength. From the above equations, the ultimate lateral strength, F_{ult}, of the bearing maybe expressed as:

$$\frac{F_{ult}}{N} = \frac{0.5w_l}{h}\left[\left(1+\frac{\alpha B}{N}\right) - \frac{N}{0.85f_c w_l w_t}\left(1+\frac{\alpha B}{N}\right)^2\right] \tag{3.22}$$

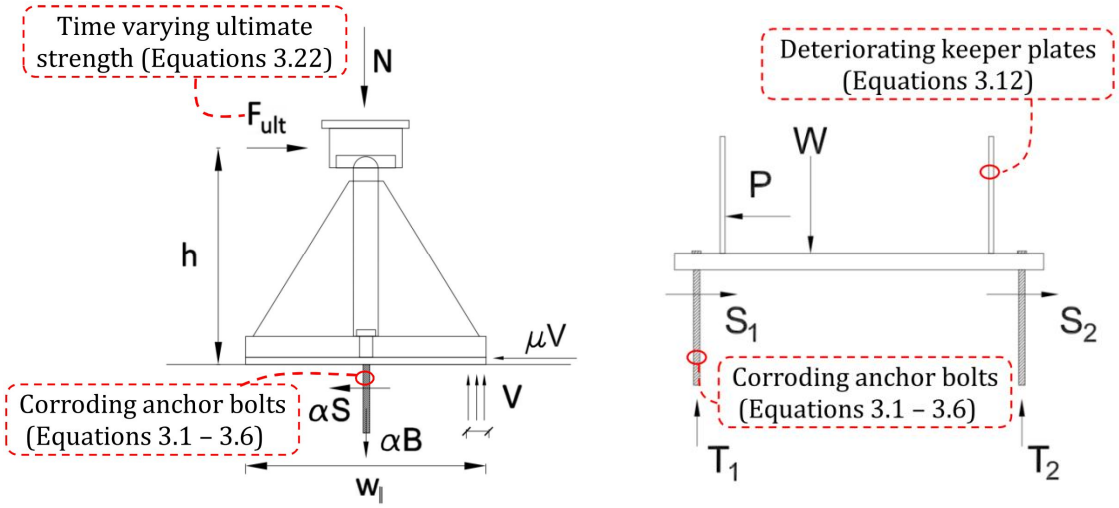

(a) (b)

Figure 3-4: a) Force distribution mechanism in fixed bearings on concrete pedestals along longitudinal direction, and b) force distribution mechanism through the anchor bolt when the keeper plate strikes the rocker (Ghosh and Padgett 2010).

While a similar relationship for estimating the ultimate strength of fixed bearing along the transverse direction can be found in available literature (Mander et al. 1996), it should be noted that the calculated strengths along both directions correspond to that of the pristine bearings. Along the service life of the bridge due to corrosion, the cross-sectional area of the bolt reduces and consequently leads to reduced ultimate lateral strengths for the deteriorated bearings. Depending on the environmental exposure condition, the cross sectional area loss of steel can be computed using Equations (3.1)–(3.7) and the deterioration parameter

distributions enlisted in Table 3.3 and Table 3.4. This reduction in cross sectional area impacts the bond strength, B, of the embedded bolt as indicated in Equation (3.21). Uncertainty in the corrosion deterioration parameters (depending on the exposure condition) enlisted in Table 3.3 – 3.6 via reduction in bond strength are then propagated through the assessment of ultimate lateral strength of the fixed bearing along the longitudinal and transverse directions. Consequently, the time-evolving probability distribution for ultimate lateral strength is accounted for in the finite element modeling for longitudinal and transverse fixed bearing response.

For the case of steel expansion (rocker) bearings, the motion in the longitudinal direction is primarily rocking, where the ultimate lateral strength is dependent on the coefficient of rocking friction of the bearing. As per suggestions by Mander et al. (1996), the coefficient of rocking friction varies from 0.04 for clean well-worn rocker bearings and 0.12 for badly corroded bearings to take into account the "locking" effect as mentioned earlier. In the absence of any further data to support time-dependent modeling of friction increase from corrosion product buildup, a linearly varying coefficient of friction is assumed for this study starting with 0.04 for the pristine bridge and 0.12 for a bridge near the end of its service life (assumed to be 100 years in this study).

The transverse motion of the steel expansion bearing initially consists of a sliding frictional component. Once the horizontal frictional force exceeds the frictional resistance of the sole plate-rocker interface, the sole plate slides on the rocker until the rocker bearing strikes the keeper plate provided to prevent excess transverse motion. With additional horizontal loading, the keeper plate bends significantly and fails by tearing of the fillet weld securing the plate (Mander et al. 1996). The free-body diagram in Figure 3-4(b) shows the distribution of forces for this phenomenon.

As it can be seen, the force P with which the rocker strikes the keeper plate gets transmitted in the form of shear forces S_1 and S_2 through the anchor bolts. For intact bearings with no deterioration, the shear strength of anchor bolt (with a typical diameter of 25.4mm) is found to be sufficient to transmit the forces, with the failure of the bearing governed solely by the tearing failure of the keeper plate. However, with corrosion deterioration, there is significant decrease in the shear strength of the anchor bolts, such that they are no longer capable to transmit the forces when the rocker strikes the keeper plate. This refers to the phase where the failure of the bearing assembly is determined by the shear failure of the anchor bolts rather than the failure of the keeper plate. In addition to the corrosion of the

concrete embedded anchor bolts, the transverse failure mechanism and ultimate strength of the expansion bearings as previously described are also a function of the chloride exposed steel keeper plates. The corrosion degradation of these keeper plates leading to reduced plate thickness are modeled using Equation (3.12) depending on the environmental exposure condition.

3.3.3. Modeling of elastomeric fixed and expansion bearings

While high-type steel fixed and expansion bearings are common in steel bridges, concrete girder and slab type bridges often employ elastomeric pad bearings. These bearing assemblies consist of two components: an elastomeric rubber pad and steel dowels for restraint as shown in Figure 3-5. Each individual component of this type of bearing assembly plays a unique role in the transfer of forces from the superstructure to the columns. For instance, the elastomeric pad transfers lateral forces by developing frictional forces, while the steel dowels offer resistance through a beam type action (Taylor 1969). The elastomeric bearing assembly can be of fixed or expansion type depending on the size of the slot in the bearing pad Figure 3-5. Corresponding to pristine bridge bearings, Choi (2002) and Nielson (2005) developed individual analytical models to capture the elastomer stiffness, sliding of

bearing, and stiffness and yield of steel dowels, eventually combining them in parallel to achieve the composite action.

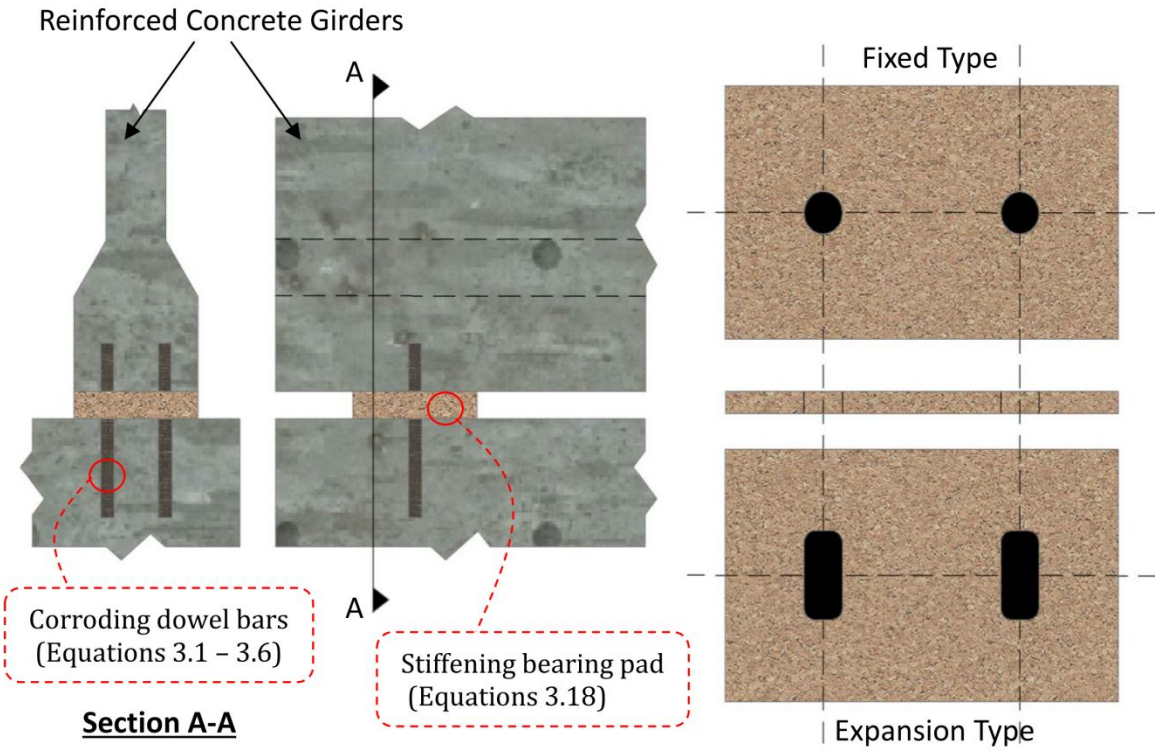

Figure 3-5: Elevation and section view of elastomeric pad bearings used for concrete bridge girders and b) fixed and expansion bearings types depending on dimensions of the slot (Ghosh and Padgett 2012).

As elaborated earlier, the rubber pads of this bearing type are affected via thermal oxidation leading to an increase in shear stiffness, while corrosion deterioration of dowel bars leads to a cross-sectional area loss of steel. Such time-dependent deterioration effects are incorporated in the analytical models of these bearings through: a) Increase in shear modulus in the analytical model of the elastomeric pad, and b) reduction in the yield strength and ultimate lateral

strength of the dowel bars calculated as a function of the dowel area as (Hwang et al. 2001; Ghosh and Padgett 2012):

$$V_{by}(t) = \frac{f_y A_d(t)}{\sqrt{3}} \tag{3.23}$$

$$V_{bu}(t) = \frac{f_u A_d(t)}{\sqrt{3}} \tag{3.24}$$

where, $V_{by}(t)$ and $V_{bs}(t)$ are the time-dependent yield shear strength and ultimate shear strength respectively, f_y and f_u are the tensile strength and ultimate shear strength of the dowel bars respectively and $A_d(t)$ is the time-dependent cross sectional area of the dowel bars.

3.3.4. Modeling of bridge bents and reinforced concrete columns

The concrete bent beams and circular reinforced concrete bridge columns in the finite element bridge models are represented by fiber-sections and modeled using nonlinear beam-column elements. Such discretized fiber sections used in the modeling of these components allows the user to specify unique constitutive models for the confined core concrete, unconfined cover concrete and the steel reinforcement. Figure 3-6 depicts the typical fiber section modeling of reinforced concrete columns and demonstrates the reduction of longitudinal and transverse

column reinforcement cross sectional area due to corrosion deterioration from chloride attacks. Depending on the exposure condition, deicing salt or marine, the cross sectional area loss of steel is modeled using Equations (3.1) - (3.7) using the deterioration parameters enlisted in Table 3.3 and Table 3.4. While the deteriorating longitudinal rebars are explicitly considered in the finite element bridge modeling of aging bridge columns, the area loss of transverse reinforcement is reflected via a reduction in confined concrete strength. The time-dependent confined concrete strength is calculated as:

$$f_{cc}(t) = K(t) f_c \tag{3.25}$$

where, f_c is the unconfined concrete compressive strength and $K(t)$ is the time-dependent confinement factor calculated as (Park et al. 1982):

$$K(t) = 1 + \frac{\rho_s(t) f_{yh}}{f_c} \tag{3.26}$$

where $\rho_s(t)$ is the ratio of volume of corroding steel hoops and f_{yh} is their yield strength. For pristine non-deteriorated CSUS columns the steel hoops are characterized by 12.7mm diameter rebars spaced at 307mm from center to center and made of grade 60 steel. Consequently for typical 906mm diameter CSUS bridge

columns, $\rho_s(t = 0 \text{ year})$ equals 2.04e – 3, which results in a $K(t = 0)$ as 1.031. The confinement factor at any other point in time in the life of the bridge depends on the exposure condition and can be computed using the deterioration equations presented in Section 3.2.1.

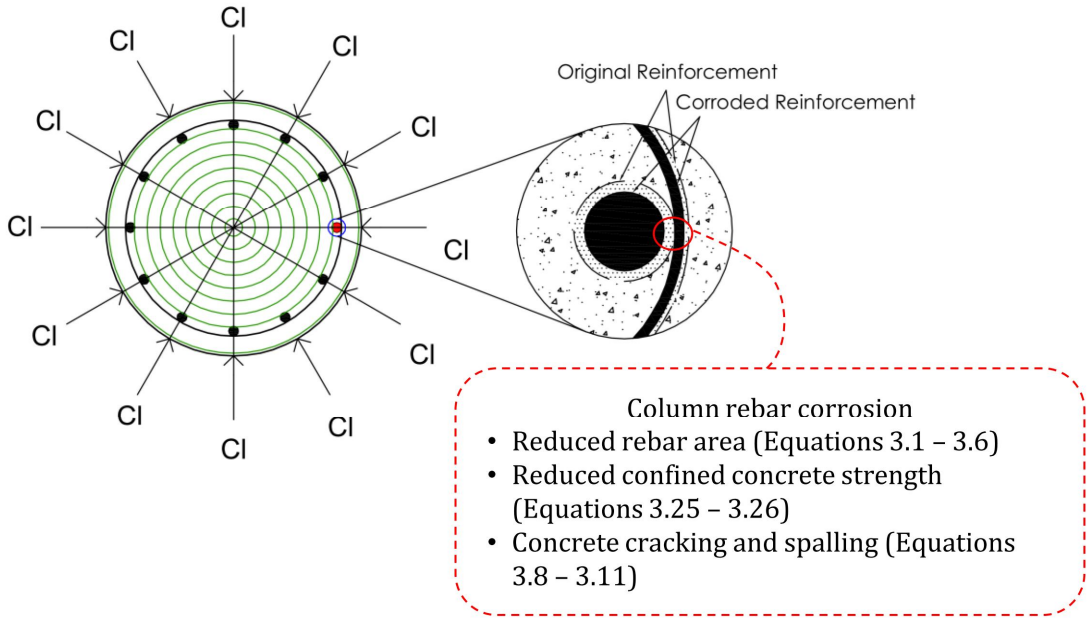

Figure 3-6: Fiber section modeling and corrosion deterioration of longitudinal and transverse resinforcement due to chloride attacks

3.3.5. Modeling of highway abutments and foundations

The most common type of bridge abutment used in CSUS bridge types is the pile bent type (Hwang et al. 2000) abutment and is consequently adopted in this study. This study does not consider aging and deterioration of highway bridge abutments and foundation, though past studies have reported cases of foundation settlement

over time (USDOT 1982). The abutments in this study are modeled in the longitudinal and transverse directions using the recommendations by Nielson (2005) based on the findings of several past studies such as CALTRANS (1999), Maroney et al. (1994), and Martin and Yan (1995). In the longitudinal direction, while the active abutment action is influenced only by the pile stiffness, the passive action is dictated by the contribution of the piles and passive pressure of the soil against the abutment backwall. In the transverse direction, the primary resistance is provided by the piles. For a majority of highway bridges within the CSUS, deep foundations employing a pile system are used (Hwang et al. 2000) and hence adopted in this study. These pile foundation systems are modeled using linear translational and rotational springs after aggregating the horizontal and rotational pile stiffnesses beneath the foundations. However, in regions characterized by potential liquefaction effects following earthquake events, explicit modeling of pile foundations is recommended (Aygün et al. 2011).

3.4. Closure

This chapter focused on the identification and modeling of different aging and deterioration mechanisms suffered by common highway bridge classes in the

Central and Southeastern United States. In this regard, available models from the literature are reviewed and adopted to model corrosion deterioration of critical bridge components, such as reinforced concrete columns, bearing anchor bolts and dowel bars, and steel keeper plates. Additionally, based on laboratory tests by past researchers, analytical models to characterize the increase in shear modulus of elastomeric bearing pads due to aging are developed. The probabilistic deterioration parameters affecting the extent of deterioration depending on the environmental exposure condition are also identified. Lastly, details on finite element modeling of deteriorating structural bridge components are provided while offering general discussions of pristine bridge component models. Additionally, finite element model validation using available experimental test results in literature of several bridge components are included in the Appendix A. The scope of aging and deterioration modeling considered in this study are also included.

Chapter 4

TIME-DEPENDENT SEISMIC FRAGILITY CURVES FOR AGING BRIDGES

This chapter evaluates the impact of aging and deterioration mechanisms on the seismic performance of aging bridge components and develops time-dependent highway bridge fragility curves at component and system level. Such fragility curves quantify the increase in probability of damage state exceedance as the bridge continues to degrade along its service life. A general time-dependent fragility methodology will be presented first followed by representative case study examples of aging multi-span continuous steel girder and multi-span simply supported concrete girder bridges under different exposure conditions. While the first example focuses on deterministic bridge geometry, the latter will consider variability in geometric characteristics. Uncertainties in ground motion characteristics, bridge modeling parameters and deterioration parameters will be considered in both cases.

4.1. Time-dependent Fragility Assessment

4.1.1. General formulation

Time-evolving fragility curves are conditional probabilistic statements representing the probability of meeting or exceeding a particular given the ground motion intensity at different points in time along the service life of the bridge. Such time-dependent vulnerability functions provide insight on the impact of aging mechanisms on bridge seismic vulnerability at both the component and system levels. The generic expression of these fragility functions follows the form:

$$P_f(t) = P[Demand(t) > Capacity(t) \mid IM] \tag{4.1}$$

where $P_f(t)$ is the probability of damage state exceedance for a particular bridge component or system at time t, $Demand(t)$ and $Capacity(t)$ are the seismic demand and capacity of the bridge component or system at the same time instant, and IM is the intensity of ground motion. This study will develop time-evolving fragility curves for critical bridge components (Table 4.1) and overall bridge system after accounting for uncertainties in deterioration parameters, bridge modeling parameters and ground motion characteristics. The components considered for fragility analysis are regarded to be most important in affecting the bridge

response, as indicated in previous studies by Nielson (2005). The following section will elaborate on the development of seismic demand and capacity models for bridge components for deriving fragility estimates.

Table 4.1: Critical bridge components and component response parameters used in this study to develop time-dependent fragility curves. Also shown are the abbreviations for different component responses that will be used throughout this study

Component	Response Parameter	Abbreviation
Column Response	Curvature Ductility	COL
Fixed Bearing Longitudinal Response	Deformation	FBL
Fixed Bearing Transverse Response	Deformation	FBT
Expansion Bearing Longitudinal Response	Deformation	EBL
Expansion Bearing Transverse Response	Deformation	EBT
Abutment Active Response	Deformation	ABA
Abutment Passive Response	Deformation	ABP
Abutment Transverse Response	Deformation	ABT

4.1.2. Time-dependent probabilistic seismic demand models

Probabilistic seismic demand models assist in the evaluation of peak structural demands on aging bridge components as a function of the intensity of ground motion. These models for different bridge components are constructed in this study using a simulation-based analytical approach rooted in nonlinear time history analysis to capture the effect of aging and deterioration. The proposed approach is similar to those presented in Nielson and DesRoches (2007b) and Padgett and

DesRoches (2008), but extended in this work to derive time-dependent seismic demand models as outlined in the following paragraphs.

Table 4.2: Probability distributions of highway bridge material and modeling parameters considered for fragility analysis in addition to the deterioration parameters outlined earlier in Chapter 3. The distribution parameters (a) and (b) correspond to the mean and coefficient and variation for Normal and Lognormal distributions and the upper and lower bounds for the Uniform distributions respectively.

Bridge Parameter	Units	Probability Distribution	Distribution Parameters	
			(a)	(b)
Steel strength	MPa	Lognormal	6.13	0.08
Concrete strength	MPa	Normal	33.8	0.13
Steel bearing stiffness[1]	-	Uniform	0.5	0.15
Steel fixed bearing COF[2] – longitudinal	-	Lognormal	0.24	0.50
Steel fixed bearing COF[2] – transverse	-	Lognormal	0.42	0.50
Steel expansion bearing COF[2] – longitudinal	-	Lognormal	0.05	0.50
Steel fixed bearing COF[2] – transverse	-	Lognormal	0.11	0.50
Abutment passive stiffness	kN/mm/m	Uniform	11.5	28.8
Abutment active stiffness	kN/mm/pile	Uniform	3.5	10.5
Mass[1]	-	Uniform	0.9	1.1
Damping ratio	-	Normal	0.045	0.27
Loading direction	Radians	Uniform	0	2π

[1]Multiplication factor applied to deterministically calculated values
[2]COF = coefficient of friction

To propagate the uncertainty associated with ground motion characteristics while developing seismic demand models, a total of 96 two component ground

motions from the Wen and Wu (2001) and Rix and Fernandez (2004) synthetic ground motion suites are used in the analysis. These ground motions are representative of a range of potential ground motions for the Central and Southeastern US region. An equal number of 96 three-dimensional bridge samples are generated through Latin Hypercube sampling, considering the potential uncertainty in structural, material, and corrosion related parameters at each point in time along the service life of the bridge. In addition to the corrosion related parameters presented earlier in Chapter 3, the probabilistic models for the random variables considered for the bridge structure include those previously identified for multi-span continuous steel bridges in the CSUS (Nielson and DesRoches 2007a) and reproduced in Table 4.2.

To develop time-dependent probabilistic seismic demand models, the 96 bridge samples generated at different points in time (e.g. 0, 25, 50, 75 years) are each subjected a seismic ground motion from the chosen earthquake record suite in a nonlinear time history analysis. Consequently, linear regression analysis is employed to develop probabilistic seismic demand models at different points in time, which reflect the relationship between median peak demands of deteriorated bridge components and ground motion intensity at that time instant. For

instance, corresponding to a particular deteriorating bridge component *m,* the probabilistic seismic demand model follows the form (Cornell et al. 2002; Nielson and DesRoches 2007b):

$$\ln\left[Demand_m\left(t\right)_{median}\right] = \ln\left[a_m(t)\right] + b_m(t)\ln\left(IM\right) \tag{4.2}$$

where, $Demand_m(t)_{median}$ is the time-evolving median value of the seismic demand for bridge component m, $a_m(t)$ and $b_m(t)$ are the component specific linear regression parameters, and IM is the intensity of ground motion. The component specific seismic demands can be probabilistically modeled with a lognormal distribution (Shinozuka et al. 2000; Mackie and Stojadinović 2005) and hence in the transformed space, the residual is modeled by a normal distribution with mean zero and standard deviation, σ. This allows estimation of the dispersion or lognormal standard deviation $\beta_{D,m}$ of the seismic demand. It is also noted that while individual component seismic demand models are sufficient for component level time-dependent fragility development, the correlation between the peak demands of different bridge components is also evaluated at this stage for eventual use in the bridge system level fragility analysis.

4.1.3. Component capacity limit states

In addition to the probabilistic model of seismic demand, the fragility analysis requires estimates of the structural capacities of the different bridge components. The limit state capacities used in this study are the lognormal capacity estimates presented by Nielson and DesRoches (2007a) for typical highway bridges in the CSUS. Although the adopted limits state capacities are not assumed to change directly throughout the life of the bridge, the effects of aging and deterioration are implicitly incorporated through either normalization (for instance, normalization of maximum column curvature with yield curvatures), or through the bridge modeling which renders achieving of the displacements easier due to changes in stiffness or yield strength. For instance, for components such as deteriorated bridge columns, the effects of corrosion on column capacity are incorporated while calculating the time-dependent curvature ductility demand ratio as a measure of seismic demand (Equation (4.3)).

$$\mu_{\varphi}(t) = \frac{\kappa_{max}(t)}{\kappa_{yield}(t)} \tag{4.3}$$

In the above equation, $\mu_{\phi}(t)$ is the column curvature ductility demand ratio at time t along the service life of the bridge, $\kappa_{max}(t)$ is the maximum observed

bridge column curvature under seismic shaking, and $\kappa_{yield}(t)$ is the column yield curvature.

The limit states for the bearing deformations were obtained by Nielson and DesRoches (2007a) following Bayesian updating of experimentally observed capacity estimates with results from a functionality based survey conducted by Padgett and DesRoches (2007). Since these limit states are based on offsets at joints, or relative displacements between the bridge superstructure and substructure, they are not affected by the level of corrosion deterioration. However they may be rendered easier to achieve in the models through the loss of doweling.

Table 4.3: Median (S_c) and dispersion (β_c) values of lognormally distributed capacity limit states for different bridge components [Adapted from Nielson and DesRoches (2007a)]

Component	Slight		Moderate		Extensive		Complete	
	S_C	β_C	S_C	β_C	S_C	β_C	S_C	β_C
Columns	1.29	0.59	2.10	0.51	3.52	0.64	5.24	0.65
Fixed bearings - longitudinal	6.0	0.25	20.0	0.25	40.0	0.47	187	0.65
Fixed bearings - transverse	6.0	0.25	20.0	0.25	40.0	0.47	186.6	0.65
Expansion bearings - longitudinal	37.4	0.60	104.2	0.55	136.1	0.59	186.6	0.65
Expansion bearings - transverse	6.0	0.25	20.0	0.25	40.0	0.47	187	0.65
Abutment - Passive	37.0	0.46	146.0	0.46	N/A	N/A	N/A	N/A
Abutment - Active	9.8	0.70	37.9	0.90	77.2	0.85	N/A	N/A
Abutment - Transverse	9.8	0.70	37.9	0.90	77.2	0.85	N/A	N/A

In general, the time-dependent effects of deterioration are incorporated in the analytical models of the bearings through a reduction in ultimate lateral strength of the bearing due to corrosion of dowel bars and also through increasing shear stiffness of bearing pads due to thermal oxidation. Future experimental studies on capacity estimates for deteriorating structures can further lead to improved fragility estimates for aging bridge components and bridge systems. The lognormally distributed component limit state capacities for each damage state (slight, moderate, extensive, and complete) are presented in Table 4.3.

4.1.4. Time-dependent bridge component and system level fragility curves

Since the probabilistic seismic demands and capacity limit states for different bridge components are lognormally distributed, time-dependent component level fragilities can be obtained by:

$$P_{f,m}(t) = \Phi\left\{\frac{\ln\left(IM\right) - \ln\left[med_m\left(t\right)\right]}{disp_m\left(t\right)}\right\} \tag{4.4}$$

where, $med_m\left(t\right)$ and $disp_m\left(t\right)$ are respectively the time-dependent median and dispersion parameters of the lognormal distribution representing the fragility

$P_{f,m}(t)$ of the m^{th} bridge component. In terms of the regression coefficients and statistical moments of the capacity estimates, the median value and dispersion can be estimated as:

$$med_m\left(t\right) = \exp\left\{\frac{\ln\left(S_{C,m}\right) - \ln\left[a_m\left(t\right)\right]}{b_m\left(t\right)}\right\} \tag{4.5}$$

$$disp_m\left(t\right) = \frac{\sqrt{\beta_{D,m}^2(t) + \beta_{C,m}^2}}{b_m(t)} \tag{4.6}$$

where, $S_{C,m}$ and $\beta_{C,m}$ are the median and dispersion of the lognormally distributed capacity of component m and $\beta_{D,m}(t)$ is the dispersion of the component specific lognormally distributed seismic demand.

Assessment of the bridge system reliability is conducted by assuming the bridge as a series system, wherein failure of a single component is representative of bridge failure. Such system level abstraction is similar to the system representation adopted in structural reliability studies for bridges [e.g. Nielson and DesRoches (2007b), Nowak and Cho (2007)], or other structural systems [Der Kiureghian and Dakessian (1998), Cimellaro et al. (2010)]. This system definition is consistent with the capacity estimates adopted in this study, which offer the limit

of component response upon which system level functionality inhibition is anticipated (bridge tagged for closure or reduced traffic), and implies that failure of any one of the components is indicative of overall bridge system failure. It is however acknowledged that recent work by Dueñas-Osorio and Padgett (2011) proposed a closed-form combinatorial approach to compute bridge system failure probabilities from component damages and offers flexibility to match capacity and demand across different limit states for added realism in system-level performance assessment from component states..

Under the presently adopted series system assumption, the probability of the bridge system is at or beyond a particular failure limit state is the union of the events that each component is in the same limit state. This can be mathematically shown as:

$$P[Failure_{system}] = P\left[\bigcup_{m=1}^{M} m^{th}\ \ Component\ \ Failure\right] \tag{4.7}$$

where, $P\left[Failure_{system}\right]$ is the probability of failure of the bridge system, and M is the total number of vulnerable bridge components. Estimates of correlation coefficients between peak component responses enables construction of a joint probability density function for component demand. The bridge system fragility is

then evaluated by comparing the joint probability density function of demand with the component capacities for each damage state via 50,000 Monte Carlo analyses to derive lognormally distributed system fragility estimates that account for component correlations at different points in time along the service life of the bridge. The overall corroded bridge system fragility can thus be mathematically represented as:

$$P_{f,system}\left(t\right) = \Phi\left\{\frac{\ln\left(IM\right) - \ln\left[med_{sys}\left(t\right)\right]}{disp_{sys}\left(t\right)}\right\} \tag{4.8}$$

where, $med_{sys}(t)$ and $disp_{sys}\left(t\right)$ are the estimated lognormal parameters of bridge system fragility.

4.2. Case Study Aging Bridge Structures: Seismic Performance and Time-dependent Fragility Curves

The purpose of this section is to assess the impact of aging and deterioration on the seismic response of aging highway bridge components followed by the development of time-evolving bridge fragility curves at the bridge component and system level. Such time-dependent seismic fragility curves will quantify the impact

of different deterioration mechanisms on bridge vulnerability to earthquake damage along the service life of the bridge. In this regard two case study highway bridge types, primarily distinguished by superstructure material type will be considered: a) Multi-span continuous (MSC) steel girder bridge exposed to chlorides stemming from deicing salt exposure (Ghosh and Padgett 2010), and b) Multi-span simply supported (MSSS) concrete girder bridge under exposure of deicing salt and also chlorides stemming from marine splash and atmospheric zones (Ghosh and Padgett 2012). For the first case study, a deterministic MSC steel girder bridge geometry will be used to investigate the impact of aging mechanisms on the seismic response of bridge components prior to fragility analysis. The MSSS concrete girder bridge example will consider uncertainty in bridge geometry and investigate the impact of deterioration mechanisms on probabilistic seismic demand models of a portfolio of bridge structures. Time-dependent fragility curves using the methodology outlined in Section 4.1 will be developed at the component and system level for both case study examples.

4.2.1. Case study aging multi-span continuous (MSC) steel girder bridge

The MSC steel girder bridge is adopted for the case study because of the prevalence of this bridge class in regions of potential seismic hazard (i.e.

attributing 13.2% of Central and Southeastern US bridges in seismic zones according to Nielson, 2005); typical design details including multiple components that are susceptible to corrosion; and concern regarding initial bridge vulnerability even prior to considering aging. Past comparative studies on classes of bridges which are particularly common in the CSUS indicate that multi-span continuous steel girder bridges are among the most vulnerable bridges to seismic damage (Nielson and DesRoches 2007b). This can be attributed to the inadequate seismic detailing of the columns having approximately 1% longitudinal reinforcement ratio along with widely placed transverse ties (307mm center to center), use of vulnerable high type steel fixed and rocker bearings, short seat widths and inadequately reinforced pile caps. Consequently, large inertial deck loads result in considerably high demands on the under-reinforced columns, expansion bearings and abutments during seismic events.

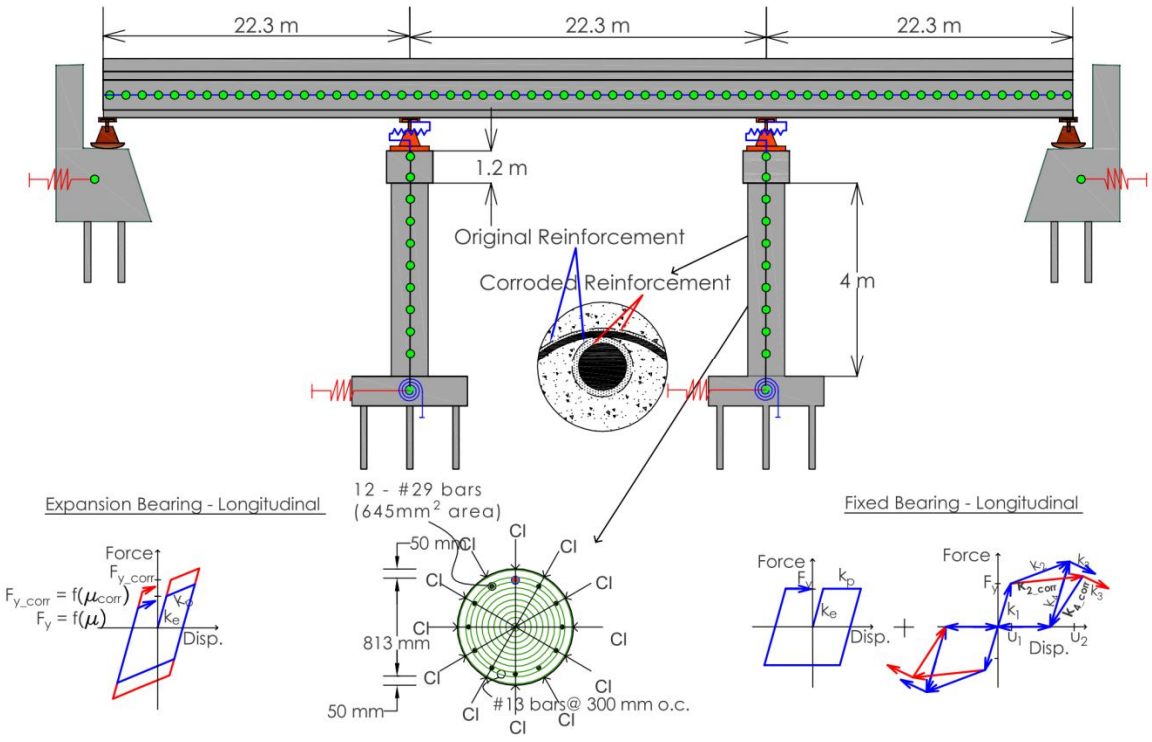

Figure 4-1: Elevation view of the 3-D nonlinear analytical finite element model of the multi-span continuous steel girder bridge. Modeling of components vulnerable to corrosion degradation in the longitudinal direction is emphasized (Ghosh and Padgett 2010)

The typical MSC steel bridge configuration used in this study is that identified by Nielson (2005) as shown in Figure 4-1, illustrating the continuity of the steel girders over the interior bents. Both the end spans and the middle span of this three span bridge are 22.30m long and 10.30m wide consisting of five steel girders. Each bent consists of three circular columns having 645mm^2 nominal cross-sectional area, reinforced with twelve #29 longitudinal bars (Metric size), and #13 (Metric size) transverse stirrups spaced at 307mm. The bridge uses high type steel

fixed bearings beneath each girder over the bent beam and high type steel expansion (rocker) bearings at the abutments. These bearings are placed on masonry plates and attached to the bridge pier and abutments using anchor bolts. Besides being highly prone to corrosion deterioration as described in Section 3.3.2, the non-ductile nature of these bearings makes them highly susceptible to seismic damage (Mander et al. 1996).

4.2.1.1. Degradation of structural components along service life

The exposure condition for the case study MSC Steel bridge constitutes chlorides stemming from deicing salt application, which has been identified by researchers as one of the most severe forms of corrosion which causes significantly higher degradation than chlorides in a marine environment (Stewart and Rosowsky 1998). As described earlier in Section 3.2.1, corrosion deterioration of reinforced concrete members consists of two distinct phases: corrosion initiation, followed by corrosion propagation. The probabilistic models for the lognormally distributed parameters for this specific case study are adopted from reported values in Table 3.3 and Table 3.5, reproduced here for convenience (Table 4.4).

Table 4.4: Descriptors of lognormal random variables affecting the corrosion deterioration of RC columns under deicing salt exposure

Descriptor	Unit	Mean	COV
Cover Depth (x)	cm	3.81	0.20
Diffusion Coefficient (D_c)	cm^2/year	1.29	0.10
Surface Chloride Concentration (C_0)	wt % concrete+	0.10	0.10
Critical Chloride Concentration (C_{cr})	wt % concrete+	0.040	0.10
Rate of Corrosion (r_{corr})	mm/year	0.127	0.30

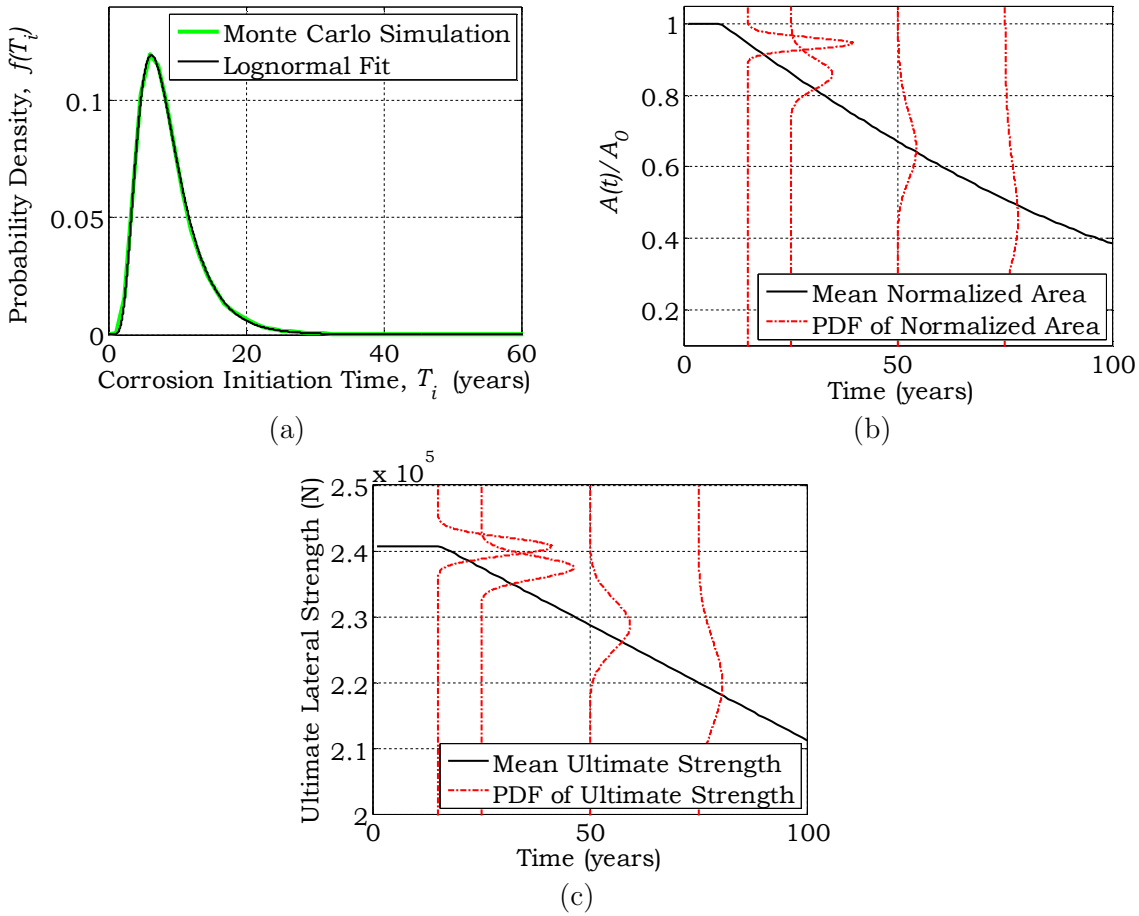

Figure 4-2: a) Lognormal fit to the corrosion initiation time (T_i) data generated using 50,000 Monte Carlo Samples, b) distribution of normalized time variant area steel rebars in RC columns along the service life of the bridge structures, and c) time-dependent reduction in ultimate lateral strength of fixed bearings in the longitudinal direction due to area loss of steel in the anchor bolts (Ghosh and Padgett 2010)

The distribution for the corrosion initiation time (Equation (3.1)) is assessed through Monte Carlo simulation having a sample size of 50,000. Using Lilliefors test, a lognormal distribution with mean 8.85 years and standard deviation of 4.5 years is found to be a good fit to the simulated data for corrosion initiation time [Figure 4-2(a)]. Once the protective passive film around the reinforcement dissolves due to continued chloride ingress, corrosion initiates and leads to gradual loss of reinforcement cross-sectional area. On the basis of the estimated distribution for corrosion initiation time presented above and anticipated corrosion rate, the area of reinforcing steel in RC columns is probabilistically assessed as a function of time (Equation (3.6)). Figure 4-2(b) shows the resulting time-dependent area reduction ratio, which is the area of reinforcing steel at time t, $A\left(t\right)$, normalized by the initial area of reinforcement, A_0 (Ghosh and Padgett 2010). This figure illustrates the reduction in steel cross sectional area over time and the increase in variability or uncertainty about that estimate of reinforcement area due to the combined effect of the variability of initial reinforcement diameter, rate of corrosion, and corrosion initiation time. Also shown in Figure 4-2(c) is the time-dependent loss of fixed bearing ultimate strength in the longitudinal direction as a result of anchor bolt corrosion, as calculated using Equation (3.22) (Ghosh and Padgett 2010). Note

that reduction in steel area or strength reduction of bridge bearings do not occur until the corrosion initiation time.

4.2.1.2. Deterministic seismic response of aging bridge components

Before conducting a full probabilistic analysis of the impact of corrosion on the fragility of this case study bridge, sample deterministic simulations are presented to illustrate the influence of time-dependent aging on the seismic response of the multi-span continuous bridge. The dynamic response is illustrated through nonlinear time history analysis of the bridge with median values for all variable parameters using a ground motion record from the synthetic suite of ground motions developed by Rix and Fernandez (2004) for Central and Southeastern US regions. This motion, shown in Figure 4-3 has peak ground acceleration (PGA) of 0.45g and duration of 29 seconds. In addition to the dynamic response of the structure in both the longitudinal and transverse directions, the influence of corrosion on the load resisting capacity is also presented. For brevity, comparisons are made between the pristine bridge at time zero and the bridge at 50 years into its service life. The following sections will illustrate the seismic response analysis for the following scenarios: a) seismic response of bridge columns while considering deterioration of the columns only, b) seismic response of bridge bearings while

considering deterioration of bearings only, and c) seismic response of both columns and bearings under joint considerations of aging mechanisms for both components.

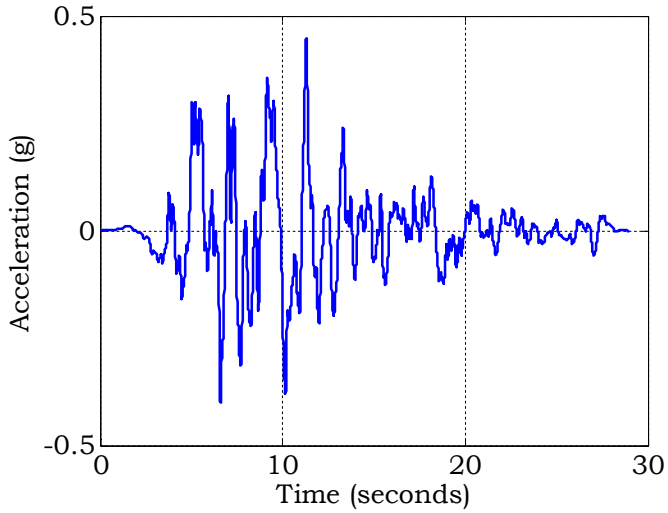

Figure 4-3: Earthquake record from the Rix and Fernandez (2004) ground motion suite used for determinitsic response analysis

4.2.1.2.1. Seismic response of corroding bridge columns

The effect of time-dependent corrosion on the seismic behavior of reinforced concrete column is first assessed. Due to corrosion and subsequent area loss of reinforcing steel, the load carrying capacity and yield curvature of the reinforced concrete columns undergo a significant reduction. This phenomenon is illustrated in Figure 4-4(a), which shows a 16.6% reduction in yield curvature and 21% reduction in the yield moment of a 50 year old corroded column as compared to that of a pristine column. Subsequently, when the bridge is subjected to the

sample ground motion, the demands placed on the corroded reinforced concrete column increase relative to the pristine column. As shown in Figure 4-4(b), while the peak curvature ductility demand of 3.3 for the pristine bridge already indicates significant damage in the form of cracking and spalling, after 50 years of exposure to deicing salts the bridge subjected to the same motion suffers peak curvature ductility demands of 5.4, which signifies a more severe damage in the form of column reinforcement buckling (Hwang et al. 2001; Buckle 2006).

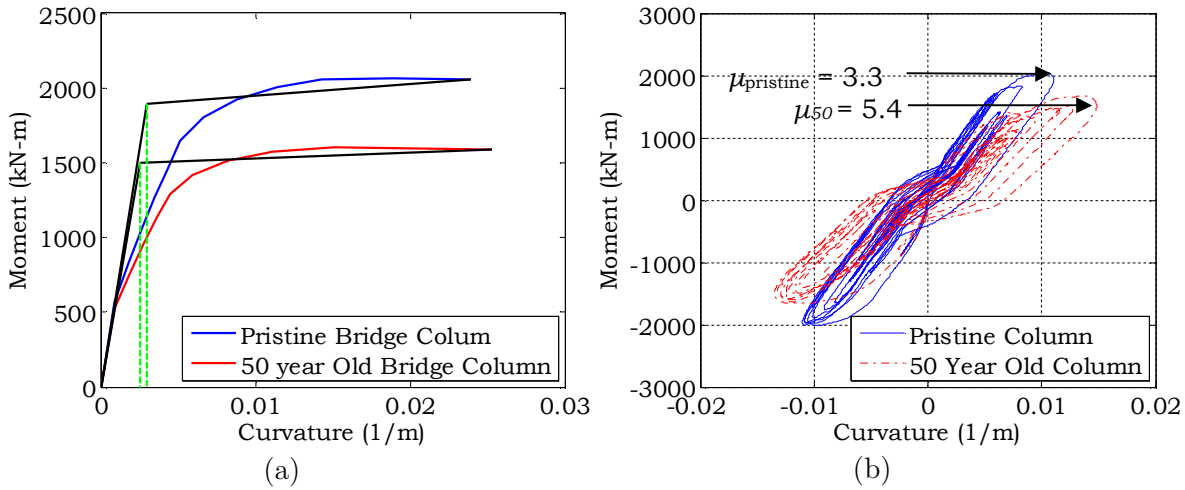

Figure 4-4: a) Reduction in column load resisting capacity and yield curvature, and b) increase in curvature ductility demand of a 50 year old column as opposed to a pristine bridge column for the same ground motion (Ghosh and Padgett 2010)

An increased seismic demand on the corroded RC columns is found to correspond to a negligible increase in demands on certain components like expansion bearings and abutments, which only show approximately a 3% and 1% increase, respectively, in peak displacement in the corroded bridge relative to the

pristine bridge. In some components, however, there is a reduction in the peak seismic demands when column corrosion is modeled. For instance, compared to the pristine bridge, there is an approximately 13% reduction in the peak longitudinal displacement of the fixed bearings in the 50 year old bridge. This reduction in bearing demands is attributed to the concentration of damage in the corroded columns as compared to the pristine bridge.

4.2.1.2.2. Seismic response of degrading steel bridge bearings

Recalling the deterioration models presented in Section 3.3.2, corrosion of the steel bearings results in reduced ultimate strength in the fixed bearing assemblies. While, this is also true for expansion bearings along the transverse direction, the increased coefficient of friction along the longitudinal direction results in increased expansion bearing stiffness. Analogous to the response of columns in the previous section, considering only bearing degradation results in an increase in the peak displacement of the fixed bearing assembly by 16% and 11% in the longitudinal and transverse directions respectively. As expected, the reduced post yield stiffness and ultimate strength due to corrosion shift the hysteretic characteristics of the bearing, and result in larger peak deformations under seismic loading. Figure 4-5(a) shows the comparative longitudinal loading response of the fixed bearings

for the pristine bridge and 50 year old bridge depicting an increase in peak bearing deformations due to corrosion deterioration.

For expansion bearings, the increase in coefficient of friction due to debris accumulation increases the yield force by 19% and reduces deformation of the expansion bearings in the longitudinal direction Figure 4-5(b). Additionally, in the transverse direction, the reduced ultimate strength of the bearing assembly results in an 18% increase in peak deformation for the 50 year old bridge bearing as compared to the pristine bearing (Ghosh and Padgett 2010).

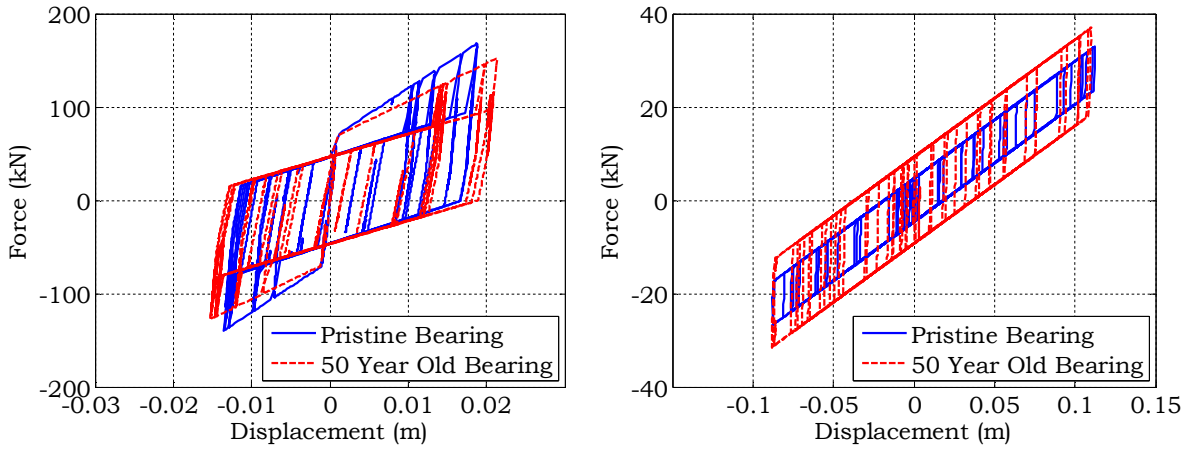

Figure 4-5: a) Decease in peak forces and increase in seismic demand on fixed bearings along longitudinal direction, and b) increase in peak forces due to additional friction and decrease in seismic demand on expansion bearings along longitudinal direction (Ghosh and Padgett 2010)

4.2.1.2.3. Seismic response of bridge components under joint consideration of column and bearing deterioration

To reflect field conditions for corroded bridges throughout their lifetime, the joint occurrence of column and bearing corrosion are evaluated in this section. Consideration of the simultaneous effects of corrosion degradation of reinforcing bars in the reinforced concrete columns and steel bridge bearing assembly reveals several interesting trends in the seismic response of the multi-span continuous steel girder bridge. Figure 4-6(a) illustrates the seismic demands on the RC columns, expansion bearings in the longitudinal direction, and fixed bearings in the transverse direction, due to joint consideration of the corrosion deterioration mechanisms of the columns, fixed and expansion bearing assembly. The 50 year and 100 year corroded bridge response are compared to the pristine, or time zero, bridge response using column moment-curvature and bearing force-displacement plots for the sample ground motion.

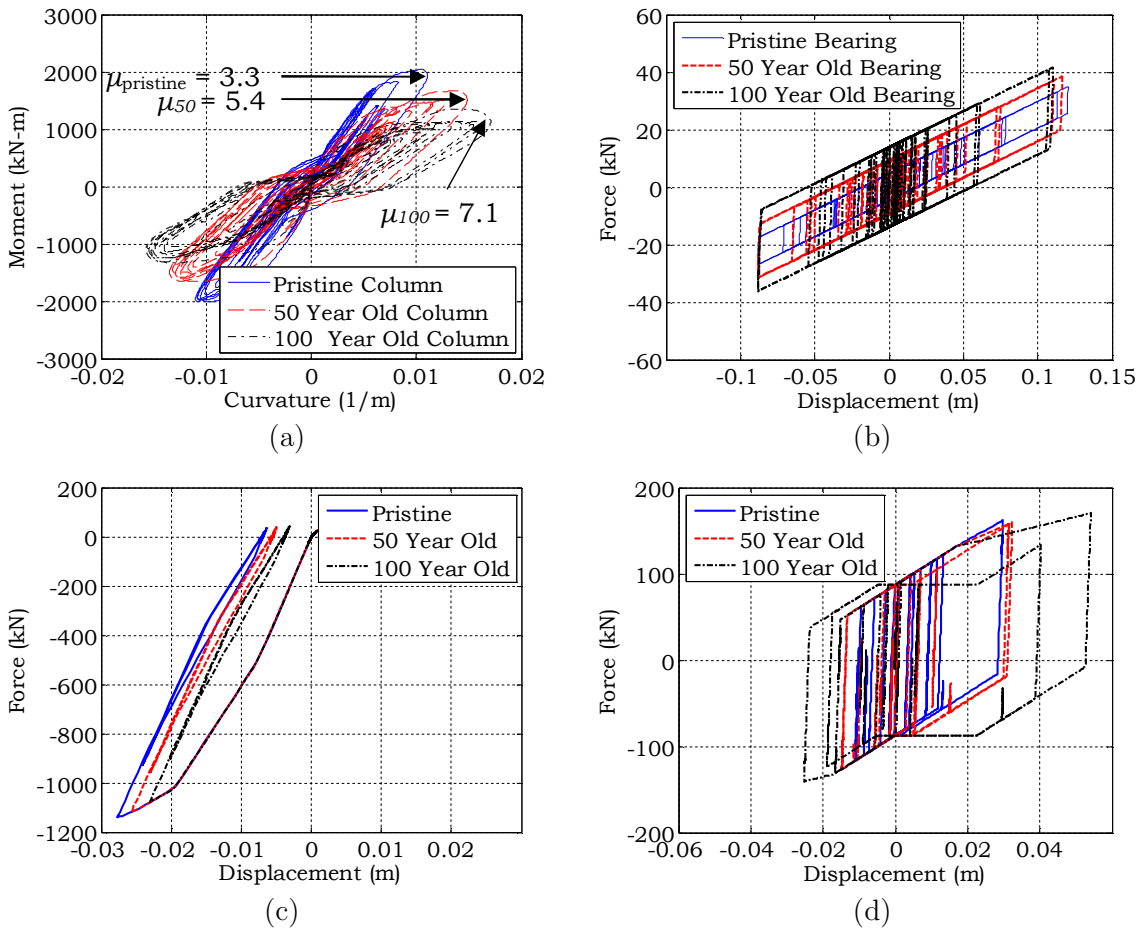

Figure 4-6: a) Increase in curvature ductility demand on corroded RC columns, b) increase in expansion bearing force and decrease in bearing deformation in longitudinal direction, c) decrease in peak abutment abutment response in the passive direction, and d) increase in peak displacement of corroded fixed bearings in transverse direction (Ghosh and Padgett 2010)

The corroded RC columns are found to show a consistent increase in the curvature ductility demand, which increases by 63% and 115% for the 50 and 100 year old column, respectively, relative to the non-deteriorated column. It is interesting to note that as opposed to earlier findings when single component (bearing) deterioration was considered, a joint consideration of column and bearing

corrosion reveals a decrease in peak deformation demand on the fixed bearings in the longitudinal direction. Quantitatively, an 11% and 44% reduction in peak deformations for the 50 and 100 year old steel fixed bearing is observed along the longitudinal direction. This reduction in fixed bearing deformations is primarily attributed to the concentration of damage in the corroded columns and the dynamic response of the bridge deck and columns as a nearly single degree of freedom system, with little deformation occurring over the columns at the location of the fixed bearings. Additionally, there is a reduction in the expansion bearing deformations in the longitudinal direction due to continued increase in coefficient of friction due to debris accumulation along the service life of the bridge [Figure 4-6(b)]. Consequently, reduced displacements in the longitudinal direction results in reduced pounding forces upon the closure of the 71mm gap between the deck and the abutment. The decrease in pounding results in a respective 11% and 27% decrease in the passive deformation of the abutments for the 50 and 100 year old corroded bridge [Figure 4-6(c)]. Both fixed and expansion bearings are found to experience large demands in the transverse direction for both pristine and corroded bridge. Additionally, the increase in seismic demand on the columns in the transverse direction is not as dramatic as that in the longitudinal direction and a

reduced post yield stiffness of the corroded fixed and expansion bearings leads to higher peak bearing displacements as the bridge nears the end of its service life. For example, the fixed bearing deformations increase by approximately 15% and 110% [Figure 4-6(d)], and the expansion bearings deformations increase by 13% and 69% in the transverse direction for the 50 and 100 year old bridge. The impacts of these findings on the seismic fragility of the bridge component and system along its service life are discussed in the subsequent sections, considering uncertainty in the bridge and ground motion realizations.

4.2.1.3. Component and system level time-dependent fragility curves

Bridge component and system time-evolving fragility curves are now evaluated using the methodology outlined in Section 4.1. Such fragility curves quantify the effect of corrosion on the seismic vulnerability at different points in time along the service life of the bridge. It is observed that at the component level, while there is a steady increase in the fragility of certain elements, some other components show a reduced vulnerability with time. This contradicting trend in the component seismic fragilities are consistent with the findings from the deterministic analysis which revealed that increased demands on typical components (like deteriorated RC columns) result in decreased demands on certain other bridge elements (like

fixed bearings in the longitudinal direction). The changes in fragilities for all bridge components, whether increasing or decreasing, for the aging bridge at different points in time along the service life relative to the pristine bridge are presented in the Appendix B.

Although consideration of joint degradation of RC columns and steel bridge bearings results in increasing fragility of some components (e.g., columns) and decreasing fragility of others (for example, fixed bearings), the overall seismic fragility at the system level increases in time as the bridge continues to corrode (Figure 4-7). For example, for a ground motion having PGA = 0.60g, there is an 30% chance of achieving complete damage for the pristine, or time zero, bridge, but after 75 years of exposure to deicing salts, the chance of complete damage for the same level of earthquake is 49%. A complete list of the median (in units of g) and dispersion values of the system fragility at all damage states is provided in Table 4.5 for different points in time. The decrease in median values of fragility for the different damage states along the service life of the deteriorated bridge is further a direct indication of the increased bridge system vulnerability due to corrosion of its critical structural components. In general there is also a slight change in the dispersion over time, indicating reduced uncertainty in estimating the PGA value

corresponding to exceedance of each damage state when the bridge is corroded. The reduction in dispersion stems from an increased likelihood of bridge component damages due to aging and degradation as opposed to their pristine counterparts. The overall increase in seismic fragility of the bridge can be attributed to the dominance of the columns, transverse and longitudinal expansion bearings, followed by the transverse fixed bearings, in dictating the bridge system vulnerability. On the whole, the seismic vulnerability of these components tends to be negatively affected by the continued corrosion of the bridge.

Table 4.5: Median and dispersion values of system fragilities for all damage states at different points in time.

Damage State / Time (years)	Slight		Moderate		Extensive		Complete	
	med_{sys}	$disp_{sys}$	med_{sys}	$disp_{sys}$	med_{sys}	$disp_{sys}$	med_{sys}	$disp_{sys}$
0	0.27	0.70	0.52	0.62	0.66	0.65	0.89	0.70
25	0.27	0.65	0.48	0.58	0.61	0.62	0.79	0.64
50	0.26	0.61	0.47	0.54	0.60	0.59	0.79	0.62
75	0.24	0.54	0.40	0.53	0.51	0.56	0.67	0.60
100	0.21	0.53	0.35	0.49	0.46	0.54	0.63	0.58

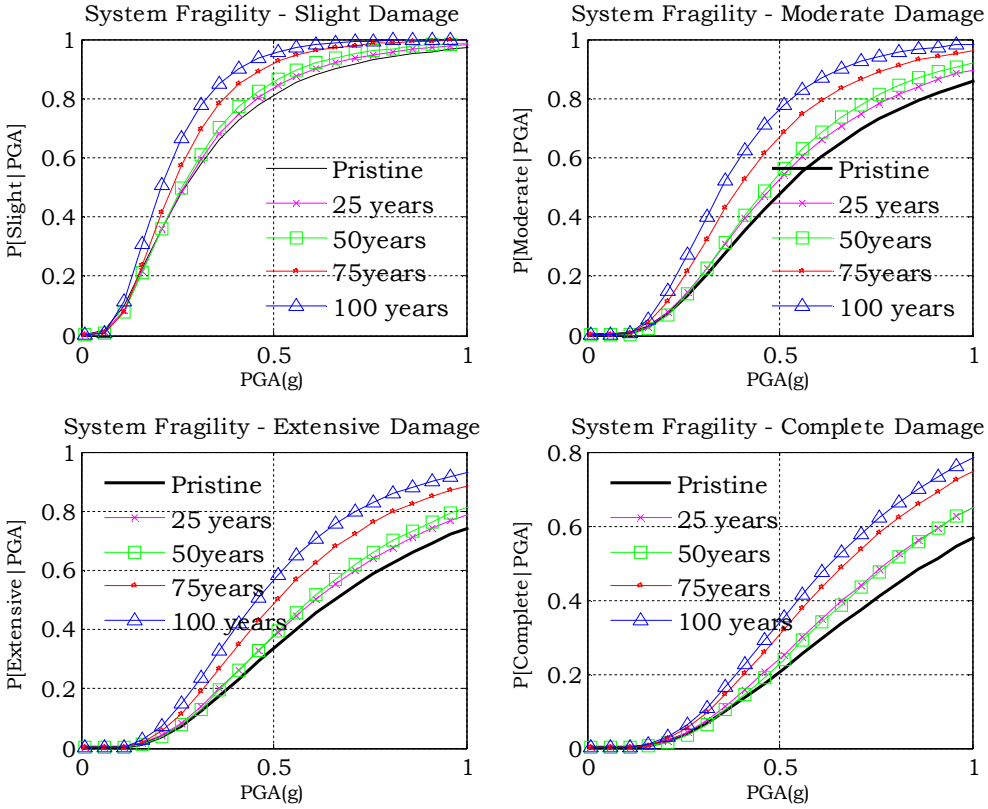

Figure 4-7: System level time-dependent seismic fragility curves corresponding to different damage states for the case study MSC steel girder bridge (Ghosh and Padgett 2010)

4.2.2. Case study multi-span simply supported (MSSS) concrete girder bridge

While the previous case study focused on the impact assessment of aging mechanisms and development of time-evolving bridge fragility curves for a typical MSC steel bridge, this section will focus on the multi-span simply supported (MSSS) concrete girder bridge class. This bridge class constitutes nearly 19% of all

bridges in CSUS and has also been identified by previous researchers (Nielson 2005; Nielson and DesRoches 2007b) as seismically vulnerable due to inadequate detailing of components. Similar to the previous case study, the RC columns of this bridge class is also characterized by insufficient transverse reinforcement consisting of #13 bars spaced at 305mm on center, inhibiting the shear resistance and ductile capacity. Additionally the elastomeric pad bearings have the potential for 'walking out' from under the girders during large deformations in seismic events, and seat widths are inadequate. Furthermore, the reinforcing steel in the concrete columns and the bridge bearings are prone to aging and deterioration. Such mechanisms include corrosion of reinforcing steel in columns and bearing dowel bars along with increase in stiffness of bearing pads due to thermal oxidation as elaborated in Section 3.2.3.

Unlike the previous example, the present case study will incorporate uncertainty within the bridge geometry and develop probabilistic seismic demand models and time-dependent fragility curves representative of the seismic vulnerability of a portfolio of bridges. This is achieved by sampling eight representative three-span, zero-skew bridges belonging to this particular bridge class from CSUS bridge inventory. The span lengths, deck widths and column

heights of all these eight bridges are obtained using Latin Hypercube Sampling techniques from the cumulative density functions of span lengths, deck widths and column heights of all such bridges in the inventory. Table 4.6 shows the representative configuration for the MSSS concrete girder bridge samples used in this study.

Table 4.6: Eight representative bridge configuration of the case study MSSS concrete bridge class

Bridge Number	Number of spans	Mid-span length (m)	Deck width (m)	Column height (m)
1	3	13.2	15.43	4.82
2	3	6.9	10.65	6.40
3	3	7.8	13.76	5.13
4	3	11.9	16.7	4.92
5	3	9.1	9.61	7.31
6	3	6.7	7.65	5.34
7	3	8.6	17.97	5.59
8	3	9.6	12.11	4.72

Figure 4-8 shows a typical finite element model of a three span, zero-skew bridge type belonging to the MSSS concrete girder bridge class under consideration. These three dimensional finite element models for each pristine and aging bridge within the bridge class are developed in this study following the modeling strategies presented in Chapter 3. For the deteriorated bridge modeling, in addition to reducing the cross-sectional area of column reinforcement to account for the effects of corrosion deterioration, the figure also shows changes in the force-

displacement curves for aging bridge bearing models as compared to the pristine state. The impact of corrosion deterioration of steel members such as reinforced concrete columns, bearing dowel bars and thermal oxidation of the elastomeric bearing pads on the seismic response and fragility of bridge components and system belonging to the bridge class under consideration will be assessed in the following sections.

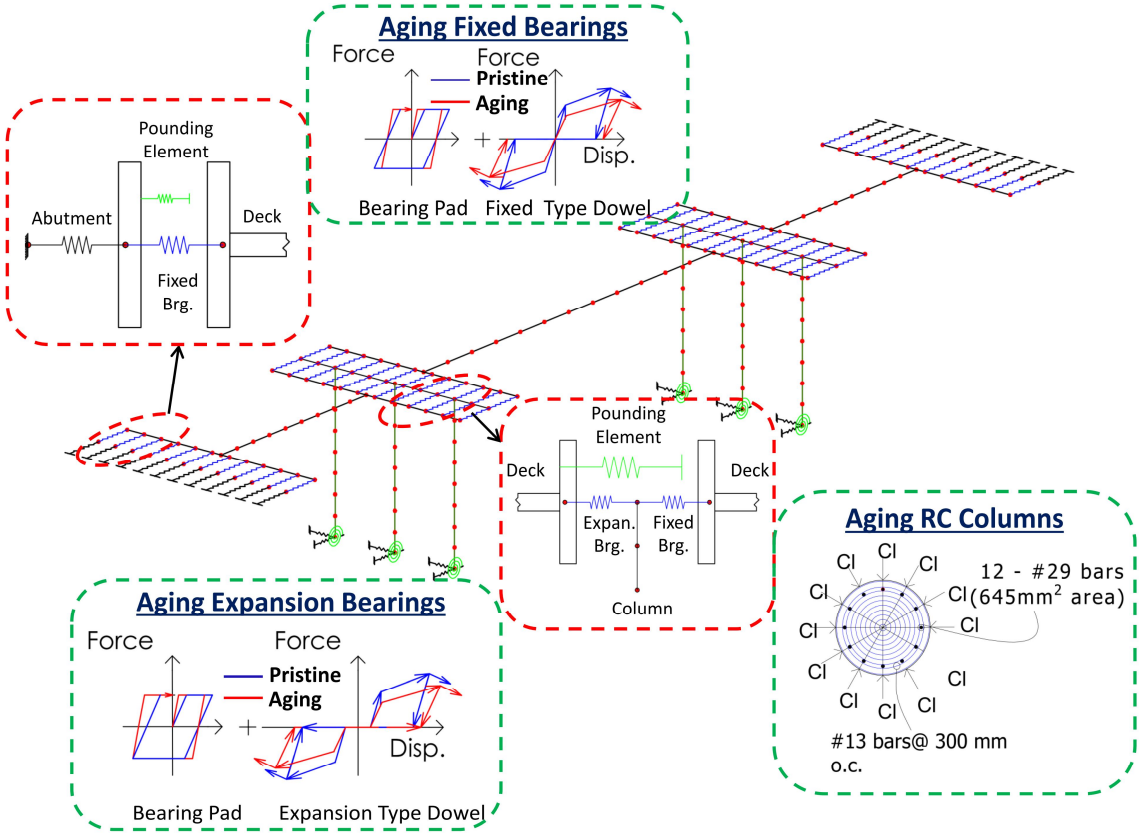

Figure 4-8: Typical finite element model of the 3 span MSSS concrete bridge sample showing potential changes in modeling parameters due to aging and deterioration (Ghosh and Padgett 2012)

4.2.2.1. Degradation of structural components along service life

In order to understand the impact of component deterioration on bridge class fragility, it is essential to assess how each of these aging components individually affects the bridge response. The component responses in turn depend on the severity of environment, point in time along the service life of the bridge class, and level of degradation of the component under consideration. The primary focus of this section will be to assess component and bridge system performances under corrosion deterioration due to chlorides from deicing salt exposure; the effects of different exposure conditions other than chlorides resulting from deicing salt on bridge fragilities (such as marine splash and atmospheric zones) will be discussed in Section 4.2.2.4 of the thesis. The parameters used to assess the corrosion deterioration of embedded steel members under deicing salt exposure condition are similar to those assumed for the previous case study as presented in Table 4.4.

Additionally, to assess the stiffening of the elastomeric bearings, a key input for the Arrhenius methodology as given in Equation (3.15) is the region specific absolute in-field exposure temperature (T_{field}) of these elastomeric pads. The region of interest chosen to assess the exposure to chlorides from deicing salts is the state of Tennessee with an average annual snowfall of 9inches and yearly average

temperature of 56°F (NOAA 2004; USDOS 2010). Under such conditions, Figure 4-9 shows how corrosion deterioration and thermal oxidation manifest in reducing the area of column reinforcing steel and bearing dowel bars while also leading to an increase in horizontal stiffness of the bearing pads. Along with the reduction in the mean value of normalized steel area, Figure 4-9(a) also shows the corresponding uncertainty associated at different points in time along the service life of the bridge. Uncertainty associated with increase in shear modulus of the elastomeric bearing pad is considered same as that of the uniformly distributed random variable model adopted by Nielson (2005) for the pristine rubber bearing with shear modulus ranging between 0.66MPa to 2.07MPa.

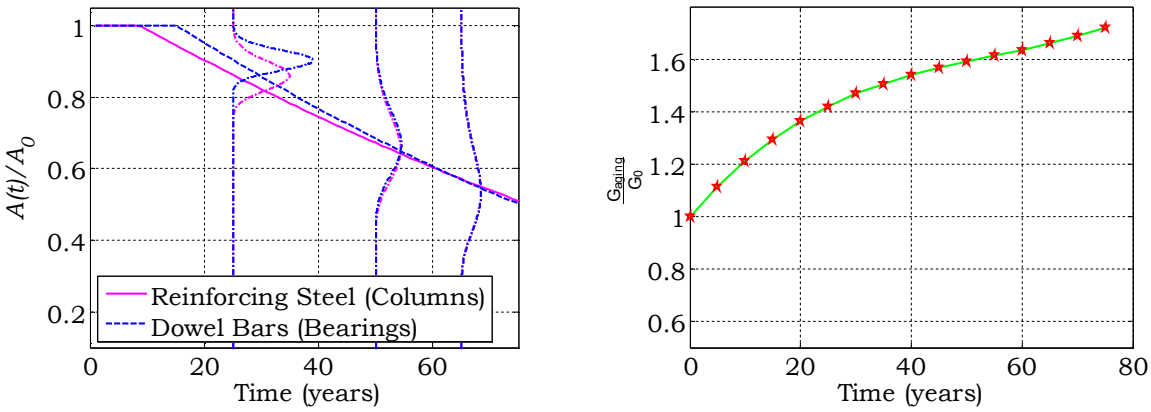

Figure 4-9: a) Normalized cross sectional area reduction of reinforcing steel in RC columns and steel dowels in elastomeric bearings, and b) increase in shear modulus of elastomeric bearing pad (Ghosh and Padgett 2012). Uncertainty associated with the increase in shear modulus is adopted from Nielson (2005)

4.2.2.2. Probabilistic seismic demand model for aging bridge components

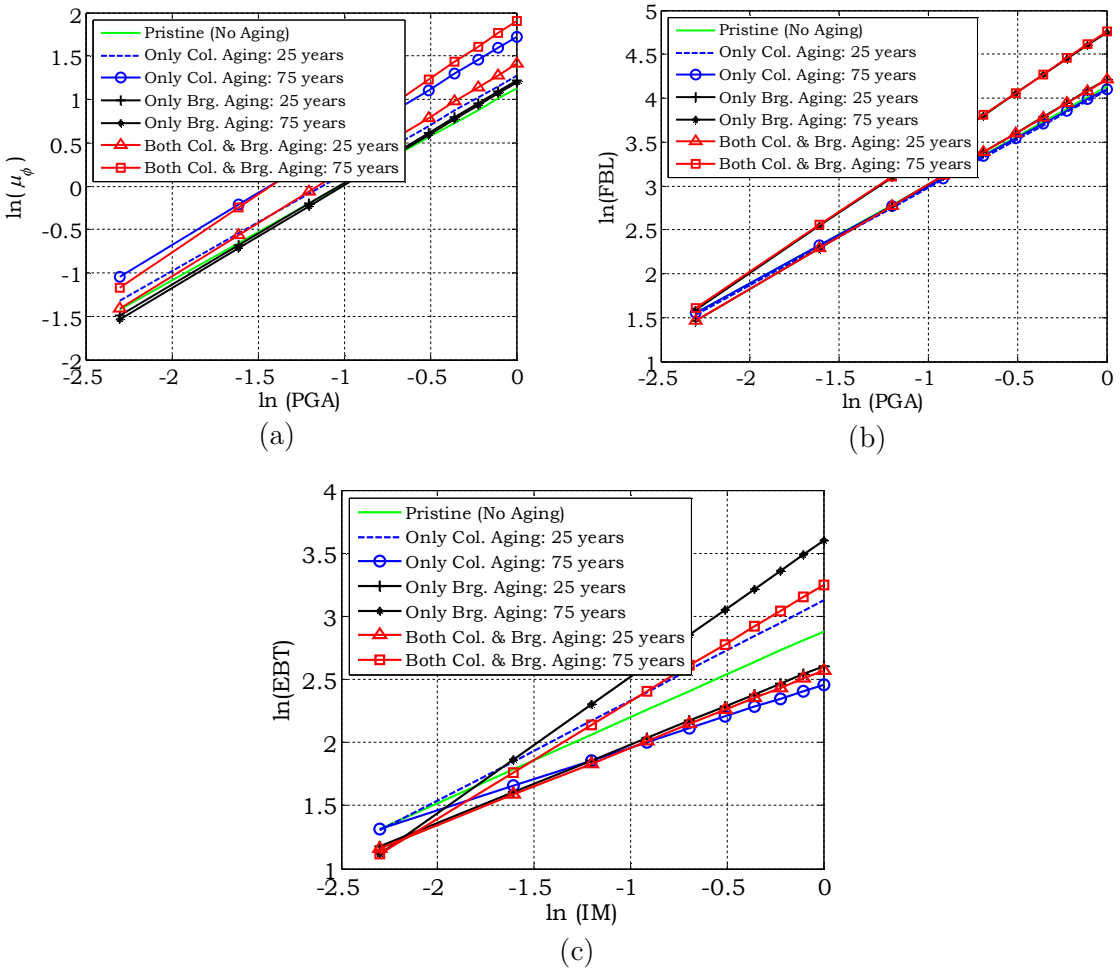

Figure 4-10:PSDMs showing median value of demand against intensity measure for a) RC bridge columns, b) fixed bearing deformation in the longitudinal direction c) expansion bearing deformation in the transverse direction for the case study MSSS concrete bridge class (Ghosh and Padgett 2012)

As described previously in Section 4.1, probabilistic seismic demand models are critical precursors to the development of time-dependent fragility curves. Such demand models of different bridge components help to highlight how the seismic demand placed on the components vary under the effects of aging and

deterioration. The demand models for the aging MSSS concrete bridge class presented in this section correspond to two points in time in the service life of the bridges (25 years and 75 years). Additionally, similar to the previous case study example of the MSC steel girder bridge, three distinct scenarios of component deterioration: a) individual cases of column deterioration, b) individual cases of bearing deterioration, and b) joint consideration of both degradation effects.

Figure 4-10(a) shows the PSDMs for demands placed upon the columns (measured in terms of curvature ductility demand) for the bridge class after 25 and 75 years of exposure to deicing salts. It can be clearly seen in the figure that if only bearing degradation is considered, regardless of the year, it has a negligible impact on the seismic demand placed on the columns. As one would expect, the deterioration of the columns only has a significant influence on the column demand which is found to increase steadily with age from 25 to 75 years. Additionally when both column and bearing deteriorations are accounted for, the demands placed on the columns are highest for that particular point in time than when the aging mechanisms are considered individually. Similarly, Figure 4-10(b) shows the impact of component deterioration on the response of fixed bearings in the longitudinal direction. Similar to the previous figure this also shows that while only column

deterioration has negligible impact on the seismic demand placed on the fixed bearings, bearing degradation has a significant impact in increasing the demand due to aging. In this case however, the joint consideration of these components does not have a significant influence on the demand than when bearing deterioration is considered individually. Furthermore, it is misleading to assume that these two individual degradation mechanisms of the columns and bearings have virtually no effect on the response of one another. This is shown in Figure 4-10(c) which depicts the PSDMs for the expansion bearings in the transverse direction. This figure shows that initial deterioration of bridge columns at 25 years (under the individual or joint consideration of aging) alone tends to increase the transverse deformation on the expansion bearings, while increased deterioration at 75 years reduces the seismic demand due to the localization of forces and energy dissipation through the heavily deteriorated bridge columns. Similarly, when the effects of bearing deterioration is considered alone, initially at 25 years the effect of increase in horizontal stiffness of bearing pads due to thermal oxidation tends to dominate over the steel area reduction of dowel bars and reduces the transverse displacement of the expansion bearings. However, as the dowel deterioration becomes more pronounced, the deformation and hence the seismic demand placed

on the expansion bearings increases far beyond the demands placed on the initial non-deteriorated expansion bearings in the transverse direction.

4.2.2.3. Fragility curves for aging MSSS concrete bridge class under deicing salt exposure

Fragility curves, using the methodology outlined in Section 4.1 are derived for the class of MSSS concrete girder bridges to assess how the joint effects of deterioration of RC columns and elastomeric bridge bearings affect the seismic reliability of key components and the system. Figure 4-11 shows the percentage changes in median fragility values of different components (with respect to the pristine bridge) for the slight damage state. A decrease in median value, or negative percent change, reveals an increase in vulnerability to seismic loading; conversely, an increase in median value, or positive percent change, reveals a reduction in seismic vulnerability of the component. The trends in variation of the median fragility parameter for different bridge components as depicted in Figure 4-11(b) are found to remain consistent across all damage states. This figure reveals two interesting trends. Firstly, the median values of certain bridge components, such as bridge columns and fixed bearings in the longitudinal direction, show a consistent decrease (hence an increase in susceptibility to seismic damage) along their service life. On

the other hand, both the fixed and expansion bearings in the transverse direction show an initial increase in median values followed by a decrease as the bridge continues to age.

The above findings are consistent with the assessment of the demand models presented earlier in Section 4.2.2.2. In the initial period, the corrosion of rebar in the columns and dowel bars in the bearings do not have a pronounced effect on the deformation response of these components which is mostly dominated by the stiffening of the elastomeric pad. Additionally, although median values for parameters such as fixed and expansion bearings in the transverse direction show a dramatic increase with a subsequent decrease in median values along the service, the effect of this component on system fragility is negligible owing to its high median value. To further highlight the relative vulnerability of each component at the slight damage state, the median values of the pristine components are shown in the legend of the figure in percent g PGA. It is noted that the relative vulnerability of these components are not consistent across each damage state, although the trends in impact of aging remains similar. Furthermore, while the median values of different bridge components either increase or decrease depending

on the point in time along the service life of the bridge, the dispersions are in general found to decrease steadily across all components Figure 4-11(b).

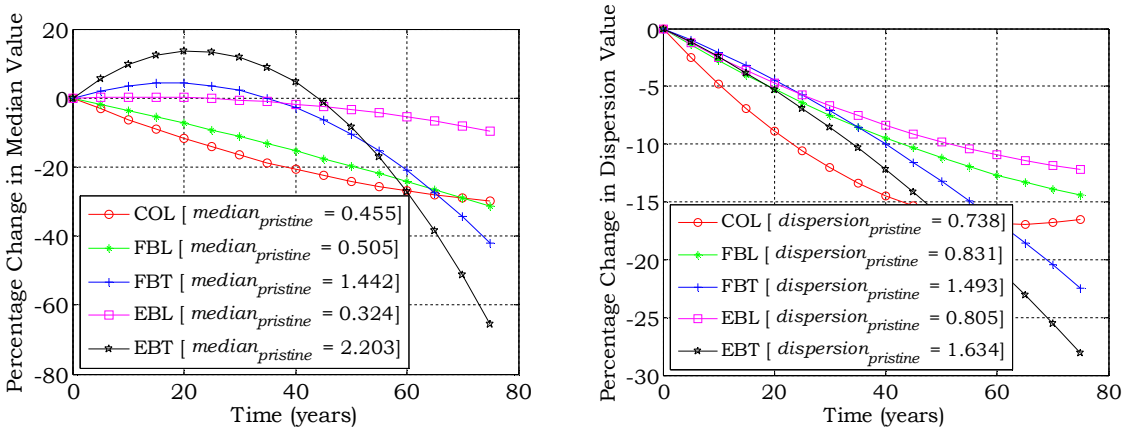

Figure 4-11: Percentage change in a) median and b) dispersion values for slight damage state across the service life of different bridge components (Ghosh and Padgett 2012)

Given the contrasting trends in impact of deterioration on bridge component fragility due to the complex dynamic response of the structure, bridge class fragility curves are developed to quantify the overall impact of aging on system vulnerability. Figure 4-12 shows the aging bridge class fragility curves at four different points in time for the moderate and extensive damage states, clearly revealing that aging and deterioration has an overall negative impact on bridge system fragility. This is in contrast to the individual fragilities of some bridge components (Figure 4-12) which tend to show a reduced fragility in the initial period of service life, such as the bridge expansion bearings in the transverse

direction. This finding underlines the need to consider the effects of multiple bridge component degradation mechanisms while assessing the seismic vulnerability of bridge classes. The results further demonstrate that even after considering uncertainty in ground motion, geometry and modeling parameters the effects of aging and deterioration emerge as critical factors in fragility modeling of the MSSS concrete girder bridge class. Time varying median and dispersion values for different components and bridge system under deicing salt exposure are presented in Appendix B.

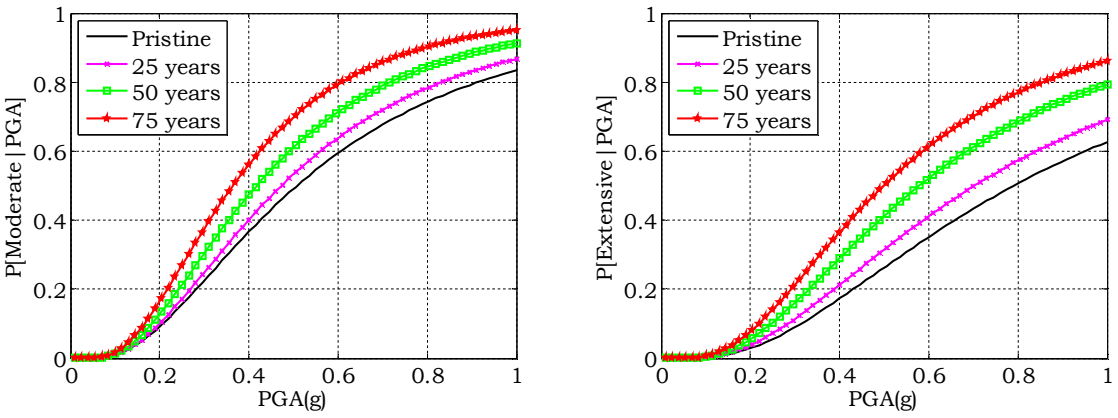

Figure 4-12: Fragility curves for case study MSSS Concrete bridge classes for the a) moderate and b) extensive damage states under deicing salt exposure (Ghosh and Padgett 2012)

4.2.2.4. Impact of exposure condition on deteriorated bridge fragility

In addition to the case of deicing salt exposure as elaborated in the preceding section, two additional exposure conditions are considered in this study. These exposure scenarios correspond to proximity to chloride ions stemming from marine sources as detailed in Chapter 3. In order to demonstrate the effects of such exposure conditions, the bridge class under consideration is assumed to be located in the state of South Carolina (SC), which is characterized by moderate seismicity with potential exposure to marine chlorides from the close proximity to the Atlantic Ocean. The probabilistically distributed deterioration parameters to calculate the corrosion initiation time and subsequent area loss of steel embedded in RC members for sea-splash and atmospheric zone are presented in Table 3.4. The average yearly temperature to evaluate the stiffening of bearing pad for bridges located in SC are 66°F - almost 10°F higher than TN where deicing salt exposure was considered.

Figure 4-13 shows the normalized area reduction of steel and increase in shear modulus of elastomeric bearing pads under the different exposure conditions and bridge locations. It can be observed that for the same reinforcement layout and cover depth in the RC columns, deicing salt exposure leads to the shortest

expected corrosion initiation time (approximately 8 years) and also results in significantly higher cross sectional area loss of steel as compared to either marine splash zone or atmospheric chloride exposure. Also, both sources of marine chloride degradation lead to a lesser uncertainty about the mean area loss of steel, relative to the deicing salt exposure due to reduced dispersion of the corrosion rates. A similar trend is observed for the cross sectional area loss of steel dowels in the bridge bearings under different exposure conditions. Additionally, a higher average annual temperature in SC is found to result in further stiffening of the neoprene rubber pad in bridge bearings as compared to TN. Another interesting observation is that for the atmospheric zone exposure, the onset of corrosion to reinforcing steel in concrete is found to be significantly delayed relative to the other exposure conditions. Hence the impact on seismic fragility under chloride exposure from atmospheric marine zone is expected to be solely due to stiffening of the bearing pad for the initial period in the bridge's service life.

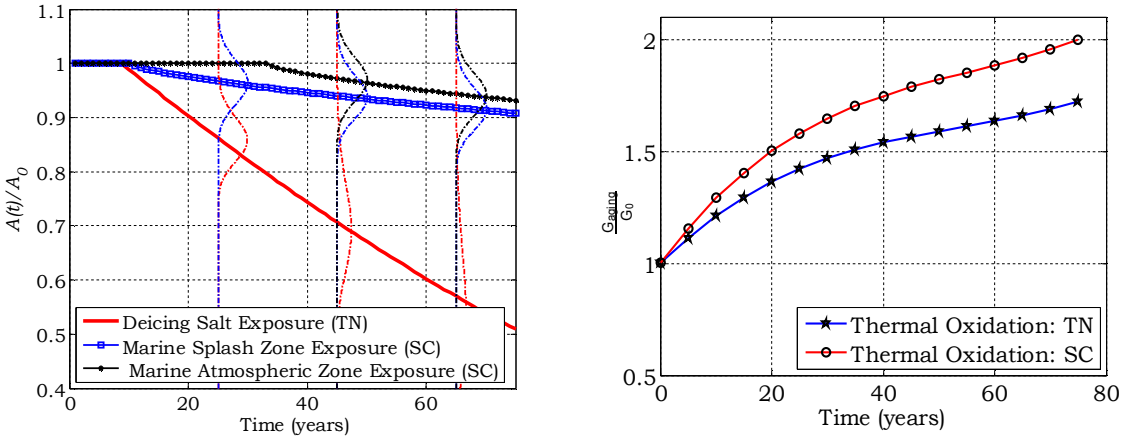

(a) (b)

Figure 4-13:a) Normalized residual area of column reinforcement under different exposure conditions and b) variation of stiffness modulus change due to thermal oxidation in Tennessee and South Carolina (Ghosh and Padgett 2012)

Comparisons of the seismic fragility of the bridge class under different exposure conditions are presented in Figure 4-14 which shows several interesting observations. For instance, Figure 4-14(a) and (b) depict the change in bridge system fragility for the moderate damage state under sea-splash and atmospheric chlorides exposure at different points in time in the service life. Although both exposure conditions clearly reveal that towards the end of service life (75 years) both exposure conditions render the bridge more vulnerable to seismic threats, the variation in bridge fragility due to aging is quite insignificant especially for the case of marine atmospheric exposure. This phenomenon is primarily because while corrosion deterioration of RC columns tends to render the bridge more fragile, stiffening of the elastomeric bearing pads is beneficial to bridge behavior by

reducing bearing displacement, as elaborated previously. However, towards the end of the service period, column deterioration dominates as revealed by a clear increase in bridge fragility at 75 years. A comparison of the impact of all three different exposure conditions on bridge fragility is shown in Figure 4-14(c) for the complete damage state. This figure clearly shows the relative comparison of the impact of severity of the three distinct exposure conditions considered in this study. The median values for the fragility curves for the atmospheric, sea-splash and deicing salt exposure are found to be 5%, 9% and 44% lesser than the median value for the as-built pristine bridge fragility. These findings highlight that while atmospheric chloride exposure has the least impact on seismic fragility of aging bridges, exposure to chlorides stemming from deicing salt exposure is most detrimental. This high level of deterioration associated with chloride ions stemming from deicing salt exposure as compared to other exposure conditions have also been validated in the past by Stewart and Rosowsky (1998) with respect to live load reliability of concrete bridges. Time varying median and dispersion values for different components and bridge system under marine splash and atmospheric exposure zone are presented in the Appendix B.

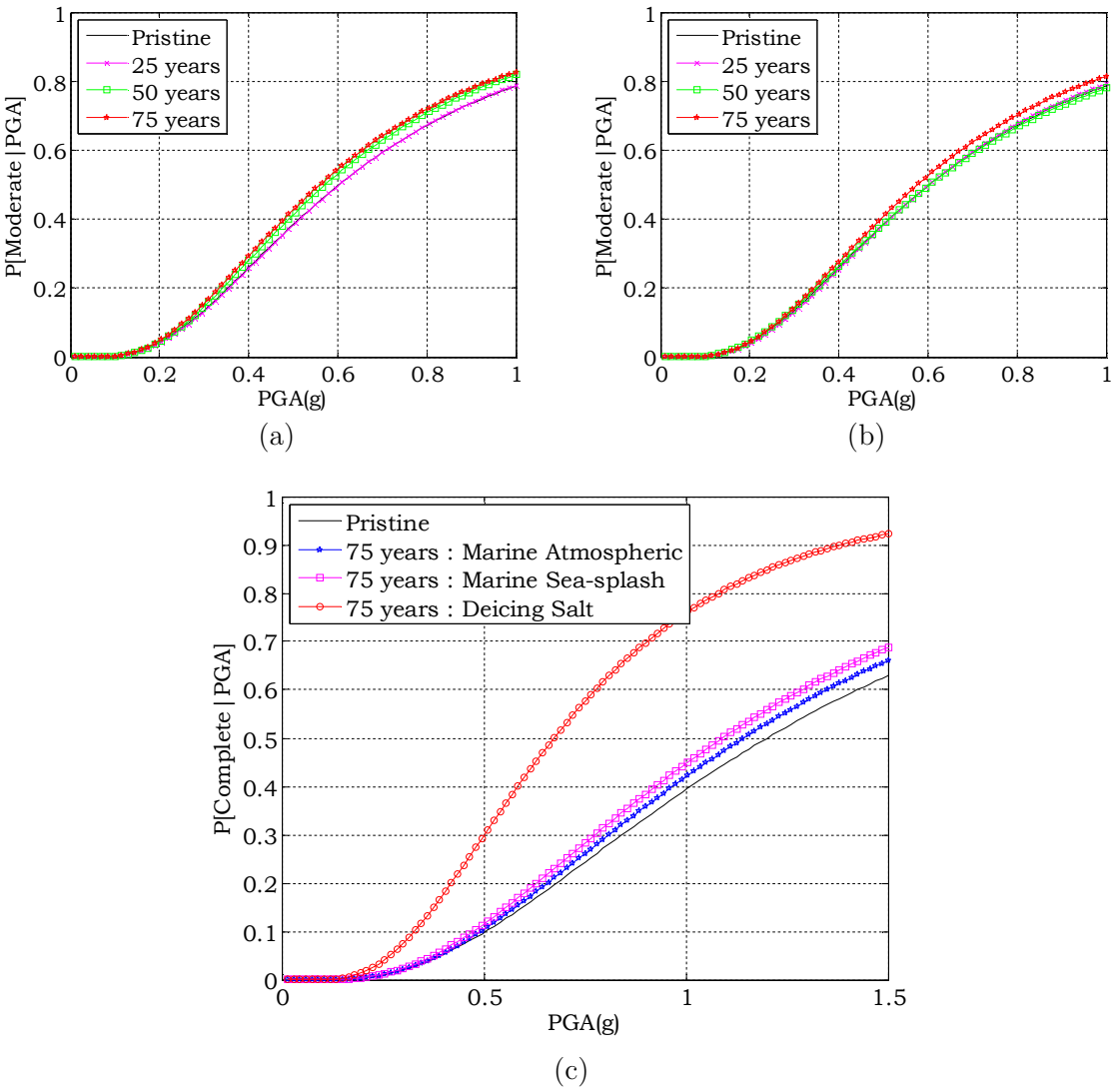

Figure 4-14: a) Aging bridge seismic fragility curves for moderate damage state under sea-splash exposure, b) aging bridge seismic fragility curves for moderate damage state under atmospheric exposure and c) comparison of fragility curves for the complete damage state under diferent exposure conditions (Ghosh and Padgett 2012)

4.3. Closure

This chapter presented the mathematical framework behind the development of time-dependent fragility curves for aging highway bridges after constructing time-evolving probabilistic seismic demand models and component capacity estimates. The impact of aging and deterioration mechanisms in addition to the development of such fragility curves are demonstrated for two structurally different case study highway bridges. The first case study comprised of a multi-span continuous steel girder bridge with deterministic bridge geometry and characterized by deteriorating concrete columns and steel bridge bearings under deicing salt exposure. The component level seismic response of this bridge was examined under the individual and joint consideration of aging mechanisms of degrading structural components. Consequently, time-dependent fragility curves were developed at component and system level using the presented methodology and after evaluating the extent of deterioration at different points along the service life of the bridge. It is observed that at the component level, while there is a steady increase in the fragility of a majority of structural components, a few components such as steel fixed and expansion bearings in the longitudinal direction show a reduced vulnerability with time. Overall, it is observed that at the bridge system level, the seismic

vulnerability significantly increases with a 32% shift in the median value of complete damage fragility near the end of the bridge's life.

The second case study focused on the fragility assessment of a suite of aging multi-span simply supported concrete girder bridges under three different exposure conditions: a) deicing salt exposure, b) sea splash exposure, and c) atmospheric exposure. This bridge type suffers from deterioration mechanisms characterized by corroding reinforced concrete columns, dowel bars, and stiffening elastomeric pads. While the bridge columns of this bridge class show a consistent increase in vulnerability with time irrespective of the exposure condition, the bearing pad assembly shows an initial decrease in vulnerability (due to increasing bearing pad stiffness) followed by an increase in vulnerability (due to the dominant effect of dowel corrosion). Overall bridge seismic vulnerability for this bridge type is also found to increase along the service life of the bridge under different exposure condition. However, the change in bridge vulnerability under marine exposure conditions, especially in the atmospheric zone, is found to be negligible compared to deicing salt exposure conditions. The results of this case study show that median values for the fragility curves for the atmospheric, sea-splash and deicing

salt exposure are found to be 5%, 9% and 44% lesser than the median value corresponding to the pristine bridge fragility.

Chapter 5

PARAMETERIZED SEISMIC FRAGILITY MODELS FOR AGING HIGHWAY BRIDGES

Previous chapters outlined the importance of accounting for bridge component deterioration mechanisms when constructing seismic fragility curves at the bridge component and the system level. Such time-dependent fragility curves can effectively quantify the impact of deterioration on the increase in vulnerability of a specific bridge structure or a portfolio of bridges along their service lives. In addition to these time-dependent fragility curves for seismic reliability estimation, this study will develop flexible parameterized aging bridge reliability models. Unlike the previously presented one-dimensional fragility functions at different time instants and typically conditioned only on the hazard parameter (PGA), these parameterized models will be conditioned on multiple critical parameters that affect the bridge response in addition to the hazard parameter. The potential

advantages of these parameterized fragility models as opposed to traditional models are reflected in their ability to: a) assess the impact of individual deteriorating structural components and geometries on bridge performance without the need for costly re-analysis (Ghosh et al. 2013a), b) incorporate new information on deterioration parameters obtained using field measurements to efficiently determine "updated" fragility estimates, and c) assist in reliability and loss estimation of aging transportation networks after using in-situ bridge reliability estimates, correlations stemming from different sources, and network theory (Ghosh et al. 2013b).

This chapter will explore the use of surrogate models, or metamodels, rooted in statistical learning techniques to develop parameterized fragility models for efficient seismic reliability assessment of aging highway bridges. In this regard, this study will focus on four different surrogate modeling techniques (Ghosh et al. 2013a): 1) polynomial response surface models with stepwise regression (PRSM), because of their prior usage in the field of structural reliability; 2) multivariate adaptive regression splines (MARS), because of their reputation of generating accurate results with manageable computational cost (Jin et al. 2008); 3) radial basis function networks (RBFN), because of their ability to efficiently analyze and

interpolate scattered multivariate data (Hardy 1971); and 4) support vector machines for regression (SVMR), because of their ability to generate nonlinear decision boundaries to train and predict responses in a projected high dimensional space. Additionally, dimensionality reduction techniques will be applied for the first time in highway bridge reliability problems to visualize the failure surface of structural components and ensure the applicability of surrogate models. The metamodel fitting and dimensionality reduction techniques will be demonstrated for the previously discussed (see Chapter 4) multi-span simply supported concrete girder bridge class. The flexibility of parameterized fragility models to incorporate field measurement data after spatial interpolation and Bayesian updating will be demonstrated in a separate network level example focusing on bridges in the state of South Carolina wherein parameterized fragility models will be developed for nine different bridge classes (Ghosh et al. 2013b).

5.1. Generalized Multidimensional Fragility Formulation

Traditional fragility functions, as described previously, are conditional uni-dimensional probabilistic statements which quantify the probability of meeting or exceeding a particular damage state of a bridge component or system given the

intensity of ground motions (*IM*), as shown earlier in Equation (4.1) and reproduced below:

$$P_f = P\left(Demand > Capacity \mid IM\right) \tag{5.1}$$

A potential disadvantage of such single-parameter fragility curves lies in their inability to assess the impact of any individual deteriorating bridge component on bridge performance during earthquakes, or to incorporate new information on deterioration parameters; both without the need for costly re-analysis. Hence, these single-parameter fragility curves can only be used to represent seismic vulnerability of a non-deteriorating bridge or a bridge with an assumed level of deterioration using historical estimates. Addressing such gaps, this study proposes generalized multidimensional fragility functions as (Ghosh et al. 2013a):

$$P_f = P\left(Demand > Capacity \mid IM, p_1, p_2, \ldots, p_k\right) \tag{5.2}$$

where $\mathbf{p} = \{p_1, p_2, \ldots, p_k\}$, is the set of k critical parameters affecting the seismic performance of the deteriorating bridge components and includes: i) critical modeling parameters, ii) deterioration affected structural parameters, and iii) bridge geometric parameters. In this study only field measurable parameters

(measurable using sensor devices or other practical techniques) are chosen to condition and update the fragility estimates herein. Other parameters which are critical but not field measurable are also considered in the fragility analysis, but treated as time-invariant random variables to propagate their uncertainty when deriving the fragility models. These parameter distributions are adopted from (Nielson 2005) and are presented in Table 4.2.

Statistical learning techniques are employed in this study to develop the proposed parameterized fragility models. The key steps involved in this procedure include (Ghosh et al. 2013a): a) fitting multidimensional surrogate models, or metamodels, to bridge component responses after devising an experimental design strategy and conducting non-linear time-history analysis of bridge models, and b) conducting logistic regression at bridge component and system level to develop parameterized fragility models. The following sections will first detail these steps along with verification of the applicability of surrogate model by confirming the smoothness of the failure surface for different components of the MSSS concrete bridge class. This will be followed by an application example of network level bridge reliability estimation after incorporating in-situ bridge conditions for an

existing transportation network in South Carolina, US consisting of nine different aging bridge classes.

5.2. Surrogate Model Fitting Rooted in Statistical Learning Techniques

In order to exemplify the surrogate modeling concept to efficiently predict bridge seismic response using statistical learning, let the predicted output variable y be the peak seismic response of a particular bridge component such as the column curvature ductility or bearing deformation, and the predictors be the ground motion intensity measure (IM) and parameter vector $\mathbf{p} = \{p_1, p_2, \ldots, p_k\}$. As described earlier, parameter vector $\mathbf{p}$ may include critical modeling parameters, geometric parameters and structural parameters affected by deterioration. Let the joint set of IM and $\mathbf{p}$ be represented by $\mathbf{x}$ such that, $\mathbf{x} = \{IM, \mathbf{p}\}$. The objective herein is to develop surrogate demand models to approximate the relationship between the seismic response y and the joint vector $\mathbf{x}$. Hence, if the true (but unknown) relationship $t(\mathbf{x})$ between the predictors $\mathbf{x}$ and the predicted variable y can be represented as:

$$y = t(\mathbf{x}) \tag{5.3}$$

then, the surrogate demand model $d(\mathbf{x})$ is said to statistically predict this complex and implicit relationship $t(\mathbf{x})$ as:

$$y = d\left(\mathbf{x}\right) + e \tag{5.4}$$

where e, is the total error resulting from lack-of-fit and is assumed to be a zero mean normal random variable (Chen et al. 2006; Simpson et al. 2001).

Table 5.1: Steps involved in the development of surrogate demand models for predicting bridge component responses (Ghosh et al. 2013a)

Step Number	Purpose	Description
1	Develop experimental design matrix	Select sets of sample points in the design parameter space of predictor variables **x** using an experimental design strategy to generate a *sequence of experiments* (finite element simulations) to be performed.
2	Conduct finite element simulations for each row of experimental design matrix	Conduct three dimensional dynamic nonlinear finite element simulations of bridge models to obtain the response (output) data **y** for component responses corresponding to the *experimental design runs*. This response data (**y**) pertaining to a particular bridge component constitutes the predicted values.
3	Fit surrogate models	Choose surrogate models $d(\mathbf{x})$ to fit the observed data obtained in Step 2 and choose the best model based on goodness-of-fit estimates.

Following traditional strategies specific for computer simulations/experiments (Simpson et al. 2001), this study will develop metamodels for approximating seismic response of bridge components using the three steps outlined in Table 5.1. The subsequent sections will detail the experimental design strategy and different metamodels analyzed in this study.

5.2.1. Experimental design methods and finite element analysis

This section elaborates on the experimental design strategy and subsequent finite element simulations that correspond to steps 1 and 2 from Table 5.1. An experimental design strategy allows a systematic combination of the predictor variables prior to metamodel fitting and helps to reduce the number of computationally expensive simulations while improving the quality of the approximation and predictive capabilities of the surrogate model (Fang et al. 2006). If the entire *sequence of experiments* of the design is represented by the matrix X, then, each *experimental design run* corresponds to each row of X. Additionally, each *experimental design run* is expressed in terms of the *factors* (predictor variables) set at specified *levels* (Simpson et al. 2001).

Although many different experimental design procedures exist in literature, this study adopts the Latin Hypercube Experimental Design. This design strategy was first introduced by McKay et al. (1979) and has been widely adopted for computer experiments which are typically deterministic, i.e. without any random noise. Pertaining to nonlinear dynamic analysis of complex finite element bridge models this means that a particular combination of bridge modeling parameters coupled with a ground motion record will always yield the same seismic response of a particular bridge component following the finite element analysis. The Latin Hypercube design operates by dividing the desired range for each element within the parameter vector $\mathbf{p}$ into n intervals of equal marginal probability $1/n$ followed by selecting a sample once from each stratum. Next, the selected n samples for the first element (p_1) are combined with the n samples of the second factor (p_2), and subsequent factors ($p_3 \ldots\ p_k$) such that it maximizes the minimum distance between the design points. Each row of this Latin Hypercube experimental design matrix is then paired with a suite of ground motions with varying intensity measures (IM), which is treated as an uncontrolled factor. Hence, if the size of original Latin Hypercube experimental design matrix is $[n, k]$ and the number of ground motions paired with each row is r, then the size of final experimental design matrix is

$[(n \times r), k]$. Next, nonlinear dynamic time history analysis of finite element bridge models corresponding to each row of the final experimental design matrix is conducted using OpenSees. The seismic responses of bridge components ($\mathbf{y}$) thereby obtained are used to fit different surrogate models, as described in the next section.

5.2.2. Surrogate demand models

This section correspond to step 3 from Table 5.1 and describes each of the metamodels adopted in this study including the mathematical details along with their relevance to parameterized seismic demand modeling of aging highway bridges (Ghosh et al. 2013a). Four different metamodels were considered including Polynomial Response Surface Models, Multivariate Adaptive Regression Splines, Radial Basis Functions for Networks, and Support Vector Machines for Regression.

5.2.2.1. Polynomial response surface models (PRSM)

Polynomial response surface models were first developed by Box and Wilson (1951) and have been widely adopted for predicting the response of complex engineering systems, such as buildings. The most widely used response surface models consist of low order polynomial functions. Simpson et al. (2001) recommended that first order polynomials shall suffice for responses characterized by low curvatures; while

second order polynomials including two factor interactions are more appropriate for significant curvatures. Other researchers have demonstrated the capability of second order polynomials to predict the dynamic response of structures in structural reliability evaluations with negligible prediction errors (Cundy et al. 2003; Seo and Linzell 2012). Consequently, second order response surface polynomials of the form shown in Equation (5.5) are adopted in this study because of enhanced goodness-of-fit measures in comparison to first order polynomial models (Ghosh et al. 2013a).

$$\hat{y} = \beta_0 + \sum_{i=1}^{l} \beta_i x_i + \sum_{i=1}^{l} \sum_{j=1, i<j}^{l} \beta_{ij} x_i x_j \tag{5.5}$$

In this equation, $\hat{y}$ represents the predicted value of the bridge component response, x_1, …, x_l, are the predictors and β_0, …, β_{ij} are the regression coefficients obtained using least square principles after fitting the response surface approximations to the component response data from nonlinear time history analysis of bridge models under seismic shaking. Additionally, this study seeks the most optimal form of the second order polynomial response (Equation (5.5)) using stepwise regression technique, which is a systematic method for adding and

removing terms from the second order model based on their statistical significance in a regression (Wang and Jain 2003).

5.2.2.2. Multivariate adaptive regression splines (MARS)

Although the polynomial response surface models provide simplistic relations between the output and input variables, their application is bounded with certain assumptions, such as, homoscedasticity of the errors, and normality of the error distribution (Ravishanker and Dey 2002). Unlike the response surface models, MARS is a nonparametric regression procedure that makes no assumption about the underlying functional relationship between the predictor and predicted variables and yet has been shown to display great accuracy in predictions due to its "adaptive" nature while being computationally efficient. This adaptive nature of MARS can be exploited to accurately predict the response of bridge components if their seismic behavior is widely different in different domains of parameter combinations. First introduced by Friedman (1991) for regression modeling of high dimensional data, the MARS model can be represented as:

$$\hat{y} = \sum_{i=1}^{l} \theta_i B_i(\mathbf{x}) \tag{5.6}$$

where, θ_i's are the constant coefficients and $B_i(\mathbf{x})$'s are the basis functions. Each basis function can in turn be represented as:

$$B_i(\mathbf{x}) = \prod_{l=1}^{L_i} [s_{l,i}(x_{v(l,i)} - t_{l,i})]_+ \tag{5.7}$$

where, L_i is the number of truncated linear functions multiplied in the i^{th} basis function, $x_{v(l,i)}$ is the input variable corresponding to the l^{th} truncated linear function in the i^{th} basis function, $t_{l,i}$ is the knot value corresponding to $x_{v(l,i)}$, and $s_{l,i}$ is +1 or -1.

The adaptive nature of the MARS metamodel is primarily attributed to the automatic partitioning of the input parameter space to determine the model basis functions (B_i ($\mathbf{x}$)'s) and associated parameters (θ_i's) through a backward/forward iterative approach. The MARS metamodeling strategy is yet to be applied for computing reliability of civil engineering structures, while it has gained significant reputation in other fields of science and engineering (Courtois and Woodside 2000; X. Wang et al. 1999). This study will test whether the bridge component response predictions by the highly flexible MARS metamodel is significantly better than the predictions obtained using other metamodeling strategies (Ghosh et al. 2013a).

5.2.2.3. Radial basis function networks (RBFN)

Radial basis function networks belong to a class of "training-based" metamodels which involves training a hidden layer of neurons based on the output responses and input variables. RBFN was first developed by Hardy (1971) for scattered multivariate data interpolation, by using linear combinations of radially symmetric functions based on Euclidian distances or other such metrics to approximate response functions. Although this class of metamodels suffers from a lack of transparency due to the hidden layer of neurons, RBFNs has been shown to generate excellent approximations to a wide range of response functions: discrete or continuous, deterministic or stochastic. Hence, it is worthwhile to assess the performance of this versatile metamodeling strategy to predict the seismic response of bridge components conditioned on multiple input parameters.

Radial basis functions consist of three sets of nodes. The first set at the input level, consists of the same number of nodes as input predictor variables (x_i's). The second set is a layer of l hidden nodes where training of neurons occur, and the third layer is at the bridge component response level giving the RBFN the following functional form:

$$\hat{y} = \alpha_0 + \sum_{i=1}^{l} \alpha_i \phi_{RBF_i}\left[w_i(\mathbf{x})\right] \tag{5.8}$$

where, $\phi_{RBF_i}\left[w_i(\mathbf{x})\right]$ is a nonlinear mapping from the input layer to the hidden later, α_0 is the bias, and α_1, …, α_l are the connection weights between the hidden layer and output bridge component response layer. The function $w_i(\mathbf{x})$ can be defined as:

$$w_i(\mathbf{x}) = \frac{|| \mathbf{x} - c_i ||^2}{\varsigma_i^2} \tag{5.9}$$

where, ς_i is a scalar parameter defining the width of the i^{th} radial unit, $|| \cdot ||$ is the Euclidian norm and c_i are the centers of the radial basis functions. The standard and most commonly adopted radial basis functions are the Gaussian function and polyharmonic spline function (Merz and Hao 2011). This study found that polyharmonic splines as radial basis functions performed best in predicting the bridge component responses and are thereby adopted.

5.2.2.4. Support vector machines for regression (SVMR)

Support Vector Machines are a modern and specific class of statistical learning algorithms and unlike the previously discussed metamodels, they are characterized by the usage of kernels, absence of local minima, and sparseness of the solution.

While support vector machines have primarily found their applications in *classification* problems, they can also be used for regression to develop non-linear functions which statistically "learn" by using linear learning machine mapping into high dimensional kernel induced feature spaces. In multi-dimensional bridge component response predictions, it is worthwhile to investigate if the nonlinear pattern of the relation between the input parameters (x_i's) and bridge component response (y) can be projected to a high dimensional feature space where they can be readily separated by linear functions (Ghosh et al. 2013a). The support vector machines are believed to perform exceptionally well if such linear functions exist in high dimensions.

SVMR starts with mapping the input vector $\mathbf{x}$ of bridge parameters onto an m-dimensional feature space using nonlinear functions, followed by the construction of a linear model in this feature space. This linear model $h(\mathbf{x},q)$ in the feature space can be represented as:

$$h(\mathbf{x},q) = \sum_{j=1}^{l} q_j n_j(\mathbf{x}) + b \tag{5.10}$$

where, $n_j(\mathbf{x})$ represents a set of nonlinear transformations, q_j are the weights, and b is the model bias. The quality of the estimated function value (bridge component

response) is measured in SVMR using the ε-sensitive loss function $Loss_{\varepsilon}[\mathbf{y},h(\mathbf{x},q)]$, first proposed by Vapnik (1998) as shown in Equation (5.11) . The primary aim of SVMR is to optimize the generalization bounds for regression (characterized by $Loss_{\varepsilon}[\mathbf{y},h(\mathbf{x},q)]$ while ignoring errors situated within certain distance of the true component response value.

$$Loss_{\varepsilon}\left[\mathbf{y},h(\mathbf{x},q)\right]=\begin{cases}0 & \text{if } |\ \mathbf{y}-h(\mathbf{x},q)\ | \ <\varepsilon \\ |\ \mathbf{y}-h(\mathbf{x},q)\ | & \text{otherwise}\end{cases} \tag{5.11}$$

While performing linear regression in the high-dimension feature space using ε-insensitive loss, SVMR simultaneously tries to reduce model complexity by minimizing $\|q^2\|$. This is achieved by introducing slack variables ξ_i, ξ_i^* i = 1, ..., I, to measure the deviation of training samples from the ε-insensitive zone. Thus, along with Equation (5.11), SVMR regression is also formulated as minimization of the following function:

$$\begin{aligned}&\min\frac{1}{2}\,||\,q^2\,||+C\sum_{i=1}^{I}\left(\xi_i+\xi_i^*\right)\\ &\text{subjected to }\begin{cases}\mathbf{y}_i-h(\mathbf{x}_i,q)\le\varepsilon+\xi_i^*\\ h(\mathbf{x}_i,q)-\mathbf{y}_i\le\varepsilon+\xi_i\\ \xi_i,\xi_i^*\ge 0, i=1,...I\end{cases}\end{aligned} \tag{5.12}$$

The optimization problem presented above can be transformed into the corresponding dual problem, which can be solved as:

$$h(x) = \sum_{i=1}^{SV} \left(\tau_i - \tau_i^*\right) K\left(\mathbf{x}_i, \mathbf{x}\right) \quad \text{subjected to } 0 \le \tau_i \le C, 0 \le \tau_i^* \le C \tag{5.13}$$

where, SV is the number of Support Vectors, C is the cost function and the kernel function $K(\mathbf{x}, \mathbf{x}_i)$ is represented as:

$$K(\mathbf{x}, \mathbf{x}_i) = \sum_{j=1}^{m} n_j(\mathbf{x}) n_j(\mathbf{x}_i) \tag{5.14}$$

5.3. Metamodel Fitting for Case Study MSSS Concrete Bridge Class

In this section, the performance of different surrogate models will be assessed on the basis of their predictive capabilities of component responses for a case study MSSS Concrete bridge class. The accuracy in prediction will be tested against results from benchmark Monte Carlo simulations (Ghosh et al. 2013a).

5.3.1. Case study bridge class description and parameter selection

The different surrogate modeling strategies are explored for their use in bridge seismic reliability analysis using the previously identified non-seismically designed multi-span simply supported (MSSS) concrete bridge classes representative of the Central and South Eastern US. As mentioned in Chapter 4, the chosen bridge class constitutes nearly 19% of all bridges in the region and has been identified by previous researchers as seismically vulnerable due to inadequate detailing of structural components (Nielson and DesRoches 2007b; Nielson 2005). Parameterized surrogate demand models are constructed for the same set of previously identified critical bridge component responses that have been traditionally regarded as critical contributors to the overall system seismic fragility. These components response descriptions are reproduced in Table 5.2 and also depicted in Figure 5-1.

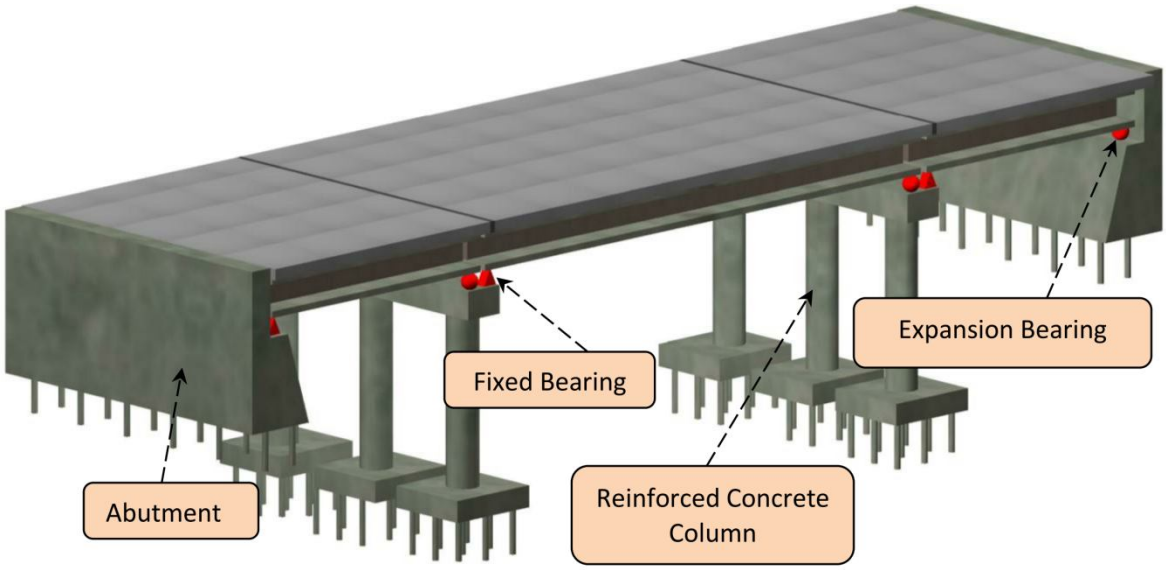

Figure 5-1: General representation of case study multi-span simply supported (MSSS) concrete bridge class depicting critical bridge components (Ghosh et al. 2013a)

Table 5.2: List of critical bridge components contributing to system reliability

Bridge Component	Component Response Parameter	Units	Abbreviation
Reinforced Concrete Columns	Column Curvature Ductility	--	COL
Fixed Bearings	Longitudinal Deformation	mm	FBL
	Transverse Deformation	mm	FBT
Expansion Bearings	Longitudinal Deformation	mm	EBL
	Transverse Deformation	mm	EBT
Abutments	Active Deformation	mm	ABA
	Passive Deformation	mm	ABP
	Transverse Deformation	mm	ABT

A preliminary step in the development of surrogate demand models involves the identification of the vector $\mathbf{x}$ of predictors that consists of the ground motion intensity (IM) and bridge modeling parameters p_1 to p_k. Unlike earlier chapters, the IM chosen for this case study example is the spectral acceleration at the geometric

mean of periods in longitudinal and transverse directions (S_a), due to its superior predictive capabilities compared to other ground motion intensity measures as revealed in a preliminary study (Ghosh et al. 2013a). It is however noted that use of this intensity measure is currently impractical for risk assessment purposes due to unavailability of region and bridge specific hazard curves for this intensity measure and the requirement to estimate periods for each bridge in a portfolio with limited structural information. For such cases, use of intensity measures such as peak ground acceleration (PGA) is more feasible, as will be demonstrated for the network level application in the South Carolina region (Ghosh et al. 2013b). The consequence of adopting PGA resulted in slightly inferior goodness-of-fit estimates for all the surrogate models investigated for the case study MSSS bridge class under consideration.

The bridge modeling parameters p_1 to p_k consists of three subsets. Studies by Nielson (2005) and Padgett and DesRoches (2009) have revealed that bridge geometric parameters are critical in affecting their seismic response and fragility. Hence a subset of conditioned parameters p_1 to p_k consist of bridge geometric parameters, such as, column height, span length and number of bridge columns per bent. An additional motivation behind adopting bridge geometric parameters lies

in the availability of highway bridge geometries in the National Bridge Inventory (Federal Highway Administration (FHWA) 2006) database, which can be readily used for rapid bridge-specific fragility analysis. The second subset consists of deterioration-affected bridge structural parameters. For the case study bridge type, Ghosh and Padgett (2012) demonstrated that the reinforced concrete columns and the elastomeric bearings are prone to aging and deterioration. Hence, conditioning the surrogate models on structural parameters affected by aging along with bridge geometric parameters will render the metamodels readily applicable across an inventory of aging bridges whose characteristics may change in time. The final subset consists of critical bridge modeling parameters as identified by Nielson (2005) from a sensitivity analysis. Since this study aims to develop flexible parameterized fragility models which will aid in rapid estimation of seismic fragility, only those critical parameters are chosen which are field measurable using sensor devices or other practical techniques. Other parameters which are critical but not field measurable are also considered in the fragility analysis, but treated as time-invariant random variables to propagate their uncertainty (Table 4.2). A complete list of the elements in vector **p** along with their descriptions and category are presented in Table 5.3 .

Table 5.3: List of parameters (elements of vector p) included as a subset of predictor variables for the parameterized metamodel development (Ghosh et al. 2013a)

Element of vector p	Description	Category
p_1	Steel strength	Critical bridge modeling parameter (Nielson 2005)
p_2	Elastomeric bearing pad friction	
p_3	Elastomeric bearing dowel gap	
p_4	Column reinforcing bar area	Deterioration-affected bridge structural parameters (Ghosh and Padgett 2012)
p_5	Elastomeric bearing dowel bar area	
p_6	Shear modulus of elastomeric bearing pads	
p_7	Concrete cover depth	
p_8	Column height	Bridge geometric parameters (Nielson 2005)
p_9	Mid-span length	
p_{10}	Number of columns per bent (proxy for deck width)	

5.3.2. Design of experiments

In order to achieve an efficient exploration of the sample space of parameter vector **p** while ensuring appropriate pairing with earthquake records with varying intensity measures, the experimental design matrix is generated in this study using a two-stage procedure. In the first stage, the Latin Hypercube design with optimal spacing is generated using parameters p_1 to p_{10} of vector **p**. The range of each of these parameters used to generate the experimental designs is presented in Table 5.4. The upper and lower levels of the critical bridge modeling parameters (p_1 to p_3) and the bridge geometric parameters (p_8 to p_{10}) are adopted from Nielson (2005). Furthermore, for the deterioration affected structural parameters (p_4 to p_7) the

upper and lower levels correspond to the pristine and severely deteriorated structural parameters, respectively, with the extent of deterioration computed using the aging models outlined in Ghosh and Padgett (2010, 2012). In Latin Hypercube design of experiments, while the user is flexible to choose the number of experimental design rows, the minimum number of design runs required for optimally spaced design points is typically at least twice the number of parameters considered (JMP 2011). To achieve computational efficiency, the present case study adopts the minimum number of experimental design rows, 20, corresponding to twice the ten parameters p_1 to p_{10}.

Table 5.4: Range of parameters p_1 to p_{10} of vector p used to generate Latin Hypercube design with optimal spacing (Ghosh et al. 2013a)

Parameter	Unit	Lower Level	Upper Level
p_1	MPa	275.79	517.11
p_2	--	0.00	2
p_3	cm	0.00	5.08
p_4	cm^2	0.90	6.45
p_5	cm^2	0.548	5.081
p_6	MPa	0.10	6.00
p_7	cm	0.00	10.16
p_8	m	3.00	7.00
p_9	m	7.50	40.00
p_{10}	--	2	4

In the second stage of generating the design matrix, each design row is paired with a subset ensemble of 24 ground motions sampled from the 96 ground

motion suite developed by Wen and Wu (2001) and Rix and Fernandez (2004), as previously adopted for fragility analysis of bridges located in Central and Southeastern US (Choi 2002; Nielson 2005; Padgett 2007). To encompass the entire suite of 96 ground motions, a subset of 24 ground motions is selected with replication for a total of 24×20 = 480 rows in the final design matrix. This step ensures that each row of the original Latin Hypercube design matrix is paired with ground motions that reflect the different range of hazard intensities in the overall suite. This is followed by nonlinear dynamic time history analysis of three dimensional finite element bridge models using OpenSees (Mazzoni et al. 2009), with bridge characteristics for each nonlinear time history run informed from the generated experimental design matrix.

5.3.3. Cross validated performance measures of surrogate models

In this stage, the adopted surrogate demand models are fitted to 480 response data generated for each of the critical bridge components following the nonlinear dynamic analyses of the bridge models subjected to seismic loading. Appropriate transformation of variables is often required in the model fitting process to attain conforming metamodels. While several forms of data transformation exist, such as square-root or inverse transformations, the logarithmic transformation used in this

study is particularly helpful when the variable of interest ranges over several orders of magnitude (Cornell et al. 2002; Shome and Cornell 1999). The transformed variables in this study include the bridge component responses and predictors p_2, p_3, p_6, and p_7, in addition to S_a. The performance of all metamodels with respect to fitting the component response data is assessed using different goodness-of-fit indicators after performing cross validation. Such cross validation minimizes the bias commonly associated with arbitrary choice of training validation samples while comparing different metamodels. The cross validation technique and different goodness-of-fit measures considered in this study are elaborated in the following subsections.

5.3.3.1. Repeated random sub-sampling cross validation

While several cross validation techniques exist, this study adopts the repeated random sub-sampling cross validation procedure (Picard and Cook 1984). In this procedure, 80% of randomly selected responses for a particular bridge component are assigned as the training data set and the remaining 20% are set aside for validation purposes. Next, each metamodel is fitted to the training set, and predictive accuracy is assessed using the validation set using goodness-of-fit estimates. This process is repeated until the variation in the average goodness-of-

fit estimate is minimized. An advantage of this cross validation technique over the commonly adopted k-fold cross validation technique (Mosteller and Tukey 1968) is that the proportion of the training/validation split is not dependent on the number of iterations (folds).

5.3.3.2. Goodness-of-fit measures

Three different goodness-of-fit measures are adopted in this study to compare the fitting and predictive capabilities of the surrogate models to the bridge finite element simulation data. The merits of each of these metrics are described below (Ghosh et al. 2013a).

Adjusted R²

This is a commonly adopted measure that reflects how well the independent variables in $\mathbf{x}$ account for the predicted dependent variable $\hat{y}$. Unlike the commonly adopted goodness-of-fit measure, R^2, the adjusted R^2 increases only if a new additional predictor variable model term improves the model more than what would be expected by chance.

$$Adjusted\ R^2 = 1 - \left[1 - \left(\frac{n\sum_{i=1}^{n} y_i \hat{y}_i - \left(\sum_{i=1}^{n} y_i\right)\left(\sum_{i=1}^{n} \hat{y}_i\right)}{\sqrt{n\left(\sum_{i=1}^{n} y_i^2\right) - \left(\sum_{i=1}^{n} y_i\right)^2}\sqrt{n\left(\sum_{i=1}^{n} \hat{y}_i^2\right) - \left(\sum_{i=1}^{n} \hat{y}_i\right)^2}} \right)^2 \right] \frac{n-1}{n-v-1} \quad (5.15)$$

In Equation (5.15), y is the actual component response from finite element simulation, $\hat{y}$ is the corresponding predicted value by the metamodel, n is the number of data samples which equals 480 in the case study, and v is the total number of regressors. The *Adjusted* R^2 goodness-of-fit measure can take values from 0 to 1, wherein a higher value generally means a better model.

Root Mean Squared Error (RMSE)

It represents the average distance of actual data points from the fitted surrogate model, measured along a vertical line. Compared to other goodness-of-fit measures, such as the *Adjusted* R^2, the *RMSE* is a better goodness-of-fit estimate being more sensitive to occasional large errors in the predicted bridge component response as compared to the actual response. The equation representing the *RMSE* of a fitted surrogate model is presented in Equation (5.16). Additionally, since this goodness-of-fit metric represents an error in prediction, a lesser value generally means a better model.

$$RMSE = \sqrt{\frac{\sum_{i=1}^{n}\left(\hat{y}_i - y_i\right)^2}{n}} \tag{5.16}$$

Symmetric Mean Absolute Percentage Error (SMAPE)

This metric is commonly used in quantitative forecasting methods because unlike other goodness-of-fit strategies it produces a measure of relative overall surrogate model fit to the bridge component response data. This statistical measure of predictive accuracy is calculated by Equation (5.17). Similar to *RMSE*, since *SMAPE* provides an estimate of the error in the model, a lower value is desirable for a better model.

$$SMAPE = \frac{1}{n}\sum_{i=1}^{n}\frac{|\,\hat{y}_i - y_i\,|}{\left(|\,\hat{y}_i\,| - |\,y_i\,|\right)/2} \tag{5.17}$$

5.3.3.3. Comparison of metamodel predictive capabilities

In this sub-section the predictive capabilities of the four different surrogate models are compared using the goodness-of-fit measures after fitting each of the four metamodels to the 480 finite element simulation results for eight different bridge components. This procedure is schematically shown in Figure 5-2(a) where four metamodels are fitted to the seismic response of a particular bridge component and

the three goodness-of-fit estimates are obtained for comparison of the metamodels (Ghosh et al. 2013a).

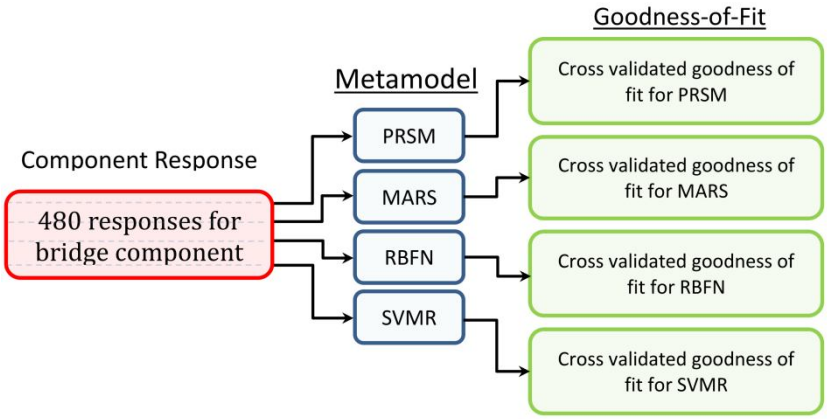

(a)

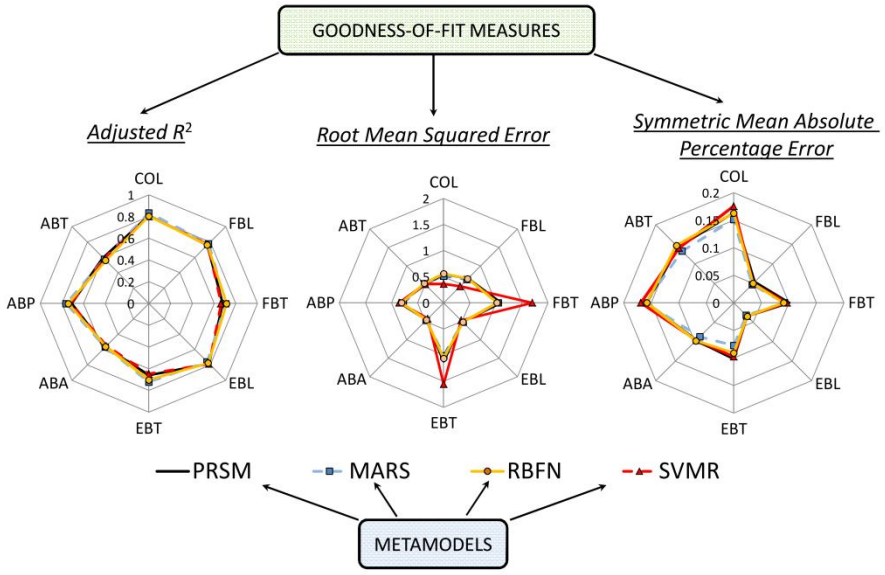

(b)

Figure 5-2: a) Schematic representation of fitting metamodels to 480 responses of a particular bridge component *k* and subsequent comparison of goodness-of-fit estimates, and b) radar plots depicting the comparison of three different goodness-of-fit estimates obtained after fitting the four metamodels to response data of eight different bridge components listed in Table 5.2 (Ghosh et al. 2013a)

Figure 5-2(b) depicts the actual comparison of the predictive capability of the metamodels derived for the eight different bridge components via the goodness-of-fit measures. A closer look into Figure 5-2(b) reveals several interesting trends. First, the radar plot for *Adjusted* R^2 shows a similar trend in the quality of prediction for all of the metamodels for almost all bridge components. For instance, all metamodels result in high values (greater than 0.70) of *Adjusted* R^2 while predicting responses of columns, fixed and expansion bearings in the longitudinal direction, and abutment passive response. For fixed and expansion bearing responses in the transverse direction however, the MARS and RBFN metamodels with high *Adjusted* R^2 (greater than 0.70) are found to perform slightly better than PRSM and SVMR (*Adjusted* R^2 lies between 0.65 to 0.70). For the abutment active and abutment transverse response the performance of all metamodels is almost identical with *Adjusted* R^2 values lying between 0.55 to 0.60. While PRSM, MARS, and RBFN are found to perform similarly while comparing the *RMSE* values in Figure 5-2(b), the comparatively poor predictive capability of SVMR is found to surface again especially when predicting fixed and expansion bearing responses in the transverse directions. This is indicative of occasional large discrepancies between the fitted SVMR predictions and actual component

responses leading to large errors. Comparison of the overall general model fitting metric, *SMAPE* reveals that for almost all bridge components, except abutment passive response, the MARS metamodel performs best and gives the least overall predictive error. For almost all bridge components, RBFN is the second ranking model on the basis of *SMAPE* followed by PRSM. The SVMR metamodel shows inferior performance compared to PRSM, MARS or SVMR. To provide an overall assessment of different surrogate models with respect to their predictive capabilities, average values of the three different goodness-of-fit metrics over the eight bridge components are presented in Table 5.5. The last column of Table 5.5 is the normalized reference index (RI) that is intended to provide a general performance measure by normalizing and scaling (along the appropriate increasing/decreasing direction) and then combining the different goodness-of-fit metrics for the four metamodels (Chou et al. 2011). For instance for the PRSM surrogate model,

$$\begin{aligned} Normalized\ Average\ R^2 &= \frac{0.696 - \min\left(Average\ R^2\right)}{\max\left(Average\ R^2\right) - \min\left(Average\ R^2\right)} \\ &= \frac{0.696 - 0.691}{0.716 - 0.691} \\ &= 0.185 \end{aligned} \tag{5.18}$$

$$Normalized\ Average\ RMSE = \frac{\left|0.719 - \max\left(Average\ RMSE\right)\right|}{\max\left(Average\ RMSE\right) - \min\left(Average\ RMSE\right)} = 0.686 \quad (5.19)$$

$$Normalized\ Average\ SMAPE = \frac{\left|0.106 - \max\left(Average\ SMAPE\right)\right|}{\max\left(Average\ SMAPE\right) - \min\left(Average\ SMAPE\right)} = 0.103 \quad (5.20)$$

$$\text{Reference Index for PRSM} = \frac{(0.185 + 0.686 + 0.103)}{3} = 0.325 \quad (5.21)$$

Table 5.5: Average goodness-of-fit measures and reference indices for the different metamodels under consideration (Ghosh et al. 2013a)

Surrogate Model	Average Adjusted R^2	Average *RMSE*	Average *SMAPE*	Reference Index (RI)
PRSM	0.696	0.719	0.106	0.325
MARS	0.716	0.685	0.097	1.000
RBFN	0.701	0.701	0.104	0.532
SVMR	0.691	0.793	0.107	0.000

Comparison of the presented reference indices, wherein a higher value of RI indicates a better metamodel, reveals that the MARS metamodel with its 'adaptive' model fitting characteristics emerges as the best metamodel. Due to its adaptive nature, the MARS metamodel partitions the sample space and fits a series of models, each of which has a lower error, and then combines them into an ensemble with an overall better performance compared to other metamodels. Moreover, since MARS metamodels do not assume any underlying functional

relationship between the predictor and predicted variables, there is complete flexibility in component response predictions which are not constrained by mathematical rules pertaining to typical underlying model assumptions. The second best surrogate model in this study is RBFN. The ability of this metamodel to generate good predictive response for different bridge components indicates that the implicit metamodel training at the level of the hidden layer of neurons is prominently adequate. Additionally, the radial basis functions chosen for RBFN in this study are the polyharmonic splines. Hence it is not surprising that this metamodel performs well since the nature of these polyharmonic spline radial basis functions can be anticipated to be similar to the adaptive regression splines in MARS metamodel. PRSM surrogate models emerge as the third most favorable while predicting seismic response of critical bridge components. Until now this simplified metamodel has been extensively adopted by researchers to compute reliabilities of civil engineering structures, buildings and bridges alike. While the PRSM metamodel performs reasonably well in the present case study example, comparative goodness-of-fit measures reveal that RBFN and MARS lead to slightly better predictive capabilities and lesser prediction errors. The least favorable metamodeling strategy for component demand prediction of the case study bridge

type is the SVMR metamodel which results in least average *Adjusted* R^2 and highest error estimates in the form of *RMSE* and *SMAPE*. As mentioned earlier, an important criterion for SVMR metamodels to perform satisfactorily is the nonlinear pattern of the data to be easily separable using linear functions in the high dimensional feature space. The poor performance of SVMR with respect to other metamodels may imply that such clear separations using linear functions in a projected space are nonexistent.

5.3.3.4. Comparison of metamodel predictions with benchmark case: Monte Carlo simulations

Since the comparison of metamodels thus far was conducted using 480 data samples generated with a Latin Hypercube design of experiments, a benchmark study is conducted using direct Monte Carlo simulations. Although the task of conducting many Monte Carlo trials is computationally intensive, nonetheless it delivers confidence in proceeding with metamodels for bridge seismic reliability analysis. For Monte Carlo simulation (MCS), 10,000 bridge samples are generated by sampling randomly from the range of parameter estimates p_1 to p_{10} in Table 5.4. This quantity of simulations are found to be more than sufficient to cover 95% of the uncertainty associated with the surrogate models and to generate enough

number of random combinations of earthquake intensities and parameter realizations to cover the entire sample spaces The generated bridge samples are then paired with earthquake records from the ground motion suite selected at random, followed by nonlinear dynamic analysis of each earthquake-structure combination using OpenSees. The generated component responses following finite element analyses (10,000 for each bridge component) are compared with the predicted responses using each metamodel originally fitted to the 480 finite element simulation results as discussed earlier. These comparisons, presented as cumulative density plots of component responses, provide a sound basis for assessment against Monte Carlo analysis by incorporating the uncertainties associated with the sampled ground motions and bridge parameters (Ghosh et al. 2013a). The error in the cumulative density plot between the metamodel predictions and MCS is quantified in this study using the symmetric mean absolute percentage error (*SMAPE*) metric elaborated earlier which is indicative of the overall model fit error. Examples of comparative cumulative density plots for the case study bridge columns and abutment active response are presented in Figure 5-3(a) and (b). These two components are chosen since they reflect the minimum and maximum *SMAPE* values for the top metamodels. The *SMAPE* values for all bridge

components and metamodels are presented in Figure 5-3(c) along with average *SMAPE* estimates across all components for each metamodel.

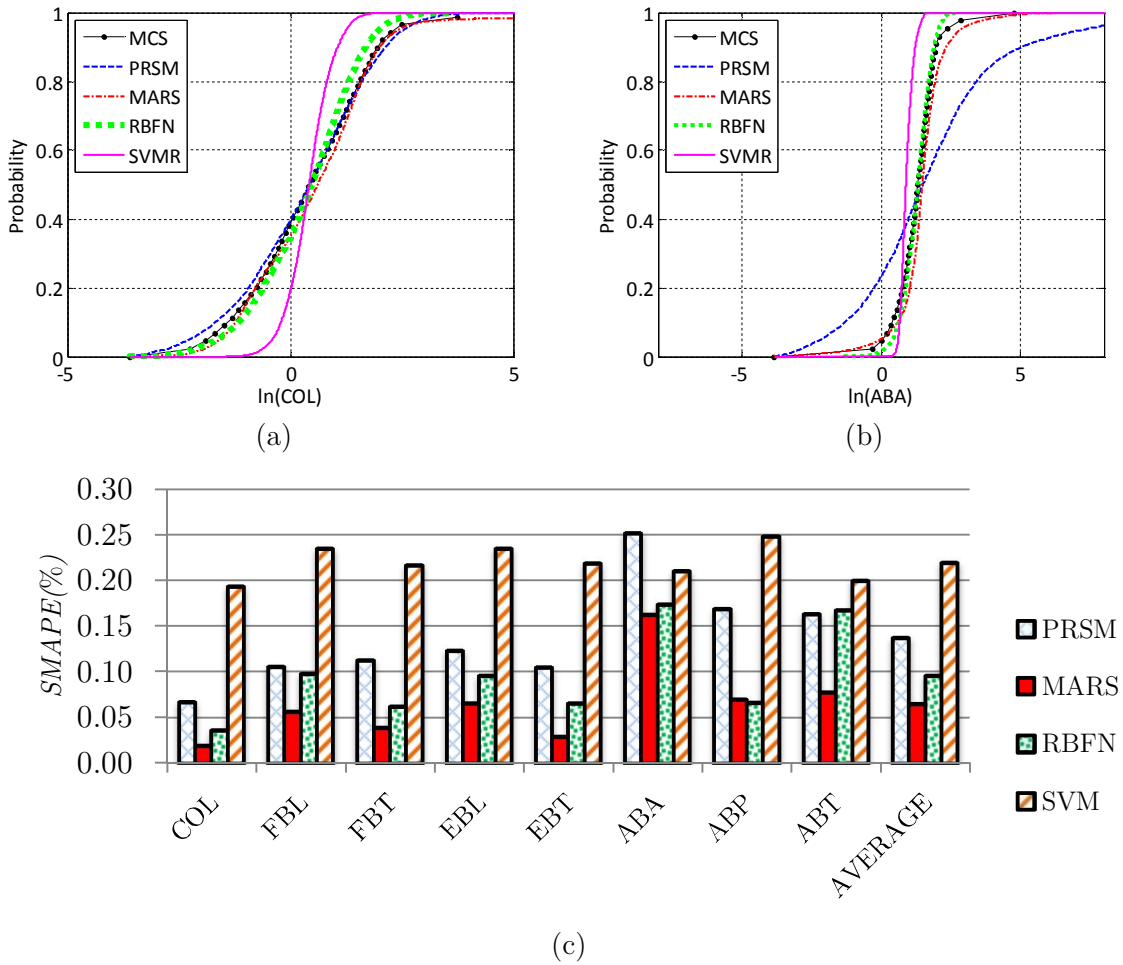

Figure 5-3: Cumulative density plots showing comparison between Monte Carlo simulation results and the surrogate model predictions for a) bridge columns and b) abutment active response, and c) SMAPE results for all bridge components and metamodels with the last table column depicting the average metamodel performances (Ghosh et al. 2013a).

The cumulative density plots and average *SMAPE* comparisons show that the MARS, RBFN and PRSM metamodels provide the least predictive deviations

from Monte Carlo simulation results and emerge as the best metamodels in this study, while the SVMR metamodel is the least favorable. This finding is consistent with the metamodel ranking results is the previous section where the surrogate models were fitted to the 480 component response results from Latin Hypercube design of experiments. It should be recalled that the primary purpose behind developing metamodels for bridge seismic reliability problems is to obtain significant computational efficiency over naïve MCS while maintaining accuracy in predictions. For instance, the 10,000 Monte Carlo simulations required approximately 2,500 hours for completion in a 3.2GHz computer with Intel Xeon processor and 2.4GB RAM. On the other hand, 480 finite element simulations from the Latin Hypercube design took just over 120 hours to complete, demonstrating a gain of over 20 times with respect to computational efficiency when compared with naïve MCS. Training of the metamodels to the component responses from these 480 simulations took negligible computation time, yet yielded reasonably accurate component response predictions. Use of the metamodels can henceforth be conducted real time for rapid generation of component response estimates corresponding to any set of parameter combinations.

5.4. Development of Parameterized Fragility Models Using Logistic Regression

In this section the multi-dimensional surrogate demand models are used in conjunction with logistic regression techniques to develop bridge component and system level parameterized fragility models conditioned on the joint vector $\mathbf{x} = \left\langle S_a, p_1, ..., p_{10} \right\rangle$. The steps involved in constructing such multidimensional fragility functions are detailed below (Ghosh et al. 2013a, 2013b):

Step 1: Generate a large number ($N_{logistic}$) of demand estimates for component m from the corresponding surrogate demand model after randomly combining $N_{logistic}$ sample realizations of parameters in input vector $\mathbf{x}$. Correlations across different bridge components responses are also accounted for while sampling realizations for a particular bridge component m.

Step 2: Sample the same number ($N_{logistic}$) of capacity estimates of the m^{th} bridge component for a particular damage state from the component specific capacity limit state distributions (adopted from Nielson and DesRoches (2007b) and reproduced in Table 4.3).

Step 3: Construct a binary vector of 0's (survival) and 1's (failures) for the m^{th} bridge component corresponding to whether the demand d (from Step 1) exceeds the capacity c (from Step 2) or not. Mathematically, the i^{th} element of this binary vector bin_m corresponding to the m^{th} bridge component can be populated as:

$$bin_{m,i} = \begin{cases} 1 & if\ d_{m,i} \geq c_{m,i} \\ 0 & if\ d_{m,i} < c_{m,i} \end{cases} \tag{5.22}$$

Step 4: Conduct logistic regression using the survive-failure vector binary vector to determine the m^{th} component failure probability model conditioned on S_a and parameters p_1 to p_{10}, as shown in Equation (5.23):

$$PF_{m|S_a,p_1,\ldots,p_{10}} = \left[bin_{m,i} = 1 | IM, p_1, p_2, \ldots, p_{10} \right] = \frac{e^{\theta_{m,0}+\theta_{m,S_a}S_a+\sum_{j=1}^{10}\theta_{m,j}p_j}}{1+e^{\theta_{m,0}+\theta_{m,S_a}S_a+\sum_{j=1}^{10}\theta_{m,j}p_j}} \tag{5.23}$$

where $\theta_{m,0}, \theta_{m,S_a}$ and $\theta_{m,j}$'s (j = 1,2,…10) are the logistic regression coefficients for the m^{th} bridge component. It is noted that $bin_{m,i} = 1$ is a statement equivalent to *Demand>Capacity*, and the above equation is equivalent to Equation (5.2) for the multidimensional fragility estimate, but at the component level.

Step 5: Construct system level binary survive-failure vectors, adopting a series system assumption that failure of any one of the bridge components is indicative of

system failure. This system level model enables the construction of a vector of binary elements (survival/failure) for the bridge system from the binary vector of each of the individual components. For instance, the binary vectors from each of the M bridge components can be arranged in matrix form as:

$$BIN = \begin{bmatrix} \vdots & \vdots & \vdots & \vdots \\ bin_1 & bin_2 & \cdots & bin_M \\ \vdots & \vdots & \vdots & \vdots \end{bmatrix} \tag{5.24}$$

Following the series system assumption, the i^{th} element of the binary vector of the system (bin_{sys}) will equal 1 (representing failure) if at least one elements in the i^{th} row of the matrix BIN equals 1. However, if *all* the elements in the i^{th} row are 0 (representing survival), then the i^{th} element of vector bin_{sys} is also 0. Consequently, logistic regression is carried out to arrive at the system level failure probability with logistic regression coefficients $\theta_{sys,0}$, θ_{sys,S_a} and $\theta_{sys,,j}$'s as shown in Equation (5.25):

$$PF_{sys|S_a,p_1,\ldots,p_{10}} = P\left[bin_{sys,i} = 1 | im, p_1, p_2, \ldots, p_{10}\right] = \frac{e^{\theta_{sys,0}+\theta_{sys,S_a}S_a+\sum_{j=1}^{10}\theta_{sys,j}p_j}}{1+e^{\theta_{sys,0}+\theta_{sys,S_a}S_a+\sum_{j=1}^{10}\theta_{sys,j}p_j}} \tag{5.25}$$

In this study, parameterized component and system level fragility models are developed for the case study MSSS Concrete girder bridge class corresponding

to the MARS metamodel owing to its superior performance relative to the other three surrogate models. Table 5.6 shows the logistic regression coefficients for the eight critical bridge components, while Equation (5.26) presents these coefficients for the 11 dimensional fragility model at the system level for extensive damage state (Ghosh et al. 2013a).

$$PF_{sys|S_a,p_1,\ldots,p_{10}} = \frac{e^{2.87+2.44\ln(S_a)-0.002p_1-0.49\ln(p_2)-0.015\ln(p_3)-0.05p_4+0.006p_5-0.47\ln(p_6)+0.11\ln(p_7)+0.03p_8+0.02p_9-0.04p_{10}}}{1+e^{2.87+2.44\ln(S_a)-0.002p_1-0.49\ln(p_2)-0.015\ln(p_3)-0.05p_4+0.006p_5-0.47\ln(p_6)+0.11\ln(p_7)+0.03p_8+0.02p_9-0.04p_{10}}} \quad (5.26)$$

Table 5.6: Logistic regression coefficients corresponding to multi-dimensional fragility models for critical bridge components of the case study MSSS concrete bridge class under consideration

	Bridge Component							
Logistic Regression Coefficient	**COL**	**FBL**	**FBT**	**EBL**	**EBT**	**ABA**	**ABP**	**ABT**
$\theta_{m,0}$	3.31E+0	-1.05E+0	-1.71E-1	-1.60E+0	-1.36E+0	-6.24E+1	-1.32E+0	-8.46E+0
θ_{m,S_a}	1.99E+0	1.58E+0	2.23E+0	2.33E+0	1.62E+0	1.31E+1	2.56E-1	-3.23E-1
$\theta_{m,1}$	-5.90E-3	4.00E-5	-1.45E-3	1.00E-5	2.10E-4	-1.01E-1	-6.90E-4	-3.01E-3
$\theta_{m,2}$	3.32E-1	-4.91E-2	-7.95E-1	-1.54E-1	-8.80E-1	-2.76E+1	-1.03E+0	4.59E-1
$\theta_{m,3}$	1.15E-2	-3.70E-2	-2.90E-2	-4.10E-3	2.05E-2	-1.93E+1	-9.99E-3	-1.67E-1
$\theta_{m,4}$	-2.12E-1	1.45E-1	-1.98E-2	1.37E-2	4.86E-2	-9.88E+0	-5.08E-2	4.47E-1
$\theta_{m,5}$	3.52E-2	-1.10E-1	-5.28E-2	-3.77E-2	1.44E-1	-3.97E+0	-1.26E+0	6.08E-1
$\theta_{m,6}$	6.98E-2	-2.88E-1	-6.97E-1	-2.08E-1	-6.59E-1	8.94E+0	-1.10E-1	1.42E+0
$\theta_{m,7}$	7.94E-3	4.63E-2	2.74E-1	1.87E-1	1.83E-2	4.31E+0	-7.19E-2	-6.25E-1
$\theta_{m,8}$	3.97E-2	3.28E-2	-6.97E-3	3.10E-2	1.75E-3	-2.04E+1	1.02E-1	-1.91E-1
$\theta_{m,9}$	5.38E-3	-2.81E-3	3.24E-2	2.29E-2	3.31E-2	1.50E-1	3.62E-3	1.11E-3
$\theta_{m,10}$	3.93E-3	-4.39E-2	-2.94E-2	-2.15E-2	-2.53E-2	1.25E+1	-2.46E-1	-2.85E-1

The parameterized component and system level fragility models presented in this study have several advantages over 'classical' fragility curves conditioned only upon the ground motion hazard intensity. Firstly, the seismic vulnerability of bridge component or system given the value of S_a can be found by simple substitution of parameters in the above equations if point estimates of the bridge parameters p_1 to p_{10} are available. Secondly, the sensitivity of fragility estimates to a specific parameter or combination of different parameters can be studied by varying them while holding the remaining ones constant. Finally, for a particular bridge with specific geometry (constant values of p_8 to p_{10}) if some, or all, of the remaining parameters p_1 to p_7 are probabilistic in nature, one may estimate the 'classical' one dimensional fragility curve (conditioned only on the earthquake intensity) by integrating over the domain of the statistical uncertainties of the parameters (Ghosh et al. 2013b). This multi-dimensional integration strategy is demonstrated in Equation (5.27) and assumes statistical independence between the predictor variables p_1 to p_7.

$$PF_{sys|S_a} = \int_{p_1}\int_{p_2}\cdots\int_{p_7} \frac{e^{\theta_{sys,0}+\theta_{sys,S_a}S_a+\sum_{j=1}^{7}\theta_{sys,j}p_j+\theta_{sys,8}p_8^{sp}+\theta_{sys,9}p_9^{sp}+\theta_{sys,10}p_{10}^{sp}}}{1+e^{\theta_{sys,0}+\theta_{sys,S_a}S_a+\sum_{j=1}^{7}\theta_{sys,j}p_j+\theta_{sys,8}p_8^{sp}+\theta_{sys,9}p_9^{sp}+\theta_{sys,10}p_{10}^{sp}}} f(p_1)\ldots f(p_7)dp_1\ldots dp_7 \quad (5.27)$$

where, p_8^{sp}, p_9^{sp}, and p_{10}^{sp} are the bridge specific column height, mid-span length and number of columns respectively, and $f(p_1)$, …, $f(p_7)$ are the associated probability density functions of parameters p_1, …, p_7 respectively.

To demonstrate the multi-dimensional integration methodology and obtain "classical" fragility curves, a specific geometric configuration of the case study bridge is chosen with 3 columns per bent, each 5m high, and a mid-span length of 30m. The probability distributions of the remaining critical bridge modeling and deterioration affected structural parameters (p_1 to p_7) are presented in Table 5.7. Figure 5-4 depicts the component and system level "classical" fragility curves conditioned only on the ground motion hazard intensity (S_a) obtained after integration of the fragility function following Equation (5.27).

Table 5.7: Probability distributions of parameters p_1 to p_7 required for demonstrating the multi-dimensional integration methodology. The means and coefficient of variations of the lognormally distributed variables are reported in the lognormal space.

Parameter	Distribution Type	Distribution Mean	COV
p_1	Lognormal†	463.00	0.08
p_2	Lognormal†	1.00	0.10
p_3	Uniform†	2.54	0.10
p_4	Lognormal‡	3.68	0.10
p_5	Lognormal‡	2.81	0.10
p_6	Uniform‡	3.05	0.10
p_7	Lognormal‡	5.08	0.10

† Adopted from Nielson (2005), ‡ Adopted from Ghosh and Padgett (2010, 2012)

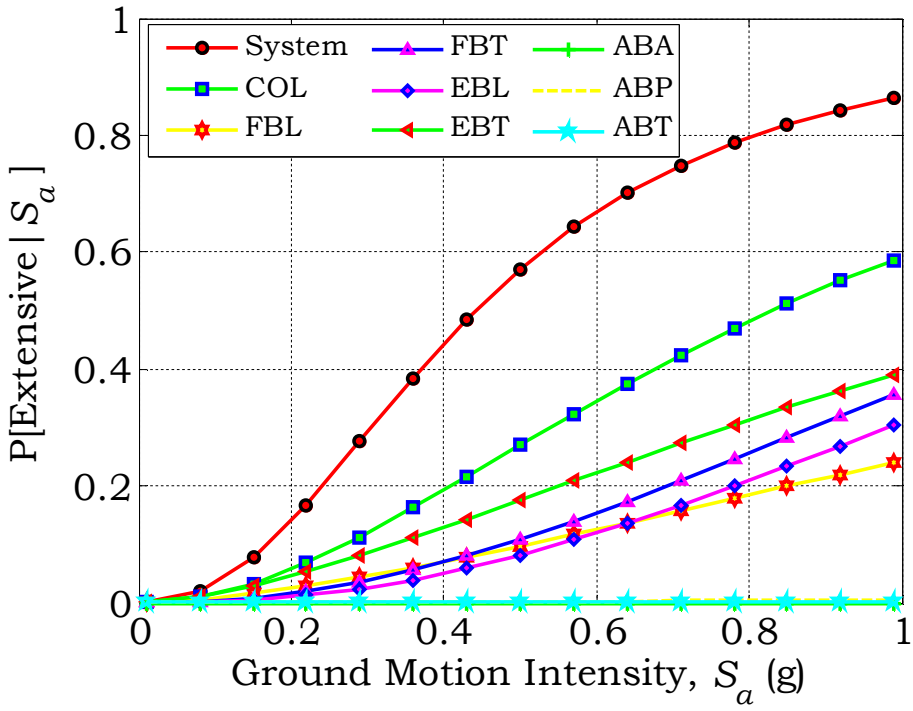

Figure 5-4: Traditional component and system level fragility curves obtained after multi-dimensional fragility models at bridge component and system level

The demonstrated multidimensional integration strategy is conducted using the mean estimates of the logistic regression coefficients reported in Table 5.6. Additionally, it is possible to compute the confidence bounds about the fragility estimates using the standard error of the mean coefficient estimates. An instance of the confidence bounds at the bridge system level is presented in Figure 5-5. In general, for all practical purposes and through the remainder of this thesis only the mean estimates of the logistic regression coefficients will be employed. Overall, the

parameterized fragility models presented in this study enables precise predictions of bridge specific seismic reliabilities with negligible computational cost. Additionally, these parameterized fragility models may be incorporated within regional risk assessment framework packages like HAZUS (FEMA 2003) for efficient computation of bridge specific reliabilities while incorporating their in-situ field condition.

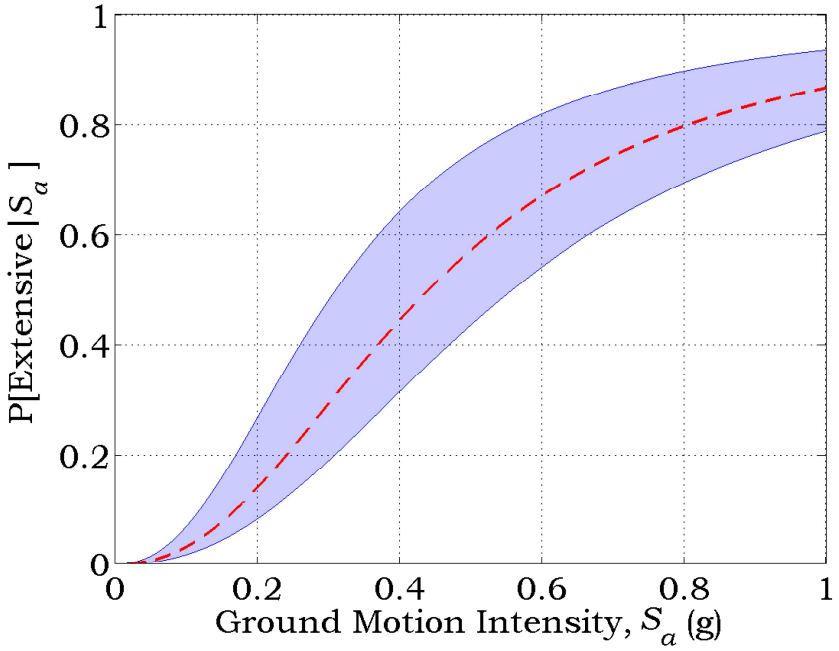

Figure 5-5: Confidence bounds of uni-dimensional system level fragilities after incorporating the standard error of the logistic regression coefficient estimates

5.5. Dimensionality Reduction and Failure Surface Visualization

The results in the previous sections have demonstrated that surrogate models can accurately and efficiently predict seismic demand of critical bridge components thereby enabling efficient reliability assessment and development of parameterized fragility models. This section will focus on the validity of applying metamodels to bridge seismic reliability problems by inspecting the shape of the failure domain (Ghosh et al. 2013a). Since prior studies have suggested potential limitations of applying metamodels for approximating limit state functions when non-smooth failure surfaces exist in hypothetical examples (Guan and Melchers 2001), this section of the study inspects if the same is true for limit state functions of bridge components under seismic excitation.

A common challenge faced by researchers is the lack of failure surface visualization tools for high dimensional limit state functions (with more than three dimensions). This problem also exists in this case study example since the adopted metamodels are 11-dimensional corresponding to the size of vector $\mathbf{x} = \{S_a, \mathbf{p}\}$. To overcome this difficulty, this research adopts the dimensionality reduction method

introduced by Hurtado (2012) which provides a simple yet powerful technique to visualize failure surfaces of multi-dimensional reliability problems reduced to only two dimensions. While this technique has been demonstrated for several benchmark problems (Hurtado 2012), dimensionality reduction methods applied to bridge reliability problems are lacking in the literature and is introduced for the first time in this study. While details of the adopted technique can be found in Hurtado (2012), the following steps outline the dimensionality reduction methodology specific to multi-dimensional bridge reliability problems.

Step 1: Formulate the limit state equation for a particular bridge component as:

$$lsf(\mathbf{x}) = c - d(\mathbf{x}) \tag{5.28}$$

where, $lsf(\mathbf{x})$ is the component limit state function, c is the component capacity, and $d(\mathbf{x})$ is the component demand equivalent to the component specific surrogate demand model. The capacity estimates c may also be considered as a function of vector **x,** however for simplicity, the probabilistic capacity estimates for different bridge components proposed by Nielson and DesRoches (2007a) are adopted in this study. While the MARS metamodel should ideally be adopted to approximate the demand function due to its superior performance compared to other metamodels, it

suffers from lack of continuity across the sample space domain and is difficult to differentiate with respect to the parameters in vector **x** (required for step 3). Hence, in this example the polynomial response surface metamodel (PRSM), which approximates component response reasonably well, is used given its mathematically explicit form of the demand model and ease of differentiability. Future studies on this topic will investigate failures surface visualizations using MARS and other metamodels used in this research. The limit state function developed using the capacity distributions and PRSMs in this step aids in the computation of the design point vector as outlined in step 2.

Step 2: Compute the design point vector $\mathbf{x}^*$ at which the limit state function *lsf*(**x**) is minimum. This step can be achieved using the classical Hasofer and Lind algorithm (1974) or any appropriate constrained nonlinear optimization problem solver. Table 5.8 shows the design vector $\mathbf{x}^* = \left\langle S_a^*, p_1^*, ..., p_{10}^* \right\rangle$ corresponding to the different bridge components for the case study bridge class. The design point vector developed herein aids estimating the vector to the center of mass of the failure domain in the next step.

Table 5.8: Vector of design points in the physical space for different bridge components at which the value of the limit state function is minimum

Component	S_a^*	p_1^*	p_2^*	p_3^*	p_4^*	p_5^*	p_6^*	p_7^*	p_8^*	p_9^*	p_{10}^*
COL	0.30	279.58	0.55	0.43	3.17	2.94	0.79	0.68	3.89	13.12	2
FBL	0.11	299.62	0.30	0.21	3.60	1.79	0.18	0.68	4.57	27.19	4
FBT	0.32	322.55	0.02	0.34	3.37	2.03	0.90	0.91	3.87	13.90	4
EBL	0.26	324.12	0.07	0.30	3.88	2.27	1.83	0.68	3.37	16.56	4
EBT	0.23	329.23	0.05	0.29	2.57	2.83	0.73	1.39	4.07	30.02	3
ABA	0.13	397.38	0.16	0.37	3.68	2.69	0.59	1.21	4.79	24.21	4
ABP	0.37	387.04	0.12	0.34	3.92	2.61	0.75	1.96	5.40	10.88	2
ABT	0.09	409.45	0.28	0.20	4.01	3.12	0.28	0.82	4.92	19.70	3

Step 3: Compute the vector $\boldsymbol{w}$ to the center of mass of the failure domain as:

$$\mathbf{w} = -\frac{\nabla lsf(\mathbf{x}^*)}{|| \nabla lsf(\mathbf{x}^*) ||} \tag{5.29}$$

where $\nabla lsf(\mathbf{x}^*)$ is the value of the gradient of the limit state function evaluated at the design point. The vector $\mathbf{w}$ developed in this step is used henceforth to develop the nonlinear transformation vectors to represent the clustering of samples in a reduced space.

Step 4: Choose random vectors across the range of input parameter space and classify as 'safe' [$c > d(\mathbf{x})$] or 'failure' [$c < d(\mathbf{x})$] samples. This step is achieved in two stages. In the first stage random realizations of parameters S_a, p_1 to p_{10} are drawn and paired to constitute vectors in the multi-dimensional sample space. Let $\mathbf{x}^r$

represent one such random vector which is then used to compute the nonlinear transformations in the reduced two dimensional space as:

$$\mathbf{v}_1^r = \| \mathbf{x}^r \| \tag{5.30}$$

$$\mathbf{v}_2^r = \cos \angle(\mathbf{x}^r, \mathbf{w}) \tag{5.31}$$

In the second stage, along with $\mathbf{v}_1^r$ and $\mathbf{v}_2^r$, an indicator variable ind^r is maintained to classify if the chosen random vector $\mathbf{x}^r$ belongs to the 'safe' (represented by 0) or 'failure' (represented by 1) domain as:

$$ind^r = \begin{cases} 1 \text{ if } c - d(\mathbf{x}^r) < 0 \\ 0 \text{ if } c - d(\mathbf{x}^r) > 0 \end{cases} \tag{5.32}$$

Step 5: Conduct step 4 (Equations (5.30) to (5.32)) N_{MC} = 10,000 times in a Monte Carlo sequence, each time choosing a different random vector $\mathbf{x}^r$ to obtain N_{MC} sets of realizations of vectors $\langle \mathbf{v}_1^r, \mathbf{v}_2^r \rangle$ and indicator functions ind^r. Graphing the vectors $\langle \mathbf{v}_1^r, \mathbf{v}_2^r \rangle$ in the two dimensional sample space while accounting for the 'safe' or 'failure' indicators yields a visualization of the multi-dimensional failure surface in two dimensions.

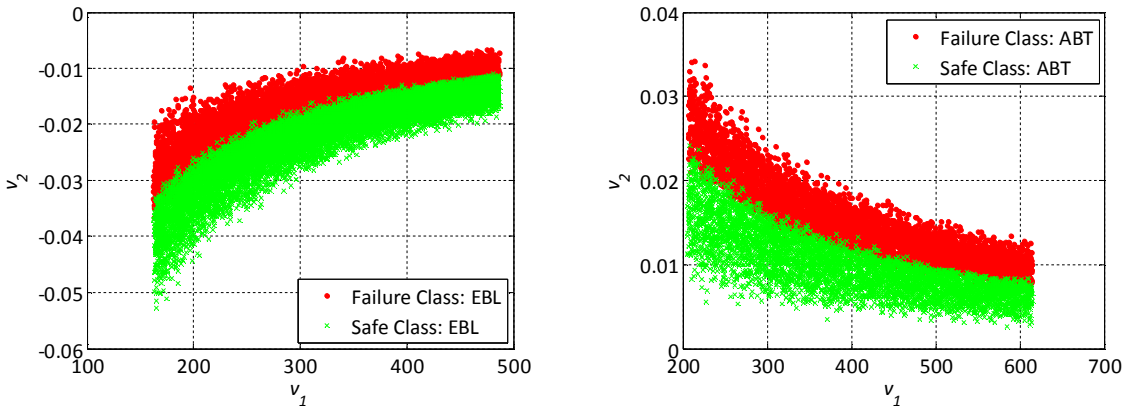

(a) (b)

Figure 5-6: Two dimensional failure surface of a) expansion bearings in the longitudinal direction and b) abutment transverse response after dimensionality reduction of multi-dimensional surrogate demand models (Ghosh et al. 2013a)

Following Steps 1-5, two dimensional failure surfaces are constructed for all bridge components. Figure 5-6(a) and (b) represent two such failure surfaces for bridge expansion bearings in the longitudinal direction and abutments in the transverse direction. These figures are developed after reducing the 11-dimensional response surface to two dimensions in order to inspect the smoothness of the failure surface and the applicability of surrogate demand models for approximating limit state functions. It is evident from Figure 5-6(a) and (b), and also similar surfaces developed for other bridge components but not reproduced here, that a 'smooth' demarcation with low curvatures exists between safe and failure domains. Such smooth surfaces, characterized by lack of sudden discontinuity, validate the applicability of the proposed surrogate demand models in approximating the bridge

component limits states and seismic responses for the range of parameters considered. Thus, this research has confirmed two important features pertaining to bridge reliability predictions using metamodels: 1) the ability of metamodels to efficiently and accurately predict seismic demand of bridge components given the input parameter realizations, and 2) the applicability of metamodels to approximate high dimensional limit states due to smoothness of the failure domain for bridge components.

5.6. Network Level Application Example: South Carolina Bridge Transportation Network

The primary purpose of this application example is to demonstrate the potential of parameterized fragility models to incorporate data available from field instrumentation of highway bridges and efficiently compute their in-situ reliability in aging transportation networks. Such fragility estimates of individual bridges in an aging transportation network can be used to achieve objectives such as computation of network reliability or risk-ranking of bridges for retrofit prioritization (Ghosh et al. 2013b; Rokneddin et al. 2013). Most of the recent aging bridge reliability work, such as those included in Chapters 2 and 4 tends to rely

upon historical evidence of deterioration parameters available in region-specific databases or on limited laboratory test data. Such estimates may lead to potential under-or-overestimation of bridge fragilities because most environmental degradation mechanisms such as corrosion deterioration are not static processes, but influenced by changes in the atmosphere, such as temperature and moisture content, amongst others (Stewart 2004; Moncmanová 2007). The primary reasons behind depending on such historical databases are the expensive and labor intensive procedures associated with the field instrumentation of bridges which makes it impractical to obtain sensor measurements of every bridge in an aging transportation network. Spatial interpolation techniques may address this issue by approximating deterioration parameters at non-instrumented bridge locations from nearby instrumented bridges in the network. While these spatial interpolation techniques have been used to predict deterioration parameters across a single bridge (Gassman and Tawhed 2004), such applications are lacking with respect to predictions across a portfolio of highway bridges distributed over a region. The interpolated or instrumented deterioration parameters can then be used to assess individual aging bridge fragilities across the network after updating the historical deterioration parameters using Bayesian methodologies. These updated

deterioration parameters can be used to compute the level of deterioration of bridge structural parameters which will eventually inform the parameterized fragility models to compute in-situ bridge reliability estimates. The following subsections will describe the bridge network and bridge classes under consideration along with demonstration examples of spatial interpolation techniques, Bayesian updating methodology, and scenario specific reliability assessment of bridges using parameterized fragility models.

5.6.1. Description of the case study bridge network and aging bridge classes

Figure 5-7 shows the case study highway bridge network in South Carolina, USA, consisting of a total of 509 highway bridges of nine different bridge classes categorized according to structure, material properties, and construction type (Table 5.9). The bridge inventory is obtained from the National Bridge Inventory (FHWA 2010) and integrated with the GIS map of the region's roadways from TELEATLAS (2010). The majority of these bridges do not include seismic detailing, and are also prone to the adverse effects of aging and deterioration given their age and proximity to the sea. A primary degrading agent, as elaborated in earlier chapters, is airborne marine chlorides from the adjoining sea coast leading

to corrosion deterioration of both exposed and embedded steel members. Two different marine exposure conditions are considered in this study based on proximity to sea coast: a) marine splash zone for bridges located within10m from the sea coast, and b) marine atmospheric exposure for other bridges. The case study network shows 30 out of the 509 bridges to be in the marine splash zone.

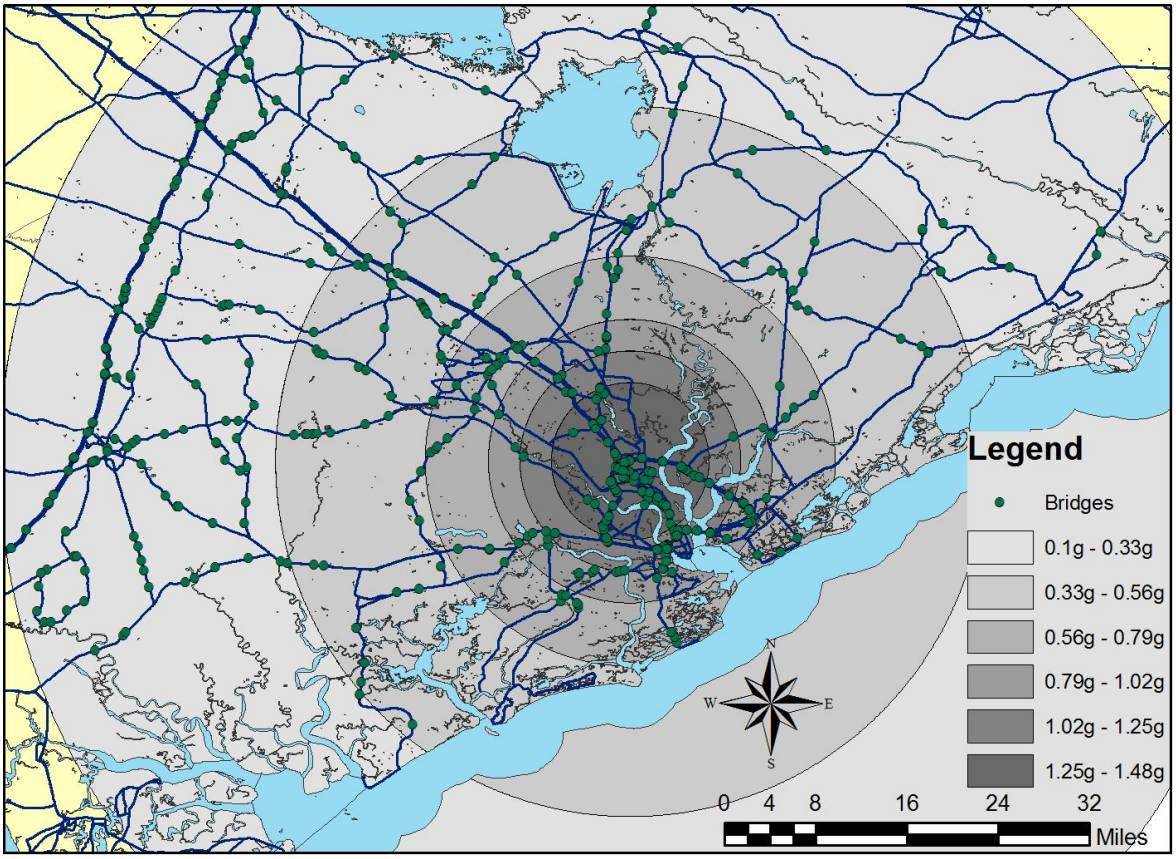

Figure 5-7: The case study area in the South Carolina transportation network showing bridge locations and PGA contours resulting from the selected seismic scenario (Rokneddin et al. 2013)

Table 5.9: Inventory of bridges in the case study transportation network showing the different classes

Bridge Classes	Number
MSSS Slab	159
MSSS Steel Girder	123
MSSS Concrete Girder	117
MSC Steel Girder	38
MSC Slab	17
SS Concrete	19
SS Steel	19
MSC Concrete Box Girder	15

MSC = Multi-span continuous, MSSS = Multi-span simply supported, SS = Simply supported

Along with the highway bridge locations, Figure 5-7 also shows the peak ground acceleration (PGA) contours resulting from a strong ground motion scenario of $M_w = 7.3$, based on the largest contributing event to the 10% exceedance probability in 50 years seismic de-aggregation map of the region (USGS 2010). The event's epicenter coincides with the epicenter of the historic 1886 Charleston earthquake, which is 20km away from the center of Charleston. The PGA contours are computed using HAZUS-MH MR4 (FEMA 2009) with the weighted average of four attenuation relationships for central and eastern US. The case study network lies in the greater Charleston area and includes bridges and roads along freeways, highways, and main roads encompassing the counties of Charleston, Berkeley, Orangeburg, Dorchester, and Colleton between Interstate-95

and the Atlantic Ocean. The objective herein is to compute the failure probabilities of each bridge within the network for the scenario earthquake using parameterized fragility models for different bridge classes and in-situ bridge conditions following spatially interpolation and statistical updating of deterioration parameters.

5.6.2. Spatial interpolation of deterioration parameters

Accurate estimates of aging highway bridge fragilities for all bridges in the network require up to date information on deterioration parameters at all bridge locations. Since it is impractical to field-monitor every bridge in the transportation network, spatial interpolation techniques are employed to estimate the values of deterioration parameters for non-instrumented bridges from data made available by a limited number of instrumented bridges. While several interpolation procedures are available in spatial data analysis, this study employs Kriging (Krige 1951), a widely popular method in the field of geostatistics. Although several strategies such as polynomial fittings, trend surface analysis, etc. exist for spatial interpolation, Kriging has several clear advantages over these methods. First, Kriging incorporates the correlation structure among observations while making predictions at unobserved locations. Second, while methods such as trend surface analysis can be significantly affected by the location of data points and produce extreme

fluctuations in predicted estimates in sparse areas, Kriging predictions are more stable over sparsely sampled regions (Mackaness and Beard 1993). However, user discretion is recommended with respect to using Kriging for spatial interpolation when localized effects or other discontinuities are present in the spatial process. Under such circumstances, the Kriging procedure is known to perform poorly and use of alternative spatial interpolation techniques, such as Bayesian Partition Modeling is recommended. It is assumed in this study that sudden discontinuities are non-existent for deterioration parameters distributed across a region and hence the Kriging procedure is adopted.

Since field instrumentation of bridges is considered to be an expensive and labor intensive procedure in practice, the number of bridges chosen for demonstration as 'field instrumented' is restricted to 100 out of the total 509 bridges in the case study network. The number of the sample points is consistent with the findings of Webster and Oliver (2008) and Trauth et al. (2010), who recommend a minimum of 100 sample points for the construction of an appropriate variogram. Field instrumentations at each of the 100 bridge locations are assumed to gather data for the following deterioration parameters which have been shown earlier (Chapter 3) as critical in affecting the corrosion deterioration of bridge

components: 1) Surface chloride concentration (C_s), 2) Chloride diffusion coefficient (D_c), and 3) Corrosion rate (r_{corr}). Along with the concrete cover depth, these parameters are the key elements used to predict the corrosion initiation time and rate of area loss of steel. Following other corrosion deterioration studies (Enright and Frangopol 1998, 1999), the deterioration parameters at monitored bridge locations are assumed to follow lognormal distributions with hypothetical mean values assigned from the range of estimates reported in Table 5.10 (based on actual field measurements reported in literature) for the two deterioration zone exposure conditions. Additionally, based on available studies, the coefficient of variation (δ) of the distribution for both C_s and D_c is assumed to be 0.5 (Suzuki et al. 1990; Vu and Stewart 2000), while δ corresponding to r_{corr} lies between 0.14-0.33 (Thoft-Christensen 1995; Frangopol et al. 1997; Val et al. 1998; Vu and Stewart 2000).

The following paragraphs will now outline the main steps involved in the Kriging procedure to exploit the data from the limited number of instrumented locations and spatially interpolate across all bridges in the network.

Table 5.10: Range of mean values of deterioration parameters assigned to instrumented bridges and used for Kriging

Deterioration Parameter	Exposure Condition	Range of Parameter Estimate	Unit
C_s	Marine Splash	3.74 – 5.54[a]	% weight of cement
	Marine Atmospheric	0.43 – 2.22[b]	% weight of cement
D_c	Marine Splash	2.13 – 4.66[c]	10^{-12} m^2/sec
	Marine Atmospheric	4.41 – 4.91[d]	10^{-12} m^2/sec
r_{corr}	Marine Splash	0.22– 0.38[e]	mm/year
	Marine Atmospheric	0.05 – 0.10[e]	mm/year

[a]Funahashi (1990) [b]Uji et al. (1990) [c]Funahashi (1990) and Liam et al. (1992)
[d]Mustafa and Yusof (1994) [e]Zen (2005)

Step 1: Construct an experimental variogram (called semivariance) which provides an estimate of the squared difference between instrumented values of deterioration parameters relative to their separation distances of the respective monitored bridge locations as follows:

$$\gamma\left(h\right) = 0.5\left(z_l - z_{l+h}\right)^2 \tag{5.33}$$

where $\gamma(h)$ is the semivariance, z_l and z_{l+h} are the instrumented deterioration parameter values at bridge location l and another location separated by distance h (also called 'lag interval') from l.

Step 2: Derive a variogram estimator, $\gamma_E(h)$, which summarizes the central tendency of observations at different instrumented bridge locations. The form of the variogram estimator is typically given by:

$$\gamma_E\left(h\right) = \frac{1}{2 * N\left(h\right)} \sum_{i=1}^{N(h)} \left(z_{l_i} - z_{l_i+h}\right)^2 \tag{5.34}$$

where $N(h)$ is the number of pairs within the lag interval h. Next, a parametric curve called the variogram model is fitted to approximate the variogram estimator with the most appropriate mathematical representation. Due to theoretical constraints, only functions satisfying certain mathematical characteristics can be used as variogram models. The most prevalently used variogram models include the spherical model, exponential model, and linear models (Trauth et al. 2010). Following the goodness of fit test results corresponding to these traditionally adopted variogram models, the exponential model with nugget effect is employed in this study. The form of this exponential variogram model is given as:

$$\gamma_{exp} = n_g + s\left(1 - e^{-\frac{3h}{a}}\right) \tag{5.35}$$

where, n_g is the nugget, s is the sill and a is the range. In the variogram model, n_g is the intercept of the variogram and represents the sub-grid scale variations, s

equals the total variance of the data set representing the value of the semivariance as lag h goes to infinity, and a controls the degree of correlation between the data points (Cressie 1993; Myers 1997; Reimann 2008).

The variogram model fitting procedure is exemplified in Figure 5-8 for surface chloride concentration C_s, revealing that the spatial process is correlated over short distances while there is little spatial dependency for separation distances beyond 8km (the "range" of the variogram). While the present case study uses only 100 out of 509 bridges for field instrumentation, the level of spatial dependency and the range of the variogram can be improved by increasing the number of instrumented bridges within the network. This further highlights the importance of instrumenting sufficient number of bridges within the network to obtain confident predictions. It is noted that the fitted variogram in Figure 5-8 results from one realization of the lognormal distribution for C_s at instrumented bridge locations, and therefore, the predicted estimates at the unobserved locations (calculated in step 3) are only point estimates of C_s.

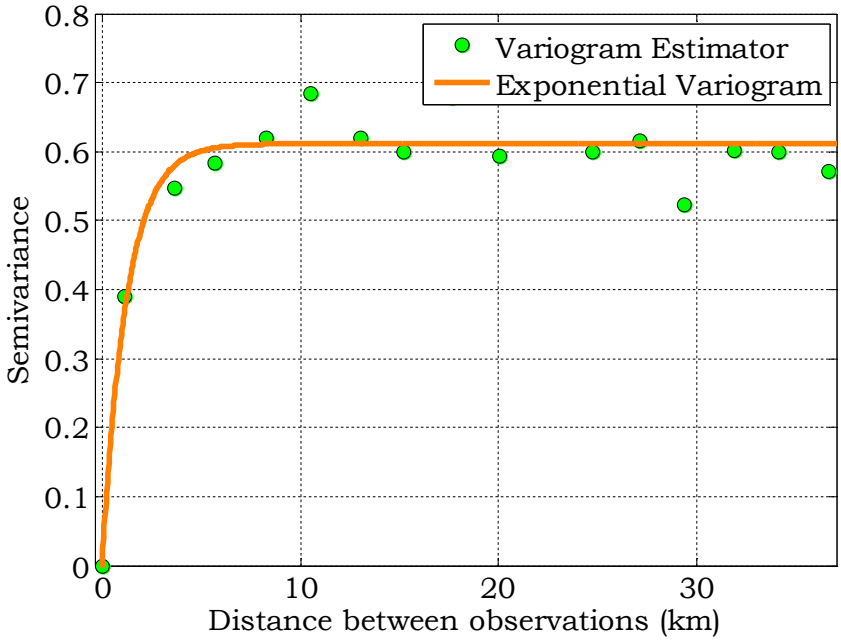

Figure 5-8: Exponential variogram for Kriging of surface chloride concentration across the network (Rokneddin et al. 2013)

Step 3: Use the exponential variogram model γ_{exp} to spatially interpolate deterioration parameters through Kriging which uses a weighted average of neighboring point observations to estimate values at unobserved locations. The weighting points λ_i's required for the interpolations are computed as:

$$\begin{pmatrix} \lambda_1 \\ \vdots \\ \lambda_t \\ \mu \end{pmatrix} = \begin{bmatrix} \gamma_{\exp}(l_1,l_1) & \cdots & \gamma_{\exp}(l_1,l_t) & 1 \\ \vdots & \ddots & \vdots & \vdots \\ \gamma_{\exp}(l_t,l_1) & \cdots & \gamma_{\exp}(l_t,l_t) & 1 \\ 1 & \cdots & 1 & 0 \end{bmatrix}^{-1} \begin{bmatrix} \gamma_{\exp}(l_1,l^*) \\ \vdots \\ \gamma_{\exp}(l_t,l^*) \\ 1 \end{bmatrix} \tag{5.36}$$

where, $\gamma_{exp}(l_i,l_j)$ represents the exponential variogram estimate between the points l_i and l_j, l^* is the non-instrumented bridge location where the interpolation estimates

of deterioration parameters are desired, t is the total number of instrumented bridge locations (100 in this case) and μ is the Lagrange multiplier used to minimize the Kriging error and satisfy the unbiasedness condition $\sum_{i=1}^{n} \lambda_i = 1$. Computation of λ_i's is followed by estimation of the deterioration parameter z_{l^*} at location l^* from Equation (5.37). It is noted that z_{l^*} denotes the mean of the Kriging estimate for deterioration parameter at the interpolated non-instrumented bridge location.

$$z_{l^*} = \begin{pmatrix} \lambda_1 & \cdots & \lambda_t \end{pmatrix} \begin{pmatrix} z_{l_1} \\ \vdots \\ z_{l_t} \end{pmatrix} \tag{5.37}$$

Although not considered in this study, the uncertainty associated with this interpolated estimate can also be quantified using Kriging variance. The variability about the mean estimate is captured to a certain extent in this study by repeating the Kriging procedure N_{krig} times for many samples from the parent distribution of the deterioration parameters at the instrumented bridge locations using a Monte Carlo scheme. Figure 5-9 demonstrates this approach of repeated sampling and Kriging interpolation across the region to determine the distribution of r_{corr} at the specified unobserved bridge location. The same procedure applies to

form the probability distributions of other deterioration parameters (D_c and r_{corr}). Both field acquired and estimated probability distributions of the deterioration parameters for all network bridges are regarded as new measurements, and are combined with historical estimates of deterioration parameters through Bayesian updating as discussed in the next section.

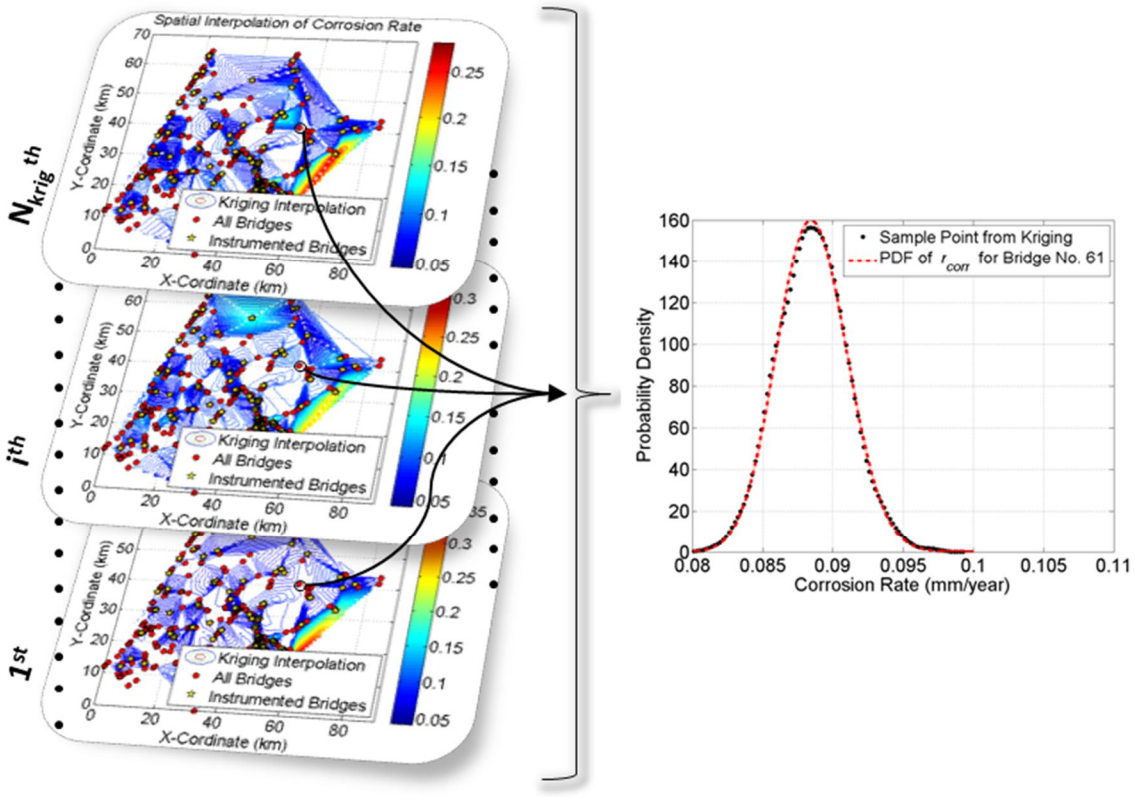

Figure 5-9: Repeated spatial interpolation of corrosion rate across the 509 bridge network using a Monte Carlo approach after drawing samples from the distribution of corrosion rate at instrumented bridge locations (Rokneddin et al. 2013)

5.6.3. Bayesian updating of deterioration parameters

The Bayesian updating technique provides a rational statistical approach to integrate the new information available from field instrumentation and historically available data from previous knowledge or experience to obtain more accurate probabilistic models of bridge conditions. The general Bayesian updating procedure is presented in Equation (5.38):

$$p\left(\varphi|\kappa\right) = \frac{q\left(\kappa|\varphi\right)p(\varphi)}{\int_{-\infty}^{\infty} q\left(\kappa|\varphi\right)p(\varphi)d\varphi} \tag{5.38}$$

where $p(\varphi|\kappa)$ is the updated posterior distribution of the deterioration parameter based on historical data and new inspection results, $p(\varphi)$ is the prior distribution of the deterioration parameter $\varphi \in \Phi$ based on historical records from region specific databases (for instance, Federal Highway Administration reports), and $q(\kappa|\varphi)$ is the likelihood function in which $\kappa \in \mathrm{K}$ is a random variable representing new deterioration parameter from field instrumentation data or spatial interpolation. While the general formulation for Bayesian updating is presented above, closed form solutions exist for typical distribution types (such as normal distributions), which relaxes the computational complexity of the updating procedure (Ang and Tang 2007). This is particularly helpful in the statistical updating of aging

parameters under consideration since they are typically lognormal and can be readily transformed to the corresponding normal distribution. For instance, if in the normal space, the mean and standard deviations of the historical distribution and the field instrumented distribution of a deterioration parameter be represented by $N(\mu,\sigma)$ and $N(\mu',\sigma')$ respectively, then the statistically updated posterior distribution also follows a normal distribution with parameters $N(\mu'',\sigma'')$ calculated using the following equations:

$$\mu'' = \frac{\mu(\sigma')^2 + \mu'(\sigma)^2}{(\sigma')^2 + (\sigma)^2} \tag{5.39}$$

$$\sigma'' = \sqrt{\frac{(\sigma')^2(\sigma)^2}{(\sigma')^2 + (\sigma)^2}} \tag{5.40}$$

The distribution of deterioration parameters representing "new information" constitute the likelihood function distribution at all bridge locations and are obtained after field instrumentation or spatial instrumentation of instrumented data, as elaborated in the preceding section. In this study, historical estimates of lognormal distributions of C_s and D_c, representing the prior distribution, are assumed to have mean values equal to the central values of the ranges outlined in Table 5.10 and the same coefficient of variation (δ) of 0.5. Additionally, the prior

historic distributions of r_{corr} are obtained as a function of cover depth and water-cement ratio based on the equation proposed by Vu and Stewart (2000). Table 5.11 reports the mean values of prior distributions of the corrosion deterioration parameters considered in this study.

Table 5.11: Mean values of prior distributions of deterioration parameters representing historically available information

Deterioration Parameter	Exposure Condition	Prior Mean	Unit
C_s	Marine Splash	4.64[f]	% weight of cement
	Marine Atmospheric	1.33 [f]	% weight of cement
D_c	Marine Splash	3.50 [f]	10^{-12} m^2/sec
	Marine Atmospheric	4.66 [f]	10^{-12} m^2/sec
r_{corr}	Marine Splash	Function of bridge age, cover depth and water-cement ratio (Vu and Stewart 2000)	mm/year
	Marine Atmospheric		mm/year

[f]Central value of ranges reported in Table 5.10

Figure 5-10 shows an example of results of updating the lognormally distributed chloride diffusion coefficient, deriving a posterior estimate of D_c that incorporates both historic knowledge and field measurement data. The posterior distribution parameters are obtained after using Equations (5.39) and (5.40) with the parameters from the historical and field measured distributions, also shown in Figure 5-10. Updated estimates of the deterioration parameters aid in determining

the extent of deterioration of bridge structural members which eventually inform aging bridge fragility assessment. Similar Bayesian updating procedures are also performed for C_s and r_{corr}.

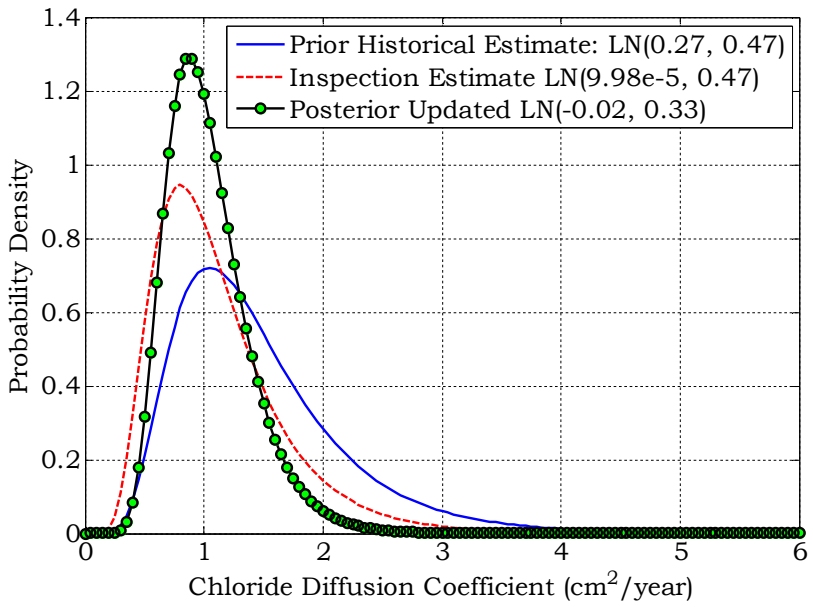

Figure 5-10: Bayesian updating example of chloride diffusion coefficient (D_c). Note that the lognormal distribution representation LN(λ, ζ) indicates λ = mean and ζ = standard deviation of the associated normal distribution (Rokneddin et al. 2013)

5.6.4. Computing bridge reliabilities using parameterized fragility models and updated deterioration parameter estimates

In order to compute the fragilities of bridges across the transportation network under consideration, parameterized fragility models are developed for all nine

different bridge classes under consideration. These parameterized models will be used in conjunction with the updated present day bridge structural condition (function of updated deterioration parameters) to derive in-situ bridge reliabilities. Additionally the following sections will provide a comparison between the fragility curves derived using the multidimensional fragility models and traditional methods.

5.6.4.1. Parameterized fragility model development for different bridge classes and comparison with traditional techniques

Parameterized fragility models for the different bridge classes are developed in this study using the same principles as described earlier in this chapter, albeit with some basic modifications. Firstly, geometric parameters are not included within the list of parameters the surrogate models or the fragility models are conditioned upon. Instead, uncertainties in geometric parameters for representative 3-span bridges are propagated through the finite element analyses (similar to the case study example in Section 4.2.2) to develop the parameterized fragility models. Fragility estimates for bridges with different span numbers are determined using modification factors proposed in HAZUS (2003). Secondly, only polynomial response surface metamodels were considered for the surrogate model development of highway bridges. While it is acknowledged that other metamodels, such as,

MARS may perform better (as revealed earlier), polynomial response surface models offer easy portability of the surrogate models without significant loss of accuracy and slight differences in goodness-of-fit estimates (Figure 5-2(b) and Table 5.5).

Table 5.12: List of parameters included as a subset of predictor variables for the surrogate model development of MSSS concrete girder bridge class within the South Carolina bridge network

Element of vector p	Description	Category
p_1	Steel strength	Critical bridge modeling parameter (Nielson 2005)
p_2	Elastomeric bearing pad friction	
p_3	Elastomeric bearing dowel gap	
p_4	Column reinforcing bar area	Deterioration-affected bridge structural parameters (Ghosh and Padgett 2012)
p_5	Elastomeric bearing dowel bar area	
p_6	Shear modulus of elastomeric bearing pads	
p_7	Concrete cover depth	

To draw parallels with the previous example on MSSS concrete girder type presented in Section 5.3, the reduced set of conditioned parameters for the same bridge type in this application example now includes parameters p_1 to p_7 (Table 5.12). The performance of polynomial response surface models for fitting the response of different bridge components is shown in Table 5.13, while Equation (5.41) shows the system level parameterized fragility model obtained using logistic regression techniques detailed in Section 5.4. Although in general the response

surface models provide a good fit to the component response data, the relatively low *Adjusted* R^2 values for certain bridge components such as abutments still offers significant improvement over traditional uni-dimensional power law demand models (Nielson 2005). The coefficients of polynomial response surface metamodels and parameterized fragility models for all nine bridge classes within the South Carolina network is included in the Appendix C.

$$P_{sys|im,x_1,x_2,\ldots,x_7} = \frac{e^{6.15+4.00\log(PGA)-0.003p_1-0.251\log(p_2)-0.025\log(p_3)-0.395p_4-0.116p_5+0.03\log(p_6)-0.148\log(p_7)}}{1+e^{6.15+4.00\log(PGA)-0.003p_1-0.251\log(p_2)-0.025\log(p_3)-0.395p_4-0.116p_5+0.03\log(p_6)-0.148\log(p_7)}} \quad (5.41)$$

Table 5.13: Goodness of fit estimates for the polynomial response surface metamodels corresponding to different components of the MSSS Concrete girder bridge class in South Carolina

Component Name	Component Response Description	*Adjusted* R^2	*RMSE*
COL	Column curvature ductility	0.82	0.54
FBL	Fixed bearing deformation (Longitudinal)	0.76	0.69
FBT	Fixed bearing deformation (Transverse)	0.68	1.00
EBL	Expansion bearing deformation (Longitudinal)	0.77	0.59
EBT	Expansion bearing deformation (Transverse)	0.70	0.98
ABA	Abutment active deformation	0.65	0.50
ABP	Abutment passive deformation	0.66	0.83
ABT	Abutment transverse deformation	0.68	0.50

5.6.4.2. Incorporation of in-situ bridge condition to compute bridge specific reliability

The field-instrumented/spatially interpolated and statistically updated deterioration parameters (C_s, D_c, and r_{corr}) at each bridge location as demonstrated earlier can be used to assess the extent of deterioration suffered by critical members of all the bridges in the network. These deterioration affected structural parameters can now be readily used in conjunction with the parameterized fragility models for different bridge classes and multi-dimensional integration techniques to derive uni-dimensional fragility curves.

Table 5.14: Statistical distribution of the deterioration affected structural parameters (p_1 to p_4) and critical bridge parameters (p_5 to p_7) corresponding to the case study MSSS Concrete Bridge

Parameter	Unit	Distribution Type	Distribution Parameters	
p_1	cm	Lognormal	λ = -4.65	ζ = 0.29
p_2	MPa	Lognormal	λ = 6.13	ζ = 0.08
p_3	-	Lognormal	λ = 0.00	ζ = 0.10
p_4	cm	Uniform	a = 0.00	b = 5.08
p_5	cm^2	Lognormal	λ = 1.49	ζ = 0.12
p_6	cm^2	Lognormal	λ = 1.36	ζ = 0.11
p_7	MPa	Uniform	a = 1.37	b = 4.35

The multi-dimensional integration strategy is demonstrated for an MSSS concrete girder bridge built in 1922 and located in the marine atmospheric

exposure zone in the South Carolina bridge network under consideration. Table 5.14 shows the statistical distributions of each of the deterioration affected structural parameters (p_4 to p_7) corresponding to the present day bridge conditions. Also shown in the table are the typical statistical distributions corresponding to critical bridge modeling parameters (p_1 to p_3) for MSSS concrete bridges located in the Central and Southeastern US as identified by Nielson (2005).

Single-parameter fragility curves for the example bridge conditioned only on *PGA* are estimated by integrating the multi-dimensional fragility estimates over the domain of the uncertainties for the different parameters as shown in Equation (5.42). This fragility curve (Figure 5-10) thus obtained, is similar to a 'classical' fragility curve, although it incorporates all the effects of aging and deterioration and their associated uncertainties. It is noted that parameters p_1 to p_7 are assumed to be statistically independent which enables the multi-dimensional integration over each parameter specific distribution without constructing the joint probability density function.

$$p_{sys|im} = \int_{p_1} \cdots \int_{p_7} \frac{e^{6.15+4.00\log(PGA)-0.003p_1-0.251\log(p_2)-0.025\log(p_3)-0.395p_4-0.116p_5+0.03\log(p_6)-0.148\log(p_7)}}{1+e^{6.15+4.00\log(PGA)-0.003p_1-0.251\log(p_2)-0.025\log(p_3)-0.395p_4-0.116p_5+0.03\log(p_6)-0.148\log(p_7)}} f(p_1)\ldots f(p_7)dp_1\ldots dp_7 \quad (5.42)$$

5.6.4.3. Comparison with fragility curves obtained using traditional methods

The fragility curves derived using the proposed parameterized formulation and subsequent multi-dimensional integration are compared with the traditional state-of-the-practice method for fragility analysis. In the conventional method (detailed in Chapter 4), surrogate demand models conditioned only on PGA are developed using component responses obtained from finite element analysis of bridge samples constructed through Latin Hypercube sampling of deterioration and modeling parameters. Finally, the derived fragility curve is characterized by a lognormal distribution with a median and dispersion value. As elaborated above, the traditional state-of-the-art methodology is considerably bridge specific and would result in intractable number of simulations while deriving fragility curves for 509 bridges in the network. This also highlights the potential advantage of proposed parameterized fragility models pertaining to their ability to efficiently generate fragility curves by integrating out the critical bridge parameters depending on application and data availability.

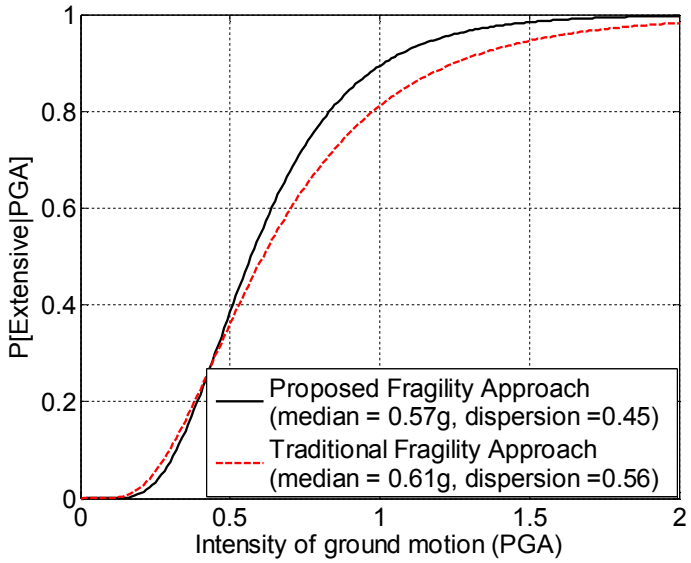

Figure 5-11: Comparison of fragility curve obtained using the proposed parameterized fragility approach and traditional fragility approach for case study MSSS Concrete girder bridge (Rokneddin et al. 2013)

Using the proposed parameterized fragility approach, the resulting fragility curve is found to have median and dispersion values of 0.57g and 0.45, while the traditional fragility methodology yields median and dispersion values of 0.61g and 0.56, respectively (Figure 5-11). Although median values differ only by 6.5%, the dispersion values vary significantly by almost 25%. The reduced dispersion value of the fragility curve obtained using the proposed approach can be attributed to the improved fit of the multi-dimensional surrogate demand models to component responses. These surrogate models benefit from extra predictors (p_1 to p_7) in addition to PGA which lead to better approximation to component responses as

compared to single-parameter demand models (conditioned only on *im*) in the state-of-the-practice fragility methodology.

Similar conditioned-on-*PGA*-only fragility curves, for the extensive damage state are developed in this study for all 509 bridges in the case study network after incorporating the effects of aging and degradation by multi-dimensional integration. After developing the uni-dimensional fragility curves for each bridge location, point estimates of damage state exceedance probabilities are identified for each bridge in the network from these fragility curves and PGA at each bridge site.

The histogram of the probabilities is presented in Figure 5-12 shows the frequency distribution of the failure probabilities corresponding to the 509 bridges in the network. Evidently, the majority of the bridges have extreme failure probabilities. A significant percentage of the bridges with very low failure probabilities are comprised of MSSS Slab, MSC Slab, SS Concrete, and SS Steel bridges which are found to be relatively non-vulnerable to the scenario seismic event owing to minimal bearing deformations and low column demands (for multi-span bridges). Bridges with high failure probabilities tend to belong to the aging MSC Steel, MSSS Steel, and MSSS Concrete girder bridge classes characterized by

high demands on column, bearing and abutment deformations and are primarily concentrated near the epicenter characterized by high PGA intensity.

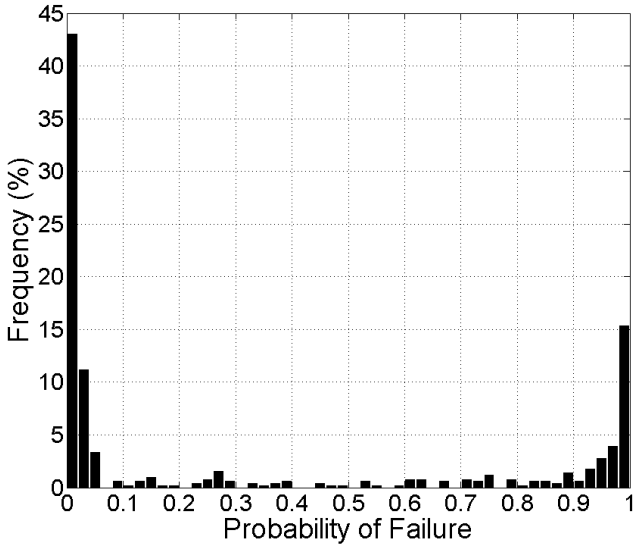

Figure 5-12: Frequency distribution of the failure probabilities corresponding to the 509 bridges in the chosen case study network in South Carolina (Rokneddin et al. 2013)

A comparison of aging bridge failure probabilities against the case when no deterioration is accounted revealed a 25% underestimation for more than 80% of the bridges in the network, thereby underlining the importance of accounting for aging and deterioration mechanisms. The bridge failure probabilities obtained is this study after implementing the parameterized fragility models and accounting for field condition can be used next to achieve other objectives, such as, network level reliability estimation and risk ranking of bridges within a network for seismic

retrofit prioritization and structural upgrades (Ghosh et al. 2013b; Rokneddin et al. 2013).

5.7. Closure

This chapter introduced highly flexible multidimensional fragility models for efficient and still accurate seismic vulnerability assessment of aging highway bridges. Such parameterized fragility models offer several advantages over traditional uni-dimensional models in their ability to: a) assess the impact of individual deteriorating structural components and geometries on bridge performance without the need for costly re-analysis, b) incorporate new information on deterioration parameters obtained using field measurements to efficiently determine "updated" fragility estimates, and c) assist in reliability and loss estimation of aging transportation networks after using in-situ bridge reliability estimates. Four different surrogate modeling strategies are explored while developing parameterized fragility models, ranging from classical polynomial response surface models to emerging metamodels, such as multivariate adaptive regression splines, radial basis function networks and support vector machines for regression. The predictive capabilities of these metamodels are assessed with the

help of three goodness-of-fit estimates and their accuracy is tested against benchmark Monte Carlo simulations. For the case study MSSS Concrete bridge class, multivariate adaptive regression splines metamodels performs best and results in least deviations from Monte Carlo results. Support vector machines for regression are found to suffer from the highest predictive errors, with the other two metamodels show intermediate performance. Applicability of surrogate models to approximate the failure domain is investigated for the first time in this study for bridge reliability using dimensionality reduction and failure surface visualization techniques. A clear demarcation between survive-failure domains and smoothness of the failure surface in two dimensions renders confidence in adopting the surrogate models to approximate the multidimensional failure surface. Consequently, bridge component and system level parameterized bridge fragility models are constructed using logistic regression techniques to express the bridge probability of failure as function of ground motion intensity and bridge modeling parameters, geometric parameters, and deterioration affected structural parameters.

The potential of parameterized fragility models to incorporate field instrumentation data is demonstrated after considering a portion of an existing

aging transportation network in the state of South Carolina comprising of 509 bridges of nine different bridge classes. Since field instrumentation of highway bridges is an expensive and labor intensive procedure, it is only feasible to monitor only a handful of bridges in a distributed transportation network. This study demonstrates the Kriging spatial interpolation procedure which helps to determine the deterioration parameter at non-instrumented bridge locations using the data available from instrumented bridges sites. Statistical distributions of deterioration parameters at all bridge locations are derived next using Bayesian updating procedures which help to preserve historically available data while incorporating new information from field measurement. Consequently, the statistically derived information on deterioration affected structural parameters is used in conjunction with parameterized bridge fragility models for different bridge classes to derive in-situ reliability estimates of all bridges within the network. The parameterized fragility models presented in this chapter constitute the next generation fragility models which enable efficient and precise estimation of bridge fragilities while also being able to exploit the data available from field instrumentation and sensor monitoring of bridges.

Chapter 6

SUPPLEMENTARY THREATS TO BRIDGE SEISMIC VULNERABILITY

The previous chapters focused on the impact of environmental degradation mechanisms on the seismic performance of aging highway bridges. This chapter will discuss other critical and prevalent, yet traditionally neglected threats to bridge structures in seismic zones. One such threat stems from the exposure of bridges to multiple earthquakes along their service lives when located in regions prone to moderate to high seismicity. Repeated shock scenarios may lead to accumulation of structural damage resulting in a reduction in structural capacity of bridge components, and thereby rendering the bridge more vulnerable to resist future earthquakes. The first part of this chapter will focus on the impact of such repeated seismic shocks on highway bridges while accounting for the probabilistic nature of earthquake hazard. The second part of this chapter will elaborate on the

impact of truck and traffic load on the component and system level bridge seismic response and vulnerability. Although the primary function of highway bridges is the safe transport of traffic and goods between different origin-destination pairs across the nation, negligible amount of literature exists on the development of a joint seismic and live load fragility framework. This chapter will develop such a framework allowing incorporation and coupling of site-specific traffic characteristics (truck gross vehicle weight histogram and truck flow) with conditional reliability estimates to arrive at bridge-specific fragility curves.

6.1. Impact of Repeated Seismic Shocks on Highway Bridge Damage

The phenomena of damage accumulation due to repeated seismic shocks will be demonstrated in this study for two distinct scenarios (Ghosh et al. 2013c): a) multiple earthquakes in the form of repeated main shocks along the service life of the structure, and b) main shock-aftershock sequences. The methodologies and results presented in this section however do not consider the impact of aging and deterioration mechanisms on lifetime seismic vulnerability assessments in addition to repeated earthquake shocks. While degradation mechanisms were a primary

focus of the previous chapters of this thesis, future studies should focus on the development of a joint framework focusing on aging and damage accumulation simultaneously after considering the probabilistic nature of both hazards.

A critical step towards a damage accumulation framework due to repeated seismic shocks is choosing an indicator which reflects the actual cumulative nature of damage under multiple earthquake pulses. In this regard, the engineering demand parameters presented earlier, such as column curvature ductility is inappropriate for repeated shock events because structural component geometry or direction of the movement during repeated earthquakes may potentially lead to recovery of plastic hinges. Addressing such shortcomings, the Park and Ang damage index (Park and Ang 1985) offers an unique indicator for measuring damage accumulation by combining two limit states of failure (Kunnath and Jenne 1994): a) monotonic structural deformation or ductility, and b) dissipated hysteretic energy. While several damage indices existing in literature focus on these limit states separately (Khashaee 2005), the Park and Ang damage index offers a combination of both limit states and has consistently resulted in good agreement with experimental test data for buildings as well as bridges (Chai et al. 1994; S. K. Kunnath and Jenne 1994; Williams and Sexsmith 1997).

The Park and Ang damage index is used in this study to develop regression models to statistically predict damage accumulation based on the earthquake intensity and past damage history. These regression models are further used to predict the probability of damage index exceedance conditioned on the number of earthquake pulses incurred by the structure. Finally, time-dependent damage index exceedance probabilities are computed using site specific hazard curves for main shocks and aftershocks characterized by homogeneous and nonhomogeneous Poisson process rates, respectively. The following section of this chapter will discuss the mathematical formulations of the proposed framework followed by an application on a representative case study single column box girder bridge located near the San Andreas Fault in California.

6.1.1. Formulation of the damage accumulation framework

6.1.1.1. Predictive regression models

The Park and Ang index for damage measurement results from a combination of ductility demand induced by the earthquake and the dissipated hysteretic energy, as shown in Equation (6.1) (Park and Ang 1985; Guzman and Ishiyama 2004):

$$D = \frac{\mu_m}{\mu_u} + \beta \frac{E_h}{M_y \theta_y \mu_u} \tag{6.1}$$

where D is the Park and Ang damage index, μ_m is the maximum ductility caused by the earthquake, μ_u is the ultimate ductility capacity under monotonic loading, E_h is the total hysteretic energy dissipated, M_y is the yield moment capacity, θ_y is the yield rotation angle and β is a dimensionless constant usually assumed to be 0.05 for reinforced concrete (RC) structures. Additionally, Table 6.1 lists the classification of damage levels suggested by Park et al. (1985) used to relate empirical observed damages to calculated damage indices.

Table 6.1: Damage level classification and correlation with calculated damage indices and damage measures as proposed by Park et al. (1985)

Damage Level	Damage Index (D)	Damage Measure
I	$D < 0.1$	No damage; localized minor cracking
II	$0.1 < D < 0.25$	Minor damage; light cracking throughout
III	$0.25 < D < 0.4$	Moderate damage; severe cracking; localized spalling
IV	$0.4 < D < 1.0$	Severe damage; crushing of concrete; reinforcement exposed
V	$D > 1.0$	Loss of element load resistance

It is clear from Equation (6.1) that the engineering demand parameters, μ_m and E_h, are directly correlated with the characteristic of the structure and the

ground motion. Based on the previously discussed power-law form of the engineering demand parameter as a function of the earthquake intensity measure *IM* (Cornell et al. 2002), both μ_m and E_h in the transformed space are linear functions of *IM*. Consequently, the damage index D is also expected to be a linearly dependent on IM as shown in Equation (6.2) for single earthquake pulses (Ghosh et al. 2013c):

$$\ln(D_1) = \alpha_1 + \beta_1 \ln(IM_1) \tag{6.2}$$

In the above equation, D_1 is the damage index after the first earthquake pulse, α_1 and β_1 are regression coefficients and IM_1 is the peak ground motion intensity of the first earthquake shock. The goodness-of-fit measures obtained confirm that this model can be adopted to predict the damage index for single shock scenarios as will be elaborated later in the representative case study section.

Unlike single shock scenarios, damage index evaluation under multiple shocks is further involved owing to its dependence on the history of shock occurrences. Under multiple earthquake events, the only parameter which can be considered strictly cumulative is the total energy dissipated (E_h), whereas, the maximum ductility μ_m could have been achieved during the most immediate

seismic pulse or in any of the previous pulses, depending on the nature of the earthquake shocks. For clarity, let us suppose that the bridge structure is subjected to two earthquake pulses along its service life and let the corresponding maximum curvature ductilities be μ_{m1} and μ_{m2} and hysteretic energies dissipated be E_{h1} and E_{h2} respectively. In order to calculate the damage index, the total energy dissipated is given by:

$$E_h = E_{h1} + E_{h2} \tag{6.3}$$

and the maximum curvature ductility is given by:

$$\mu_m = \max(\mu_{m1}, \mu_{m2}) \tag{6.4}$$

Hence, from the above equations it is clear that while total dissipated energy increases with the number of shocks, the maximum curvature ductility is solely dependent on the strongest pulse in the history of shocks the bridge is subjected to along its service life. It is however noted that the curvature ductility also depends also on the level of degradation since it reflects, for instance, a reduction in the stiffness. Thus it is expected that μ_{m2} should always be greater than μ_{m1}; however, the influence of other aspects, such as geometry or direction of the movement, may in a few specific cases lead to a case where $\mu_{m1} > \mu_{m2}$

(Abdelnaby 2012). Regardless of these instances, the damage index of a structure is a quantity that is strictly increasing with the number of earthquake shocks as shown in Equation (6.5):

$$D_n > D_{n-1} > \ldots > D_2 > D_1 \tag{6.5}$$

where, D_n is the damage index after the structure has been subjected to n shocks. Consequently, the damage index after n earthquake shocks can be described as a multilinear regression model as follows (Ghosh et al. 2013c):

$$\ln(D_n) = \alpha_n + \beta_n \ln(IM_n) + \gamma_n \ln(D_{n-1}) + \delta_n \ln(IM_n)\ln(D_{n-1}) \tag{6.6}$$

where, D_n is the damage index after the n^{th} earthquake shock with ground motion intensity IM_n; α_n, β_n, γ_n and δ_n are regression coefficients, and D_{n-1} is the damage index after n-1 earthquake shocks. This multilinear regression model with interaction coefficients is similar to the model form presented in Section 5.2.2.1 and in this context can be seen as an extension of the model previously presented in Equation (6.2) since the damage index of the structure after the n^{th} shock naturally depends on how 'weak' the structure has become after being exposed to the previous (n-1) shocks (quantified by D_{n-1}).

In order to arrive at either of the regression Equation (6.2) or Equation (6.6), the structure needs to be subjected to a series of ground motions either individually (for one shock) or in combinations as earthquake trains (for multiple shocks). It is noted that the predictive regression equations for the damage index based on the earthquake intensity are approximate statistical relationships and the error in model prediction is propagated throughout the results developed in this study. In addition to the adopted model form (Equation (6.6)), regression models with linear, interaction and quadratic terms were also tested. The improvement in model goodness-of-fit estimates was however found to be negligible and hence the present model form is adopted in this study for simplicity.

6.1.1.2. Damage index exceedance probability computations

After predictive regression equations are formulated, the probability of exceeding different levels of damage indices are computed, given that the structure is subjected to a certain number of shocks. This probability, represented as $P[D>d \mid n \textit{ shocks}]$, can be evaluated using Monte Carlo simulations. In this approach, first a large number of earthquake intensity measures are sampled based on earthquake occurrence probabilities corresponding to site specific seismic hazard curves. Second, the total energy dissipated and subsequent damage indices are computed

using Equations (6.2)-(6.6), while accounting for the uncertainty about the predictive regression models. Finally, the probability of exceeding a certain level of energy dissipated is computed as:

$$P\left[D > d \mid n \ \ shocks\right] = \frac{1}{N_{MC}} \sum_{i} I[D_{n_i} > d] \tag{6.7}$$

where, N_{MC} is the total number of Monte Carlo trials, D_{n_i} is a realization of the damage index after n shocks for the i^{th} Monte Carlo trial, $I[\cdot]$ is the indicator function which equals 1 when $[\cdot]$ is true or equals 0 if $[\cdot]$ is false. This study employs 50,000 Monte Carlo trials (N_{MC}) to arrive at accurate estimates of damage index exceedance probabilities as per Equation (6.7) although a preliminary investigation revealed that the results stabilize with fewer trials (approximately 10,000 trials).

The probability of damage index exceedance calculated using Equation (6.7) is dependent on the number of shock occurrences. However, it is often of practical importance to compute the chance of exceeding limiting values of damage index given a time period of interest. Such time durations may include the service life of a structure for life-cycle analysis or the time interval immediately following a main shock when aftershock occurrences are highly probable. Using the total probability

theorem, the time-dependent exceedance probabilities may be computed as (Ghosh et al. 2013c):

$$P\left[D > d|T\right] = \sum_{n=1}^{\infty} P\left[D > d|n\,shocks\right] P\left[n,T\right] \tag{6.8}$$

where, T is the time period of interest, $P[n, T]$ is the probability of experiencing n shocks in time T, and $P[D>d \mid n\ shocks]$ is computed using Equation (6.7).

This study computes the probability $P[n, T]$ for two distinct circumstances:

1. *Main shocks*: using a constant main shock hazard occurrence rate λ_m for the service lifetime of the structure (e.g., $T = 50$ years), and
2. *Aftershocks*: using time-dependent aftershock hazard occurrence rate $\lambda_a(t)$ for a time interval of one year (i.e., $T = 365$ days) following a main shock event, after which the threat of aftershock occurrence usually decays to an insignificant level (FEMA 2000; Luco et al. 2002).

These aforementioned constant (for main shocks) or time varying (for aftershocks) hazard occurrence rates can be obtained from region specific hazard curves, as will be demonstrated in the case study section. Using the constant or time varying hazard rates and characteristics of a homogeneous or

nonhomogeneous Poisson process for main shocks or aftershocks respectively, the probability $P[n,\ T]$ can be computed as:

$$P[n,T] = \begin{cases} \dfrac{\left(\lambda_m T\right)^n}{n!} e^{-\lambda T} \ \ for\ main\ shock\ scenario \\ \dfrac{\left[\int_0^T \lambda_a(t)\right]^n}{n!} e^{-\int_0^T \lambda_a(t)} \ \ for\ aftershock\ scenario \end{cases} \tag{6.9}$$

6.1.2. Representative case study example

The formulations and the framework developed in the preceding section will be demonstrated using a typical representative case study single column integral concrete box girder bridge located in California. The finite element model of this bridge along with deterministic examples of damage accumulation is presented first followed by time-dependent damage accumulation examples for multiple main shocks and main shock-aftershock scenarios.

6.1.2.1. Case study bridge and finite element model

Figure 6-1 depicts the geometric and structural properties of the case study single column bridge under consideration. Based on the dimensions and material properties of the deck superstructure the weight of the superstructure is 2850kN.

While the superstructure elements such as the bridge deck and the abutments are not explicitly modeled in this study, the superstructure mass is assumed to be represented as a lumped mass on top of the bridge column and the superstructure weight propagated as axial load in addition to the self-weight of the column. The axial load ratio of the column is assumed to be 0.06, typical of single column bridges in California (Brandenberg et al. 2011). The diameter of the bridge column is assumed to be 1.28m and the longitudinal steel ratio in the column is 2.5% of the gross cross sectional area distributed as 22 #14 rebars, each with a nominal diameter of 43mm. The nonlinear finite element model of the bridge column, idealized as a beam-column element fixed at the base, is analyzed for seismic excitation using the finite element software package OpenSees also used earlier(Mazzoni et al. 2009). The column section is modeled using a nonlinear fiber section with distributed plasticity in which the column concrete is modeled using the *Concrete04* material and the steel is modeled using the *uniaxialMaterial Hysteretic* capable of capturing strength degradation from repeated loading cycles. While the simplistic modeling assumptions are adopted to demonstrate the damage accumulation framework, future studies should consider explicit finite element modeling of the overall bridge system in addition to investigating the sensitivity of

ground motion direction on bridge damage. With the present case study bridge, the following sections will demonstrate:

a) Computation of the damage index under a single shock or train of earthquake shocks,

b) Formulation of the regression equations to predict the damage index from future shocks, and

c) Evaluation of the damage index exceedance probability under two distinct cases of main shock and aftershock hazards.

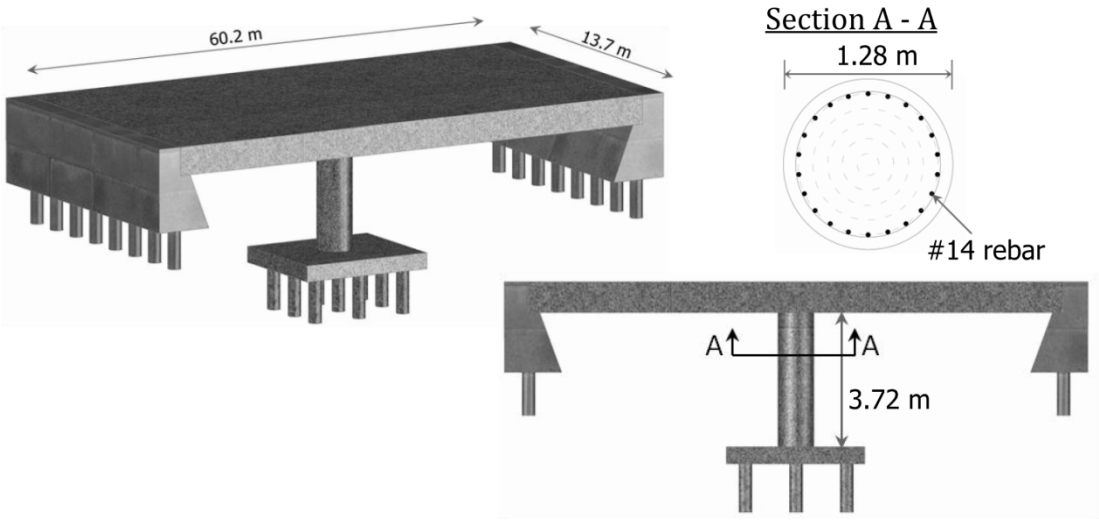

Figure 6-1: Representative case study single column box girder bridge to demonstrate the damage accumulation framework presented in this study (Ghosh et al. 2013c)

6.1.2.2. Deterministic damage accumulation examples

Damage index measurement following the nonlinear time history analysis of the bridge structure under seismic excitation requires estimation of maximum curvature ductility demand and the total hysteretic energy dissipated. In this study earthquake pulses from a suite of 100 ground motions for California developed by Gupta and Krawinkler (2000) and Krawinkler et al. (2003) are adopted for the finite element simulations. The selected ground motion records are characterized by PGAs between 0.03g to 1.3g, and durations between 18.7 seconds to 99.96 seconds. Additionally magnitudes ranged between 4.7 to 6.5, and distances between 3.6km to 60km. Pertinent structural characteristics required for the damage index estimation, such as, yield moment capacity, ultimate curvature ductility, and yield rotation angle are presented in Table 6.2.

Table 6.2: Structural characteristics of the example bridge column required for damage index measurement (Ghosh et al. 2013c)

Structural Characteristic	Symbol	Unit	Value
Yield curvature	ϕ_y	1/m	0.0052
Ultimate ductility capacity under monotonic loading	μ_u	--	17.024
Yield moment	M_y	kN-m	8751.35
Yield rotation angle	θ_y	rad	0.0042

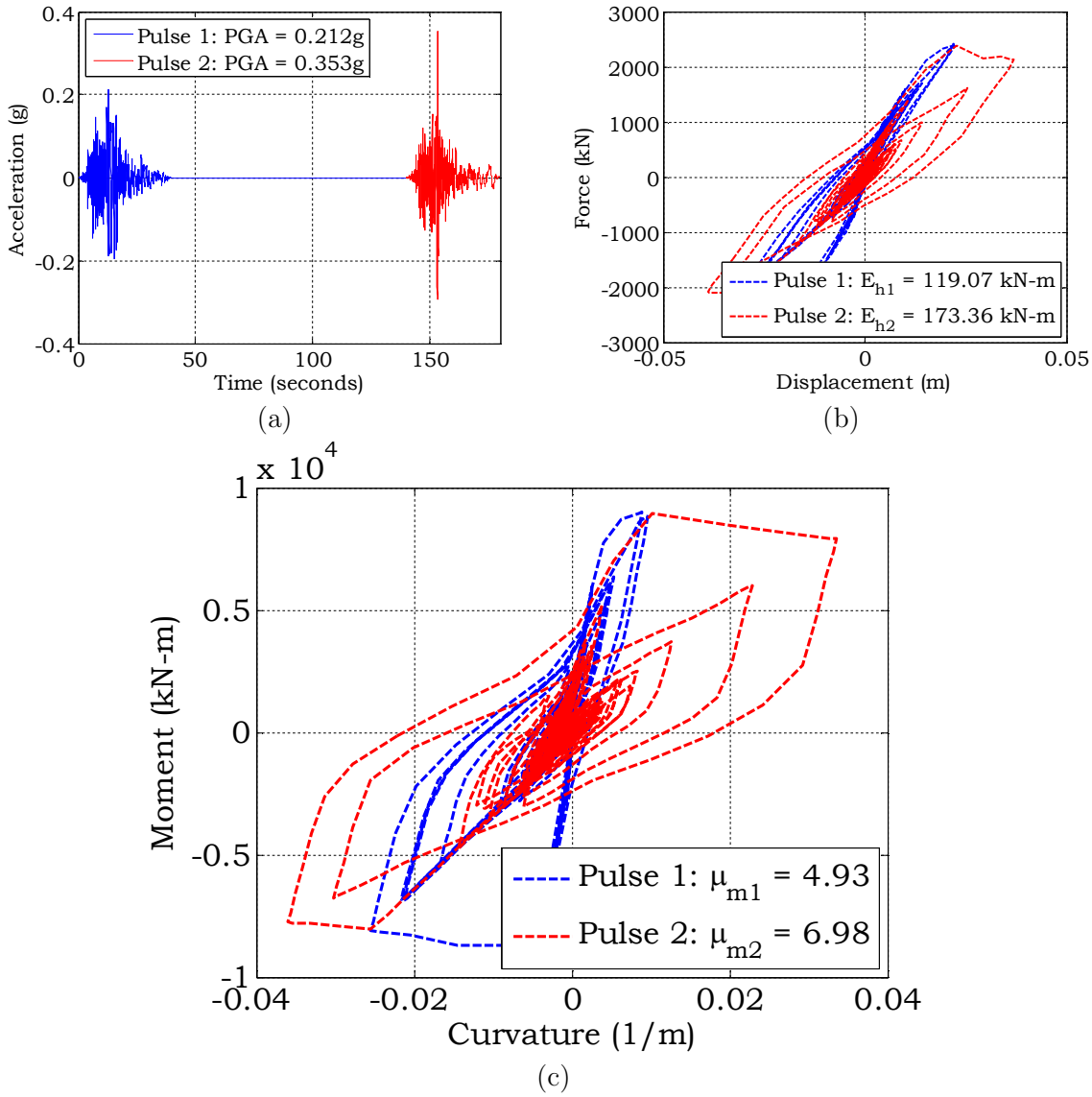

Figure 6-2: (a) Train of two earthquake pulses used for deterministic illustration of damage index computation; (b) force –displacement plot of bridge column response depicting the total hysteretic energy dissipation; and (c) moment-curvature plot depicting the maximum curcature ductilities incurred during the two-pulse shock scenario (Ghosh et al. 2013c)

To demonstrate the procedure for damage index quantification, consider the case study bridge column subjected to two consecutive earthquake shocks with

peak ground acceleration (PGA) intensities of 0.21g and 0.35g [Figure 6-2(a)]. The second pulse is appended to the first pulse following a gap representing the no-loading condition such that the vibration response from the first pulse dampens out prior to re-loading (taken as a period of 100 seconds in this study). Additionally, in a generic sense, if the first pulse represents a main shock, the second pulse can either represent another main shock pulse occurring at a later point in time along the service life of the bridge, or an aftershock immediately following the main shock. Figure 6-2(b) shows the force-displacement curve of the bridge structure which can be used to compute the individually dissipated hysteretic energy for the two earthquake pulses: $E_{h,1} = 119.07$kN-m and $E_{h,2} = 173.36$kN-m for earthquake shocks 1 and 2 respectively. Additionally, Figure 6-2(c) shows the moment-curvature relation at the column plastic hinge location corresponding to the two-pulse earthquake train with the lower intensity earthquake (pulse 1) leading to a lower value of maximum curvature ductility $\mu_{m,1} = 4.93$ as compared to the relatively stronger earthquake (pulse 2) which results in a maximum curvature ductility $\mu_{m,2} = 6.98$. It is noted that maximum ductility for the n^{th} shock ($\mu_{m,\text{n}}$) is obtained by normalizing the maximum observed curvature by the yield curvature as shown in the following equation:

$$\mu_{m,n} = \frac{\phi_{m,n}}{\phi_y} \tag{6.10}$$

where, $\phi_{m,n}$ is the maximum curvature observed during the n^{th} earthquake pulse, and ϕ_y is the yield curvature.

To demonstrate the concept of damage accumulation with number of shocks, the damage index will be evaluated for two cases. The first case involves damage index measurement for the bridge structure subjected only to the first shock. Using Equation (6.2) discussed earlier, this damage index D_1 can be computed using as:

$$D_1 = \frac{4.93}{17.02} + 0.05 * \frac{119.07}{8751.35 * 0.0042 * 17.02} = 0.30 \tag{6.11}$$

A damage index of 0.30 corresponds to level III in the Park and Ang damage scale (Table 6.1) and is indicative of moderate damage characterized by severe cracking and localized spalling. In the second case, when both earthquake pulses are considered, the dissipated hysteretic energy used to predict the damage index after two shocks is now cumulative and equals $E_h = E_{h1} + E_{h2} = 119.07 + 173.36 = 292.43$kN-m, while the maximum curvature ductility is $\mu_m = \max(\mu_{m1}, \mu_{m2}) = 6.98$. The damage index is therefore computed as shown in Equation (6.12):

$$D_2 = \frac{6.98}{17.02} + 0.05 * \frac{292.43}{8751.35 * 0.0042 * 17.02} = 0.44 \quad (6.12)$$

In this case the computed damage index of 0.44 corresponds to damage level IV in the Park and Ang damage scale (Table 6.1) and indicates severe damage characterized by crushing of concrete and exposure of steel reinforcement. The above example thus demonstrates the phenomena of damage accumulation with increasing number of shocks. While the presented results correspond to the case where the second shock has a stronger intensity than the first shock (as might occur when the structure is subjected to two independent main shocks along the service life), the proposed framework is capable of capturing damage accumulation when the first shock is predominantly stronger than the second shock (for example, during main shock-aftershock scenarios). For instance, when the structure is subjected to the above earthquakes, but in the reverse order, maximum curvature ductility for the second shock is 2.9 as opposed to 3.3 for the first shock. However, even though there is a reduction in the curvature ductility, the computed Park and Ang damage index increases from 0.19 to 0.21. When applied to realistic examples, such as the main shock – after shock sequence during the Darfield and Christchurch earthquakes in New Zealand, the damage index for the case study structure increases from 0.38 to 0.41. The following section will formulate the

regression equations to predict the damage index and quantify the associated uncertainty following single or multiple shock scenarios based on the ea rthquake intensity and past damage history.

6.1.2.3. Formulating Regression Equations to Predict Damage Index

Regression equations representing statistical relationships between the predictors and predicted variable (elaborated in Chapter 5) can be employed in the context of this study to approximate the damage index for future shocks as a function of ground motion intensity and previous earthquake history (in case of multiple shock scenarios). For the single shock scenario, regression models similar to Equation (6.2) are constructed after subjecting the case study bridge structure to the adopted 100 ground motion pulses. The data cloud and the fitted regression line in logarithmic space are depicted in Figure 6-3(a) and the regression equation is shown in Equation (6.13).

$$\ln\left(D_1\right) = 1.91 + 2.51\ln\left(PGA_1\right) \tag{6.13}$$

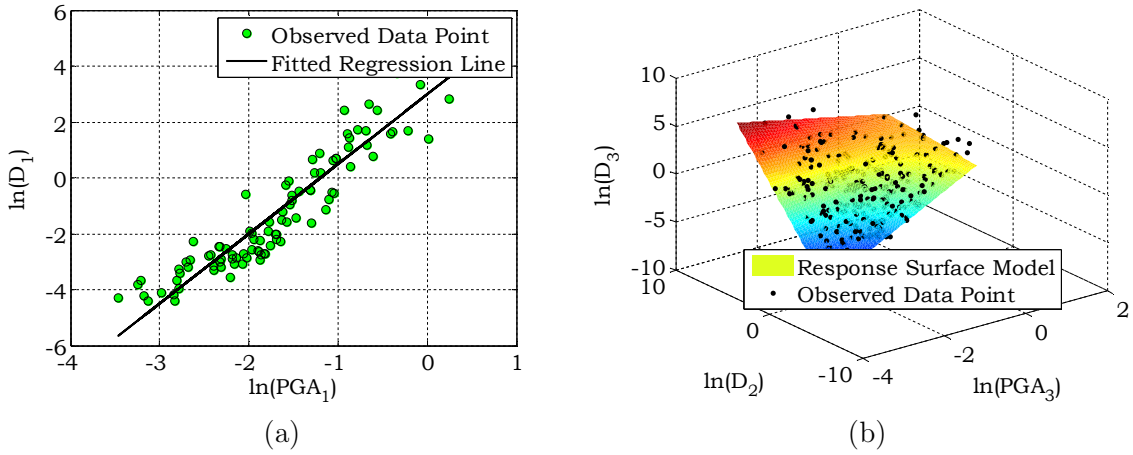

Figure 6-3: (a) Linear regression model for predicting the damage index following single shock occurrences, and (b) Multilinear regression model for predicting the damage index after three shocks as a function of the PGA of the third shock and damage index incurred up to the second shock (Ghosh et al. 2013c)

A high value of the coefficient of determination, $R^2 = 0.87$, and a relatively low estimate mean square error (MSE) = 0.70 indicates an adequate model fit to the generated damage index data. To construct similar polynomial regression models to predict the damage index for two or more consecutive shocks, the bridge structure is subjected to train of appended earthquake records [similar to Figure 6-2(a)], randomly selected and paired from the same suite of 100 ground motions. The fitted multilinear regression models will now follow the form shown earlier in Equation (6.6), conditioned on the PGA intensity of the latest pulse and the damage index incurred until the previous shock. For instance, Equation (6.14)

shows the fitted regression model for 2 shocks with an R^2 value of 0.86 and a MSE= 0.68.

$$\ln\left(D_2\right) = 1.82 + 0.77\ln\left(PGA_2\right) + 0.12\ \ln\left(D_1\right) - 0.33\ln\left(PGA_2\right).\ln(D_1) \qquad (6.14)$$

These multilinear regression models consistently perform well for a higher number of shocks as tabulated in Table 6.3 and shown in Figure 6-2(b) for three consecutive shock scenario. Additionally, it is observed that the coefficients of the regression models for 2 shocks and higher are marginally different from one another suggesting that earthquake damage has the Markovian property. Furthermore, this similarity can be used with advantage to develop an "average" model to predict the damage index efficiently. The regression coefficients for the average model in addition to those for original models for the multiple repeated shocks are also presented in Table 6.3 (Ghosh et al. 2013c). Consistently high R^2 values confirm that the average model performs adequately as well as the original models with negligible loss of accuracy and imparts confidence to adopt this model to capture damage accumulation and predict damage index exceedance probabilities as shown in the next section.

Table 6.3: Comparison of regression model coefficients and goodness of fit estimates for the original and average models for more than one shock scenario (Ghosh et al. 2013c)

Model	Number of shocks (n)	α_n	β_n	γ_n	δ_n	Original Model R^2	Average model R^2
Original	2	1.82	0.77	0.12	-0.33	0.86	0.85
Original	3	1.48	0.64	0.19	-0.33	0.90	0.89
Original	4	1.64	0.74	0.27	-0.32	0.91	0.90
Average	--	1.65	0.71	0.19	-0.33	--	--

6.1.2.4. Time-dependent damage index exceedance probabilities: Lifetime main shocks and main shock-aftershock sequences

In addition to the regression models developed in the preceding section, estimation of damage index exceedance probabilities requires information on the hazard potential where the bridge is located. In this study it is assumed that the case study bridge is located near the Stanford University campus site, 10 km away from the San Andreas Fault in California. This site is specifically chosen in this study to aid in exceedance probability computations (demonstrated in a later section), after adopting the available aftershock probabilistic seismic hazard data available in Yeo and Cornell (2009). It is noted that development of aftershock probabilistic seismic hazard curves is not an easy task in itself because of the time-dependent nature of the problem and is an area of ongoing research. Consequently, the amount of literature on this topic is limited. Unlike aftershocks, probabilistic seismic hazard

curves for main shocks can be easily obtained from the USGS (2012). The following sections will exemplify damage index exceedance probability calculation for two distinct scenarios (Ghosh et al. 2013c): 1) lifetime main shock hazard, and 2) aftershock hazard.

6.1.2.4.1. Scenario I: Main shock hazard

Figure 6-4 shows the main shock hazard curve for the chosen site near the San Andreas Fault, representing the annual probability of exceeding different PGA intensities. Main shock hazard occurrence is typically considered to be a Poisson process such that the annual earthquake exceedance probabilities are constant over the service life of the structure. The earthquake *occurrence* probabilities for different PGA intensities ranges can be obtained by calculating successive differences of the PGA *exceedance* probabilities from the hazard curve. A critical step in the lifetime damage index exceedance probability computation involves evaluation of $P[D>d \mid n \text{ shocks}]$. This solution was obtained by using Monte Carlo simulation (outlined in Equation (6.7)) with the following characteristics: a) sampling 50,000 earthquake intensity measures based on earthquake occurrence probabilities; and b) using the regression equations with the associated uncertainties developed in the previous section to estimate damage indices

depending on the number of shocks. In this study the authors have considered earthquake intensities with PGA levels of 0.1g and higher because earthquake intensities below this level are found to cause insignificant bridge damage (Nielson and DesRoches 2007a).

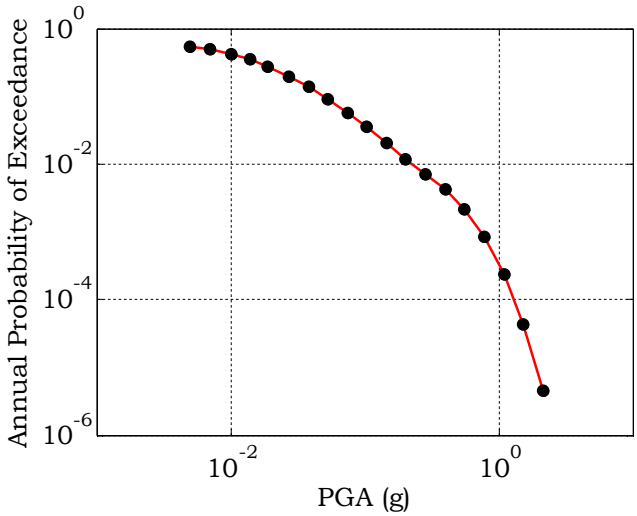

Figure 6-4: Main shock hazard near Stanford University campus site, 10 km away from the San Andreas Fault (USGS 2012).

Figure 6-5(a) depicts the probability of exceeding different levels of damage index as the structure is subjected to repeated earthquake shocks. This increasing probability of failure clearly indicates the need to consider multiple shocks within the damage accumulation framework. Additionally, the number of shocks is restricted to 8 because the probability of having more than these many number of shocks in the lifetime of the bridge structure (assumed as $T = 50$ years) is found to be negligible. The probability of number of shock occurrences during the lifetime of

the structure is shown in Figure 6-5(b) after computing earthquake occurrence probabilities using the Poisson assumption (Equation (6.9)). The constant Poisson hazard occurrence rate λ_m is calculated from the hazard curve after adding the individual annual occurrence rates of different PGA intensity ranges, which are individually Poissonian.

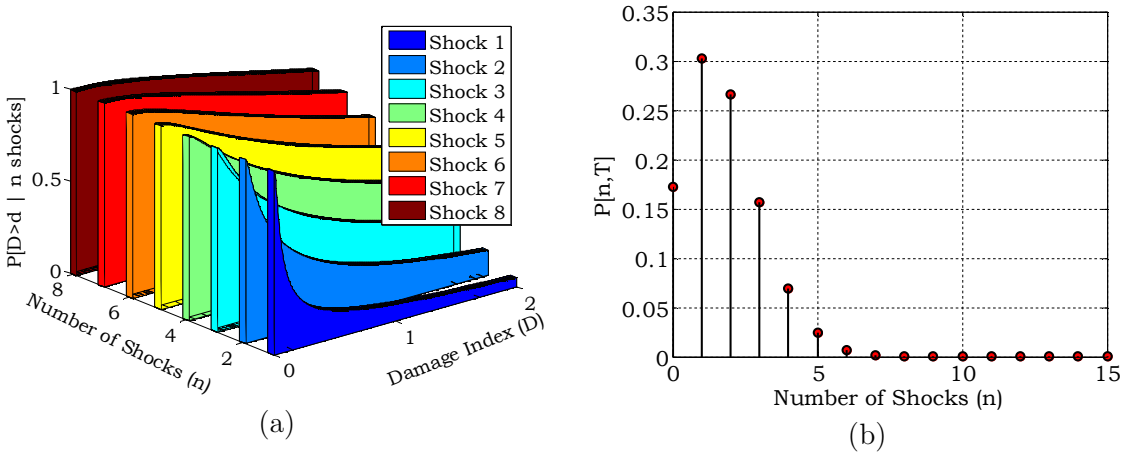

Figure 6-5: (a) Probability of exceedance of different levels of damage index depending on the number of shocks (P[$D>d$ | n shocks]), and (b) Probability of incurring n shocks in lifetime $T = 50$ years (Ghosh et al. 2013c)

In order to make the probability of damage index exceedance independent of the number of shocks, the lifetime exceedance probabilities $P[D>d \mid T]$ are computed using Equation (6.8). These probabilities are of particular interest to bridge owners and decision makers since they provide information on the chance of damage index exceedance for the structural service life. Such information may aid in devising potential retrofit strategies or structural upgrades to reduce lifetime

risks associated with bridges located in seismic zones. Figure 6-6 shows the accumulation of lifetime damage index exceedance probabilities for the case study bridge structure. Each color band within Figure 6-6 represents the contribution from the exceedance probabilities given the number of shocks and the chance of incurring that many shocks within structural lifetime (i.e., $P[D>d \mid n \text{ shocks}] \times P[n, T]$). Also shown is the cumulative contribution of exceedance probabilities for all shocks experienced by the bridge structure, which is equivalent to the lifetime probability of exceedance as indicated in the figure.

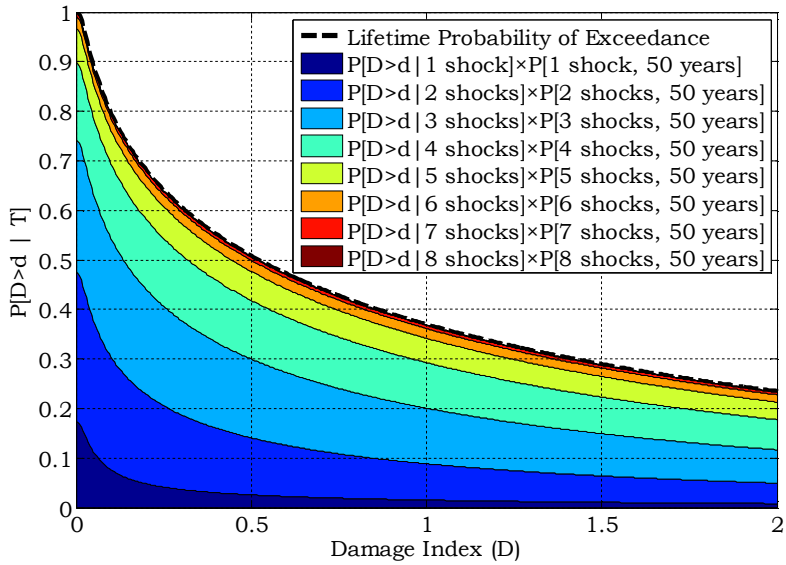

Figure 6-6: Probability of exceeding different damage index levels along the lifetime of the structure. The different color bands in the figure correspond to the joint contributions of exceedance probabilities given the number of shocks and the chance of incurring that many shocks within structural lifetime (i.e., P[$D>d \mid n$ shocks]×P[n, T]) (Ghosh et al. 2013c)

6.1.2.4.2. Scenario II: Aftershock hazard

Unlike main shock hazards, aftershock hazard rates are not constant over time and depend heavily on the number of days elapsed since the main shock event (Utsu and Ogata 1995; Yeo and Cornell 2009). While data on site specific aftershock exceedance rates is scarce, Yeo and Cornell (2009) recognize the nonhomogeneous Poisson characteristics of this phenomenon and provide sufficient information from which time-dependent aftershock probabilistic hazard curves can be derived. It is however noted that the assumed nonhomogeneous Poissonian nature of the aftershocks in Yeo and Cornell's (2009) model is yet to be validated using available techniques. Additionally, this model assumes that aftershocks are uniformly distributed along the fault rupture or concentrated at the ends, which according to Boyd (2012) is unrealistic. The purpose of this study, however, is to present a framework to compute damage index exceedance during main shock-aftershock sequences. While aftershock modeling is not the primary focus of this research, the proposed methodology is flexible to incorporate any emerging aftershock models and Yeo and Cornell's (2009) model is adopted herein for simplicity.

Since aftershock occurrence rates are significantly influenced by the magnitude of the main shock (Ōmori 1894; Utsu and Ogata 1995), this study will focus on aftershock occurrences following a magnitude $Mw = 7$ main shock event. Such an event is simulated in this study by subjecting bridge structure to the Imperial Valley earthquake record from the PEER ground motion database (PEER 2012). With respect to a magnitude 7 earthquake, Yeo and Cornell (2009) provide: a) instantaneous daily aftershock rates as a function of time elapsed from the main shock, and b) the probability of hazard exceedance at the site given an aftershock of random magnitude in the aftershock zone. This data is reproduced in Figure 6-7(a) and Figure 6-7(b) respectively. Additionally, Yeo and Cornell (2009) also indicate that the instantaneous daily aftershock rates multiplied to the probability of hazard exceedance will generate time-dependent aftershock probabilistic hazard curves, as derived in Figure 6-7(c). The number of aftershock occurrences within a year (T= 365 days) following the main shock is shown in Figure 6-7(d) calculated using the nonhomogeneous Poisson process rate λ_a(t) from the time-dependent aftershock hazard curves.

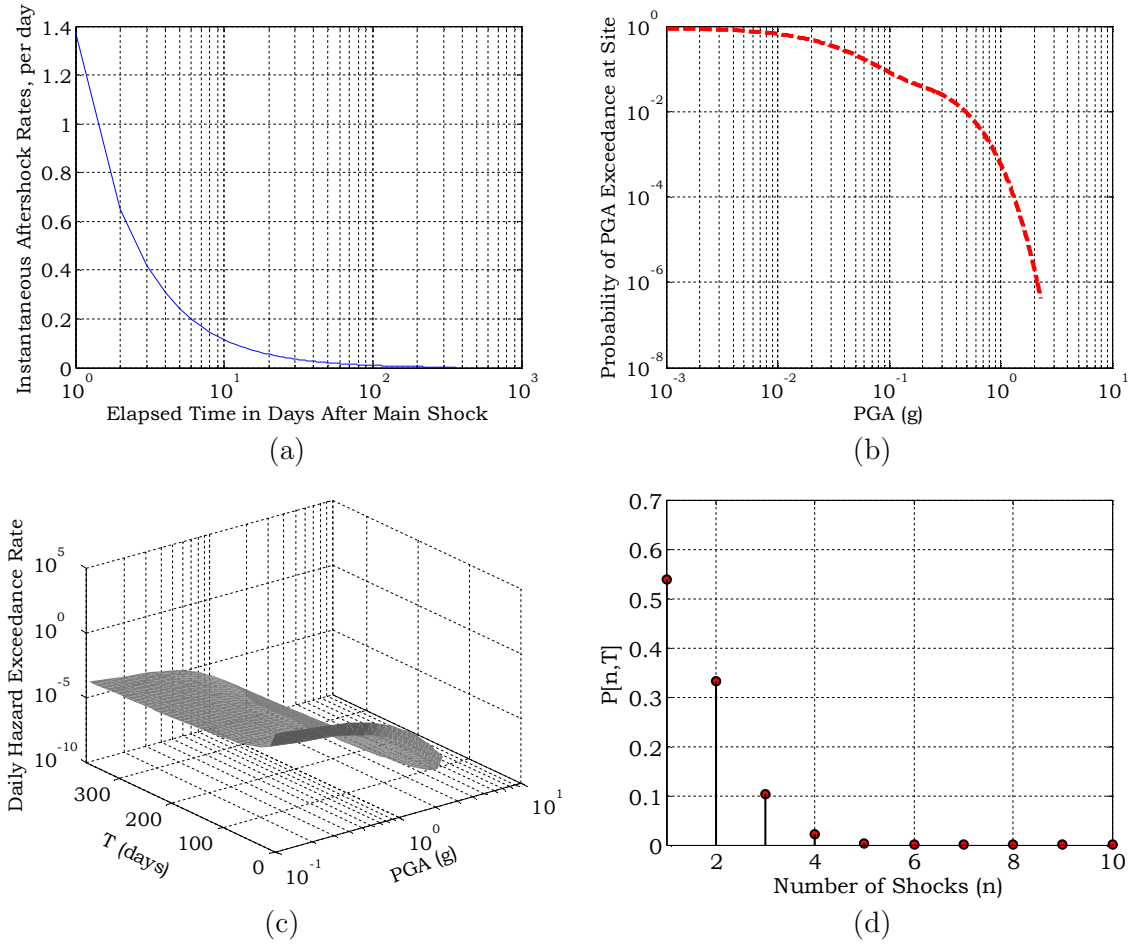

Figure 6-7: (a) Instantaneous daily aftershock exceedance rate as a function of time following the main shock [adopted from Yeo and Cornell (2009)], (b) probability of hazard exceedance at site given an aftershock of random magnitude in the aftershock zone [adopted from Yeo and Cornell (2009)], (c) time-dependent aftershock probabilistic seismic hazard curve for the case study site, and (d) probability of incurring *n* shocks in 365 days following the main shock occurrence calculated using the nonhomogeneous Poisson process rate from the time-dependent aftershock hazard curves (Ghosh et al. 2013c)

Due to the initial magnitude 7 Imperial valley earthquake, which already induces some level of structural damage, the shock dependent exceedance probabilities $P[D>d \mid n \text{ shocks}]$ for the aftershock scenario are higher compared to the main shock scenario presented earlier. This conditional exceedance probability

is shown in for the first seven shocks, beyond which the probability of an aftershock occurrence is minimal [Figure 6-8(a)]. Additionally, Figure 6-8(b) depicts the probability of exceeding different levels of damage index for 365 days following the main shock, after which the chance of aftershock occurrence is minimal. A closer observation of the color bands in Figure 6-8(b) reveals that contribution of the first three shocks to the cumulative probability of damage is most significant attributed to their high probability of occurrence as compared to other shocks.

While a comparison between Figure 6-8(b) and Figure 6-6 may potentially indicate that aftershock damage exceedance risks are higher than lifetime main shocks, it should be noted that the aftershock results presented in this are valid only following a strong initial main shock of magnitude 7. Hence it is intuitive to expect a potentially higher risk of cumulative damage following a given strong earthquake event than in the case of uncertain lifetime main shocks. Future studies on this topic should investigate aftershock damage index exceedance probabilities for different main shock magnitudes, in addition to building a methodology to study main shocks and aftershocks damages under the same framework.

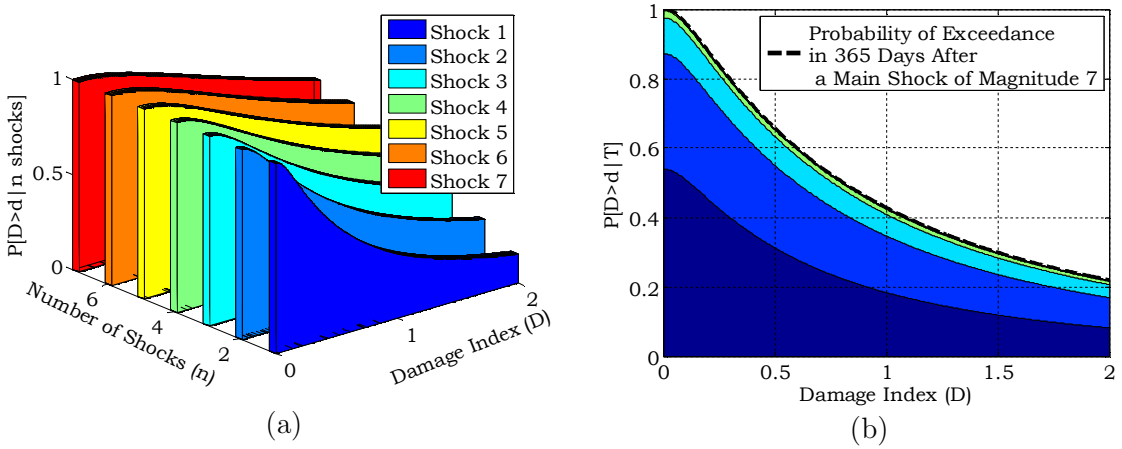

Figure 6-8: a) Probability of exceedance of different levels of damage index depending on the number of aftershocks (P[$D>d|n$ shocks]), and b) Probability of exceeding different damage index levels for 365 days after main shock occurrence (Ghosh et al. 2013c)

The results presented in this study revealed that for both main shock and aftershock scenarios, there is a significant increase in the probability of damage index exceedance under repeated shock scenarios within the chosen time windows. The developed probabilistic estimates of damage index exceedance will inform bridge owners or stakeholders about the associated seismic risks and assist in devising potential retrofit strategies or structural upgrades to reduce lifetime risks associated with bridges located in seismic zones. The increase in probability of damage index exceedance presented in this study highlights the importance of considering repeated earthquake threats detrimental to the seismic performance of bridge structures in addition to the previously discussed aging and deterioration mechanisms. Other traditionally neglected features of seismic risk assessment for

bridges also deserve further exploration, like the impact of traffic loads on bridge performance during earthquakes as will be discussed next.

6.2. Impact of Traffic Loads on Bridge Reliability

While the previous section of this chapter focused on the impact of repeated seismic events, this section will focus on another commonly neglected, yet widely prevalent phenomenon while computing bridge vulnerability: impact of truck presence on bridge component and system level response. A joint seismic and live load fragility framework is presented in this study which investigates such impacts while rendering flexibility to incorporate vehicle weight distribution and truck flow rate for site specific bridge reliability estimates (Ghosh et al. 2013d). The proposed framework is developed corresponding to a realistic site specific traffic model in the state of Alabama and representative case study bridge. It is however noted that the suggested methodology is applicable for other traffic models and bridge types.

6.2.1. Influence of truck vehicle weight and position on bridge performance

The governing truck vehicle weight and truck position atop the bridge deck are random variables. This section will investigate the impact of these two parameters on component and system level vulnerability of a case study highway bridge.

6.2.1.1. Case study bridge model

The case study MSC-steel bridge configuration introduced earlier in Chapter 4 is also adopted herein to demonstrate the joint seismic and live load assessment framework. The only difference between the adopted bridge models however is the presence of a truck at a random position atop the bridge deck [Figure 6-9(a)]. The three dimensional finite element bridge model is developed using OpenSees adopting the same modeling principles described earlier for pristine bridge structures. Future studies should explicitly model the deck using improved material models, such as shell elements, as opposed to the base spline model used in this study. Additionally, the aging and deterioration mechanisms discussed previously also need to be incorporated within the proposed live load-seismic fragility framework. The weight of the superimposed truck axles at any position on the

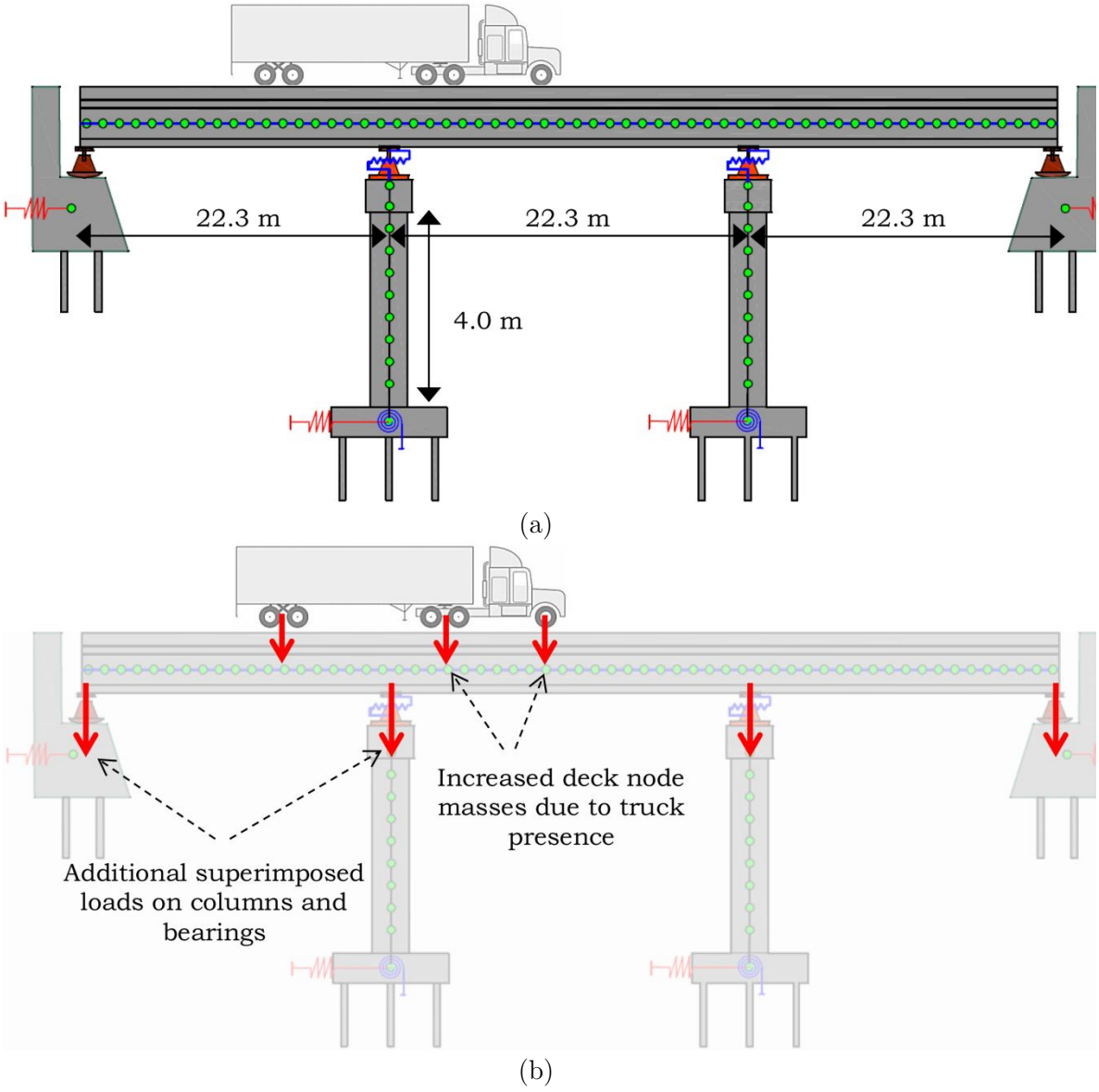

Figure 6-9: a) Case study multi-span continuous (MSC) steel girder with a superimposed truck load at any random location atop the bridge deck, and b) additional loads on bridge deck and other critical bridge components due to truck presence

bridge deck is now reflected via increased modal masses of the pertinent deck nodes, additional vertical forces on steel fixed and expansion bearings and increased axial forces on bridge columns as shown schematically in Figure 6-9(b).

These additional loads on different bridge components due to truck presence are calculated using structural analysis principles after assuming the bridge deck in the form of a spine model spanning over multiple supports as a continuous beam (Ghosh et al. 2013d).

6.2.1.2. Site specific traffic model

The realistic truck-traffic data used in this study is obtained from a regional network of 11 Weigh-In-Motion (WIM) stations across northern Alabama where approximately 21.4 million trucks were recorded thereby providing a robust database of traffic demands. The truck-traffic is represented by a standard WB-20 truck which by Transportation Research Board (2003) is a FHWA Class 9 vehicle, subtype S3 (FHWA 2011) making it the most common type of truck in the recorded database. The geometric configuration of the truck along with the axle distributions of the gross-vehicle-weight (GVW) is depicted in Figure 6-10(a). Additionally, Figure 6-10(b) shows the histogram of WB-20 truck GVW at the Alabama site. It shows two modes at 17.2 and 35.4 tonnes, representing empty and fully loaded trucks (partial loads are inefficient and so are fewer), with a GVW range of about 10 to 55 tonnes.

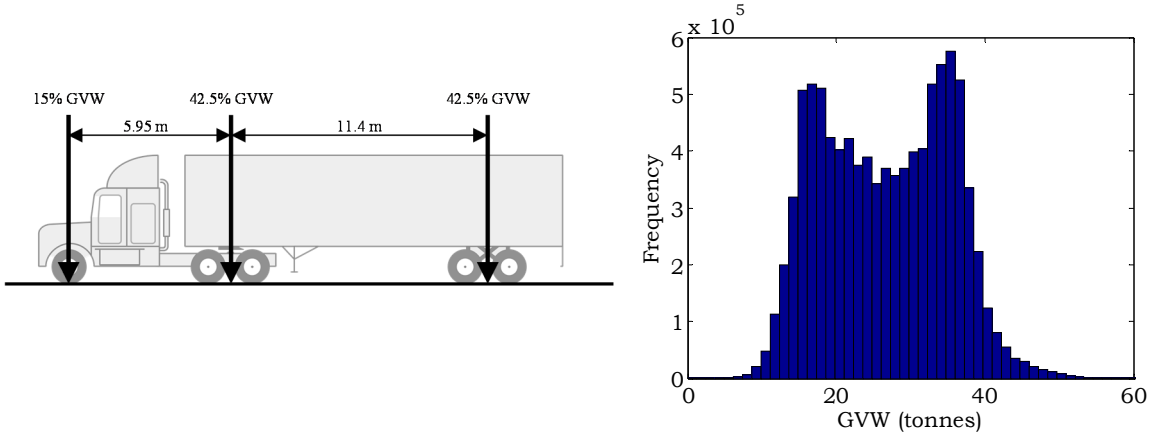

(a) (b)

Figure 6-10: a) Geometric configuration and axle distributions of the gross vehicle weight (GVW) for a WB-20 truck, and b) recorded GVW histogram for all WB-20 type trucks at the chosen case study site (Ghosh et al. 2013d)

6.2.1.3. Identification of most unfavorable truck location and component response analysis

The position of the truck atop the bridge deck is random and can be located anywhere from the left end to the right end of the bridge in the longitudinal direction. To identify the truck position which makes the case study bridge most vulnerable to seismic shaking, several different truck positions atop the bridge deck are investigated. These positions range from Load Case 1 to Load Case 18 [Figure 6-11(a)] in increments of 2.90 m to cover the entire length of the bridge from the left end to the right, offering sufficient discretization to investigate the influence of truck position on bridge component and system level fragilities. These fragilities

are computed using the same procedures as outlined in Chapter 4 for the following case: a) Standalone bridge with no superimposed truck load ($P\left[DS|PGA,\text{No Truck}\right]$), and b) bridge with WB-20 truck of a given GVW (w) at any random location atop the bridge deck ($P\left[DS|PGA,w,\text{Truck}\right]$) with the superimposed load appropriately reflected in the finite element bridge model as described earlier. The fully-loaded truck GVW mode of 35.4tonnes [Figure 6-10(b)] is used in this stage of the analysis [Figure 6-11(a)], but the impact of different truck GVW will be found in the next section. Additionally, it is noted that the symmetry of the case study MSC steel bridge about the bridge centerline in terms of bridge column and bearing configuration averts the need to redo the computationally expensive bridge fragility analysis with the WB-20 truck positioned in the opposite direction.

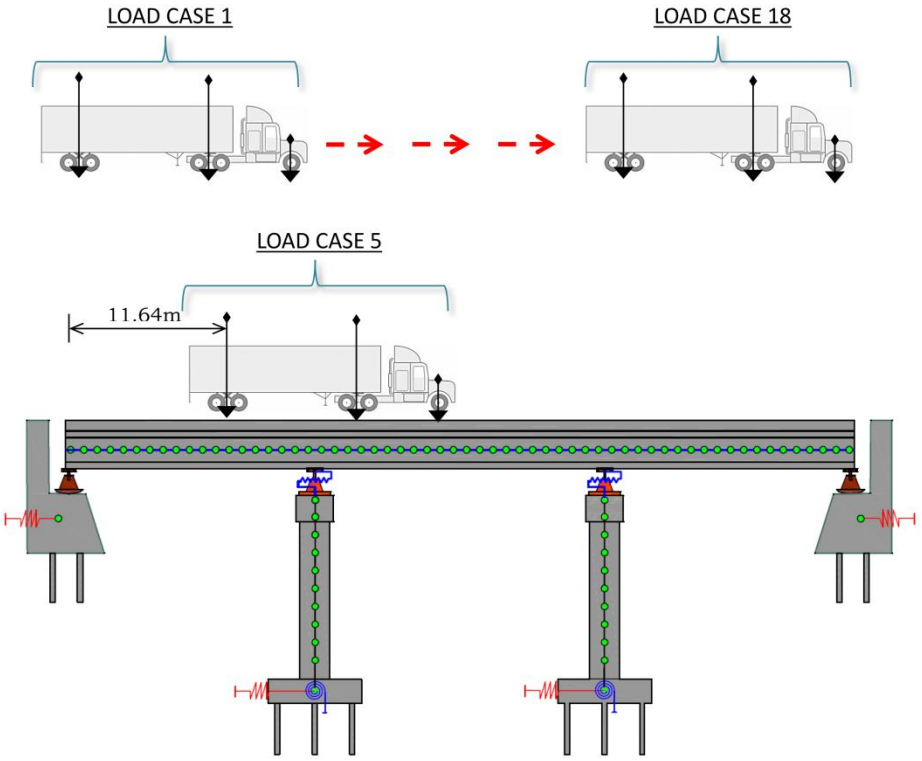

(a)

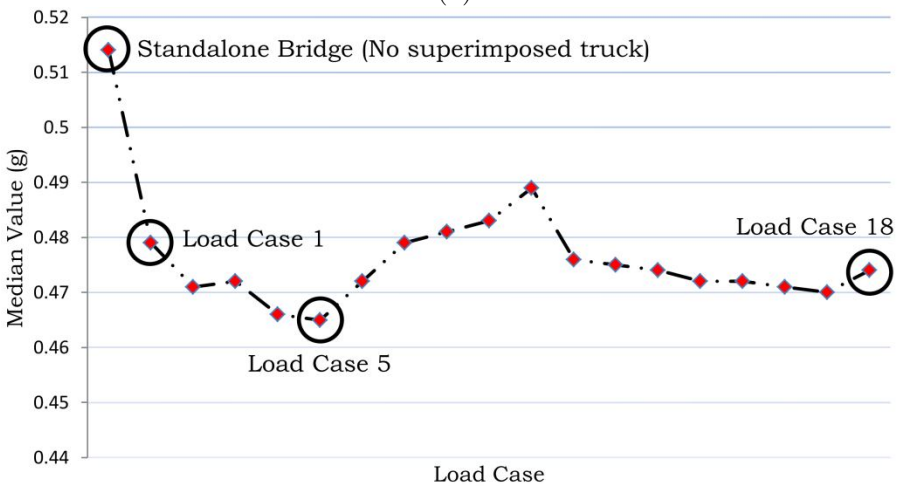

(b)

Figure 6-11: a) Different WB-20 truck locations investigated in this study (ranging from Load Case 1 to Load Case 18) to assess the impact on bridge system fragility, and b) median values of bridge system fragility for the standalone bridge with no superimposed truck and Load Cases 1 to 18. Note that Load Case 5 leads to the highest change in median values and hence corresponds to the most unfavorable truck position (Ghosh et al. 2013d)

Corresponding to each truck position, from Load Case 1 to Load Case 18, fragility analyses are conducted to arrive at the median and dispersion values of bridge component and system level fragility. Figure 6-11(b) shows the median values of bridge system fragility for the extensive damage state for the different load cases in addition to median value for the standalone bridge without any superimposed truck load. At the extensive damage state the damage to bridge components in visible, requires repair and results in closure of the bridge for at least a week after the seismic event (Padgett and DesRoches 2007). All the results presented in this chapter will correspond to this damage state although the methodology is applicable to other damage states as well. Since the median value of fragility corresponds to the PGA intensity which indicates 50% probability of damage state exceedance, a reduction in median value signifies a more seismically vulnerable bridge. Hence, it is evident from Figure 6-11(b) that regardless of the location, presence of a superimposed truck load on a bridge leads to a decrease in median value of fragility and hence an increase in bridge vulnerability. Of all load cases considered, however, Load Case 5 [Figure 6-11(a)] is found to be the most unfavorable to the case study bridge fragility leading to approximately 10% reduction in median values as compared to the pristine bridge structure. It also

noted that irrespective of the position of superimposed WB-20 truck load, the variation in the dispersion of fragility estimates is negligible compared to the standalone bridge and approximately equals 0.50. This is in contrast to the time-dependent aging fragility curves developed earlier which revealed the potential impact of aging and deterioration mechanisms on both median and dispersion estimates.

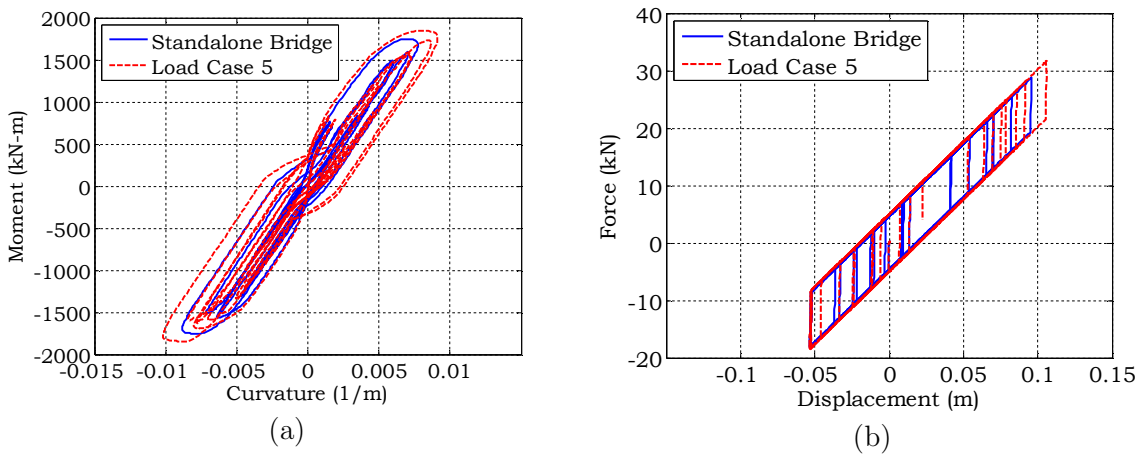

Figure 6-12: Increase in peak component responses of a) reinforced concrete columns and b) expansion bearings in the longitudinal direction when the case study bridge with WB-20 truck in Load Case 5 position is subjected to a deterministic ground motion with peak ground acceleration of 0.47g. Comparisons are shown with respect to the component behaviors of the standalone bridge with no superimposed truck load subjected to the same ground motion (Ghosh et al. 2013d)

A closer inspection of the seismic response of the case study highway bridge for the most unfavorable truck position (Load Case 5) reveals an increase in seismic demand of critical bridge components as compared to the standalone bridge

without any superimposed truck load. For instance Figure 6-12(a) shows an increased peak column curvature of the case study bridge column in the first bent when the bridge is subjected to a deterministic ground motion record from the Rix and Fernandez (2004) ground motion suite with peak ground acceleration of 0.47g. Additionally Figure 6-12(b) shows the increase in peak expansion bearing deformation in the second bent along the longitudinal direction as compared to the standalone bridge. It is noted that although Load Case 5 results in the maximum increase in the seismic demand of critical bridge components which eventually leads to highest reduction in median value of bridge fragilities [Figure 6-12(b)], the trend of observing a steady increase in seismic demand of these components due to superimposed truck load is consistent for all load cases.

6.2.1.4. Influence of truck weight on seismic fragility

Given the identification of the most unfavorable position of the WB-20 truck load, fragility surfaces are derived herein corresponding to this truck position for different truck GVWs. As shown in Figure 6-10(b) depicting the truck GVW histogram, it is evident that truck weight is a random variable and can vary widely across a specific site. The impact of variable truck GVW corresponding to the most unfavorable truck position (Load Case 5) is investigated by conducting the fragility

analysis after successively increasing the truck vehicle weight from 10 to 60 tonnes in increments of 10 tonnes to cover the entire range of truck GVW in the site-specific WIM data of Figure 6-10(a).

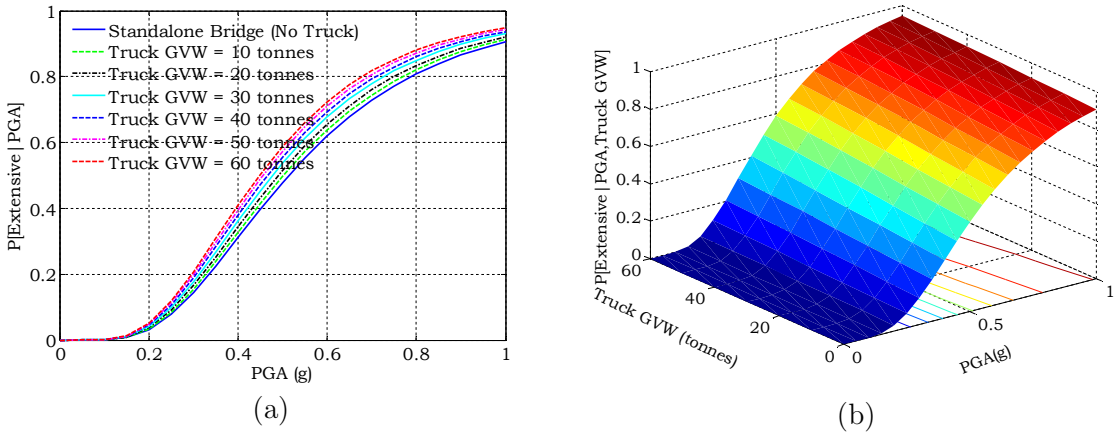

(a) (b)

Figure 6-13: a) Case study bridge system level fragility curves for different GVWs of the WB-20 truck positioned at Load Case 5 location, and b) interpolated three dimensional fragility surface depicting the joint impact of the PGA of seismic shaking and truck GVW (Ghosh et al. 2013d)

Figure 6-13 shows the fragility curves for different truck GVW occurrences in addition to the interpolated fragility surface. The steady increase in bridge fragility underlines the enhanced susceptibility of bridge damage state exceedance to increased superimposed truck load. The median fragility estimates for the present case study bridge are found to change by 13% for the 60 tonne truck GVW as opposed to case when there is no superimposed truck load atop the bridge deck. It is however acknowledged that the chances of observing the heaviest truck at the worst location is rare.

6.2.2. Joint seismic and live load framework: Seismic fragility convolution with live load models

The previous sections demonstrated that that presence of truck load atop the bridge deck may lead to noticeable changes in bridge vulnerability depending on the truck position and gross vehicle weight. The developed fragility surface will now be convolved with the case study site specific GVW histogram and truck flow rate to determine site specific conditional bridge fragility.

6.2.2.1. General convolution methodology

To develop a site-specific model, the presence of only a single truck is assumed in this study which is deemed reasonable for bridge lengths less than about 100m. The fragility surface previously defined [Figure 6-13(b)] is conditional on the presence of one truck, and the associated truck GVW, in addition to the traditional hazard intensity measure (PGA). Thus the fragility curve can be expressed by integrating on the truck GVW distribution, denoted $f_{\mathrm{GVW}}\left(\cdot\right)$ (Ghosh et al. 2013d):

$$P\left[\text{Extensive} \mid \text{PGA}, \text{Truck}\right] = \int P\left[\text{Extensive} \mid \text{PGA}, w, \text{Truck}\right] \cdot f_{\mathrm{GVW}}\left(w\right) dw \quad (6.15)$$

where w is a dummy integration variable. Then, the fragility curve is given by:

$$P\left[\text{Extensive} \mid \text{PGA}\right] = P\left[\text{Extensive} \mid \text{PGA}, \text{Truck}\right] \cdot P\left[\text{Truck}\right] + P\left[\text{Extensive} \mid \text{PGA}, \text{No Truck}\right] \cdot P\left[\text{No Truck}\right] \quad (6.16)$$

The term $P\left[\text{Extensive} \mid \text{PGA}, \text{No Truck}\right]$ is just the standard seismic fragility curve for the standalone bridge without any superimposed traffic loads.

The site-specific elements of the proposed model are twofold: it requires the truck GVW distribution, and the probability of occurrence of a truck, a function of the truck density at the site, which is in turn a function of the flow rate and mean speed at the site. While the truck GVW distribution can be readily obtained from WIM data at the site [Figure 6-10(b)], the following section on truck presence modeling will demonstrate truck occurrence probability computations.

6.2.2.2. Truck Presence Modeling

This section will summarize the truck presence model adopted in this study, which may be found in further details in (Ghosh et al. 2013d). The mean truck density (trucks per km) is adopted as the traffic metric in this study for site specific convolution and may be expressed as:

$$\rho = \frac{Q}{v} \tag{6.17}$$

where Q (i.e. the truck flow rate) and v (km/h) is the constant (or mean) speed of the traffic stream. In addition to the mean truck density, vehicle presence modeling also needs to account for the minimum length within which no arrival can occur: this includes the physical vehicle length, as well as a minimum gap that drivers will keep in jammed conditions, usually assumed to be about 2m. Denoting this length as Δ, Haight (1963) provides the general result for n vehicles. For simplicity however, the presence of one truck at a time on the bridge is slightly overestimated by neglecting multiple truck presences and writing (Ghosh et al. 2013d):

$$P\left[1 \text{ truck}\right] \approx 1 - P\left[\text{No trucks}\right] = 1 - \left\{\frac{\Gamma\left(1, \mu\left[L - \Delta\right]\right)}{\Gamma\left(1\right)} - \frac{\Gamma\left(0, \mu L\right)}{\Gamma\left(0\right)}\right\} \tag{6.18}$$

where, $\Gamma\left(n, x\right)$ denotes the upper incomplete gamma function, $\Gamma\left(n\right)$ the complete gamma function, L is the length of the bridge, μ is the mean truck density in trucks/m ($\rho \times 10^{-3}$); and the other parameters are as previously defined. The assumptions underlying Equation (6.18), such as constant speed of the traffic and that all truck occupancy lengths are the same (Δ), have been tested using Monte Carlo simulation of a heterogeneous traffic stream based on the model described in

O'Brien and Caprani (2005). Ghosh et al. (2013d) found that Equation (6.18) offers a slightly conservative estimation of the probability of occurrence of a truck on a length of road, given a truck flow rate and velocity distribution. As such, this model is deemed appropriate for modest truck flows and bridge lengths under about 100m.

For the current case study bridge of length 66.9m, and assuming $\Delta = 22$m [20m length for the WB-20 truck plus 2m full stop bumper-to-bumper minimum gap (Caprani 2012)], and a free-flow speed of 80km/h (about 50mph), the probabilities of 1 truck occurring, based on Equation (6.18), are 4.4% for 80trucks per hour (truck density of 1truck/km) increasing to 16.4% for 320trucks per hour (4 trucks/km) (Ghosh et al. 2013d). Figure 6-14 shows the variation of this probability by flow rate for the case study bridge and other bridge lengths. It can be seen that the probability is more sensitive to bridge length than truck density, and may be reasonably well approximated by straight line fits enveloped by (Ghosh et al. 2013d):

$$P\left[1 \text{ truck}\right] \approx \left(L - 18\right) Q \times 10^{-5} \tag{6.19}$$

where L is the bridge length ($25 \leq L \leq 100\,\text{m}$) and Q ($0 \leq Q \leq 600\,\text{trucks/hr}$) is the mean hourly truck flow, and a mean traffic speed of 80-90km/h is assumed.

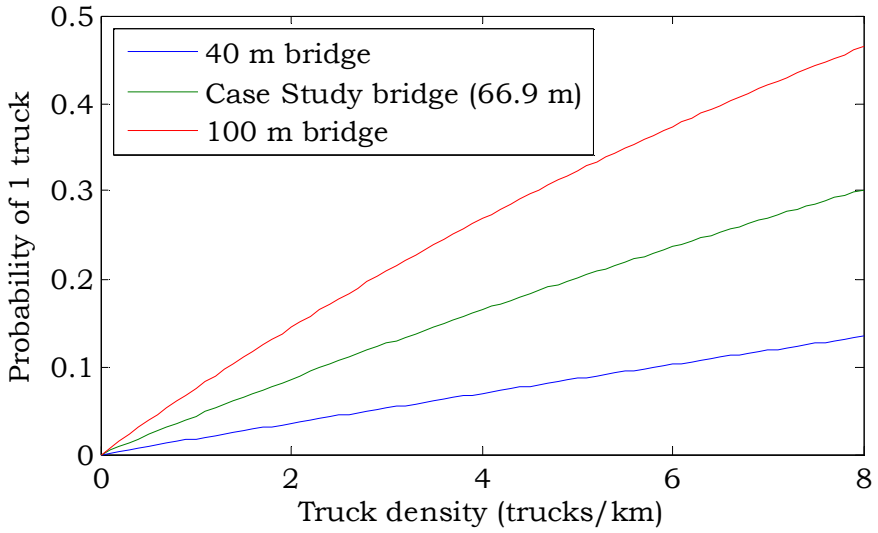

Figure 6-14: Probabilities of observing one truck by truck density and bridge length, assuming Δ = 22m (Ghosh et al. 2013d)

It should be noted that all of the above discussion relates to one traffic lane only. If it is assumed that the truck arrivals in adjacent lanes are independent (and there is some evidence to suggest that they are not, but the correlation is generally weak [OBrien and Enright 2011)], then the probability of one truck being present on multiple lanes is found from Equation (6.18) using the combined truck density across the lanes.

6.2.2.3. Results for the case study bridge and site traffic load data

For a one-lane bridge, using the approach described, the fragility curves are shown below in Figure 6-15 for the following cases: (a) no truck is present, representing current practice; (b) one truck is present which has GVW histogram given by Figure 6-10(b) and the fragility curve estimated using Equation (6.15) and; (c) the fragility curve, estimated from Equation (6.16), which allows for the probability of occurrence of the truck for a density of 4trucks/km found to be 16.4% using Equation (6.18). These cases can otherwise be summarized as comparing the traditional assumption of no truck (i.e. P[Extensive | PGA, No Truck]); the consideration of live load with realistic distribution of truck weight and an assumption that the truck is present, (i.e. P[Extensive | PGA, Truck]); the consideration of live load with realistic distribution of truck weight and likelihood of truck presence (i.e. P[Extensive | PGA]). The median fragilities for these cases are: (a) 0.514g; (b) 0.481g, and; (c) 0.508g, showing reductions of 6.33% and 1.07% for (b) and (c) from the no-truck case. Hence, although the previous sections demonstrated that presence of truck atop the bridge deck may cause noticeable changes in fragility, after accounting for the GVW distribution and truck density the impact is found negligible for the present site specific investigation.

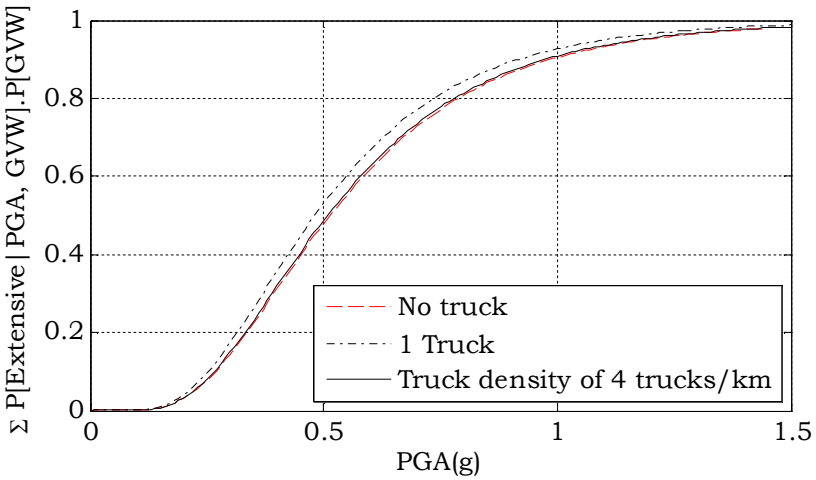

Figure 6-15: Change in seismic fragility when traffic loading is included (Ghosh et al. 2013d)

6.3. Closure

This chapter investigated two supplementary threats which are commonly neglected while assessing the seismic vulnerability of highway bridges. One such threat is the phenomena of repeated earthquake exposure in regions characterized by moderate to high seismicity. In this chapter, a framework is developed to estimate the probability of structural damage due to repeated earthquake occurrences while also accounting for the random nature of hazard occurrence. As an indicator of accumulated damage the Park and Ang damage index is chosen which helps to quantify damage using the maximum curvature ductility induced by the earthquake and the amount of energy dissipated by the structure. A

preliminary step in the damage accumulation framework involves the development of linear (for single shocks) or multilinear (for multiple shocks) regression equations to statistically predict the damage index as a function of the earthquake intensity and past damage history. The developed regression equations are independent of the hazard rates and can be applied to the bridge structure without any prior knowledge on the site specific hazard. Since the probability of earthquake occurrences are different for different PGA intensities, the site specific hazard curves are used in conjunction with a Monte Carlo strategy to develop probabilistic estimates of damage index exceedance conditioned on the number of shocks. Finally, time-dependent damage index exceedance probabilities are estimated after computing the likelihood of occurrences of different number of shocks using the constant homogeneous (for main shocks) or time-dependent nonhomogeneous (for aftershocks) Poisson process rates. The proposed damage accumulation framework is applied to a representative case study single column box girder bridge located near the San Andreas Fault, California. Results indicate that for both repeated main shocks as well as main shock-aftershock sequences, there is a significant increase in the probability of bridge damage with the number of earthquake shocks.

While the primary function of highway bridges is to ensure the safe passage of truck-traffic, the impact of these loads has been traditionally ignored within the traditional fragility framework. The second half of this chapter focused on this issue by evaluating the influence of truck loads on the seismic vulnerability of bridges and proposing a framework for the joint seismic and live load fragility assessment. An example bridge and a large database of real traffic data are used to demonstrate the approach. A WB-20 truck, representative of the truck-traffic, is used to assess the influence of the presence of a single truck on the seismic fragility. The impact of truck location is assessed by positioning the truck at different locations atop the bridge deck and subsequently computing the bridge fragilities. After determining the most influential truck position, a fragility surface is constructed conditioned on the ground motion intensity and gross vehicle weight. The fragility surface revealed an appreciable increase in bridge seismic fragility for the heaviest truck load when positioned at the worst case location. Finally, this work also proposes a means to include the probability of a truck presence, given the truck density at the site, in a seismic fragility assessment. For the bridge and traffic studied, even for heavy truck flows, the median PGA is found to reduce by a negligible percentage. Hence, unless the site specific GVW distribution is

significantly different from the present case study, even for high flow rates the truck-traffic does not have a significant effect on the seismic fragility. Future studies should investigate if these findings are consistent across other bridge classes investigated in this thesis. If the impact of truck-traffic is revealed significant for other bridge classes, then network level reliability estimation studies (as indicated in Chapter 5) is warranted after incorporating truck-traffic data across the network level.

Chapter 7

APPLICATION OF TIME-EVOLVING FRAGILITY FUNCTIONS: SEISMIC LOSS ASSESSMENT OF AGING BRIDGES

Previous chapters of this thesis focused on the development fragility functions for aging highway bridges highlighting the increase in the probability of meeting or exceeding a particular damage state due to aging and deterioration or other supplementary threats along the service life of the bridge. This chapter will focus on the assessment of lifetime economic loss attributed to repair of seismic damage to bridges. In particular, this chapter applies the time-dependent fragility curves developed in Chapter 4 to assess seismic losses, although in general the parameterized fragility functions may also be adopted. In this regard, a framework based on a nonhomogeneous Poisson process is developed which is capable of incorporating time-dependent bridge vulnerability, uncertainty in repair procedures

and correlations between component repair costs (Ghosh and Padgett 2011). The following sections will highlight the mathematical principles behind the development of this framework, along with case study examples of seismic loss estimation of aging highway bridges.

7.1. Nonhomogeneous Poisson Process Formulation for Seismic Loss Estimation of Deteriorating Highway Bridges

Accurate predictions of seismic loss estimates of highway bridges require explicit consideration of the effects of structural degradation, which have traditionally been ignored. Under the assumption of time invariant structural strength, the seismic failure probability of bridge components does not change along the structure's service life and thereby losses can be computed using pristine bridge fragility curves. However, the time-dependent fragility curves presented in Chapter 4, confirms that exposure to unfavorable environmental conditions leads to changes in damage exceedance probabilities with time. These time-dependent fragility curves will be used here within a nonhomogeneous Poisson process framework to model lifetime seismic loss estimates (Ghosh and Padgett 2011).

7.1.1. Component level seismic loss estimation of aging bridges

Given a constant annual earthquake occurrence rate at the bridge site, the time-dependent annual rate of occurrence of a particular damage state i for a bridge component m at time t can be as a nonhomogeneous Poisson process given by:

$$\lambda_{i,m}(t) = \nu P_{i,m}(t) \tag{7.1}$$

where, ν is the constant site specific earthquake occurrence rate, $P_{i,m}(t)$ is the time-dependent annual probability of exceedance of damage state i for the m^{th} bridge component at time t. The time between events in a homogeneous Poisson process with a constant rate (r) can be modeled by an exponential distribution, with the probability density function (PDF), $f_\tau(t)$ and the cumulative density function (CDF), $F_\tau(t)$ following the equations (Melchers 1999):

$$F_\tau\left(t\right) = 1 - e^{-rt} \tag{7.2}$$

$$f_\tau\left(t\right) = re^{-rt} \tag{7.3}$$

In the context of this study involving the nonhomogeneous Poisson process with a time varying rate parameter $\lambda_{i,m}(t)$, the same equations as above can be

adopted but now with r replaced by $\lambda_{i,m}(t)$ and e^{-rt} replaced by $e^{-\int_0^t \nu P_{i,m}(t)dt}$ as shown:

$$F_\tau\left(t\right) = 1 - e^{-\int_0^t \nu P_{i,m}(t)dt} \tag{7.4}$$

$$f_\tau\left(t\right) = \lambda_{i,m}(t) e^{-\int_0^t \nu P_{i,m}(t)dt} \tag{7.5}$$

These equations reflect the distribution of the time between the beginning of exposure of the deteriorating bridge component to earthquakes ($t = 0$), and the occurrence of first failure ($t = \tau$). The CDF, $F_\tau\left(t\right)$, as shown in Equation (7.4), is also equivalent to the probability of exceeding the limit state of the deteriorating bridge component in the period $[0, T]$.

Additionally, C_{i,m_t} is defined as the cost associated with damage state i to restore the bridge component m to its original full functionality at time t. As formulated by Beck et al. (2002) for seismic loss estimation of buildings, the present value of total seismic losses ($SLS_{i,m}$)corresponding to damage state i along the service life of the bridge component is given by:

$$SLS_{i,m} = \sum_{t=1}^{T} \left[C_{i,m_t} \left(1+d\right)^{-t} \right] \tag{7.6}$$

where, d is the after-inflation risk-free discount ratio to convert future costs into present values and T is the service life of the bridge. The probabilistic tools described for a nonhomogeneous Poisson process, along with Equation (7.6) which converts future losses into present values, are used to derive the statistical moments of seismic loss estimates of deteriorating bridge components with uncertainty in repair procedures. These derivations are detailed in the equations presented in the following sections.

Given the definition of the discount ratio presented, the cost to restore the structure at time t is the same as the present day repair cost (Nuti and Vanzi 2003), or $C_{i,m_t} = C_{i,m_0} = C_{i,m}$. The expected value of seismic losses can therefore be calculated as:

$$E\left[SLS_{i,m}\right] = E\left[\sum_{t=1}^{T} \left[C_{i,m} \left(1+d\right)^{-t} \right]\right] \tag{7.7}$$

This expression can be expanded using a geometric series and further simplified to estimate the expected seismic losses as shown in Equation (7.8):

$$E\left[SLS_{i,m}\right] = \left[\sum_{t=1}^{T} P(C_{i,m_t}).C_{i,m} \right].\frac{1-\left(1+d\right)^{-T}}{d} \tag{7.8}$$

where, $P(C_{i,m_t})$ is the probability of incurring the cost $C_{i,m}$ at time t and can be replaced by the probability density function of the time elapsed from beginning of exposure to hazard occurrence as given in Equation (7.5), but in the discrete space. Furthermore, a summation is introduced given n distinct damage states to evaluate the total expected cost across all damage states for a single component:

$$E\left[SLS_{m}\right] = \left[\sum_{i=1}^{n}\sum_{t=1}^{T} \lambda_{i,m}\left(t\right) e^{-\sum_{t=1}^{t=T}\lambda_{i,m}(t)}.C_{i,m} \right].\frac{1-\left(1+d\right)^{-T}}{d} \tag{7.9}$$

In reality, several options may exist for repairing a particular damage state for the bridge component and the preference of one repair strategy over another depends on the discretion of the owner and availability of resources. Hence, instead of having a single repair cost, $C_{i,m}$ (and hence a single repair strategy), the expected seismic loss can be written as follows by considering multiple repair strategies using the theorem of total probability (Ghosh and Padgett 2011):

$$E\left[SLS_{m}\right] = \left[\sum_{i=1}^{n}\sum_{t=1}^{T}\sum_{j=1}^{J} \lambda_{i,m}\left(t\right) e^{-\sum_{t=1}^{t=T}\lambda_{i,m}(t)}.P\left(C_{i,m,j}\right).C_{i,m,j} \right].\frac{1-\left(1+d\right)^{-T}}{d} \tag{7.10}$$

where, $P\left(C_{i,m,j}\right)$ is the probability of adopting the j^{th} repair strategy, which has an associated cost $C_{i,m,j}$, and J is the total number of viable repair options.

Similar to the expected value, the variance of the seismic loss estimate for a single repair strategy can be calculated from first principles as:

$$Var\left[SLS_{i,m}\right] = Var\left[\sum_{t=1}^{T} C_{i,m}\left(1+d\right)^{-t}\right] \tag{7.11}$$

This expression can also be expanded using a geometric series as shown in Equation (7.12)(Ghosh and Padgett 2011):

$$Var\left[SLS_{i,m}\right] = \left[E\left(C_{i,m}{}^{2}\right) - \left(E\left(C_{i,m}\right)\right)^{2}\right].\left(\frac{1-\left(1+d\right)^{-2T}}{d(2+d)}\right) \tag{7.12}$$

Given the potential for different repair strategies to restore a particular component, to the variance in the seismic losses considering the contribution of all damage states for components m is found as (Ghosh and Padgett 2011):

$$Var\left[SLS_{i,m}\right] = \left[\sum_{i=1}^{n}\left(\sum_{t=1}^{T}\sum_{j=1}^{J}\lambda_{i,m}\left(t\right)e^{-\sum_{t=1}^{t=T}\lambda_{i,m}(t)}.P\left(C_{i,m,j}\right).C_{i,m,j}^{2} - \left\{\sum_{t=1}^{T}\sum_{j=1}^{J}\lambda_{i,m}\left(t\right)e^{-\sum_{t=1}^{t=T}\lambda_{i,m}(t)}.P\left(C_{i,m,j}\right).C_{i,m,j}\right\}^{2}\right)\right].\left(\frac{1-\left(1+d\right)^{-2T}}{d(2+d)}\right) \tag{7.13}$$

where all variables have been previously defined.

In the preceding equations, the mean annual rate of failure, $\lambda_{i,m}(t)$, due to occurrence of a particular damage state i, can be approximated by the annual probability of damage due to damage state i only as (Melchers 1999):

$$\lambda_{i,m}\left(t\right) = PA_{i,m}\left(t\right) - PA_{i+1,m}(t) \tag{7.14}$$

where, in the context of this study, $PA_{i,m}(t)$ is the annual probability of exceedance of damage state i at time t for the m^{th} bridge component. To estimate these annual probabilities of exceeding different damage states, key input parameters are the time-dependent fragility curves described in Chapter 4. For instance, for the bridge component m, the time-dependent fragility for the i^{th} damage state may be evaluated using Equation (4.4), reproduced in Equation (7.15) as:

$$P_{f,i,m}(t) = \Phi\left[\frac{\ln\left(PGA\right) - \ln(med_{i,m}(t))}{disp_{i,m}(t)}\right] \tag{7.15}$$

where, $med_{i,m}(t)$ and $disp_{i,m}(t)$ are the median value and logarithmic standard deviation at time t in the service life of the bridge component m, PGA is the peak ground acceleration as a measure of the intensity of ground motion, and $\Phi(\bullet)$ is the standard normal cumulative distribution function. To evaluate the annual probability of exceedance, the time-dependent bridge fragilities can be convolved with the bridge site specific hazard curve as:

$$PA_{i,m}(t) = \int \Phi\left[\frac{\ln(pga) - \ln(med_{i,m}(t))}{disp_{i,m}(t)}\right]\left|\frac{dH(pga)}{d(pga)}\right| d(pga) \tag{7.16}$$

where, $H(pga)$ is the hazard curve that quantifies the annual probability of exceeding a specific level of $PGA = pga$ at a site.

7.1.2. System level seismic loss estimation of aging bridges

Moving from the component level to system level seismic loss estimate requires aggregation of component level losses. However, the damage scenarios for the different bridge components are not statistically independent. For instance, damage to one bridge component (e.g. bearings) might have a direct influence on the demand placed upon and subsequent damage caused to other bridge components (e.g. columns or abutments). Such correlations between bridge

components can be accounted for by introducing a correlation matrix which specifies the degree of interaction between each component pair during a seismic event in terms of the demands placed. In the present study, seismic loss correlation between different bridge components is assumed to be the same as component demand correlation. Although the component correlations do not have an impact on the expected seismic loss estimate for the entire bridge found by aggregating the expected cost of M components, it has a direct influence on computing the associated variance as shown below.

The expected value and variance in total seismic losses incurred for the bridge system can consequently be aggregated as (Ghosh and Padgett 2011):

$$E\left[TSLS\right] = \sum_{m=1}^{M} E\left[SLS_m\right] \tag{7.17}$$

$$Var\left[TSLS\right] = \sum_{m=1}^{M} Var\left[SLS_m\right] + 2\sum_{x=1}^{M}\sum_{y<x}\sqrt{Var\left(SLS_x\right).Var\left(SLS_y\right)}.Corr(SLS_x, SLS_y) \tag{7.18}$$

where, $Corr(SLS_x, SLS_y)$ is the correlation between seismic losses for components x and y.

In the methodology outlined above, the incorporation of time-dependent seismic fragility curves via the nonhomogeneous Poisson process model more accurately reflects seismic losses than traditional models that neglect structural deterioration in time. Additionally, correlations in component damage and loss contributions are captured along with the likelihood of adopting different repair procedures for the same damage level to restore bridge functionality, which is typically neglected in seismic repair modeling and loss estimation approaches. The input parameters (such as time-dependent fragility curves, repair/restoration methods, and associated costs) needed for the proposed loss assessment frameworks are presented in the following sections for two representative case studies.

7.2. Input Models for Seismic Loss Estimates of Deteriorating Bridges

To evaluate seismic losses of the case study aging bridges, several critical parameters are required, including: 1) time-dependent fragility curves of deteriorating bridge components convolved with the location specific hazard map, 2) relative preferences of repair/restoration methods for seismically damaged bridge

components; and 3) repair cost estimates for each identified repair method. The input models adopted for these parameters are discussed below.

7.2.1. Representative case study aging bridges and hazard curves

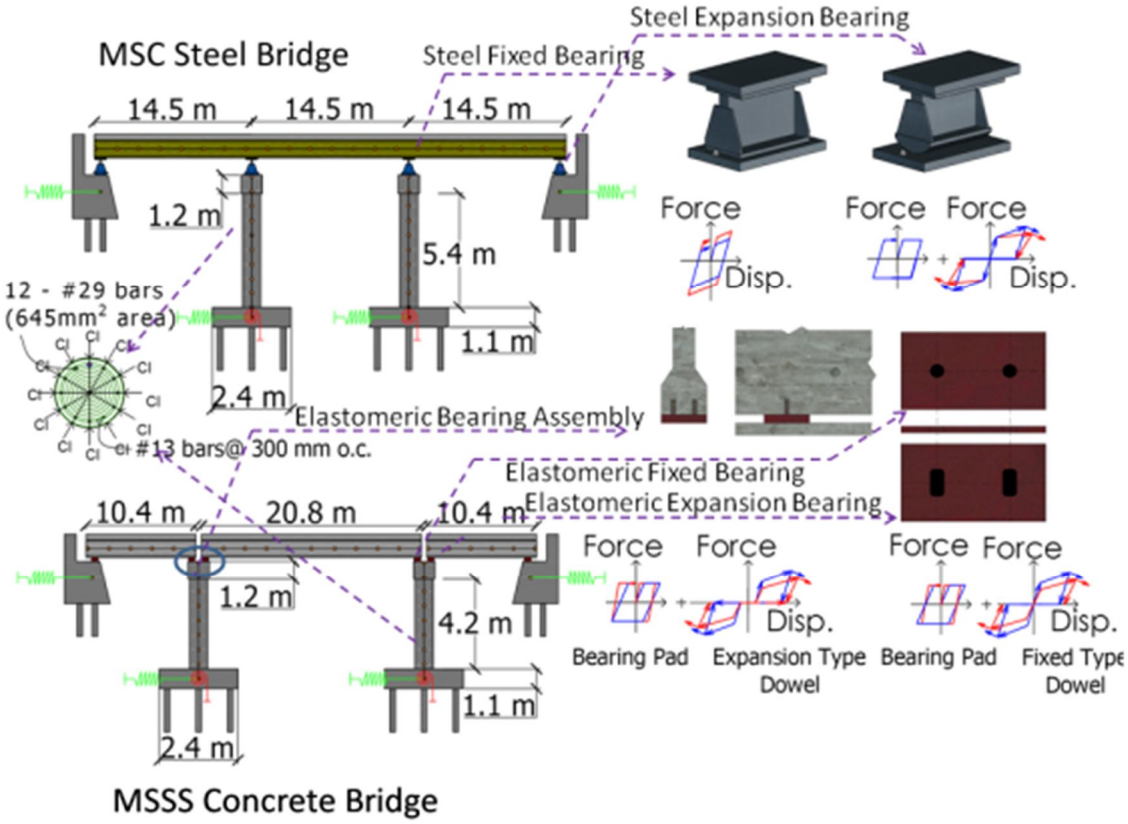

Figure 7-1: Representative case study MSC steel and MSSS concrete girder bridges showing bridge geometries and different bridge components affected by corrosion deterioration (Ghosh and Padgett 2011)

Bridge types from the same bridge classes (MSC steel girder and MSC concrete girder) considered in Chapter 4 are adopted as case study examples to demonstrate the proposed loss assessment framework. The primary motivation behind choosing

these two geometrically and structurally dissimilar bridge types is to demonstrate the varying effect of deterioration mechanisms on different bridge components and subsequent impact on loss estimates. While the deterioration mechanisms of critical structural components belonging to both bridge types and their typical non-seismic detailing have already been detailed in Chapter 3 and Chapter 4, Figure 7-1 shows the geometry and representative finite element model for the two case study bridges considered in this chapter.

Time-dependent fragility curves are derived for each bridge components at different points along the service of the bridge using the methodologies described Chapter 4. For instance, Figure 7-2 (a) illustrates a time varying fragility curve for the deteriorating RC columns of the MSSS concrete girder bridge for the moderate damage state. It should be noted that while deterioration results in an increase in the seismic vulnerability in time for some components (e.g. RC columns), it may lead to a decrease in the seismic fragility for other components (e.g. expansion bearings in longitudinal direction for the MSC steel bridge as discussed in Chapter 4 and shown in Figure 7-2(b) for the present case study bridge). A complete list of the time-dependent fragility parameters corresponding to different components of both case study bridges at different points in time along the service life of the

bridge are presented in Appendix D. These time-dependent fragility curves for each component at this step are convolved next at each point in the service life with the local seismic hazard estimate, as presented in Equation (7.16).

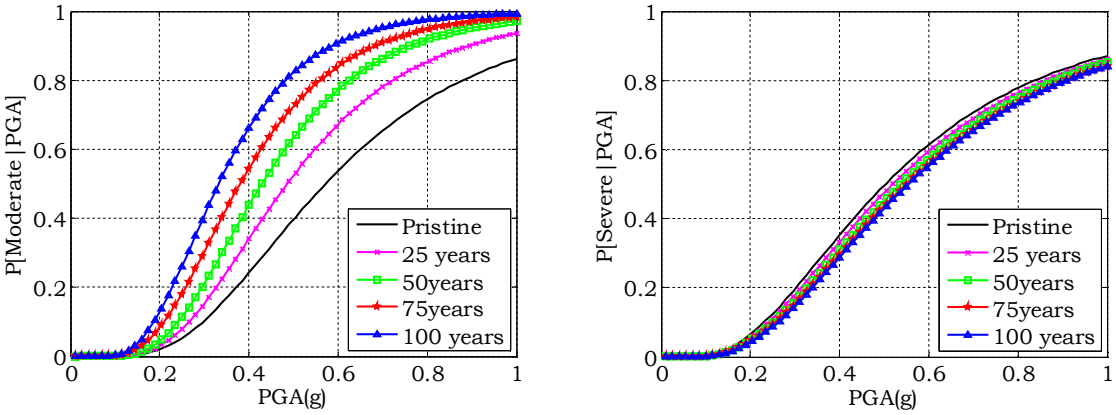

Figure 7-2: Example time-dependent fragility curves for a) RC columns of MSSS concrete bridge, b) expansion bearings in the longitudinal direction of MSC Steel Bridge(Ghosh and Padgett 2011)

For the case study conducted, the seismic hazard curve for Nutbush, located in the southeastern edge of the New Madrid seismic zone in the state of Tennessee is obtained from the USGS (2012)(Figure 7-3) to arrive at the time varying annual probability of bridge component failure used in the proposed seismic loss assessment framework. This region can be characterized as a moderate seismic zone in which low probability high consequence events dominate the seismic hazard. Although the proposed methodology is extendable to other bridge types, deterioration exposure conditions, and hazard levels, this New Madrid region is

particularly crucial for implementation of the proposed methodology due to the significant potential for corrosive exposure, such as deicing salts, rendering time variation in the seismic vulnerability, coupled with limited seismic detailing. Furthermore, the importance of such a risk-based approach is critical in such regions for propagating the range of sources of uncertainty in the loss estimation. Consequently, the associated seismic fragility model and repair cost model presented in the next section are typically representative of bridges in the CSUS. However, to assess the impact of the seismic hazard curve or bridge siting, the case study section of this chapter also includes a comparative seismic loss estimate for the bridges using the hazard curve of Los Angeles, California also shown in Figure 7-3. This will be addressed in Section 7.3.2.2.

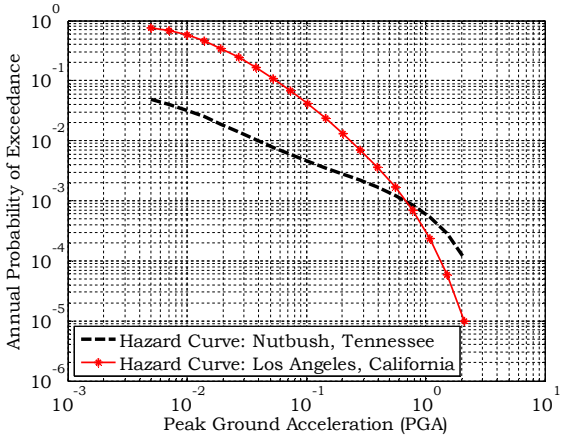

Figure 7-3: Seismic hazard curves for Nutbush, TN and Los Angeles, CA adopted from USGS (2012)

7.2.2. Repair model

Corresponding to each damage state of the individual bridge components, different repair strategies may exist in practice. Preference of one repair strategy over another depends on the level of damage, the discretion of the bridge engineer and the ease of availability of resources. The viable repair strategies for the different bridge components are obtained in this study from analysis of the results of a web based survey conducted by Padgett and DesRoches (2007). In the previous study, twenty eight practicing bridge inspectors and officials indicated their recommended repair procedure for various levels of damage to critical bridge components. Further details on the survey methodology and results can be found in Padgett and DesRoches (2007). The responses obtained reflect a range of preferences for repair items and are adopted as the probabilistic repair procedure model for the case study conducted in this chapter (Padgett and DesRoches 2007).

To illustrate the repair model assumed, Figure 7-4 shows a sample of the responses for repair strategies that might be adopted to (a) repair damage to multiple-column bents and (b) address repair strategies that might be needed due to longitudinal offset over the piers following a seismic event. The latter case of longitudinal offset is assumed to be equivalent to the longitudinal deformation of

steel rocker bearings (for the MSC steel bridge) and elastomeric fixed and expansion bearings (for the MSSS concrete bridge) following the suggestions of Nielson (2005). It is also assumed in this study that complete damage state of the bearings in the longitudinal direction is also indicative of imminent deck collapse and hence requires both bearing and bridge deck replacement as the preferred repair strategy for this damage state. Similar results from the past study provide models of repair preferences for damage to other bridge components for use in the case study loss assessment. These are presented in Appendix D.

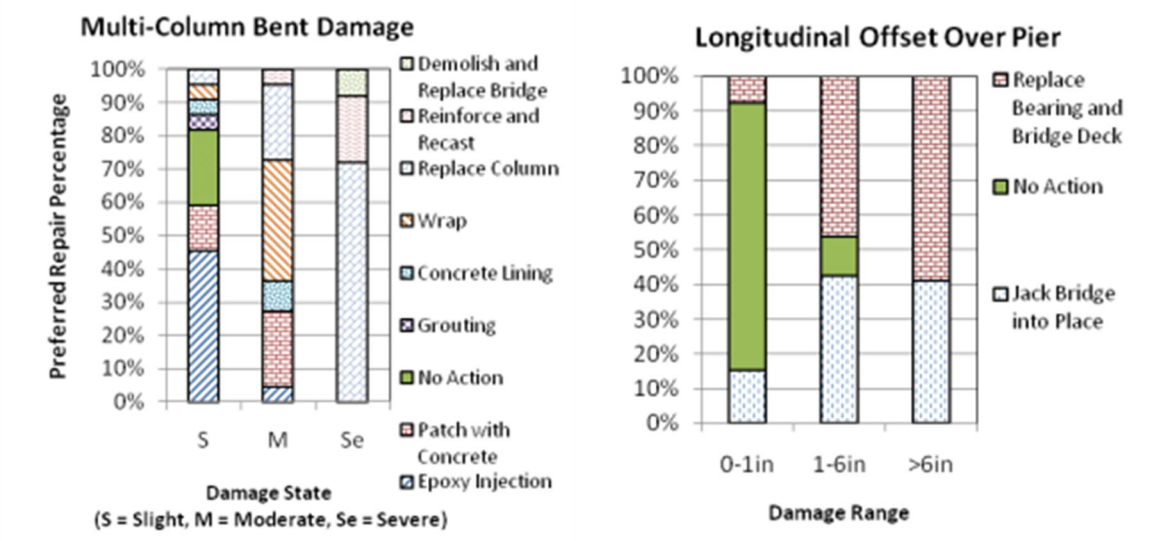

(a) (b)

Figure 7-4: Repair strategies adopted to address a) damage to multicolumn bent and b) longitudinal offset over pier. The figures indicate the probability of each repair method based on survey responses from (Padgett and DesRoches 2007b)

7.2.3. Repair cost estimates

In addition to the repair methods for each component, costs associated with each repair item are required. To reduce uncertainty in cost estimates that arise from variability of pricing from one state to another, the repair costs considered are primarily based on the state of Tennessee – the location of the case study. The repair and replacement cost items are adopted from the *Average Unit Prices for 2009 Awarded Contracts Manual* for highway bridge construction and repair items available from the website of Tennessee Department of Transportation (TNDOT 2010).

Table 7.1: Unit costs of different repair items used in repair/restoration of various bridge components. The reported costs are for the year 2010.

Item	Corresponding bridge component	Unit	Average Unit Price
Epoxy Injection*	Columns, Abutment Passive	ft	$ 46.98
Concrete Patch*	Columns, Fixed Bearings, Abutment Passive	sq. yd.	$ 48.00
Grout*	Columns, Abutment Passive	cu ft	$ 11.58
Concrete Lining*	Columns	each	$ 93.10
Jack bridge into place*	Expansion Bearings	each	$ 2,500.00
Anchor Bolt Replacement*	Fixed and Expansion Bearings	each	$ 13.00
Replace Bearing†	Fixed and Expansion Bearings	each	$ 1,198.50
Regrade and Resurface Approach*	Abutment Active	Lump sum	$ 20,103.00
Add Fill and Asphalt*	Abutment Active	sq. yd.	$ 45.00

Source: *(TNDOT 2010), † (ODOT 2010)

Supplemental cost data not available in the unit price manual are adopted from the Public Works Costbook 2010 (Mahoney 2009) and from the DOT of the neighboring state, Ohio (ODOT 2010). The average unit costs of the different repair items and the bridge components in context of which these repair methods are used following a seismic damage are presented in Table 7.1.

7.3. Case Study Seismic Loss Estimation and Applicability of the Proposed Framework

In this section, probabilistic seismic loss assessments are conducted for the two case study aging bridges to gain insight into the methodology proposed and results obtained with and without deterioration. The proposed methodology based on the nonhomogeneous Poisson process model is applied using the time-dependent component fragility curves, repair model, and repair costs outlined above. Following these formulations, the statistical moments of seismic loss, such as expected values and variances, are evaluated as presented in the following sections. The influence of parameters such as bridge aging mechanisms, different seismic hazard scenarios on the economic losses is compared for both bridge types. The results also provide insight on component damage contributing the most to overall

repair costs or seismic losses, as well as the sensitivity of the loss estimates to modeling assumptions, such as discount rate, remaining service life and hazard curves. These findings are followed by a discussion of the flexibility of application of the proposed methodology within the framework of seismic loss estimation for civil infrastructure.

7.3.1. Expected value and variance of seismic loss estimate of deteriorating bridges

The base case assumed for estimating probabilistic seismic losses includes an after-inflation risk-free discount rate of 3% and a remaining service life of 75 years for the deteriorating bridge located in Nutbush, Tennessee. In reality, the after-inflation risk-free discount rate is practically found to vary from 1% to 7% (Beck et al. 2002) and hence the 3% assumption of the discount rate is believed to be realistic. A sensitivity of the expected losses to the discount rate is presented in a later section. Under the assumption of 3% discount rate, the expected seismic loss estimates of the aging representative MSC steel and MSSS concrete girder bridges are computed following the proposed method.

Figure 7-5 summarizes the results of the loss assessment for both bridge types, and compares the expected seismic losses for the pristine bridge, where deterioration is neglected, to the aging bridge. In addition, the figure also depicts the contribution of different components to the total loss. A change in the relative contribution of component damage to the total losses for the pristine and aging bridge is apparent and consistent with the findings of the fragility analysis for the two bridges. For instance, for the MSC steel bridge, the relative lifetime seismic losses incurred to repair the columns increases in the case where aging is considered, while the fixed bearing contribution actually decreases. Fragility analyses for this type of bridge have revealed that these components tend to be less vulnerable as the bridge approaches the end of its service life, as previously discussed. Overall, the analysis shows an increase of 14% in the total expected seismic losses for the deteriorating MSC steel bridge as compared to the pristine bridge. The relative change observed in seismic loss estimate for the MSSS concrete girder bridge is significantly higher with an increase of approximately 44%. This finding is also a direct reflection of the fact that nearly all of the components of the MSSS concrete bridge become increasingly vulnerable with age.

These results underline the importance of capturing the effects of time-dependent vulnerability in the life-cycle analysis of deteriorating bridge infrastructure.

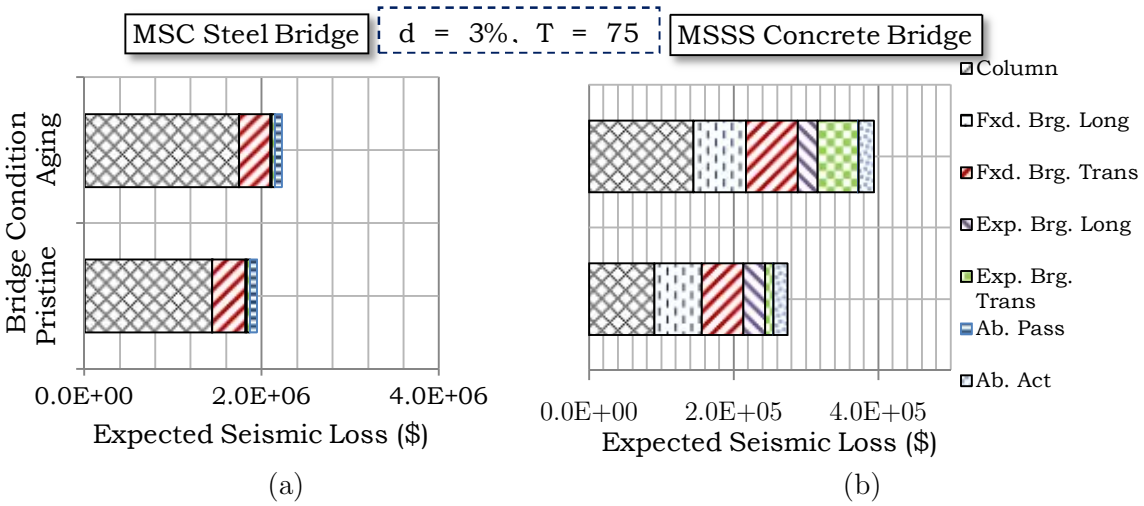

Figure 7-5:Expected seismic loss estimates for the representative a) MSC steel girder bridge and b) MSSS concrete girder bridge for the assumed base case (Ghosh and Padgett 2011)

Table 7.2: Correlation coefficients between demands placed on different bridge components for the MSC steel bridge (Ghosh and Padgett 2011)

	COL	FBL	FBT	EBL	EBT	ABP	ABA
COL	1.00	0.54	0.66	0.82	0.79	0.78	0.60
FBL	0.54	1.00	0.32	0.67	0.62	0.60	0.34
FBT	0.66	0.32	1.00	0.53	0.74	0.43	0.47
EBL	0.82	0.67	0.53	1.00	0.70	0.91	0.77
EBT	0.79	0.62	0.74	0.70	1.00	0.57	0.43
ABP	0.78	0.60	0.43	0.91	0.57	1.00	0.64
ABA	0.60	0.34	0.47	0.77	0.43	0.64	1.00

The total variance in seismic loss is also found for both bridge types after evaluating the variances for individual components from Equation (7.13).

Computing the total variance requires the covariance matrix between the component seismic damage. Table 7.2 shows an example of correlation coefficient matrix between the different components for the representative pristine MSC steel bridge. These coefficients are calculated during the fragility assessment by estimating the correlations between the peak responses of each bridge component from the results of nonlinear time history analysis of the analytical bridge models under a suite of ground motions. The correlation coefficients used in this study correspond to the pristine case study bridges. It is observed from a sensitivity study that the correlation coefficients change negligibly with aging of the bridge, having an insignificant impact on the variance of seismic loss estimates. Additionally, Nielson (2005) found that the correlation coefficients depend negligibly on earthquake intensity of the adopted ground motion suites and can be assumed as constant. Based on these observations, the correlation coefficients for the pristine bridges are adopted in the present study and assumed as time invariant. The seismic loss variances calculated for the correlated bridge components and bridge system reflect the uncertainty in the hazard, structural vulnerability, and repair procedure modeled in the loss assessment framework. The expected values and standard deviations of the total seismic loss estimates for both

bridge types are summarized in Table 7.3 for the base case assumptions. It is worthwhile to note that neglecting the effects of correlation between component damages would result in a significant underestimation of the standard deviation in losses and therefore on probabilities of exceeding budget constraints. For instance, for the aging MSC steel girder bridge the standard deviation of seismic losses are underestimated by as much as 23% if correlations are completely neglected. Additionally, if both the influence of aging and multiple correlated components are neglected in computing the seismic losses, it is found that the expected losses and variances are underestimated by 12.5% and 49.5%, respectively. These findings further highlight the importance of considering the effects of deterioration and correlation between component repairs to estimate seismic losses, as captured in the proposed methodology.

Table 7.3: Summary of seismic loss estimates for representative case study bridges corresponding to the base case (Ghosh and Padgett 2011)

Bridge Type	Bridge condition	Expected Value	Std. Dev.
MSC steel	Pristine	$ 1942363	$ 1044214
	Aging	$ 2221423	$ 1107601
MSSS concrete	Pristine	$ 274197	$ 242280
	Aging	$ 393675	$ 321199

7.3.2. Sensitivity of expected seismic loss estimates to parameter variations

As indicated earlier, the expected values of seismic loss estimates of bridge components and system depend on parameters such as the discount rate and remaining service life of the degrading bridge. Additionally the seismic loss estimates in the previous section were evaluated after convolving the component fragilities with a single hazard curve for Nutbush, Tennessee. The main focus of this section is to evaluate to sensitivity of expected losses to variations of these above mentioned factors.

7.3.2.1. Impact of variations in discount ratio and remaining service life on expected seismic losses

To assess the influence of modeling parameter variations, the after-inflation risk-free discount rate is reasonable assumed to differ from 1% to 7% (Beck et al. 2002) while the remaining service life of the bridge is assumed to vary from 25 years to 100 years, with an assumed total service life of 100 years. Figure 7-6 shows the sensitivity of the expected seismic loss estimate when one of these parameters is held constant at the base value and the other is varied across its range.

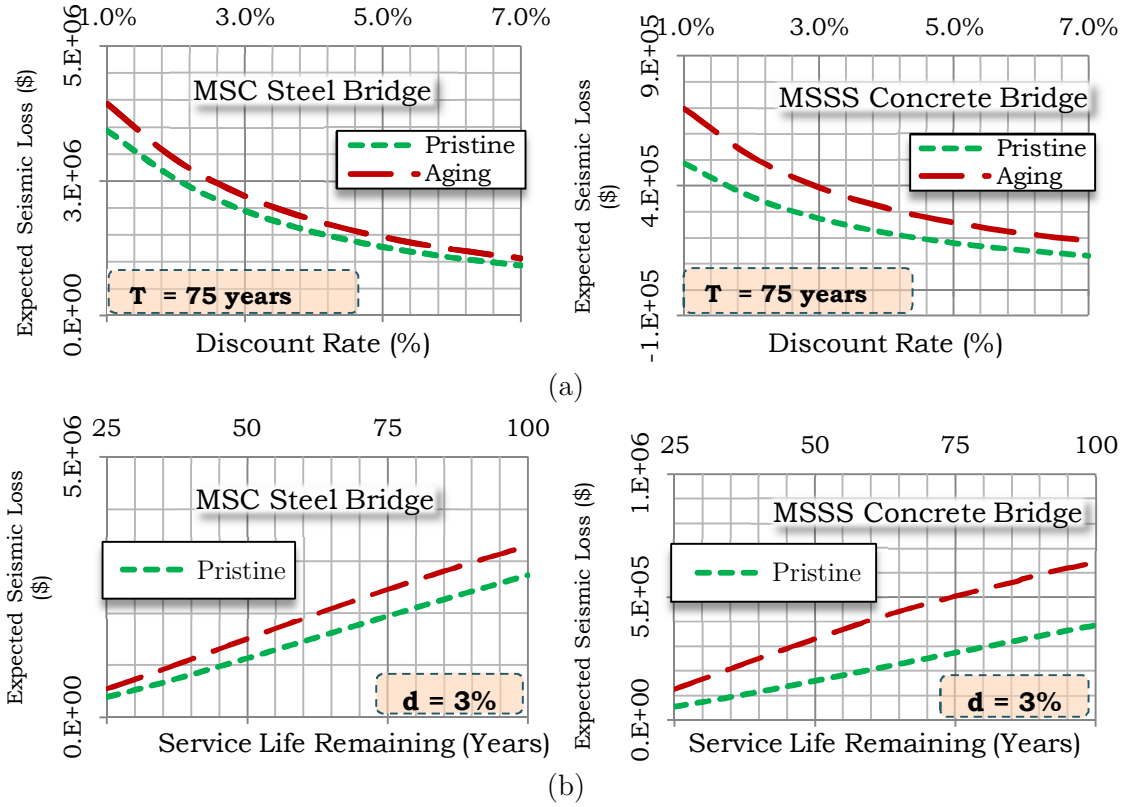

Figure 7-6: Sensitivity of expected seismic loss of representative case study pristine and aging bridges to variations in a) after-inflation risk-free discount rate and b) remaining service life. Note the difference in scale of the y-axis for the two bridge types (Ghosh and Padgett 2011)

The results show that a change in remaining service life tends to have a more significant effect on the losses than does variation in the discount rate. In general, an increase in the discount rate tends to decrease the estimated seismic losses, while an increase in remaining service life escalates the expected seismic losses, as anticipated. For the aging MSSS concrete bridge with 100 year remaining service life, the expected seismic losses increase by 66% when compared to the pristine bridge. A 20% increase in expected losses is observed for the 100

year aging MSC steel bridge relative its pristine counterpart. For both bridge types, the aging bridge loss estimate is more sensitive to variation in discount ratio and remaining service life than the pristine bridge losses. Furthermore, the ratio of aging to pristine bridge losses for the MSSS concrete bridge is more sensitive to variations in discount rate and remaining service life than the MSC steel bridge.

These sensitivity studies for both bridge types further highlight the importance of taking into account the effects of aging and deterioration in the seismic loss estimates of highway bridges. As the results reveal, depending upon the after-inflation risk-free discount rate and remaining service life of the bridge, the seismic losses may be significantly higher than those calculated assuming no environmental degradation.

7.3.2.2. Impact of hazard curve on seismic loss estimates

While the results in the previous section are based on the seismic hazard for Nutbush, Tennessee, seismic loss estimates are now assessed for comparative purposes based on the hazard curve for Los Angeles, California to assess the influence of different hazard curves on the seismic loss estimates. It is noted that the bridge details, component repair costs and deterioration levels are assumed to

be identical and the results in this section are only meant to highlight the impact of hazard curve on seismic losses. Figure 7-3 presented earlier shows a comparison between the hazard curves of these two regions. The figure clearly reveals the differences between the West Coast versus Central and Southeastern US hazards, typically characterized by the relative flatness of the Nutbush, Tennessee hazard curve as compared to the one for Los Angeles, California. While low consequence events have a higher probability of occurrence in California, large infrequent events are more likely to occur in regions of CSUS, such as Tennessee.

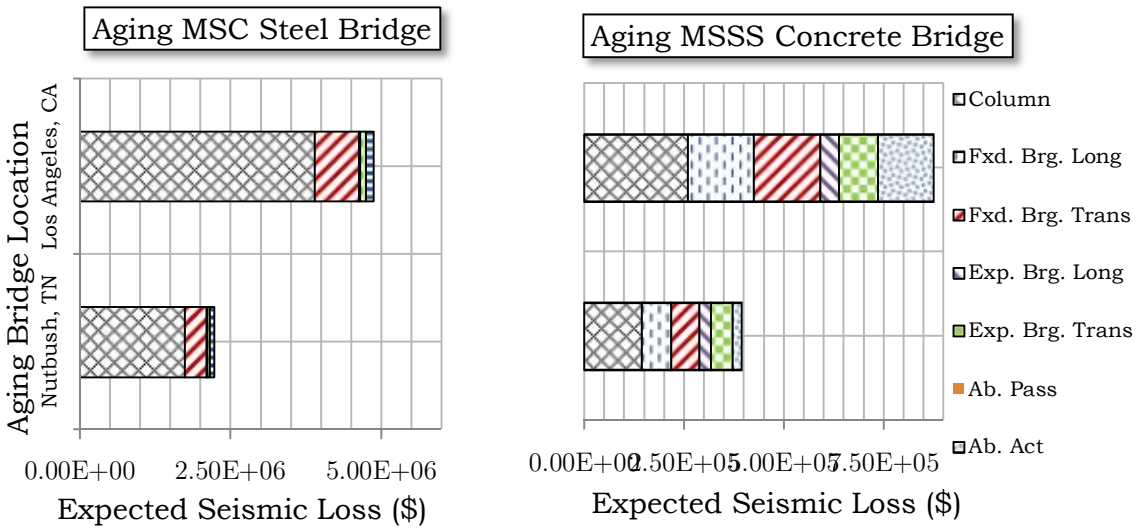

Figure 7-7:Comparison of expected seismic loss estimates for Nutbush, TN and Los Angeles, CA for a) aging MSC steel girder bridge and b) MSSS concrete girder bridge (Ghosh and Padgett 2011). Bridge details, component repair costs and deterioration levels are assumed to be identical at both locations and the presented results highlight only the impact of hazard curve on seismic losses estimates

To assess the impact of the hazard exposure, the seismic losses for the deteriorated bridges are compared for the base case discount ratio and exposure period in Nutbush, Tennessee and Los Angeles, California as shown in Figure 7-7. For both the MSC steel and MSSS concrete girder bridges the total expected seismic losses were found to be approximately 2.2 times higher for the same bridge in California as compared to Tennessee. In this particular case study, the low consequence-high probability seismic events for California dominate the seismic losses as compared to the relatively 'flat' hazard curve of Tennessee. The lifetime seismic losses for the deteriorated bridge are found to be significantly higher than the pristine counterpart, with approximately a respective 25% and 22% increase in expected value and variance for seismic losses related to the MSC steel bridge for the West Coast hazard. The corresponding expected losses and variances for the aging MSSS concrete bridge are found to be 46% and 69% higher as compared to the pristine counterpart.

7.4. Range of applicability of the developed seismic loss estimation methodology

The case studies highlighted in this chapter illustrated the application of the proposed framework in estimating statistical moments of seismic losses for deteriorating bridges. The results highlight the merits of the proposed methodology in capturing the effects of corrosion deterioration of multiple correlated bridge components on seismic losses, as well as propagating the commonly neglected uncertainty in repair action and associated costs. Furthermore they highlight the importance of capturing correlations amongst components for evaluating the standard deviation in losses for aging bridges. However, it is worthwhile to note that the developed methodology is not restricted to applications for deteriorating highway bridges alone.

The proposed methodology arrives at system level seismic loss estimates by aggregating the component level losses given potential time variation in failure probability and a range of sources of uncertainty from hazard occurrence to repair cost model. In this context, the framework is applicable to any number civil structures or infrastructures (such as buildings, bridges, etc.) that consist of an

assemblage of components vulnerable to seismic threats. The framework is rendered more flexible by incorporating effects such as degradation of structural resistance and uncertainty in repair procedures. In this chapter, specific examples of bridges are chosen to highlight seismic loss estimation of these key elements of the deteriorating transportation infrastructure. However, for civil infrastructures situated further away from sources of deterioration, the proposed nonhomogeneous framework can be easily transformed into a homogeneous Poisson framework by assuming $\lambda_{i,m}(t)$ in Equation (7.1) as time invariant, such that $\lambda_{i,m}\left(t_1\right) = \lambda_{i,m}\left(t_2\right) = \lambda_{i,m}$. For instances where there is no uncertainty in repair procedures or only one viable repair strategy $(j=1)$, the cost parameters $C_{i,m,j}$ and $P\left(C_{i,m,j}\right)$ in Equations (7.10) and (7.13) can be simply taken as $C_{i,m}$ and $P\left(C_{i,m}\right)$. Component correlations ranging from full, to partial, to negligible correlation can be explicitly considered is illustrated in the case study. Thus while the methodology permits accounting for the effects of deterioration and uncertainty in repair of multiple correlated components, the formulations are flexible for consistent application when there is no deterioration, correlation, or uncertainty in repair procedures. The nonhomogeneous Poisson process framework presented in this study however assumes that the bridge repair strategies and limit states are

uncorrelated. Future studies are necessary to extend the presented methodology to account for any such possible correlations.

7.5. Closure

A new approach for aging bridge seismic loss estimation is proposed in this chapter which explicitly incorporates time-dependent seismic vulnerability via a framework based on a nonhomogeneous Poisson process. The approach proposed also accounts for the contribution of individual component repair costs, uncertainty in repair procedure, and correlation between component damage to arrive at the total losses incurred for the entire bridge system. Since previous chapters have revealed that deterioration affects the seismic vulnerability of bridge components in dissimilar ways, this aggregation of component contributions to probabilistic loss estimates is an important advance over global repair cost modeling approaches for aging bridges. This methodology can be effectively used to arrive at more accurate estimates of the statistical moments of direct economic losses for bridges, including total expected value and variance of the repair costs from lifetime seismic exposure to facilitate decision making.

Viable input models and insights from applying the proposed methodology are provided by the case study of two typically non-seismically designed bridges (MSC steel and MSSS concrete) located in the state of Tennessee. The differences in deterioration effects, geometric properties, structural characteristics, and seismic vulnerability of these two aging bridge types are reflected in the seismic loss estimates. While column damage tends to contribute the most to the losses, other repairs associated with bearing damage also contribute significantly to the total cost. When aging is considered, the relative contribution of these components changes and also differs by bridge type. Sensitivity of seismic loss estimates to discount rate, remaining service life, and region specific seismic hazard are also presented in this chapter

Chapter 8

CONCLUSIONS, KEY CONTRIBUTIONS AND FUTURE WORK

8.1. Conclusions

Exposed to the harsh external environment, highway bridges are affected by the aging and deterioration mechanisms. Additionally, bridges located in such regions as the Central and Southeastern US are typically characterized by lack of proper seismic detailing thereby rendering these non-seismically designed degrading bridges significantly more vulnerable to earthquakes when compared to pristine structures. This study focused on the efficient and precise seismic vulnerability assessment and loss estimation of aging highway bridge classes after considering deterioration mechanisms of multiple structural components.

The first step towards the development of an aging bridge fragility framework involved the identification of aging mechanisms depending on the location and structural characteristics of bridge components. Existing probabilistic models are reviewed and adopted to predict corrosion deterioration under different exposure conditions for embedded steel members (such as, column reinforcements, bearing anchor bolts and dowel bars) and exposed steel members (such as, steel bridge girders, bearing keeper plates). For embedded steel members the corrosion deterioration effects considered in this study included cross sectional area loss of steel due to corrosion and cracking and spalling of cover concrete due to the expansive forces exerted by the accumulated rust products. In addition to these adopted deterioration mechanisms, a new analytical model is proposed to compute the stiffening of elastomeric bridge bearing pads based on the experimental tests by past researchers.

The aging mechanisms are used to compute the extent of deterioration suffered by deteriorating bridge components along the service life of a bridge. Three dimensional high-fidelity finite element models are subsequently developed for nonlinear time history analysis using the software package OpenSees to ascertain the impact of aging mechanisms on the seismic response and

vulnerability. In this regard, two popular bridge classes prevalent in the Central and Southeastern US are considered for case study purposes. The first case study comprised of a multi-span continuous steel girder bridge with deterministic geometry exposed under chlorides stemming from deicing salt applications. For this bridge type, deterioration of key structural components affect the lateral force resisting system under seismic loading, resulting in reduced moment capacity and yield curvature of the columns, reduced ultimate lateral strength of the fixed and expansion bearings, and increased coefficient of friction in the bearings due to debris accumulation. The nonlinear deterministic time history analysis illustrated that when the deterioration of bridge components are considered individually, there is a significant shift in the dynamic response of the bridge producing an increase in the seismic demand on the individual components. However, joint consideration of the component corrosion effects revealed that while the seismic demand on some components e.g., RC columns and fixed bearings shows a steady increase along the service life of the bridge, there is a decrease in the demand on some components such as the fixed bearings in the longitudinal direction. A full probabilistic analysis is conducted to evaluate the component and system level time-dependent seismic fragility curves given uncertainty in bridge, ground motion, and deterioration

parameters. The bridge system fragility curves for each damage state revealed a significant increase in the bridge system vulnerability over time due to aging. For example, after 75 years of exposure to chlorides, the median value PGA for the complete damage state decreases by 27%.

The second case study to assess the impact of aging and deterioration mechanisms consisted of a portfolio of multi-span simply supported concrete girder bridges under chlorides stemming from three different exposure conditions: deicing salt exposure, marine sea splash exposure, and marine atmospheric exposure. Assessment of the probabilistic seismic demand models for this portfolio of structures also revealed the variable impact on component vulnerability, as shown in the prior case study. Additionally, a comparison between different exposure conditions indicated that the impact of corrosion deterioration is highest when highway bridges are exposed to chlorides stemming from deicing salt exposure condition. The median values for the complete damage fragility curves after 75 years of exposure to deicing salt exposure are found to decrease by 44% compared to the pristine bridge fragility. On the other hand, the reduction in median values in atmospheric and sea-splash exposure zones is found to be only 5% and 9%. Hence, when located near marine sources, especially in atmospheric zones, the

impact of corrosion deterioration may be neglected unless the highway bridge structure is marked by a significantly old service life. While corrosion effects can be neglected, one still needs to consider the continued stiffening of elastomeric bearing pads due to thermal oxidation and aging.

In addition to developing time-dependent bridge fragility curves using traditional approaches, this study also developed flexible multidimensional fragility models which offer several advantages over conventional uni-dimensional models. These models are conditioned to ground motion intensity as well as bridge modeling parameters, deterioration affected structural parameters, and bridge geometric parameters. Development of such multidimensional fragility models required assessment of four surrogate modeling strategies: polynomial response surface models, multivariate adaptive regression splines, radial basis function networks, and support vector machines for regression. For a case study multi-span simply supported bridge class it was observed that multivariate adaptive regression splines performs the best and provides least deviations from benchmark Monte Carlo simulations, while support vector machines for regression performs the worst. Polynomial response surface models and radial basis function networks shows intermediate performance. Hence, this study recommends the use of multivariate

adaptive regression splines metamodel for approximating the seismic response of bridge components using multiple predictor variables. The multidimensional surrogate models developed using this metamodel are used conjunction with component capacity estimates to develop parameterized fragility models using logistic regression techniques. These multidimensional models developed using statistical learning techniques offer significant improvements over traditional single-parameter conditioned fragility curves. Dimensionality reduction techniques are employed for the first time in bridge reliability problems to visualize the multidimensional failure surface in two dimensions and ascertain the smoothness of the failure surface. A smooth demarcation between survival-failure domains confirms the applicability of proposed surrogate models for approximating bridge component response.

An application example is presented where similar multidimensional fragility functions are developed for nine different bridge classes in an existing aging transportation network in South Carolina consisting of 509 bridges. This application example demonstrates the potential of parameterized fragility models to incorporate deterioration parameter data available from field instrumentation of highway bridges. Since field measurement and sensor monitoring of bridges are

expensive and labor intensive procedures, this study recommends the Kriging spatial interpolation technique to determine aging parameter estimates at non-monitored bridge locations using the data at monitored bridge sites. Additionally, to preserve information from historical estimates and simultaneously use information from field instrumentation Bayesian updating techniques should be employed. This case study also revealed that failure probabilities for more than 80% of the bridges within the network can be potentially underestimated by as much as 25% when the effect of aging and deterioration are not taken into consideration.

In addition to the aging and deterioration mechanisms, this study investigates the impact of additional threat scenarios commonly ignored during seismic vulnerability estimation of highway bridge structures. One such threat stems from the exposure of highway bridges to repeated earthquake shocks along their service lives when located in earthquake prone regions. This study proposes a new framework to predict damage accumulation in such structures under multiple shock scenarios after developing damage index prediction models and accounting for the probabilistic nature of the hazard. The versatility of the proposed framework is demonstrated on a case study highway bridge located in California

for two distinct hazard scenarios: a) multiple main shocks along the service life, and b) multiple aftershock earthquake occurrences following a single main shock. Results reveal that in both cases there is a significant increase in damage index exceedance probabilities due to repeated shocks within the time windows of interest and should be considered while computing lifetime seismic vulnerability of highway bridge structures when located in earthquake prone regions.

This study also presents a framework for joint live load and seismic reliability assessment of highway bridges, and provides insights into the potential effects of truck load and position on seismic vulnerability. The study evaluates the impact of truck position and governing vehicle weight on the seismic behavior of structural components as well as the overall bridge system of multi-span continuous steel highway bridges using existing Weigh-In-Motion traffic load data. A full probabilistic analysis accounting for variation in bridge parameters, ground motion, and truck position is conducted to develop bridge system level fragility curves in order to identify the critical position of truck atop the bridge deck which renders the bridge most vulnerable to seismic events. A fragility surface is derived for the critical truck position in which the failure probability is conditioned on the governing vehicle weight in addition to ground motion intensity, thus depicting the

impact of truck load on bridge seismic fragility. It is found that the median bridge fragilities may change by as much as 14% when high GVW trucks are placed at the critical location as opposed to the no-truck scenario. The fragility surface is convolved with the governing vehicle weight distribution (obtained from Weigh-In-Motion distribution) and probability of truck occurrence (function of truck flow rate) to determine site specific bridge conditional reliability estimates. For the truck GVW histogram in the state of Alabama, which served as the case study site, the change in fragilities were found to be negligible even for high truck flow rates. Hence for practical purposes, unless the truck GVW histogram is considerably different than what is considered in this study, the impact of truck loads on bridge seismic fragility can be neglected.

Finally, this study employs a novel nonhomogeneous Poisson process approach compute lifetime seismic losses of aging highway bridges using time-varying fragility functions. Results reveal that if one were to ignore aging and deterioration under deicing salt exposure conditions, the monetary seismic losses may be significantly underestimated by as much as 44% for multi-span simply supported concrete girder bridges and 14% for multi-span continuous steel girder bridges. The proposed loss estimation approach also accounts for the contribution

of individual component repair costs, uncertainty in repair procedure, and correlation between component damage to arrive at the total losses incurred for the entire bridge system. Additionally, the aggregation of component contributions to probabilistic loss estimates is an important advance over traditionally adopted global repair cost modeling approaches for aging bridges.

8.2. Key Contributions

This study provides a rigorous approach to probabilistic assessment of the impact of aging and deterioration mechanisms and other important threats on the seismic vulnerability of aging highway bridge structures. This resulted in a number of significant contributions which include:

1. Three dimensional analytical bridge models with deterioration affected structural components allowing for the study of the influence of aging on the seismic response of common bridge classes in the Central and Southeastern US.
2. A mathematical framework to derive time-dependent seismic fragility curves after incorporating uncertainty in deterioration parameters, bridge modeling parameters, and ground motion characteristics while providing insights

regarding the impacts of different exposure conditions on bridge fragility. Such fragility curves can inform bridge engineers and department of transportations on the seismic fragility of deteriorating highway bridges and prompt structural upgrades.

3. A method to derive parameterized aging bridge fragility models, which recommends viable experimental design and surrogate modeling techniques to structural response of bridge components under seismic loading. The multidimensional fragility models enable rapid assessment of structure specific vulnerability by conditioning the models on hazard parameters, bridge geometry parameters, critical bridge modeling parameters and deterioration affected structural parameters. A case study example revealed a gain of computational efficiency by 20 times when parameterized models are used in place of naïve Monte Carlo simulations to achieve the same level of accuracy.
4. A framework to utilize parameterized fragility models for determining in-situ fragility estimates of highway bridges spatially distributed across a transportation network after conducting spatial interpolation and Bayesian updating of deterioration parameter data available from field-

instrumentation. The proposed framework can be used in conjunction with network reliability theory and offer risk ranking prioritization of bridges within bridge networks leading to more resilient transportation infrastructure systems.

5. A methodology to incorporate the effect of damage accumulation in bridges from repeated seismic events in the form of multiple main shocks and main shock-aftershock scenarios after incorporating the probabilistic nature of the hazard. The developed methodology can support targeted risk based design wherein the bridge structure can be structurally designed for a target level of damage index exceedance at any point of time along the service life of the structure. Additionally, the regression models for damage index prediction after single or multiple earthquake shocks can prompt decisions on viable repair strategies to be adopted immediately after a seismic event.
6. A joint seismic–live load fragility assessment framework for impact assessment of truck-traffic load on seismic reliability after incorporating site specific data on gross vehicle weight and truck occurrence rate. This framework should find ready application by practitioners for more refined seismic assessment of problem bridges, and offer guidance for risk analysts

regarding the relative importance of considering simultaneous live loads and earthquake hazards.

7. A nonhomogeneous Poisson process methodology for seismic life-cycle cost assessment of aging bridges highlighting the importance of accounting for degradation effects while predicting life-cycle cost estimates. This framework will aid bridge owners and stake holders in efficiently channeling monetary resources for risk mitigation of aging bridges.

8.3. Recommendations for Future Work

This research focused on investigating the impact of aging and deterioration mechanisms and relevant supplementary threats on the seismic vulnerability of highway bridges. Potential areas in which this work can be extended through additional research include the following:

1. This study focused on some of the most prevalent deterioration mechanisms in the form of corrosion deterioration of embedded and exposed steel members and elastomeric bearing pads. Future studies could evaluate the impact of additional aging mechanisms, such as concrete degradation and

fatigue, as well deterioration of other bridge components, such as, foundation settlements.

2. This study provided model validation examples for several bridge components in their pristine state. Future studies should focus towards extensive experimental testing of the dynamic behavior of aging bridge columns and bearings to generate data towards the validation of analytical models.

3. Among the surrogate models tested in this study, the multivariate adaptive regression splines performed the best for multi-span simply supported concrete girder bridge class. Future work is required if this claim is valid for other bridge classes in addition to investigating other surrogate modeling strategies like Random Forests or ensemble based statistical learning techniques.

4. The parameterized fragility models developed for typical bridge classes in South Carolina incorporate the uncertainty associated with bridge geometric parameters. These models can be extended to explicitly condition on other parameters such as traffic loads for more precise estimates of bridge fragility. Additionally, this study focused on static trucks atop bridge decks

while assessing the impact of live loads on seismic bridge fragility. Future work should consider dynamic vehicle modeling and investigate if the impact is significantly different than present findings.

5. The proposed frameworks on damage accumulation due to repeated earthquakes does not account for aging and deterioration mechanism. Future studies should incorporate these mechanisms in addition to the probabilistic nature of the earthquake hazard to compute lifetime risks of damage occurrence due to repeated earthquakes. Additionally this framework should be extended towards computing lifetime monetary seismic losses owing to advantages over traditional life cycle estimation approaches which typically assumes complete repair of bridge structure after every earthquake, however insignificant the damage.

APPENDIX A – FINITE ELEMENT MODEL VALIDATION

This appendix will provide validation results for analytical models of some structural components used for bridge finite element modeling in this study. These components include highway bridge columns and bridge bearings. The software platform Opensees (Mazzoni et al. 2009) is used throughout this study for analytical modeling of these structural components and their responses will be validated herein using laboratory experimental test results.

A.1 Model Validation for Reinforced Concrete Columns

Reinforced concrete columns constitute critical sub-structural components within the bridge system responsible for transmission of gravity loads to the foundation during normal functioning as well as lateral loads during earthquakes. For model validation purposes, a thorough literature review revealed a lack of experimental test data for bridge columns with exact geometric and reinforcement detailing as commonly adopted for CSUS bridges used in this study. However, the PEER Structural Performance Database (PEER 2013) in conjunction with the Kawashima Research Laboratories in The University of Tokyo provides test data

for several different column configurations. Experimental test result for one such column is used for model validation purposes, the basic assumption being if the finite element models developed using OpenSees provide analytical results close to experimental data, then the same principles can be adopted for modeling CSUS columns.

A.1.1 Experimental test set-up

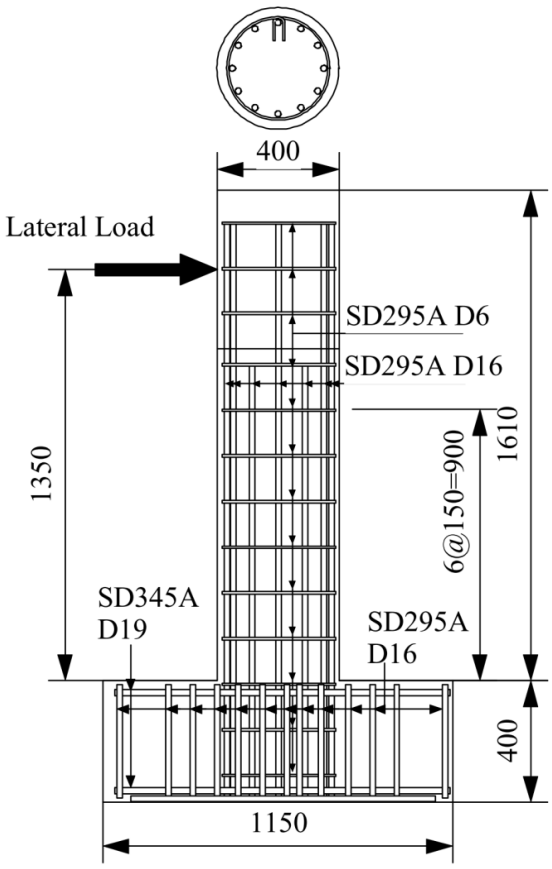

Figure A-1: Set-up configuration of bridge column tested in Kawashima Research Laboratories in The University of Tokyo (PEER 2013)

Figure A1 shows the set up of the experimental circular bridge column tested under lateral cyclic load in Kawashima Research Laboratories in The University of Tokyo. Additionally, Table A1 presents the specifications of the specimen including material properties and geometric configuration.

Table A-1: Material and geometric characteristsics for experimental column tested in the Kawashima Research Laboratories in the University of Tokyo

Section diameter (mm)	Effective height (mm)	Longitudinal reinforcement ratio (%)	Volumetric tie reinforcement ratio (%)	Concrete compressive strength (MPa)	Longitudinal Reinforcement	Tie Reinforcement
400	1350	1.89	0.26	30.0	SD295 D16 (Yield Strength = 374MPa)	SD295 D6 (Yield Strength = 363MPa)

The test column was subjected to cyclic displacement controlled loading hysteresis (Figure A-2) and parameters such as lateral forces and lateral displacements were measured at each step.

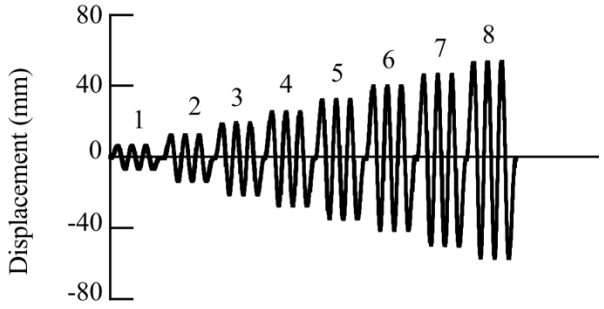

Figure A-2: Displacement controlled loading hysteresis of test column (PEER 2013)

A.1.2 Analytical modeling using OpenSees and validation

Finite element model of the bridge column is developed using OpenSees using state-of-the-art constitutive material models for capturing the mechanical characteristics and strength degradation. Column concrete is modeled using the *Conrete04 Material* which is essentially a uniaxial Popovics concrete material with degraded unloading/reloading stiffness according to the work of Karsan and Jirsa (1969) and tensile strength with exponential decay. The concrete compressive strength is taken as 30MPa from the experimental result, while the tensile strength is considered to be standard 3MPa. Additionally, the maximum concrete compressive strain and maximum tensile strain are assumed to be 0.002 and 0.0002 respectively. The column reinforcing steel is modeled using *uniaxialMaterial hysteretic* material model This command is used to construct a uniaxial bilinear hysteretic material object with pinching of force and deformation, damage due to ductility and energy, and degraded unloading stiffness based on ductility. The yield strength for longitudinal steel is taken to be 374MPa from the test results and the steel post yield stress is considered to be 561MPa. Additionally, default parameters to capture degradation of steel due to cyclic loading and unloading are employed.

The analytical column model developed using OpenSees is subjected to the cyclic load pattern shown in Figure A-2. A comparison between the lateral force and displacement at the top of the column presented in Figure A3 reveals that the analytical model can capture the experimental test result data with reasonable accuracy. This observation renders confidence in adopting the same strategies while modeling the columns for CSUS bridges. The use of material models such as *Concrete04* and *uniaxialMaterial hysteretic* which explicitly capture strength degradation during earthquake loading offers significant improvements over the traditionally adopted *Concrete01* and *Steel01* to model concrete and steel respectively in bridge columns (Nielson 2005). In the present study, the improved constitutive material models are adopted while developing parameterized fragility models (Chapter 5) and proposing damage accumulation framework under repeated earthquakes and assessing the impact of truck-traffic loads on bridge seismic fragility (Chapter 6). However the finite element models for the development of time-dependent fragility curves and seismic loss estimation of aging bridges (Chapters 4 and 7) relied on *Concrete01* and *Steel01* material. Future studies should incorporate the advanced constitutive modeling techniques in the finite

element models while developing time-evolving fragility curves and evaluating lifetime seismic losses.

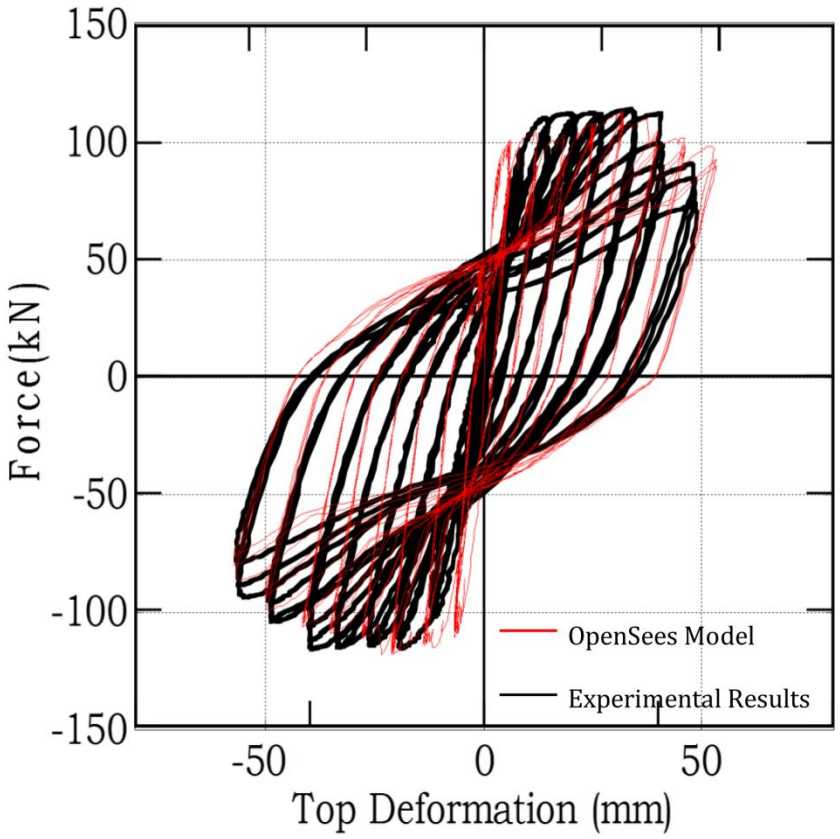

Figure A-3: Comparison between the experimental test results and analytical model results developed using OpenSees. The figure depicts that the analytical model approximates the experimental data reasonably well.

A.2 Model Validation for Bridge Bearings

Analytical modeling of high-type steel bearings relies heavily on the experimental test results by Mander et al. (1996a). In their study, a number of steel bearings were salvaged from steel girder bridges located in New York and cyclic lateral load

tests were conducted both the longitudinal and transverse directions with similar conditions to when they were installed in the bridge. In addition to the experimental tests, Mander et al. (1996a) also proposed non-linear analytical models in Drain-2DX that closely approximate the experimentally obtained behavior of each bearing type. On the basis of these models, Nielson (2005) developed the corresponding constitutive models for steel bearings using OpenSees. Figure A5 shows the performance of these models in approximating the experimentally obtained test results.

While the detailed analytical modeling of bridge bearings can be found in in Nielson (2005), this study adopts these to model pristine and aging bridge bearings after suitable ultimate strength reduction and increase in bearing friction due to corrosion. In addition to the steel bearings, this study also adopts the elastomeric bearing model from Nielson (2005). While the model for the individual components of this bearing type, such as bearing dowel and elastomeric pad, are developed using first principles, future studies should investigate the overall response using experimental results.

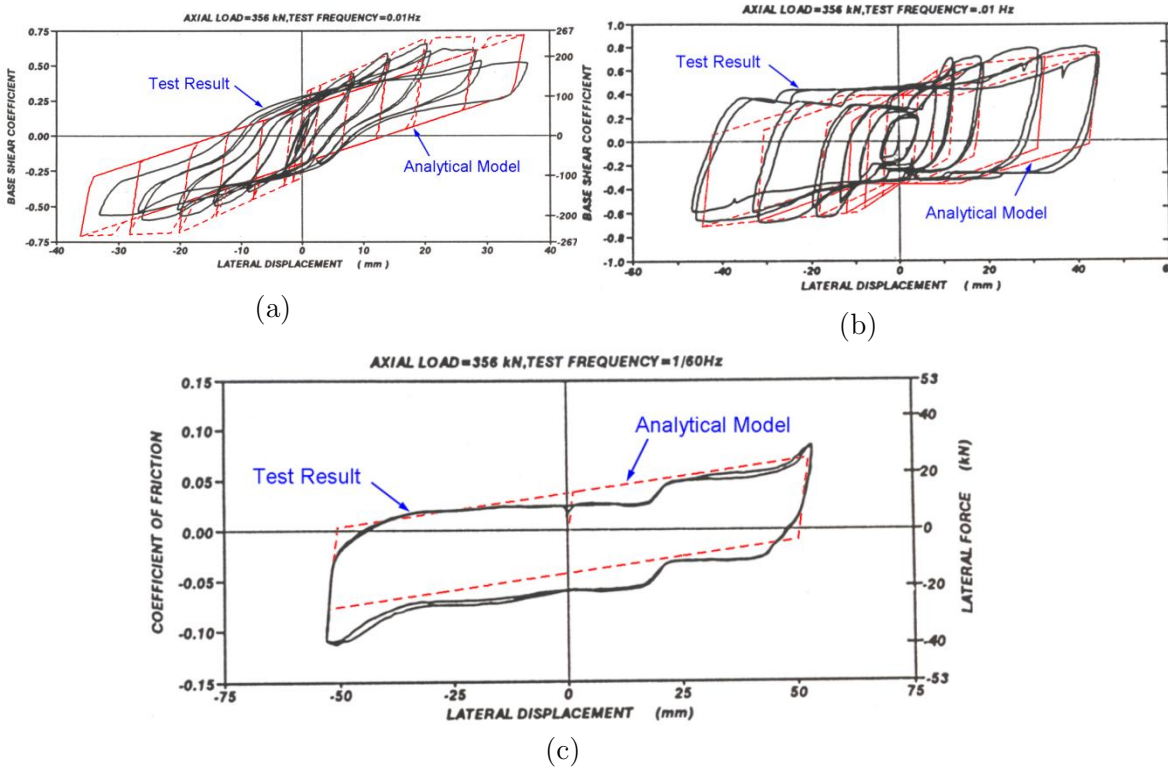

Figure A-4: Experimental and analytical response of a) fixed bearings in the longitudinal direction, b) fixed bearings in the longitudinal direction, b) fixed bearings in the tranverse direction, and c) expansion bearings in the longitudinal direction. These analytical models adopted in this sudy were initially developed by Nielson (2005).

A.3 General Note on Model Validation

The previous sections revealed that the analytical models for bridge components developed using OpenSees provides a close match with the experimentally obtained results. Additional system level validation of analytical bridge models is presented in Padgett et al. (2010) wherein a one-fourth scale, four span, concrete slab bridge was testd experimentally at the University of Nevada, Reno. Modeling strategies similar to such experimentally verified analytical models are adopted in this study

to generate three dimensional nonlinear finite element models and thereby generate bridge fragility functions after accounting for the effects of aging and deterioration. It should however be noted that the validation results for bridge columns and bearings presented in this study and those included in Padgett et al. (2010) are primarily for pristine bridge structures. Future studies should validate the analytical prediction of corroded component responses with experimental test results. The primary hindrance behind such endeavors is the lack of experimental test results for component level testing. While for corroding concrete columns a very limited amount of experimental test results exist, mostly for stout columns dominated by shear failure, laboratory test data for corroding bridge bearings is even more scarce. These deficits underline the need for extensive experimental tests of corroded bridge components in the future to understand their performance under dynamic loads and calibrate the analytical models if necessary.

APPENDIX B – TIME-DEPENDENT FRAGILITIES FOR CASE STUDY BRIDGES

The fragility curves for the case study bridges in Chapter 4 are presented in this Appendix. The medians are given in terms of gravitational acceleration g. Whenever the estimated median is larger than 4.0, the median and dispersion values are replaced by 99.00 and 0.00 respectively. This indicates that this particular component is not significant for that limit state. The curves are presented for intensity measure of PGA and derived using 96 ground motions from the Rix and Fernandez (2004) and the Wen and Wu (2001) ground motion suite.

B.1 Time varying median and dispersion for the components of case study MSC steel girder bridge presented in Chapter 4

Table B-1: Time t = 0 years (Pristine State) component fragilities for case study MSC steel girder bridge presented in Chapter 4

Component	Slight		Moderate		Extensive		Complete	
	med (g)	*disp*	*med* (g)	*disp*	*med* (g)	*disp*	*med* (g)	*disp*
COL	0.49	0.56	0.67	0.53	0.92	0.58	1.19	0.58
FBL	0.93	0.71	2.01	0.71	3.11	0.75	99.00	0.00
FBT	0.59	0.57	1.15	0.57	1.68	0.61	3.93	0.66
EBL	0.36	1.00	0.78	0.99	0.96	1.00	1.23	1.02
EBT	0.37	0.61	0.73	0.61	1.07	0.65	2.51	0.70
ABP	2.05	0.93	99.00	0.00	99.00	0.00	99.00	0.00
ABA	99.00	0.00	99.00	0.00	99.00	0.00	99.00	0.00
ABT	1.08	0.95	99.00	0.00	99.00	0.00	99.00	0.00

Table B-2: Time t = 25 years component fragilities for case study MSC steel girder bridge presented in Chapter 4

Component	Slight		Moderate		Extensive		Complete	
	med (g)	*disp*	*med* (g)	*disp*	*med* (g)	*disp*	*med* (g)	*disp*
COL	0.45	0.55	0.60	0.52	0.82	0.57	1.05	0.57
FBL	0.95	0.67	1.98	0.67	3.02	0.72	99.00	0.00
FBT	0.56	0.58	1.07	0.58	1.55	0.62	3.52	0.66
EBL	0.34	0.86	0.68	0.84	0.82	0.85	1.02	0.87
EBT	0.36	0.60	0.71	0.60	1.05	0.64	2.51	0.69
ABP	1.53	0.85	3.10	0.85	99.00	0.00	99.00	0.00
ABA	99.00	0.00	99.00	0.00	99.00	0.00	99.00	0.00
ABT	1.04	0.91	99.00	0.00	99.00	0.00	99.00	0.00

Table B-3: Time t = 50 years component fragilities for case study MSC steel girder bridge presented in Chapter 4

Component	Slight		Moderate		Extensive		Complete	
	med (g)	*disp*	*med* (g)	*disp*	*med* (g)	*disp*	*med* (g)	*disp*
COL	0.41	0.54	0.55	0.51	0.75	0.56	0.95	0.56
FBL	1.65	0.65	3.99	0.65	99.00	0.00	99.00	0.00
FBT	0.60	0.59	1.15	0.59	1.68	0.63	3.89	0.67
EBL	0.38	0.92	0.82	0.90	0.99	0.91	1.25	0.94
EBT	0.32	0.53	0.59	0.53	0.84	0.57	1.82	0.61
ABP	3.47	1.09	99.00	0.00	99.00	0.00	99.00	0.00
ABA	99.00	0.00	99.00	0.00	99.00	0.00	99.00	0.00
ABT	1.17	0.91	99.00	0.00	99.00	0.00	99.00	0.00

Table B-4: Time t = 75 years component fragilities for case study MSC steel girder bridge presented in Chapter 4

Component	Slight		Moderate		Extensive		Complete	
	med (g)	*disp*	*med* (g)	*disp*	*med* (g)	*disp*	*med* (g)	*disp*
COL	0.36	0.58	0.46	0.56	0.61	0.60	0.76	0.60
FBL	3.25	0.72	99.00	0.00	99.00	0.00	99.00	0.00
FBT	0.47	0.57	0.83	0.57	1.16	0.60	2.43	0.64
EBL	0.37	0.77	0.75	0.75	0.89	0.77	1.11	0.79
EBT	0.26	0.51	0.46	0.51	0.64	0.55	1.33	0.59
ABP	99.00	0.00	99.00	0.00	99.00	0.00	99.00	0.00
ABA	99.00	0.00	99.00	0.00	99.00	0.00	99.00	0.00
ABT	1.57	1.06	99.00	0.00	99.00	0.00	99.00	0.00

Table B-5: Time t = 100 years component fragilities for case study MSC steel girder bridge presented in Chapter 4

Component	Slight		Moderate		Extensive		Complete	
	med (g)	*disp*	*med* (g)	*disp*	*med* (g)	*disp*	*med* (g)	*disp*
COL	0.33	0.56	0.43	0.54	0.57	0.57	0.71	0.58
FBL	99.00	0.00	99.00	0.00	99.00	0.00	99.00	0.00
FBT	0.40	0.55	0.68	0.55	0.92	0.58	1.79	0.61
EBL	0.38	0.89	0.79	0.87	0.95	0.89	1.19	0.91
EBT	0.22	0.47	0.39	0.47	0.53	0.50	1.10	0.55
ABP	3.30	1.11	99.00	0.00	99.00	0.00	99.00	0.00
ABA	99.00	0.00	99.00	0.00	99.00	0.00	99.00	0.00
ABT	99.00	0.00	99.00	0.00	99.00	0.00	99.00	0.00

B.2 Time varying median and dispersion at the component and system level for case study MSSS concrete girder bridge presented in Chapter 4 under different exposure conditions

B.2.1 Deicing salt exposure condition

Table B-6: Time t = 0 (Pristine State) years component fragilities for case study MSSS concrete girder bridge presented in Chapter 4 under deicing salt exposure

Component	Slight		Moderate		Extensive		Complete	
	med (g)	*disp*	*med* (g)	*disp*	*med* (g)	*disp*	*med* (g)	*disp*
COL	0.64	0.74	0.99	0.69	1.58	0.77	2.25	0.78
FBL	0.51	0.83	1.59	0.80	2.01	0.82	2.67	0.86
FBT	1.44	1.49	99.00	0.00	99.00	0.00	99.00	0.00
EBL	0.32	0.81	1.19	0.77	1.56	0.79	2.15	0.84
EBT	2.02	1.63	99.00	0.00	99.00	0.00	99.00	0.00
ABP	2.36	0.73	99.00	0.00	99.00	0.00	99.00	0.00
ABA	0.47	1.07	2.19	1.26	99.00	0.00	99.00	0.00
ABT	0.93	1.06	3.81	1.22	99.00	0.00	99.00	0.00

Table B-7: Time t = 25 years component fragilities for case study MSSS concrete girder bridge presented in Chapter 4 under deicing salt exposure

Component	Slight		Moderate		Extensive		Complete	
	med (g)	*disp*	*med* (g)	*disp*	*med* (g)	*disp*	*med* (g)	*disp*
COL	0.56	0.67	0.83	0.62	1.27	0.70	1.77	0.71
FBL	0.49	0.83	1.44	0.80	1.81	0.82	2.35	0.85
FBT	2.19	1.55	99.00	0.00	99.00	0.00	99.00	0.00
EBL	0.36	0.83	1.19	0.79	1.52	0.82	2.05	0.86
EBT	3.62	1.68	99.00	0.00	99.00	0.00	99.00	0.00
ABP	2.56	0.86	99.00	0.00	99.00	0.00	99.00	0.00
ABA	0.55	1.20	2.45	1.36	99.00	0.00	99.00	0.00
ABT	1.02	0.94	99.00	0.00	99.00	0.00	99.00	0.00

Table B-8: Time t = 50 years component fragilities for case study MSSS concrete girder bridge presented in Chapter 4 under deicing salt exposure

Component	Slight		Moderate		Extensive		Complete	
	med (g)	*disp*	*med* (g)	*disp*	*med* (g)	*disp*	*med* (g)	*disp*
COL	0.48	0.61	0.71	0.57	1.06	0.64	1.44	0.65
FBL	0.39	0.71	0.99	0.69	1.20	0.70	1.51	0.73
FBT	0.93	1.22	2.95	1.15	99.00	0.00	99.00	0.00
EBL	0.30	0.69	0.83	0.66	1.03	0.68	1.32	0.72
EBT	1.18	1.28	99.00	0.00	99.00	0.00	99.00	0.00
ABP	2.13	0.72	99.00	0.00	99.00	0.00	99.00	0.00
ABA	0.86	1.29	99.00	0.00	99.00	0.00	99.00	0.00
ABT	1.04	0.92	99.00	0.00	99.00	0.00	99.00	0.00

Table B-9: Time t = 75 years component fragilities for case study MSSS concrete girder bridge presented in Chapter 4 under deicing salt exposure

Component	Slight		Moderate		Extensive		Complete	
	med (g)	*disp*	*med* (g)	*disp*	*med* (g)	*disp*	*med* (g)	*disp*
COL	0.45	0.62	0.65	0.58	0.96	0.65	1.30	0.65
FBL	0.36	0.74	0.92	0.71	1.12	0.73	1.41	0.76
FBT	1.11	1.22	3.76	1.14	99.00	0.00	99.00	0.00
EBL	0.31	0.74	0.87	0.71	1.08	0.73	1.39	0.77
EBT	1.13	1.25	3.91	1.17	99.00	0.00	99.00	0.00
ABP	2.24	0.72	99.00	0.00	99.00	0.00	99.00	0.00
ABA	1.81	1.66	99.00	0.00	99.00	0.00	99.00	0.00
ABT	1.44	0.99	99.00	0.00	99.00	0.00	99.00	0.00

Table B-10: Time varying system fragilities for case study MSSS concrete girder bridge presented in Chapter 4 under deicing salt exposure

Time (years)	Slight		Moderate		Extensive		Complete	
	med (g)	*disp*	*med* (g)	*disp*	*med* (g)	*disp*	*med* (g)	*disp*
0	0.18	0.76	0.51	0.70	0.79	0.72	1.14	0.74
25	0.20	0.75	0.47	0.67	0.70	0.71	0.98	0.72
50	0.19	0.71	0.42	0.64	0.58	0.67	0.78	0.68
75	0.18	0.67	0.36	0.61	0.50	0.64	0.65	0.64
100	0.18	0.76	0.51	0.70	0.79	0.72	1.14	0.74

B.2.2 Marine atmospheric exposure condition

Table B-11: Time t = 25 years component fragilities for case study MSSS concrete girder bridge presented in Chapter 4 under marine atmospheric exposure condition

Component	Slight		Moderate		Extensive		Complete	
	med (g)	*disp*	*med* (g)	*disp*	*med* (g)	*disp*	*med* (g)	*disp*
COL	0.50	0.69	0.78	0.63	1.24	0.72	1.77	0.73
FBL	0.58	0.88	1.85	0.85	2.35	0.88	3.13	0.91
FBT	99.00	0.00	99.00	0.00	99.00	0.00	99.00	0.00
EBL	0.35	0.75	1.11	0.71	1.41	0.74	1.88	0.78
EBT	99.00	0.00	99.00	0.00	99.00	0.00	99.00	0.00
ABP	2.73	0.72	99.00	0.00	99.00	0.00	99.00	0.00
ABA	0.52	1.05	2.35	1.23	99.00	0.00	99.00	0.00
ABT	0.85	0.84	2.90	0.98	99.00	0.00	99.00	0.00

Table B-12: Time t = 50 years component fragilities for case study MSSS concrete girder bridge presented in Chapter 4 under marine atmospheric exposure condition

Component	Slight		Moderate		Extensive		Complete	
	med (g)	*disp*	*med* (g)	*disp*	*med* (g)	*disp*	*med* (g)	*disp*
COL	0.50	0.76	0.79	0.71	1.29	0.80	1.89	0.80
FBL	0.61	0.89	1.99	0.86	2.54	0.88	3.40	0.92
FBT	99.00	0.00	99.00	0.00	99.00	0.00	99.00	0.00
EBL	0.34	0.74	1.07	0.71	1.35	0.73	1.79	0.77
EBT	99.00	0.00	99.00	0.00	99.00	0.00	99.00	0.00
ABP	2.91	0.72	99.00	0.00	99.00	0.00	99.00	0.00
ABA	0.53	1.05	2.50	1.24	99.00	0.00	99.00	0.00
ABT	0.89	0.85	3.19	1.01	99.00	0.00	99.00	0.00

Table B-13: Time t = 75 years component fragilities for case study MSSS concrete girder bridge presented in Chapter 4 under marine atmospheric exposure condition

Component	Slight		Moderate		Extensive		Complete	
	med (g)	*disp*	*med* (g)	*disp*	*med* (g)	*disp*	*med* (g)	*disp*
COL	0.46	0.70	0.72	0.65	1.14	0.74	1.64	0.74
FBL	0.57	0.82	1.74	0.79	2.20	0.81	2.90	0.85
FBT	99.00	0.00	99.00	0.00	99.00	0.00	99.00	0.00
EBL	0.34	0.73	1.04	0.69	1.32	0.72	1.73	0.76
EBT	99.00	0.00	99.00	0.00	99.00	0.00	99.00	0.00
ABP	3.02	0.71	11.00	0.71	99.00	0.00	99.00	0.00
ABA	0.52	1.04	2.42	1.23	99.00	0.00	99.00	0.00
ABT	0.91	0.86	3.34	1.02	99.00	0.00	99.00	0.00

Table B-14: Time varying system fragilities for case study MSSS concrete girder bridge presented in Chapter 4 under marine atmospheric exposure condition

Time (years)	Slight		Moderate		Extensive		Complete	
	med (g)	*disp*	*med* (g)	*disp*	*med* (g)	*disp*	*med* (g)	*disp*
0	0.21	0.69	0.60	0.64	0.87	0.66	1.20	0.68
25	0.23	0.69	0.60	0.62	0.87	0.64	1.21	0.66
50	0.23	0.68	0.60	0.65	0.89	0.68	1.23	0.70
75	0.23	0.66	0.58	0.62	0.83	0.64	1.14	0.66

B.2.3 Marine splash exposure condition

Table B-15: Time t = 25 years component fragilities for case study MSSS concrete girder bridge presented in Chapter 4 under marine splash exposure condition

Component	Slight		Moderate		Extensive		Complete	
	med (g)	*disp*	*med* (g)	*disp*	*med* (g)	*disp*	*med* (g)	*disp*
COL	0.51	0.71	0.80	0.66	1.28	0.75	1.84	0.75
FBL	0.59	0.89	1.92	0.86	2.45	0.88	3.27	0.91
FBT	99.00	0.00	99.00	0.00	99.00	0.00	99.00	0.00
EBL	0.34	0.75	1.10	0.71	1.39	0.74	1.85	0.78
EBT	99.00	0.00	99.00	0.00	99.00	0.00	99.00	0.00
ABP	2.86	0.72	99.00	0.00	99.00	0.00	99.00	0.00
ABA	0.52	1.06	2.38	1.23	99.00	0.00	99.00	0.00
ABT	0.83	0.83	2.83	0.97	99.00	0.00	99.00	0.00

Table B-16: Time t = 50 years component fragilities for case study MSSS concrete girder bridge presented in Chapter 4 under marine splash exposure condition

Component	Slight		Moderate		Extensive		Complete	
	med (g)	*disp*	*med* (g)	*disp*	*med* (g)	*disp*	*med* (g)	*disp*
COL	0.46	0.70	0.72	0.65	1.15	0.74	1.67	0.75
FBL	0.53	0.79	1.58	0.77	1.98	0.79	2.59	0.82
FBT	99.00	0.00	99.00	0.00	99.00	0.00	99.00	0.00
EBL	0.34	0.74	1.06	0.71	1.34	0.73	1.78	0.77
EBT	99.00	0.00	99.00	0.00	99.00	0.00	99.00	0.00
ABP	2.87	0.69	99.00	0.00	99.00	0.00	99.00	0.00
ABA	0.54	1.07	2.60	1.26	99.00	0.00	99.00	0.00
ABT	0.89	0.85	3.23	1.01	99.00	0.00	99.00	0.00

Table B-17: Time t = 75 years component fragilities for case study MSSS concrete girder bridge presented in Chapter 4 under marine splash exposure condition

Component	Slight		Moderate		Extensive		Complete	
	med (g)	*disp*	*med* (g)	*disp*	*med* (g)	*disp*	*med* (g)	*disp*
COL	0.45	0.70	0.70	0.65	1.11	0.73	1.59	0.74
FBL	0.52	0.80	1.53	0.77	1.92	0.79	2.50	0.82
FBT	99.00	0.00	99.00	0.00	99.00	0.00	99.00	0.00
EBL	0.34	0.72	1.02	0.69	1.28	0.71	1.68	0.75
EBT	99.00	0.00	99.00	0.00	99.00	0.00	99.00	0.00
ABP	2.93	0.70	99.00	0.00	99.00	0.00	99.00	0.00
ABA	0.56	1.08	2.80	1.28	99.00	0.00	99.00	0.00
ABT	0.92	0.86	3.35	1.02	99.00	0.00	99.00	0.00

Table B-18: Time varying system fragilities for case study MSSS concrete girder bridge presented in Chapter 4 under marine splash exposure condition

Time (years)	Slight		Moderate		Extensive		Complete	
	med (g)	*disp*	*med* (g)	*disp*	*med* (g)	*disp*	*med* (g)	*disp*
0	0.21	0.69	0.60	0.64	0.87	0.66	1.20	0.68
25	0.23	0.68	0.60	0.63	0.89	0.66	1.24	0.68
50	0.23	0.67	0.57	0.61	0.83	0.63	1.15	0.65
75	0.23	0.66	0.56	0.62	0.80	0.63	1.09	0.65

APPENDIX C – SUROGATE MODELS AND PARAMETERIZED FRAGILITY

This appendix provides the surrogate model coefficients of the polynomial response surface metamodels and parameterized fragility models for different bridge classes within the South Carolina network (Chapter 5). Additionally, median and dispersion values of the in-situ bridge fragility curves after multidimensional integration are presented for all the 509 bridges in the network.

C.1 Coefficients for the polynomial response surface models for different bridge classes within the case study South Carolina Network

As presented in Chapter 5, the adopted polynomial response surface model follows the form:

$$\hat{y} = \beta_0 + \sum_{i=1}^{k} \beta_i x_i + \sum_{i=1}^{k} \sum_{j=1, i<j}^{k} \beta_{ij} x_i x_j \tag{C.1}$$

where, $\hat{y}$ represents the predicted value of the bridge component response, x_1, …, x_k, are the predictors and β_0, …, β_{ij} are the regression coefficients obtained using least square principles after fitting the response surface approximations to the component response data from nonlinear time history analysis of bridge models

under seismic shaking. Additionally, the parameterized fragility model after logistic regression follows the form:

$$P_f = \frac{e^{\theta_0 + \sum_{j=1}^{n} \theta_j x_j}}{1 + e^{\theta_0 + \sum_{j=1}^{n} \theta_j x_j}} \tag{C.2}$$

where, θ_0, θ_j's ($j = 1,2,\ldots,k$) are the logistic regression coefficients. For each bridge class the following sections will present the chosen critical and field measurable predictor variables polynomial response surface metamodel regression coefficients for predicting the component responses, and logistic regression coefficients for parameterized regression models.

C.1.1 MSC Slab Bridge Class

Table C-1: Predictor variables for MSC Concrete Bridge Class

Parameter	Unit	Description
x_1	g	Peak ground acceleration
x_2	-	Elastomeric pad coefficient of friction
x_3	Mpa	Shear modulus of elastomeric bearing pads
x_4	cm^2	Elastomeric bearing pad dowel area
x_5	cm^2	Column rebar area
x_6	cm	Column cover depth

Table C-2: Polynomial response surface model coefficients for different bridge components

Predictor term	Regression Coefficient estimate							
	COL	FBL (mm)	FBT (mm)	EBL (mm)	EBT (mm)	ABA (mm)	ABP (mm)	ABT (mm)
Intercept	1.524	3.400	1.430	3.467	1.425	2.550	3.601	3.345
$\ln(x_1)$	1.610	1.527	1.100	1.578	1.098	0.952	1.170	1.004
$\ln(x_2)$	-0.073	-0.475	-0.508	-0.436	-0.498	-0.045	0.261	0.338
$\ln(x_3)$	-0.169	-0.637	-0.819	-0.537	-0.827	-0.069	-0.123	0.064
x_4	-0.102	-0.292	-0.197	-0.221	-0.193	-0.077	-0.104	0.051
x_5	-0.284	-0.129	-0.004	-0.069	-0.004	-0.004	-0.060	-0.049
$\ln(x_6)$	0.172	-0.151	0.160	-0.195	0.153	-0.056	-0.172	0.027
$\ln(x_1)$*$\ln(x_2)$	0.058	0.048	0.036	0.070	0.041	-0.012	0.039	0.054
$\ln(x_1)$*$\ln(x_3)$	0.000	0.033	0.036	0.102	0.035	-0.072	-0.022	-0.001
$\ln(x_1)$*x_4	-0.059	-0.097	-0.105	-0.097	-0.103	-0.039	-0.033	0.030
$\ln(x_1)$*x_5	-0.084	-0.065	-0.031	-0.029	-0.031	0.011	-0.017	-0.016
$\ln(x_1)$*$\ln(x_6)$	0.032	-0.029	0.006	-0.055	0.004	-0.029	-0.034	0.001
$\ln(x_2)$*$\ln(x_3)$	-0.003	-0.113	-0.131	-0.130	-0.131	0.035	-0.005	0.039
$\ln(x_2)$*x_4	0.036	0.077	0.060	0.044	0.059	0.029	-0.059	-0.029
$\ln(x_2)$*x_5	-0.017	-0.025	-0.015	-0.014	-0.015	-0.004	-0.007	-0.021
$\ln(x_2)$*$\ln(x_6)$	0.021	0.015	-0.010	0.013	-0.009	-0.027	0.027	0.034
$\ln(x_3)$*x_4	0.024	0.028	0.049	0.013	0.050	-0.004	0.000	0.005
$\ln(x_3)$*x_5	-0.009	-0.018	0.004	-0.004	0.006	-0.002	0.000	0.004
$\ln(x_3)$*$\ln(x_6)$	-0.017	-0.024	-0.030	-0.030	-0.030	-0.017	-0.024	-0.022
x_4*x_5	0.005	0.016	-0.005	0.013	-0.006	0.013	0.017	0.013
x_4*$\ln(x_6)$	0.002	0.019	-0.034	0.002	-0.033	0.007	0.028	0.014
x_5*$\ln(x_6)$	0.003	-0.002	-0.022	0.013	-0.022	-0.001	0.000	-0.013

Table C-3: Coefficients of parameterized fragility model at bridge system level

Predictor term	Logistic Regression Coefficient
Intercept	0.056
$\ln(x_1)$	2.730
$\ln(x_2)$	-0.071
$\ln(x_3)$	-0.397
x_4	-0.223
x_5	-0.565
$\ln(x_6)$	0.269

C.1.2 MSC Concrete Girder Bridge Class

Table C-4: Predictor variables for MSC Concrete Bridge Class

Parameter	Unit	Description
x_1	g	Peak ground acceleration
x_2	cm^2	Column rebar area
x_3	cm^2	Elastomeric bearing dowel bar area
x_4	MPa	Shear modulus of elastomeric bearing pads
x_5	cm	Abutment gap
x_6	cm	Column cover depth

Table C-5: Polynomial response surface model coefficients for different bridge components

Predictor term	Regression Coefficient estimate							
	COL	FBL (mm)	FBT (mm)	EBL (mm)	EBT (mm)	ABA (mm)	ABP (mm)	ABT (mm)
Intercept	4.392	4.665	6.878	4.689	6.865	4.373	1.322	1.865
$\ln(x_1)$	1.958	1.008	1.879	1.050	1.878	1.435	0.248	0.497

x_2	-0.425	0.088	0.017	0.112	0.007	0.119	0.079	-0.004
x_3	-0.054	-0.177	-0.725	-0.151	-0.723	-0.259	0.437	0.461
$\ln(x_4)$	0.249	-0.053	-0.465	-0.044	-0.372	-0.333	0.461	0.320
$\ln(x_5)$	0.138	0.395	0.060	0.291	0.073	-0.088	-0.030	-0.020
$\ln(x_6)$	-0.269	0.114	0.201	0.148	0.158	-0.006	-0.035	-0.098
$\ln(x_1)*x_2$	-0.114	0.026	0.028	0.033	0.023	0.036	0.008	-0.036
$\ln(x_1)*x_3$	-0.015	-0.017	-0.177	-0.039	-0.173	-0.124	0.081	0.112
$\ln(x_1)*\ln(x_4)$	-0.002	0.103	-0.082	0.087	-0.056	-0.152	0.093	0.015
$\ln(x_1)*\ln(x_5)$	0.017	0.079	-0.006	0.017	0.003	0.041	-0.056	-0.045
$\ln(x_1)*\ln(x_6)$	-0.037	-0.015	0.071	0.006	0.059	0.029	-0.039	-0.027
x_2*x_3	0.008	0.004	0.036	-0.002	0.039	-0.012	-0.028	-0.025
$x_2*\ln(x_4)$	-0.005	-0.003	-0.007	-0.004	-0.018	0.000	0.000	-0.014
$x_2*\ln(x_5)$	-0.003	-0.012	-0.013	-0.014	-0.014	-0.003	-0.009	-0.006
$x_2*\ln(x_6)$	0.010	-0.050	-0.040	-0.042	-0.035	-0.018	-0.018	-0.005
$x_3*\ln(x_4)$	-0.024	0.002	0.013	0.008	0.013	0.006	-0.037	0.000
$x_3*\ln(x_5)$	-0.022	0.008	-0.010	0.000	-0.006	0.006	0.008	-0.018
$x_3*\ln(x_6)$	0.021	0.022	0.020	0.019	0.021	0.041	0.000	0.005
$\ln(x_4)*\ln(x_5)$	-0.028	0.012	-0.001	0.004	-0.004	0.005	-0.009	-0.014
$\ln(x_4)*\ln(x_6)$	-0.026	-0.023	-0.025	-0.023	-0.023	0.024	0.010	-0.021
$\ln(x_5)*\ln(x_6)$	0.035	-0.005	0.034	-0.016	0.036	-0.008	0.000	0.006

Table C-6: Coefficients of parameterized fragility model at bridge system level

Predictor term	**Logistic Regression Coefficient**
Intercept	5.32
$\ln(x_1)$	2.75
x_2	-0.36
x_3	-0.22
$\ln(x_4)$	-0.11
$\ln(x_5)$	0.12
$\ln(x_6)$	-0.17

C.1.3 MSC Steel Girder Bridge Class

Table C-7: Predictor variables for MSC Concrete Bridge Class

Parameter	Unit	Description
x_1	g	Peak ground acceleration
x_2	-	Coefficient of friction of expansion bearings in the longitudinal direction
x_3	-	Coefficient of friction of fixed bearings in the longitudinal direction
x_4	-	Multiplicative factor for initial stiffness of fixed bearings
x_5	cm	Abutment gap
x_6	cm^2	Column rebar area
x_7	cm^2	Steel bearing anchor bolt area
x_8	cm	Expansion bearing cover plate thickness
x_9	cm	Cover depth

Table C-8: Polynomial response surface model coefficients for different bridge components

	Regression Coefficient estimate							
Predictor term	COL	FBL (mm)	FBT (mm)	EBL (mm)	EBT (mm)	ABA (mm)	ABP (mm)	ABT (mm)
Intercept	3.306	-0.341	0.961	4.276	6.082	-0.392	0.221	0.528
$\ln(x_1)$	1.897	0.562	0.559	1.214	1.445	0.275	-0.098	0.148
$\ln(x_2)$	0.125	0.217	0.321	-0.043	0.279	-0.443	0.298	0.059
$\ln(x_3)$	0.386	-0.412	-0.579	0.122	-0.089	0.322	0.196	0.113
x_4	0.910	-0.809	-0.259	0.358	0.678	1.896	0.411	-0.069
$\ln(x_5)$	0.000	-0.020	0.049	0.241	0.142	-0.255	0.023	-0.014
x_6	-0.116	0.232	0.228	0.119	0.011	0.401	0.114	0.008
x_7	-0.092	-0.120	-0.147	-0.038	-0.174	-0.200	-0.045	-0.100
x_8	1.093	1.783	0.586	0.725	-1.175	2.501	1.148	1.905
$\ln(x_9)$	-0.343	-0.004	0.183	-0.222	-0.072	-0.057	0.131	0.090
$\ln(x_1)$*$\ln(x_2)$	0.089	0.066	0.045	0.046	0.058	-0.196	-0.100	-0.002
$\ln(x_1)$*$\ln(x_3)$	0.063	-0.120	-0.067	0.019	-0.029	0.097	0.026	0.004
$\ln(x_1)$*x_4	0.293	-0.056	0.116	0.148	0.472	0.715	0.053	-0.085
$\ln(x_1)$*$\ln(x_5)$	0.050	0.022	0.025	0.051	0.035	0.070	0.056	0.006
$\ln(x_1)$*x_6	-0.075	0.040	0.062	-0.013	0.012	0.001	-0.005	-0.009

$\ln(x_1)*x_7$	0.008	-0.025	0.001	-0.013	0.023	-0.039	0.015	-0.001
$\ln(x_1)*x_8$	0.252	0.499	0.198	0.181	0.143	0.421	0.205	0.600
$\ln(x_1)*\ln(x_9)$	-0.036	-0.028	0.010	-0.043	-0.002	-0.099	-0.003	0.030
$\ln(x_2)*\ln(x_3)$	0.011	0.045	0.050	0.025	0.008	0.040	0.026	0.025
$\ln(x_2)*x_4$	-0.143	-0.172	-0.201	-0.117	-0.074	-0.165	-0.077	-0.014
$\ln(x_2)*\ln(x_5)$	-0.012	0.000	0.031	-0.001	0.013	0.061	-0.032	0.007
$\ln(x_2)*x_6$	0.020	0.012	0.008	0.023	0.002	0.060	0.025	0.008
$\ln(x_2)*x_7$	-0.012	0.001	-0.010	-0.018	-0.010	-0.011	-0.016	-0.003
$\ln(x_2)*x_8$	0.053	0.024	-0.008	0.044	-0.075	0.209	0.073	-0.059
$\ln(x_2)*\ln(x_9)$	0.012	0.001	0.016	0.010	0.034	0.027	0.024	0.016
$\ln(x_3)*x_4$	-0.078	0.163	0.036	-0.058	0.013	0.018	-0.021	-0.037
$\ln(x_3)*\ln(x_5)$	-0.022	-0.004	-0.025	-0.015	-0.002	-0.008	-0.012	-0.003
$\ln(x_3)*x_6$	-0.022	-0.015	-0.016	-0.011	-0.027	-0.029	-0.009	-0.008
$\ln(x_3)*x_7$	-0.021	-0.009	-0.024	-0.004	-0.013	-0.008	-0.015	-0.012
$\ln(x_3)*x_8$	0.101	0.032	0.102	0.104	0.143	0.077	0.043	0.051
$\ln(x_3)*\ln(x_9)$	-0.003	-0.010	0.015	0.005	-0.005	0.020	0.001	-0.008
$x_4*\ln(x_5)$	0.060	0.045	0.026	-0.013	0.008	0.083	0.013	0.023
x_4*x_6	-0.102	-0.065	-0.042	-0.072	-0.061	-0.135	-0.025	-0.009
x_4*x_7	0.028	0.027	0.053	-0.030	0.087	0.013	0.014	0.019
x_4*x_8	-0.337	-0.237	-0.254	0.069	0.083	-0.066	-0.404	-0.216
$x_4*\ln(x_9)$	0.107	-0.027	-0.095	-0.009	0.049	-0.101	-0.054	-0.025
$\ln(x_5)*x_6$	0.000	0.009	0.001	0.008	-0.005	0.010	0.010	0.003
$\ln(x_5)*x_7$	-0.009	-0.009	-0.008	-0.016	-0.010	-0.012	-0.005	-0.004
$\ln(x_5)*x_8$	0.074	0.010	0.043	0.035	-0.007	0.072	0.048	0.002
$\ln(x_5)*\ln(x_9)$	0.008	0.006	-0.018	0.002	0.002	-0.001	0.002	0.004
x_6*x_7	0.005	0.013	0.012	-0.003	0.007	0.018	0.001	0.005
x_6*x_8	-0.097	-0.116	-0.088	-0.107	0.017	-0.286	-0.095	-0.044
$x_6*\ln(x_9)$	0.004	0.002	-0.001	0.014	-0.020	-0.004	-0.005	-0.009
x_7*x_8	0.034	0.004	0.023	0.032	0.088	0.011	0.042	0.043
$x_7*\ln(x_9)$	0.006	-0.010	-0.012	0.013	0.003	0.018	-0.022	-0.006
$x_8*\ln(x_9)$	0.139	-0.002	0.065	0.089	0.073	-0.041	0.031	0.032

Table C-9: Coefficients of parameterized fragility model at bridge system level

Predictor term	Logistic Regression Coefficient
Intercept	3.464
$\ln(x_1)$	2.623
$\ln(x_2)$	0.100
$\ln(x_3)$	-0.083
x_4	0.733
$\ln(x_5)$	0.132
x_6	-0.132
x_7	-0.043
x_8	-0.259
$\ln(x_9)$	-0.131

C.1.4 MSSS Concrete Girder Bridge Class

Table C-10: Predictor variables for MSC Concrete Bridge Class

Parameter	Unit	Description
x_1	g	Peak ground acceleration
x_2	cm^2	Column rebar area
x_3	cm^2	Elastomeric bearing dowel bar area
x_4	MPa	Steel strength
x_5	-	Elastomeric pad coefficient of friction
x_6	cm	Elastomeric pad bearing dowel gap
x_7	MPa	Shear modulus of elastomeric bearing pads
x_8	cm	Column cover depth

Table C-11: Polynomial response surface model coefficients for different bridge components

Predictor term	Regression Coefficient estimate							
	COL	FBL (mm)	FBT (mm)	EBL (mm)	EBT (mm)	ABA (mm)	ABP (mm)	ABT (mm)
Intercept	4.309	5.662	3.856	5.115	3.883	2.777	1.117	1.371
$\ln(x_1)$	1.453	1.192	0.955	1.055	0.777	1.412	0.365	0.633
x_2	-0.245	-0.134	-0.162	-0.010	-0.172	-0.024	-0.041	-0.067
x_3	-0.066	-0.137	-0.537	-0.072	-0.644	0.005	0.378	0.323
x_4	-0.003	-0.001	0.005	0.000	0.005	0.001	-0.001	-0.001
$\ln(x_5)$	0.230	-0.137	-0.789	-0.015	-0.667	-0.142	0.221	0.261
$\ln(x_6)$	0.030	0.075	-0.077	0.011	-0.062	-0.045	-0.174	-0.082
$\ln(x_7)$	0.327	-0.106	-0.309	0.014	-0.357	0.011	0.078	0.173
$\ln(x_8)$	-0.330	-0.261	-0.244	-0.211	-0.246	-0.370	0.053	-0.132
$\ln(x_1)$*x_2	-0.064	-0.036	-0.012	-0.007	0.004	-0.031	-0.004	-0.015
$\ln(x_1)$*x_3	-0.009	0.041	-0.227	-0.007	-0.232	-0.072	0.097	0.107
$\ln(x_1)$*x_4	0.000	0.001	0.002	0.001	0.003	0.001	0.000	0.000
$\ln(x_1)$*$\ln(x_5)$	0.012	0.004	-0.160	0.030	-0.154	-0.059	0.027	0.040
$\ln(x_1)$*$\ln(x_6)$	-0.008	-0.008	-0.012	-0.027	0.013	0.007	-0.054	0.000
$\ln(x_1)$*$\ln(x_7)$	0.098	0.085	0.050	0.120	0.052	-0.006	0.045	0.080
$\ln(x_1)$*$\ln(x_8)$	-0.017	-0.033	-0.034	-0.036	-0.019	-0.074	-0.001	0.002
x_2*x_3	0.004	-0.002	0.007	-0.001	0.016	-0.014	0.001	0.004
x_2*x_4	0.000	0.000	0.000	0.000	0.000	0.000	0.000	0.000
x_2*$\ln(x_5)$	-0.002	0.008	0.008	0.004	0.000	0.003	-0.003	-0.008
x_2*$\ln(x_6)$	0.001	0.002	0.016	0.005	0.016	0.010	0.011	0.002
x_2*$\ln(x_7)$	-0.024	-0.016	-0.021	-0.018	-0.010	-0.027	-0.010	-0.009
x_2*$\ln(x_8)$	0.009	0.007	0.016	-0.010	0.020	-0.002	-0.006	0.006
x_3*x_4	0.000	0.000	0.000	0.000	0.000	0.000	0.000	0.000
x_3*$\ln(x_5)$	-0.033	0.019	0.036	0.011	0.041	-0.002	-0.032	-0.028
x_3*$\ln(x_6)$	0.006	0.001	0.012	0.011	0.020	0.003	0.018	-0.001
x_3*$\ln(x_7)$	-0.008	0.018	0.084	0.025	0.080	0.031	-0.039	-0.033
x_3*$\ln(x_8)$	0.022	0.022	0.026	0.027	0.025	0.026	0.002	0.005
x_4*$\ln(x_5)$	0.000	0.000	0.000	0.000	0.000	0.000	0.000	0.000
x_4*$\ln(x_6)$	0.000	0.000	0.000	0.000	0.000	0.000	0.000	0.000
x_4*$\ln(x_7)$	0.000	0.000	0.000	0.000	0.000	0.000	0.000	0.000
x_4*$\ln(x_8)$	0.000	0.000	0.000	0.000	0.000	0.000	0.000	0.000
$\ln(x_5)$*$\ln(x_6)$	-0.010	-0.024	-0.027	-0.011	-0.037	-0.012	-0.008	-0.004

$\ln(x_5)$*$\ln(x_7)$	0.001	-0.048	-0.103	-0.042	-0.103	-0.014	-0.004	-0.010
$\ln(x_5)$*$\ln(x_8)$	-0.015	-0.015	0.001	-0.019	-0.007	-0.017	0.011	0.004
$\ln(x_6)$*$\ln(x_7)$	0.000	-0.001	-0.004	0.008	0.008	0.006	0.008	0.001
$\ln(x_6)$*$\ln(x_8)$	-0.007	-0.014	-0.009	-0.009	-0.007	-0.017	0.005	0.000
$\ln(x_7)$*$\ln(x_8)$	-0.002	-0.009	-0.018	-0.018	-0.016	-0.020	0.009	0.011

Table C-12: Coefficients of parameterized fragility model at bridge system level

Predictor term	Logistic Regression Coefficient
Intercept	6.146
$\ln(x_1)$	3.992
x_2	-0.395
x_3	-0.116
x_4	-0.003
$\ln(x_5)$	-0.251
$\ln(x_6)$	-0.025
$\ln(x_7)$	0.03
$\ln(x_8)$	-0.148

C.1.5 MSSS Slab Bridge Class

Table C-13: Predictor variables for MSC Concrete Bridge Class

Parameter	Unit	Description
x_1	g	Peak ground acceleration
x_2	MPa	Concrete strength
x_3	-	Elastomeric pad coefficient of friction
x_4	MPa	Shear modulus of bearing pad
x_5	cm^2	Elastomeric bearing pad dowel area
x_6	cm	Abutment gap
x_7	cm^2	Column rebar area
x_8	cm	Column cover depth

Table C-14: Polynomial response surface model coefficients for different bridge components

Predictor term	Regression Coefficient estimate							
	COL	FBL (mm)	FBT (mm)	EBL (mm)	EBT (mm)	ABA (mm)	ABP (mm)	ABT (mm)
Intercept	1.366	2.431	0.699	2.597	0.725	2.186	3.205	2.885
$\ln(x_1)$	1.245	1.086	0.698	1.141	0.688	0.724	1.051	0.970
x_2	-0.001	0.004	0.002	0.002	0.001	0.005	0.005	0.002
$\ln(x_3)$	0.068	-0.315	-0.265	-0.383	-0.250	0.148	0.227	0.316
$\ln(x_4)$	-0.433	-0.903	-0.826	-0.744	-0.810	-0.208	-0.448	-0.063
x_5	0.067	-0.151	-0.075	-0.062	-0.078	0.105	0.029	0.048
$\ln(x_6)$	-0.010	0.085	-0.041	0.044	-0.034	-0.094	0.039	-0.060
x_7	-0.221	0.043	0.027	0.025	0.019	-0.038	0.009	0.103
$\ln(x_8)$	0.071	-0.104	0.001	-0.035	0.004	0.005	0.017	0.062
$\ln(x_1)$*x_2	0.002	0.002	0.001	0.002	0.001	0.004	0.003	0.002
$\ln(x_1)$*$\ln(x_3)$	0.097	0.092	0.106	0.073	0.115	0.032	0.087	0.060
$\ln(x_1)$*$\ln(x_4)$	-0.016	0.003	0.011	0.057	0.009	-0.082	-0.107	-0.071
$\ln(x_1)$*x_5	-0.018	-0.059	-0.022	-0.049	-0.019	0.008	-0.027	-0.014
$\ln(x_1)$*$\ln(x_6)$	-0.006	0.014	0.001	0.010	0.006	-0.017	0.001	-0.014
$\ln(x_1)$*x_7	-0.036	0.008	0.019	0.007	0.019	-0.044	-0.024	0.007
$\ln(x_1)$*$\ln(x_8)$	0.019	-0.045	-0.006	-0.030	-0.003	-0.018	-0.049	-0.002
x_2*$\ln(x_3)$	0.000	0.001	0.000	0.000	0.000	0.001	0.001	0.000
x_2*$\ln(x_4)$	0.001	0.002	0.001	0.001	0.000	0.001	0.001	0.001
x_2*x_5	-0.001	0.000	0.000	0.000	0.000	0.000	0.000	0.000
x_2*$\ln(x_6)$	0.000	0.000	0.001	0.001	0.001	0.000	0.000	0.000
x_2*x_7	0.001	0.000	0.000	0.000	0.000	0.001	0.000	0.000
x_2*$\ln(x_8)$	0.000	0.000	-0.001	0.000	-0.001	0.000	-0.001	0.000
$\ln(x_3)$*$\ln(x_4)$	0.006	-0.095	-0.143	-0.117	-0.141	0.045	0.025	0.075
$\ln(x_3)$*x_5	0.013	0.035	0.018	0.013	0.020	-0.019	-0.011	0.004
$\ln(x_3)$*$\ln(x_6)$	-0.004	-0.007	-0.007	0.000	-0.004	0.013	0.017	-0.008
$\ln(x_3)$*x_7	0.023	0.019	0.005	0.009	0.002	0.023	0.015	0.020
$\ln(x_3)$*$\ln(x_8)$	-0.003	-0.005	0.004	-0.003	0.007	-0.019	-0.010	-0.006
$\ln(x_4)$*x_5	0.013	0.048	0.018	0.016	0.016	-0.013	-0.002	-0.011
$\ln(x_4)$*$\ln(x_6)$	-0.009	-0.019	0.002	-0.012	0.004	0.013	-0.009	-0.006
$\ln(x_4)$*x_7	0.034	0.011	-0.004	0.011	-0.007	0.013	0.025	0.009
$\ln(x_4)$*$\ln(x_8)$	0.005	-0.003	0.008	0.010	0.010	0.010	0.003	0.013
x_5*$\ln(x_6)$	0.000	-0.002	0.001	-0.001	0.000	0.012	0.002	0.006

x_5*x_7	-0.015	-0.003	0.003	-0.010	0.005	-0.022	-0.021	-0.019
x_5*ln(x_8)	-0.005	0.003	0.011	-0.004	0.011	-0.012	-0.015	-0.017
ln(x_6)*x_7	0.002	-0.008	0.002	-0.006	0.004	0.000	0.000	0.005
ln(x_6)*ln(x_8)	0.004	-0.007	-0.001	-0.002	-0.001	-0.001	0.000	0.005
x_7*ln(x_8)	-0.007	0.002	-0.003	-0.004	-0.002	-0.008	-0.011	-0.010

Table C-15: Coefficients of parameterized fragility model at bridge system level

Predictor term	Logistic Regression Coefficient
Intercept	-0.686
ln(x_1)	3.068
x_2	0.004
ln(x_3)	0.367
ln(x_4)	-0.614
x_5	-0.097
ln(x_6)	0.009
x_7	-0.454
ln(x_8)	0.114

C.1.6 MSSS Steel Bridge Class

Table C-16: Predictor variables for MSC Concrete Bridge Class

Parameter	Unit	Description
x_1	g	Peak ground acceleration
x_2	MPa	Steel Strength
x_3	-	Coefficient of friction of expansion bearings in the longitudinal direction
x_4	-	Multiplicative factor for initial stiffness of fixed bearings
x_5	cm	Abutment gap
x_6	cm	Hinge gap
x_7	cm^2	Column rebar area

x_8	cm^2	Bearing anchor bolt area
x_9	cm	Cover depth

Table C-17: Polynomial response surface model coefficients for different bridge components

	Regression Coefficient estimate							
Predictor term	COL	FBL (mm)	FBT (mm)	EBL (mm)	EBT (mm)	ABA (mm)	ABP (mm)	ABT (mm)
Intercept	6.906	4.871	1.853	5.963	7.227	2.840	2.945	3.114
$\ln(x_1)$	2.461	1.774	1.281	1.716	2.197	1.110	0.631	0.935
x_2	-0.006	0.001	-0.001	0.000	-0.001	0.002	-0.001	-0.002
$\ln(x_3)$	0.142	-0.331	-0.893	0.074	0.042	0.015	0.208	-0.029
x_4	-0.705	-0.501	-0.326	-0.195	-0.512	0.172	0.233	-0.473
$\ln(x_5)$	0.171	0.279	0.083	0.136	0.061	-0.080	0.057	0.019
$\ln(x_6)$	0.124	0.248	0.113	0.236	0.332	0.107	0.139	0.083
x_7	-0.381	-0.207	-0.089	-0.065	-0.123	-0.197	-0.070	-0.033
x_8	-0.097	-0.180	-0.197	-0.084	-0.655	-0.107	0.101	-0.003
$\ln(x_9)$	-0.441	-0.223	-0.222	-0.385	-0.527	-0.323	-0.278	-0.283
$\ln(x_1)$*x_2	0.000	0.001	0.000	0.000	0.001	0.001	0.000	0.000
$\ln(x_1)$*$\ln(x_3)$	0.061	0.013	0.040	0.113	-0.060	-0.062	-0.028	-0.047
$\ln(x_1)$*x_4	-0.178	0.195	0.075	-0.104	-0.139	-0.054	0.172	-0.044
$\ln(x_1)$*$\ln(x_5)$	0.039	0.057	-0.003	0.033	0.022	-0.029	0.025	0.012
$\ln(x_1)$*$\ln(x_6)$	0.010	0.042	0.002	0.015	0.062	0.001	-0.004	0.016
$\ln(x_1)$*x_7	-0.092	-0.038	-0.024	-0.022	-0.030	-0.060	-0.031	-0.023
$\ln(x_1)$*x_8	-0.010	-0.062	-0.009	-0.018	-0.170	-0.029	0.025	0.000
$\ln(x_1)$*$\ln(x_9)$	-0.017	0.027	-0.040	-0.019	-0.016	-0.027	-0.050	-0.033
x_2*$\ln(x_3)$	0.000	0.000	0.000	0.000	0.000	0.000	0.000	0.000
x_2*x_4	0.000	-0.001	0.000	-0.001	0.001	-0.001	0.001	0.001
x_2*$\ln(x_5)$	0.000	0.000	0.000	0.000	0.000	0.000	0.000	0.000
x_2*$\ln(x_6)$	0.000	0.000	0.000	0.000	0.000	0.000	0.000	0.000
x_2*x_7	0.000	0.000	0.000	0.000	0.000	0.000	0.000	0.000
x_2*x_8	0.000	0.000	0.000	0.000	0.000	0.000	0.000	0.000
x_2*$\ln(x_9)$	0.000	0.000	0.000	0.000	0.001	0.000	0.000	0.000
$\ln(x_3)$*x_4	-0.082	0.078	0.164	0.015	-0.024	-0.004	-0.015	0.012
$\ln(x_3)$*$\ln(x_5)$	0.010	0.015	0.011	0.010	0.012	0.039	0.003	0.010
$\ln(x_3)$*$\ln(x_6)$	-0.039	-0.012	-0.011	-0.023	-0.034	0.000	0.013	-0.009
$\ln(x_3)$*x_7	0.006	-0.002	-0.004	0.002	0.001	-0.002	0.005	0.014

$\ln(x_3)*x_8$	0.019	0.016	0.009	0.007	0.010	0.004	-0.016	-0.009
$\ln(x_3)*\ln(x_9)$	-0.010	-0.013	-0.021	-0.019	-0.001	0.012	0.008	0.010
$x_4*\ln(x_5)$	-0.041	-0.027	-0.061	-0.004	-0.006	0.009	-0.027	-0.024
$x_4*\ln(x_6)$	0.006	-0.004	-0.013	0.009	-0.047	-0.012	0.006	0.008
x_4*x_7	0.026	0.029	-0.016	0.014	-0.043	0.074	0.009	0.008
x_4*x_8	-0.004	0.105	0.074	0.029	0.006	0.008	0.014	0.007
$x_4*\ln(x_9)$	0.106	0.053	0.004	0.114	0.105	0.093	-0.003	0.042
$\ln(x_5)*\ln(x_6)$	-0.008	-0.042	-0.002	-0.038	0.005	-0.004	-0.003	0.005
$\ln(x_5)*x_7$	-0.002	0.002	0.000	-0.002	0.004	-0.001	0.001	-0.001
$\ln(x_5)*x_8$	0.001	-0.003	-0.011	0.001	-0.017	-0.004	-0.003	-0.008
$\ln(x_5)*\ln(x_9)$	-0.001	0.010	0.004	-0.001	0.000	-0.003	0.002	0.002
$\ln(x_6)*x_7$	0.001	-0.004	-0.001	0.001	-0.002	-0.001	0.001	-0.003
$\ln(x_6)*x_8$	-0.021	-0.035	-0.029	-0.026	-0.033	-0.029	-0.025	-0.031
$\ln(x_6)*\ln(x_9)$	-0.005	-0.003	0.007	-0.004	0.028	0.001	0.001	0.008
x_7*x_8	0.006	0.006	0.007	0.001	0.007	0.012	0.007	0.006
$x_7*\ln(x_9)$	0.015	0.009	0.010	0.001	0.035	0.025	0.014	0.008
$x_8*\ln(x_9)$	-0.008	-0.021	-0.019	0.003	-0.008	-0.002	-0.003	-0.012

Table C-18: Coefficients of parameterized fragility model at bridge system level

Predictor term	**Logistic Regression Coefficient**
Intercept	8.051
$\ln(x_1)$	4.205
x_2	-0.004
$\ln(x_3)$	-0.13
x_4	-0.321
$\ln(x_5)$	0.158
$\ln(x_6)$	0.077
x_7	-0.314
x_8	-0.252
$\ln(x_9)$	-0.203

C.1.7 MSC Concrete Box Girder Bridge Class

Table C-19: Predictor variables for MSC Concrete Bridge Class

Parameter	Unit	Description
x_1	g	Peak ground acceleration
x_2	cm^2	Column rebar area
x_3	cm^2	Elastomeric bearing dowel bar area
x_4	MPa	Shear modulus of elastomeric bearing pads
x_5	cm	Abutment gap
x_6	cm	Column cover depth

Table C-20: Polynomial response surface model coefficients for different bridge components

Predictor term	Regression Coefficient estimate							
	COL	FBL (mm)	FBT (mm)	EBL (mm)	EBT (mm)	ABA (mm)	ABP (mm)	ABT (mm)
Intercept	4.392	4.665	6.878	4.689	6.865	4.373	1.322	1.865
$\ln(x_1)$	1.958	1.008	1.879	1.050	1.878	1.435	0.248	0.497
x_2	-0.425	0.088	0.017	0.112	0.007	0.119	0.079	-0.004
x_3	-0.054	-0.177	-0.725	-0.151	-0.723	-0.259	0.437	0.461
$\ln(x_4)$	0.249	-0.053	-0.465	-0.044	-0.372	-0.333	0.461	0.320
$\ln(x_5)$	0.138	0.395	0.060	0.291	0.073	-0.088	-0.030	-0.020
$\ln(x_6)$	-0.269	0.114	0.201	0.148	0.158	-0.006	-0.035	-0.098
$\ln(x_1)*x_2$	-0.114	0.026	0.028	0.033	0.023	0.036	0.008	-0.036
$\ln(x_1)*x_3$	-0.015	-0.017	-0.177	-0.039	-0.173	-0.124	0.081	0.112
$\ln(x_1)*\ln(x_4)$	-0.002	0.103	-0.082	0.087	-0.056	-0.152	0.093	0.015
$\ln(x_1)*\ln(x_5)$	0.017	0.079	-0.006	0.017	0.003	0.041	-0.056	-0.045
$\ln(x_1)*\ln(x_6)$	-0.037	-0.015	0.071	0.006	0.059	0.029	-0.039	-0.027
x_2*x_3	0.008	0.004	0.036	-0.002	0.039	-0.012	-0.028	-0.025
$x_2*\ln(x_4)$	-0.005	-0.003	-0.007	-0.004	-0.018	0.000	0.000	-0.014
$x_2*\ln(x_5)$	-0.003	-0.012	-0.013	-0.014	-0.014	-0.003	-0.009	-0.006

x_2*ln(x_6)	0.010	-0.050	-0.040	-0.042	-0.035	-0.018	-0.018	-0.005
x_3*ln(x_4)	-0.024	0.002	0.013	0.008	0.013	0.006	-0.037	0.000
x_3*ln(x_5)	-0.022	0.008	-0.010	0.000	-0.006	0.006	0.008	-0.018
x_3*ln(x_6)	0.021	0.022	0.020	0.019	0.021	0.041	0.000	0.005
ln(x_4)*ln(x_5)	-0.028	0.012	-0.001	0.004	-0.004	0.005	-0.009	-0.014
ln(x_4)*ln(x_6)	-0.026	-0.023	-0.025	-0.023	-0.023	0.024	0.010	-0.021
ln(x_5)*ln(x_6)	0.035	-0.005	0.034	-0.016	0.036	-0.008	0.000	0.006

Table C-21: Coefficients of parameterized fragility model at bridge system level

Predictor term	**Logistic Regression Coefficient**
Intercept	5.32
ln(x_1)	2.75
x_2	-0.36
x_3	-0.22
ln(x_4)	-0.11
ln(x_5)	0.12
ln(x_6)	-0.17

APPENDIX D – TIME-DEPENDENT FRAGILITIES AND ADOPTED REPAIR STRATEGIES FOR SEISMIC LOSS ANALYSIS

The time-dependent fragilities for the case study bridges in Chapter 7 for computing lifetime seismic losses are presented in this Appendix. The medians are given in terms of gravitational acceleration g. Whenever the estimated median is larger than 4.0, the median and dispersion values are replaced by 99.00 and 0.00 respectively. This indicates that this particular component is not significant for that limit state. The curves are presented for intensity measure of PGA and, as derived using 96 ground motions from the Rix and Fernandez (2004) and the Wen and Wu (2001) ground motion suite. In addition to the fragility curves, preferred repair strategies for different damage states associated with different bridge components are also presented.

D.1 Time varying median and dispersion for the components of case study MSC steel girder and MSSS concrete girder bridges under deicing salt exposure for seismic loss estimation

D.1.1 MSC steel girder bridge

Table D-1: Time t = 0 years (Pristine State) component fragilities for case study MSC steel girder bridge presented in Chapter 7

Component	Slight		Moderate		Extensive		Complete	
	med (g)	*disp*	*med* (g)	*disp*	*med* (g)	*disp*	*med* (g)	*disp*
COL	0.19	0.42	0.24	0.42	0.35	0.48	0.72	0.48
FBL	2.88	0.68	99.00	0.00	99.00	0.00	99.00	0.00
FBT	0.36	0.56	0.65	0.56	0.91	0.59	2.22	0.59
EBL	0.09	0.54	0.31	0.54	0.50	0.61	0.72	0.61
EBT	0.18	0.54	0.33	0.54	0.47	0.58	1.20	0.58
ABP	0.58	0.64	0.97	0.64	2.01	0.63	2.01	0.63
ABA	99.00	0.00	99.00	0.00	99.00	0.00	99.00	0.00
ABT	0.64	0.66	3.56	0.66	99.00	0.00	99.00	0.00

Table D-2: Time t = 25 years component fragilities for case study MSC steel girder bridge presented in Chapter 7

Component	Slight		Moderate		Extensive		Complete	
	med (g)	*disp*	*med* (g)	*disp*	*med* (g)	*disp*	*med* (g)	*disp*
COL	0.18	0.44	0.23	0.44	0.33	0.48	0.65	0.48
FBL	3.60	0.62	99.00	0.00	99.00	0.00	99.00	0.00
FBT	0.37	0.58	0.67	0.58	0.94	0.61	2.32	0.61
EBL	0.10	0.54	0.33	0.54	0.52	0.60	0.73	0.60
EBT	0.18	0.55	0.33	0.55	0.46	0.59	1.18	0.59
ABP	0.60	0.65	1.04	0.65	2.24	0.64	2.24	0.64
ABA	99.00	0.00	99.00	0.00	99.00	0.00	99.00	0.00
ABT	0.67	0.67	3.89	0.67	99.00	0.00	99.00	0.00

Table D-3: Time t = 50 years component fragilities for case study MSC steel girder bridge presented in Chapter 7

Component	Slight		Moderate		Extensive		Complete	
	med (g)	*disp*	*med* (g)	*disp*	*med* (g)	*disp*	*med* (g)	*disp*
COL	0.17	0.43	0.21	0.43	0.30	0.48	0.58	0.48
FBL	99.00	0.00	99.00	0.00	99.00	0.00	99.00	0.00
FBT	0.38	0.58	0.69	0.58	0.97	0.61	2.41	0.61
EBL	0.10	0.53	0.34	0.53	0.54	0.59	0.76	0.59
EBT	0.17	0.47	0.29	0.47	0.40	0.51	0.95	0.51
ABP	0.62	0.65	1.10	0.65	2.47	0.64	2.47	0.64
ABA	99.00	0.00	99.00	0.00	99.00	0.00	99.00	0.00
ABT	0.70	0.68	99.00	0.00	99.00	0.00	99.00	0.00

Table D-4: Time t = 75 years component fragilities for case study MSC steel girder bridge presented in Chapter 7

Component	Slight		Moderate		Extensive		Complete	
	med (g)	*disp*	*med* (g)	*disp*	*med* (g)	*disp*	*med* (g)	*disp*
COL	0.15	0.44	0.19	0.44	0.27	0.48	0.50	0.48
FBL	99.00	0.00	99.00	0.00	99.00	0.00	99.00	0.00
FBT	0.37	0.55	0.67	0.55	0.94	0.58	2.33	0.58
EBL	0.10	0.53	0.35	0.53	0.55	0.60	0.78	0.60
EBT	0.15	0.46	0.26	0.46	0.36	0.49	0.84	0.49
ABP	0.66	0.66	1.22	0.66	2.88	0.65	2.88	0.65
ABA	99.00	0.00	99.00	0.00	99.00	0.00	99.00	0.00
ABT	0.87	0.70	99.00	0.00	99.00	0.00	99.00	0.00

Table D-5: Time t = 100 years component fragilities for case study MSC steel girder bridge presented in Chapter 7

Component	Slight		Moderate		Extensive		Complete	
	med (g)	disp	med (g)	disp	med (g)	disp	med (g)	disp
COL	0.14	0.463	0.174	0.463	0.237	0.498	0.433	0.498
FBL	99.00	0.00	99.00	0.00	99.00	0.00	99.00	0.00
FBT	0.354	0.574	0.636	0.574	0.892	0.606	2.198	0.606
EBL	0.106	0.524	0.35	0.524	0.555	0.587	0.781	0.587
EBT	0.128	0.458	0.225	0.458	0.31	0.494	0.733	0.494
ABP	0.654	0.651	1.22	0.651	2.927	0.641	2.927	0.641
ABA	99.00	0.00	99.00	0.00	99.00	0.00	99.00	0.00
ABT	3.881	0.958	99.00	0.00	99.00	0.00	99.00	0.00

D.1.2 MSSS concrete girder bridge

Table D-6: Time t = 0 years (Pristine State) component fragilities for case study MSSS concrete girder bridge presented in Chapter 7

Component	Slight		Moderate		Extensive		Complete	
	med (g)	*disp*	*med* (g)	*disp*	*med* (g)	*disp*	*med* (g)	*disp*
COL	0.37	0.51	0.57	0.51	1.06	0.63	3.47	0.63
FBL	0.18	0.54	0.70	0.54	1.18	0.62	1.75	0.62
FBT	0.31	1.03	2.14	1.03	99.00	0.00	99.00	0.00
EBL	0.12	0.56	0.83	0.56	1.78	0.71	3.15	0.71
EBT	0.39	1.09	3.89	1.09	99.00	0.00	99.00	0.00
ABP	2.27	0.61	99.00	0.00	99.00	0.00	99.00	0.00
ABA	0.72	0.82	99.00	0.00	99.00	0.00	99.00	0.00
ABT	0.92	0.68	99.00	0.00	99.00	0.00	99.00	0.00

Table D-7: Time t = 25 years component fragilities for case study MSSS concrete girder bridge presented in Chapter 7

Component	Slight		Moderate		Extensive		Complete	
	med (g)	*disp*	*med* (g)	*disp*	*med* (g)	*disp*	*med* (g)	*disp*
COL	0.33	0.47	0.49	0.47	0.85	0.58	2.50	0.58
FBL	0.19	0.55	0.70	0.55	1.17	0.63	1.71	0.63
FBT	0.35	0.95	2.65	0.95	99.00	0.00	99.00	0.00
EBL	0.11	0.49	0.71	0.49	1.39	0.62	2.30	0.62
EBT	0.30	0.89	1.74	0.89	3.46	0.97	99.00	0.00
ABP	2.51	0.58	99.00	0.00	99.00	0.00	99.00	0.00
ABA	0.91	0.86	99.00	0.00	99.00	0.00	99.00	0.00
ABT	0.86	0.63	3.74	0.63	99.00	0.00	99.00	0.00

Table D-8: Time t = 50 years component fragilities for case study MSSS concrete girder bridge presented in Chapter 7

Component	Slight		Moderate		Extensive		Complete	
	med (g)	*disp*	*med* (g)	*disp*	*med* (g)	*disp*	*med* (g)	*disp*
COL	0.30	0.45	0.43	0.45	0.74	0.55	2.08	0.55
FBL	0.17	0.54	0.63	0.54	1.03	0.61	1.49	0.61
FBT	0.30	0.91	1.78	0.91	3.55	0.99	99.00	0.00
EBL	0.10	0.47	0.63	0.47	1.18	0.59	1.87	0.59
EBT	0.28	0.87	1.51	0.87	2.91	0.95	99.00	0.00
ABP	2.35	0.60	99.00	0.00	99.00	0.00	99.00	0.00
ABA	1.89	1.01	99.00	0.00	99.00	0.00	99.00	0.00
ABT	0.98	0.65	99.00	0.00	99.00	0.00	99.00	0.00

Table D-9: Time t = 75 years component fragilities for case study MSSS concrete girder bridge presented in Chapter 7

Component	Slight		Moderate		Extensive		Complete	
	med (g)	*disp*	*med* (g)	*disp*	*med* (g)	*disp*	*med* (g)	*disp*
COL	0.27	0.46	0.38	0.46	0.64	0.55	1.73	0.55
FBL	0.16	0.52	0.59	0.52	0.97	0.59	1.41	0.59
FBT	0.24	0.79	1.04	0.79	1.85	0.85	2.84	0.85
EBL	0.09	0.49	0.59	0.49	1.07	0.59	1.65	0.59
EBT	0.23	0.71	0.93	0.71	1.60	0.78	2.39	0.78
ABP	1.91	0.58	99.00	0.00	99.00	0.00	99.00	0.00
ABA	2.67	1.02	99.00	0.00	99.00	0.00	99.00	0.00
ABT	1.18	0.67	99.00	0.00	99.00	0.00	99.00	0.00

Table D-10: Time t = 100 years component fragilities for case study MSSS concrete girder bridge presented in Chapter 7

Component	Slight		Moderate		Extensive		Complete	
	med (g)	*disp*	*med* (g)	*disp*	*med* (g)	*disp*	*med* (g)	*disp*
COL	0.24	0.44	0.33	0.44	0.54	0.53	1.39	0.53
FBL	0.16	0.52	0.57	0.52	0.94	0.59	1.36	0.59
FBT	0.21	0.61	0.76	0.61	1.24	0.68	1.78	0.68
EBL	0.08	0.49	0.56	0.49	0.99	0.59	1.50	0.59
EBT	0.21	0.61	0.77	0.61	1.26	0.68	1.83	0.68
ABP	2.08	0.67	99.00	0.00	99.00	0.00	99.00	0.00
ABA	99.00	0.00	99.00	0.00	99.00	0.00	99.00	0.00
ABT	1.55	0.71	99.00	0.00	99.00	0.00	99.00	0.00

D.2 Preferred repair strategies and repair percentages for bridge components

Associated Bridge Component	Repair Strategies	Preferred Repair Percentages by Damage State			
Reinforced Concrete Columns[1]		Slight	Moderate	Severe	Complete
	Epoxy Injection	45%	5%	0%	0%
	Patch with Concrete	14%	23%	0%	0%
	No Action	23%	0%	0%	0%
	Grouting	5%	0%	0%	0%
	Concrete Lining	5%	9%	0%	0%
	Wrap	5%	36%	0%	0%
	Replace Column	5%	23%	72%	0%
	Reinforce and Recast	0%	5%	20%	0%
	Demolish and Replace Bridge	0%	0%	8%	100%
Steel Fixed Bearings – Longitudinal[2]		Slight	Moderate	Severe	Complete
	No Action	50%	0%	0%	0%
	Patch with Concrete	50%	0%	0%	0%
	Rehabilitate (Anchor Bolt Replacement)	0%	100%	50%	0%
	Replace Bearing and Bridge Deck	0%	0%	50%	100%
		Slight	Moderate	Severe	Complete
Steel Fixed Bearings – Transverse[2]	No Action	50%	0%	0%	0%
	Patch with Concrete	50%	0%	0%	0%
	Rehabilitate (Anchor Bolt Replacement)	0%	100%	50%	0%
	Replace Bearing	0%	0%	50%	100%
Steel		Slight	Moderate	Severe	Complete

Expansion Bearing - Longitudinal[1]	Jack Bridge into Place	15%	42%	41%	0%
	No Action	77%	12%	0%	0%
	Replace Bearing and Bridge Deck	8%	46%	59%	100%
Steel Expansion Bearing - Transverse[2]		Slight	Moderate	Severe	Complete
	No Action	50%	0%	0%	0%
	Patch with Concrete	50%	0%	0%	0%
	Rehabilitate (Anchor Bolt Replacement)	0%	100%	50%	0%
	Replace Bearing	0%	0%	50%	100%
Elastomeric Fixed and Expansion Bearing - Longitudinal[1]		Slight	Moderate	Severe	Complete
	Jack Bridge into Place	15%	42%	41%	0%
	No Action	77%	12%	0%	0%
	Replace Bearing and Bridge Deck	8%	46%	59%	100%
Elastomeric Fixed and Expansion Bearing - Transverse[1]		Slight	Moderate	Severe	Complete
	Jack Bridge into Place	13%	58%	40%	25%
	No Action	88%	4%	0%	0%
	Replace Bearing	0%	17%	25%	25%
	Replace Joint	0%	8%	0%	0%
	Add Steel Plates	0%	8%	20%	0%
	Demolish and Replace Bridge	0%	4%	15%	50%
Abutment - Passive[1]		Slight	Moderate		
	Epoxy Injection	50%	28%		
	Patch with Concrete	12%	17%		
	No Action	19%	6%		
	Add Reinforcement and Cover	15%	6%		
	Grouting	4%	33%		
	Demolish and Replace Bridge	0%	11%		

		Slight	Moderate	Severe	
Abutment – Active[1]	Regrade and Resurface	23%	41%	15%	
	Add Fill and Asphalt	19%	59%	62%	
	No Action	58%	0%	0%	
	Replace Structural Section	0%	0%	23%	

[1]Adopted from survey results in Padgett and DesRoches (2007); [2]Assumed repair strategy adopted from CALTRANS (2008) in absence of proper mapping from survey results.

REFERENCES

AASHTO. (1993). *Guidelines for bridge management systems*. American Association of State Highway and Transportation Officials.

AASHTO. (2012). *LRFD Bridge Design Specifications*. American Association of State Highway and Transportation Officials.

Abdelnaby, A. (2012). "Multiple earthquake effects on degrading reinforced concrete structures." <http://hdl.handle.net/2142/34345>.

Akgul, F., and Frangopol, Dan M. (2004). "Lifetime performance analysis of existing prestressed concrete bridge superstructures." *Journal of Structural Engineering*, 130(12), 1889–1903.

Akiyama, M., Frangopol, Dan M, and Matsuzaki, H. (2011). "Life-cycle reliability of RC bridge piers under seismic and airborne chloride hazards." *Earthquake Engineering & Structural Dynamics*.

Alam, M. S., Bhuiyan, M. A. R., and Billah, A. H. M. M. (2012). "Seismic fragility assessment of SMA-bar restrained multi-span continuous highway bridge isolated by different laminated rubber bearings in medium to strong seismic risk zones." *Bulletin of Earthquake Engineering*, 10(6), 1885–1909.

Albrecht, P., and Naeemi, A. H. (1984). *Performance of weathering steel in bridges*. National Cooperative Highway Research Program, Washington D.C.

Alipour, A., Shafei, B., and Shinozuka, M. (2010). "Performance Evaluation of Deteriorating Highway Bridges Located in High Seismic Areas." *Journal of Bridge Engineering*, 1(1), 117.

Amadio, C., Fragiacomo, M., and Rajgelj, S. (2003). "The effects of repeated earthquake ground motions on the non-linear response of SDOF systems." *Earthquake Engineering & Structural Dynamics*, 32(2), 291–308.

Amato, A., Azzara, R., Chiarabba, C., Cimini, G. B., Cocco, M., Bona, M. D., Margheriti, L., Mazza, S., Mele, F., Selvaggi, G., Basili, A., Boschi, E., Courboulex, F., Deschamps, A., Gaffet, S., Bittarelli, G., Chiaraluce, L., Piccinini, D., and Ripepe, M. (1998). "The 1997 Umbria-Marche, Italy, Earthquake Sequence: A first look at the main shocks and aftershocks." *Geophysical Research Letters*, 25(15), 2861–2864.

Ang, Alfredo Hua-Sing, and Tang, W. H. (2007). *Probability concepts in engineering*. Wiley.

Aquino, W., and Hawkins, N. M. (2007). "Seismic retrofitting of corroded reinforced concrete columns using carbon composites." *ACI Structural Journal*, 104(3), 348–356.

ASCE. (2013). "ASCE: Infrastructure Fact Sheet." <http://www.infrastructurereportcard.org/>.

ATC. (1991). *Seismic Vulnerability and Impact of Disruption of Lifelines in the Conterminous United States*. Applied Technology Council.

Aygün, B., Dueñas-Osorio, L., Padgett, J. E., and DesRoches, R. (2011). "Efficient Longitudinal Seismic Fragility Assessment of a Multispan Continuous Steel Bridge on Liquefiable Soils." *Journal of Bridge Engineering*, 16(1), 93–107.

Basöz, N. I., and Kiremidjian, Anne S. (1998). "Evaluation of bridge damage data from the Loma Prieta and Northridge, California earthquakes." *Technical Report MCEER*, (98-0004).

Basoz, N., and Mander, J. B. (1999). *Enhancement of the highway transportation module in HAZUS*. National Institute of Building Sciences Report.

Basoz, Nesrin, and Kiremidjian, Anne S. (1999). "Development of empirical fragility curves for bridges." *Technical Council on Lifeline Earthquake Engineering Monograph*, (16), 693–702.

Beck, J. L., Porter, Keith A, Shaikhutdinov, R. V., Au, S. K., Mizukoshi, K., Miyamura, M., Ishida, H., Moroi, T., Tsukada, Y., and Masuda, M. (2002). "Impact of Seismic Risk on Lifetime Property Values." Monograph, , <http://caltecheerl.library.caltech.edu/342/> (Mar. 6, 2011).

Bertolini, L., Elsener, B., Pedeferri, P., and Polder, R. B. (2004). *Corrosion of steel in concrete: prevention, diagnosis, repair*. Wiley-VCH.

Box, G. E. P., and Wilson, K. B. (1951). "On the Experimental Attainment of Optimum Conditions." *Journal of the Royal Statistical Society. Series B (Methodological)*, 13(1), 1–45.

Boyd, O. S. (2012). "Including Foreshocks and Aftershocks in Time-Independent Probabilistic Seismic-Hazard Analyses." *Bulletin of the Seismological Society of America*, 102(3), 909–917.

Bradley, B. A, and Lee, D. S. (2009). "Component correlations in structure-specific seismic loss estimation." *Earthquake Engineering & Structural Dynamics*, 39(3), 237–258.

Bradley, Brendon A., and Cubrinovski, M. (2011). "Near-source Strong Ground Motions Observed in the 22 February 2011 Christchurch Earthquake." *Seismological Research Letters*, 82(6), 853–865.

Brandenberg, S. J., Zhang, J., Kashighandi, P., Huo, Y., and Zhao, M. (2011). *Demand Fragility Surfaces for Bridges in Liquefied and Laterally Spreading Ground*. PEER.

Broomfield, J. (1997). *Corrosion of steel in concrete understanding, investigation, and repair*. E & FN Spon,, New York :

Broomfield, J. P. (1997). *Corrosion of steel in concrete*. Taylor & Francis.

Buckle, G. (2006). *Seismic retrofitting manual for highway structures*. MCEER.

CALTRANS. (1999). "Seismic Design Criteria." <http://www.dot.ca.gov/hq/esc/techpubs/manual/othermanual/other-engin-manual/seismic-design-criteria/sdc.html> (Jan. 22, 2013).

CALTRANS (2008). "Element Level Inspection Manual. California Department of Transportation." <http://www.dot.ca.gov/hq/structur/strmaint/eli.pdf>

Chai, Y. H., Priestley, M. J. N., and Seible, F. (1994). "Analytical model for steel-jacketed RC circular bridge columns." *Journal of Structural Engineering*, 120(8), 2358–2376.

Chang, S. E. (2000). "Disasters and transport systems: loss, recovery and competition at the Port of Kobe after the 1995 earthquake." *Journal of Transport Geography*, 8(1), 53–65.

Chen, V. C. P., Tsui, K.-L., Barton, R. R., and Meckesheimer, M. (2006). "A review on design, modeling and applications of computer experiments." *IIE Transactions*, 38(4), 273–291.

Choe, D.-E., Gardoni, Paolo, Rosowsky, D., and Haukaas, T. (2008). "Probabilistic capacity models and seismic fragility estimates for RC columns subject to corrosion." *Reliability Engineering & System Safety*, 93(3), 383–393.

Choe, D.-E., Gardoni, Paolo, Rosowsky, D., and Haukaas, T. (2009). "Seismic fragility estimates for reinforced concrete bridges subject to corrosion." *Structural Safety*, 31(4), 275–283.

Choi, E. (2002). "Seismic Analysis and Retrofit of Mid-America Bridges." PhD Thesis, Georgia Institute of Technology, Atlanta, Georgia.

Choi, Eunsoo, DesRoches, R., and Nielson, B. G. (2004). "Seismic fragility of typical bridges in moderate seismic zones." *Engineering Structures*, 26(2), 187–199.

Chou, J., Chiu, C., Farfoura, M., and Al-Taharwa, I. (2011). "Optimizing the Prediction Accuracy of Concrete Compressive Strength Based on a Comparison of Data-Mining Techniques." *Journal of Computing in Civil Engineering*, 25(3), 242–253.

Cimellaro, G. P., Reinhorn, A. M., and Bruneau, M. (2010). "Seismic resilience of a hospital system." *Structure and Infrastructure Engineering: Maintenance, Management, Life-Cycle Design and Performance*, 6(1), 127.

Cornell, C. Allin, Jalayer, F., Hamburger, R. O., and Foutch, D. A. (2002). "Probabilistic Basis for 2000 SAC Federal Emergency Management Agency Steel Moment Frame Guidelines." *Journal of Structural Engineering*, 128(4), 526–533.

Courtois, M., and Woodside, M. (2000). "Using regression splines for software performance analysis." *Proceedings of the 2nd international workshop on Software and performance*, WOSP '00, ACM, New York, NY, USA, 105–114.

Cressie, N. A. C. (1993). *Statistics for spatial data*. J. Wiley.

Cundy, A. L., Hemez, F. M., Inman, D. J., and Park, G. (2003). "Use of response surface metamodels for damage identification of a simple nonlinear system." *Key Engineering Materials*, 245, 167–174.

Czarnecki, A. A., and Nowak, A. S. (2007). "Reliability-based evaluation of steel girder bridges." *Proceedings of the ICE-Bridge Engineering*, 160(1), 9–15.

Czarnecki, Artur A., and Nowak, Andrzej S. (2008a). "Time-variant reliability profiles for steel girder bridges." *Structural Safety*, 30(1), 49–64.

Czarnecki, Artur A., and Nowak, Andrzej S. (2008b). "Time-variant reliability profiles for steel girder bridges." *Structural Safety*, 30(1), 49–64.

Das, P. C. (1999). *Management of highway structures*. Thomas Telford.

DesRoches, Reginald, Choi, Eunsoo, Leon, R. T., Dyke, S. J., and Aschheim, M. (2004). "Seismic response of multiple span steel bridges in central and southeastern United States. i: As built." *Journal of Bridge Engineering*, 9(5), 464–472.

Du, J. S., and Au, F. T. K. (2005). "Deterministic and reliability analysis of prestressed concrete bridge girders: comparison of the Chinese, Hong Kong and AASHTO LRFD codes." *Structural safety*, 27(3), 230–245.

Dueñas-Osorio, L., and Padgett, J. (2011). "Seismic Reliability Assessment of Bridges with User-Defined System Failure Events." *Journal of Engineering Mechanics*, 137(10), 680–690.

Duracrete. (2000). *Probabilistic Performance Based Durability Design of Concrete Structures: Final Technical Report*. The European Union – Brite EuRam III.

Edwards, R. V. (2006). *Processing random data*. World Scientific.

Ellingwood, B. R., and Wen, Y.-K. (2005). "Risk-benefit-based design decisions for low-probability/high consequence earthquake events in Mid-America." *Progress in Structural Engineering and Materials*, 7(2), 56–70.

Elnashai, A. S., Bommer, J. J., and Martinez-Pereira, A. (1998). "Engineering implications of strong-motion records from recent earthquakes." *Proceedings of 11th European conference on earthquake engineering, Paris*.

Enright, M. P., and Frangopol, Dan M. (1998). "Probabilistic analysis of resistance degradation of reinforced concrete bridge beams under corrosion." *Engineering Structures*, 20(11), 960–971.

Enright, M. P., and Frangopol, Dan M. (1999). "Condition Prediction of Deteriorating Concrete Bridges Using Bayesian Updating." *Journal of Structural Engineering*, 125(10), 1118–1125.

Estes, Allen C, and Frangopol, Dan M. (2003). "Updating Bridge Reliability Based on Bridge Management Systems Visual Inspection Results." *Journal of Bridge Engineering*, 8(6), 374–382.

Fang, C., Lundgren, K., Chen, L., and Zhu, C. (2004). "Corrosion influence on bond in reinforced concrete." *Cement and Concrete Research*, 34(11), 2159–2167.

Fang, K., Li, R., and Sudjianto, A. (2006). *Design and modeling for computer experiments*. CRC Press.

Federal Highway Administration (FHWA). (2006). *National bridge inventory data*.

FEMA. (2000). *FEMA 352: Recommended Post-Earthquake Evaluation and Repair Criteria for Welded Steel Moment-Frame Buildings*. ATC Council.

FEMA. (2003). *HAZUS*. Earthquake Model, Technical Manual, Federal Emergency Management Agency, Washington DC.

FEMA. (2009). "FEMA Library - HAZUS®MH MR4 Earthquake Model User Manual." <http://www.fema.gov/library/viewRecord.do?id=3732> (Mar. 11, 2011).

FHWA. (2008). "LTBP: Long-Term Bridge Performance Program-LTBP: Long-Term Bridge Performance Program--." <http://www.fhwa.dot.gov/research/tfhrc/programs/infrastructure/structures/ltbp/> (Mar. 21, 2012).

FHWA. (2009). "FHWA Bridge Programs NBI Data." <http://www.fhwa.dot.gov/bridge/britab.cfm>.

FHWA. (2010). "NBI ASCII Files - NBI - Programs - Integrated - Bridge - FHWA." <http://www.fhwa.dot.gov/bridge/nbi/ascii.cfm?year=2010> (Mar. 11, 2011).

FHWA. (2011). "Federal Highway Administration Vehicle Classification." <http://www.fhwa.dot.gov/policy/ohpi/vehclass.htm> (Jan. 29, 2013).

Frangopol, D.M., Kai-Yung Lin, and Estes, A.C. (1997). "Reliability of reinforced concrete girders under corrosion attack." *Journal of structural engineering New York, N.Y.*, 123(3), 286–297.

Frangopol, D.M., Lin, K. Y., and Estes, A.C. (1997). "Reliability of reinforced concrete girders under corrosion attack." *Journal of Structural Engineering*, 123(3), 286.

Friedman, J. H. (1991). "Multivariate adaptive regression splines." *The annals of statistics*, 1–67.

Funahashi, M. I. (1990). "Predicting corrosion-free service life of a concrete structure in a chloride environment." *ACI Materials Journal*, 87(6).

Furuta, H., Dogaki, M., Koyama, K., Kataoka, H., and Sugimoto, H. (2004). "Life-cycle cost for bridge structures considering earthquake effects." *Journal of the Society of Materials Science, Japan*, J. Soc. Mater. Sci. Jpn. (Japan), 53(3), 339–44.

Gardoni, P., Mosalam, K. M., and Kiureghian, A. D. (2003). "probabilistic seismic demand models and fragility estimates for RC bridges." *Journal of Earthquake Engineering*, 7(sup001), 79–106.

Gassman, S. L., and Tawhed, W. F. (2004). "Nondestructive Assessment of Damage in Concrete Bridge Decks." *Journal of Performance of Constructed Facilities*, 18(4), 220–231.

Ghosh, J., and Padgett, J. E. (2010). "Aging Considerations in the Development of Time-Dependent Seismic Fragility Curves." *Journal of Structural Engineering*, 136(12), 1497–1511.

Ghosh, J., and Padgett, J. E. (2011). "Probabilistic seismic loss assessment of aging bridges using a component-level cost estimation approach." *Earthquake Engineering & Structural Dynamics*, 40(15), 1743–1761.

Ghosh, J., and Padgett, J. E. (2012). "Impact of Multiple Component Deterioration and Exposure Conditions on Seismic Vulnerability of Concrete Bridges." *Earthquakes and Structures*, 3(5), 649–673.

Ghosh, J., Padgett, J. E., and Dueñas-Osorio, Leonardo. (2013a). "Surrogate Modeling and Failure Surface Visualization for Efficient Seismic Vulnerability Assessment of Highway Bridges." *Probabilistic Engineering Mechanics*, (In Review).

Ghosh, J., Rokneddin, K., Padgett, J. E., and Dueñas-Osorio, Leonardo. (2013b). "Seismic Reliability Assessment of Aging Highway Bridge Networks with Field Instrumentation Data and Correlated Failures. I: Methodology." *Earthquake Spectra*, (Accepted (In Press)).

Ghosh, J., Padgett, J. E., and Sanchez-Silva, Mauricio. (2013c). "Seismic Damage Accumulation of Highway Bridges in Earthquake Prone Regions." *Earthquake Spectra*, (Accepted (In Press)).

Ghosh, J., Caprani, C. C., and Padgett, J. E. (2013d). "Influence of Traffic Loading on the Seismic Reliability Assessment of Highway Bridge Structures." *Journal of Bridge Engineering*, (In Review).

Goulet, C. A., Haselton, C. B., Mitrani-Reiser, J., Beck, J. L., Deierlein, G. G., Porter, Keith A., and Stewart, Jonathan P. (2007). "Evaluation of the seismic performance of a code-conforming reinforced-concrete frame building - from seismic hazard to collapse safety and economic losses." *Earthquake Engineering & Structural Dynamics*, 36(13), 1973–1997.

Guan, X. L., and Melchers, R.E. (2001). "Effect of response surface parameter variation on structural reliability estimates." *Structural Safety*, 23(4), 429–444.

Gupta, A., and Krawinkler, H. (2000). "Behavior of ductile SMRFs at various seismic hazard levels." *Journal of Structural Engineering*, 126, 98.

De Guzman, P., and Ishiyama, Y. (2004). "Collapse assessment of building structures using damage index." *Proceedings of the 13th WCEE*.

Hardy, R. L. (1971). "Multiquadric Equations of Topography and Other Irregular Surfaces." *Journal of Geophysical Research*, 76(8), PP. 1905–1915.

Hasofer, A. M., and Lind, N. C. (1974). "Exact and Invariant Second-Moment Code Format." *Journal of the Engineering Mechanics Division*, 100(1), 111–121.

Hoeke, L. J. L., Singh, P. M., Moser, R. D., Kahn, L. F., and Kurtis, K. E. (2009). "Degradation of steel girder bridge bearing systems by corrosion." *Corrosion 2009, March 22, 2009 - March 26, 2009*, NACE - International Corrosion Conference Series, National Assoc. of Corrosion Engineers International, Atlanta, GA, United states, Carboline; Multi–chem; Corrpo; Champion Technologies; Loresco.

Hoffman, Paul C., and Weyers, Richard E. (1996). "Probabilistic durability analysis of reinforced concrete bridge decks." *Proceedings of the 1996 7th Specialty Conference on Probabilistic Mechanics and Structural Reliability, August 7, 1996 - August 9, 1996*, Probabilistic

Mechanics and Structural and Geotechnical Reliability, Proceedings of the Specialty Conference, ASCE, Worcester, MA, USA, 290–293.

Hurtado, J. E. (2012). "Dimensionality reduction and visualization of structural reliability problems using polar features." *Probabilistic Engineering Mechanics*, 29(0), 16–31.

Le Huy, M., and Evrard, G. (1998). "Methodologies for lifetime predictions of rubber using Arrhenius and WLF models." *Die Angewandte Makromolekulare Chemie*, 261-262(1), 135–142.

Hwang, H., Jernigan, J., and Lin, Y. (2000). "Evaluation of Seismic Damage to Memphis Bridges and Highway Systems." *Journal of Bridge Engineering*, 5(4), 322–330.

Hwang, Howard, Liu, J. B., and Chiu, Y.-H. (2001). "Seismic Fragility Analysis of Highway Bridges." <http://hdl.handle.net/2142/9267> (Mar. 12, 2010).

Itoh, Y., and Gu, H. S. (2009). "Prediction of Aging Characteristics in Natural Rubber Bearings Used in Bridges." *Journal of Bridge Engineering*, 14, 122.

Itoh, Yoshito, Gu, H., Satoh, K., and Kutsuna, Y. (2006). "Experimental investigation on ageing behaviors of rubbers used for bridge bearings." *Structural Engineering/Earthquake Engineering*, 23(1), 17s–31s.

Jin, Y., Yang, Q., and Li, Q. (2008). "Integrated Risk Management of Typhoon Disaster to Light Steel Building." *International Conference on Risk Management Engineering Management, 2008. ICRMEM '08*, 422 –427.

JMP. (2011). "JMP, Version 7. SAS Institute Inc., Cary, NC, 1989-2007." <http://www.jmp.com/support/faq/jmp1733.shtml> (Sep. 9, 2012).

Karsan, I. D., and Jirsa, J. O. (1969). "Behavior of concrete under compressive loadings." *Journal of the Structural Division*.

Kayser, J. R., and Nowak, Andrzej S. (1989). "Capacity Loss Due to Corrosion in Steel-Girder Bridges." *Journal of Structural Engineering*, 115(6), 1525–1537.

Kelly, J. M. (1997). *Earthquake-resistant design with rubber*. Springer.

Khashaee, P. (2005). "Damage-based seismic design of structures." *Earthquake spectra*, 21, 371.

Der Kiureghian, A., and Dakessian, T. (1998). "Multiple design points in first and second-order reliability." *Structural Safety*, 20(1), 37–49.

Komp, M. E. (1987). "Atmospheric corrosion ratings of weathering steels-calculation and significance." *Materials Performance*, Mater. Perform. (USA), 26(7), 42–4.

Krawinkler, H., Medina, R., and Alavi, B. (2003). "Seismic drift and ductility demands and their dependence on ground motions." *Engineering structures*, 25(5), 637–653.

Krige, D. G. (1951). *A statistical approach to some mine valuation and allied problems on the Witwatersrand*. Univ. of the Witwatersrand.

Kumar, R., Gardoni, P., and Sanchez-Silva, M. (2009). "Effect of cumulative seismic damage and corrosion on the life-cycle cost of reinforced concrete bridges." *Earthquake Engineering and Structural Dynamics*, 38(7), 887–905.

Kunnath, S. K., and Jenne, C. (1994). "Seismic damage assessment of inelastic RC structures." *Proceedings of 5th US National Conference on Earthquake Engineering, EERI, Oakland, CA*, 55–64.

Kunnath, Sashi K., Larson, L., and Miranda, E. (2006). "Modelling considerations in probabilistic performance-based seismic evaluation: case study of the I-880 viaduct." *Earthquake Engineering & Structural Dynamics*, 35(1), 57–75.

Li, J., Gong, J., and Wang, L. (2009). "Seismic behavior of corrosion-damaged reinforced concrete columns strengthened using combined carbon fiber-reinforced polymer and steel jacket." *Construction and Building Materials*, 23(7), 2653–2663.

Liam, K., Roy, S., and Northwood, D. (1992). "Chloride ingress measurements and corrosion potential mapping study of a 24-year-old reinforced concrete jetty structure in a tropical marine environment." *Magazine of Concrete Research*, 44(160), 205–215.

Lindquist, L. (2008). "Corrosion of steel bridge girder anchor bolts." MS Thesis, Georgia Institute of Technology, Atlanta, Georgia.

Liu, C. (2005). "Evolutionary multiobjective optimization in engineering management: An empirical study on bridge deck rehabilitation." *6th International Conference on Parallel and Distributed Computing, Applications and Technologies, PDCAT 2005, December 5, 2005 - December 8, 2005*, Parallel and Distributed Computing, Applications and Technologies, PDCAT Proceedings, Institute of Electrical and Electronics Engineers Computer Society, Dalian, China, 773–777.

Lower, S. (2010). "Electrochemical corrosion - University of California Davis." <http://chemwiki.ucdavis.edu/Analytical_Chemistry/Electrochemistry/Electrochemistry_7%3A_Electrochemical_Corrosion> (Mar. 16, 2013).

Luco, N., Cornell, C.A., and Yeo, G. L. (2002). "Annual limit-state frequencies for partially-inspected earthquake-damaged buildings." *Structural Safety*, 24(2–4), 281–296.

Mackaness, W., and Beard, K. (1993). "Visualization of interpolation accuracy." *AUTOCARTO-CONFERENCE-*, 228–228.

Mackie, K. R., and Stojadinovic, B. (2006). "Post-earthquake functionality of highway overpass bridges." *Earthquake Engineering & Structural Dynamics*, 35(1), 77–93.

Mackie, K. R., and Stojadinović, B. (2005). "Comparison of Incremental Dynamic, Cloud, and Stripe Methods for Computing Probabilistic Seismic Demand Models."

Mackie, K., and Stojadinović, B. (2001). "Probabilistic Seismic Demand Model for California Highway Bridges." *Journal of Bridge Engineering*, 6(6), 468.

Mackie, Kevin R., Wong, J.-M., and Stojadinovic, B. (2010). "Post-earthquake bridge repair cost and repair time estimation methodology." *Earthquake Engineering & Structural Dynamics*, 39(3), 281–301.

Mahoney, W. (2009). *BNI Public Works 2010 Costbook*. Bni (building News).

Mander, J. B., Kim, D. K., Chen, S. S., and Premus, G. J. (1996a). "Response of Steel Bridge Bearings to Reversed Cyclic Loading." <https://ir.lib.buffalo.edu/xmlui/handle/10465/5686> (Jan. 16, 2012).

Mander, J. B., Kim, D. K., Chen, S. S., and Premus, G. J. (1996b). *Response of steel bridge bearings to reversed cyclic loading*. NCEER.

Maroney, B., Kutter, B., Romstad, K., Cahi, Y. H., and Vanderbilt, E. (1994). "Interpretation of large scale bridge abutment test results." *Proceedings of 3rd Annual Seismic Research Workshop*.

Martin, G. R., and Yan, L. (1995). "Modeling Passive Earth Pressure for Bridge Abutments." ASCE, 1–16.

Mase, G. T., and Mase, G. E. (1999). *Continuum mechanics for engineers*. CRC Press.

Mazzoni, S., McKenna, F., Scott, M. H., and Fenves, G. L. (2009). *OpenSees Command Language Manual*. Command Language Manual, University of California, Berkeley.

McKay, M. D., Beckman, R. J., and Conover, W. J. (1979). "A Comparison of Three Methods for Selecting Values of Input Variables in the Analysis of Output from a Computer Code." *Technometrics*, 21(2), 239–245.

Melchers, R. E. (1999). *Structural Reliability Analysis and Prediction*. John Wiley & Sons Ltd (Import).

Melchers, Robert E., and Frangopol, Dan M. (2008). "Probabilistic modelling of structural degradation." *Reliability Engineering & System Safety*, 93(3), 363.

Merz, P., and Hao, J.-K. (2011). *Evolutionary Computation in Combinatorial Optimization: 11th European Conference, EvoCOP 2011, Torino, Italy, April 27-29, 2011, Proceedings*. Springer.

Moncmanová, A. (2007). *Environmental deterioration of materials*. WIT Press.

Mosteller, F., and Tukey, J. W. (1968). *Data analysis, including statistics*.

Murià-Vila, D., and Toro Jaramillo, A. M. (1998). "Effects of several events recorded at a building founded on soft soil." *11th European Conference on Earthquake Engineering, Paris*.

Mustafa, M., and Yusof, K. (1994). "Atmospheric chloride penetration into concrete in semitropical marine environment." *Cement and Concrete Research*, 24(4), 661–670.

Muthukumar, S. (2003). "A Contact Element Approach with Hysteresis Damping for the Analysis and Design of Pounding in Bridges." Dissertation, , <https://smartech.gatech.edu/handle/1853/5286> (Jan. 22, 2013).

Myers, J. C. (1997). *Geostatistical Error Management: Quantifying Uncertainty for Environmental Sampling and Mapping*. John Wiley and Sons.

National Safety Commission. (2007). "The National Safety Commission Alerts: Nation's Road Infrastructure Under Great Stress." <http://alerts.nationalsafetycommission.com/2007/09/nations-road-infrastructure-under-great.php> (Mar. 25, 2012).

Nielson, B. G. (2005). "Analytical fragility curves for highway bridges in moderate seismic zones." PhD Thesis, Georgia Institute of Technology, Atlanta, Georgia.

Nielson, B. G., and DesRoches, R. (2007a). "Analytical Seismic Fragility Curves for Typical Bridges in the Central and Southeastern United States." *Earthquake Spectra*, 23(3), 615–633.

Nielson, B. G., and DesRoches, R. (2007b). "Seismic fragility methodology for highway bridges using a component level approach." *Earthquake Engineering & Structural Dynamics*, 36(6), 823–839.

Nilsson, E. (2008). "Seismic risk assessment of the transportation network of Charleston, South Carolina." MS Thesis, Georgia Institute of Technology.

NOAA (National Oceanic and Atmospheric Administration). (2004). "Climatography of the United States." <http://cdo.ncdc.noaa.gov/climatenormals/clim20/tn/406402.pdf>.

Nowak, A. S., Park, C. H., and Casas, J. R. (2001). "Reliability analysis of prestressed concrete bridge girders: comparison of Eurocode, Spanish Norma IAP and AASHTO LRFD." *Structural safety*, 23(4), 331–344.

Nowak, Andrzej S., and Cho, T. (2007). "Prediction of the combination of failure modes for an arch bridge system." *Journal of Constructional Steel Research*, 63(12), 1561–1569.

Nuti, C., and Vanzi, I. (2003). "To retrofit or not to retrofit?" *Engineering Structures*, 25(6), 701–711.

O'Brien, E. J., and Caprani, Colin C. (2005). "Headway modelling for traffic load assessment of short to medium span bridges."

OBrien, E. J., and Enright, B. (2011). "Modeling same-direction two-lane traffic for bridge loading." *Structural Safety*, 33(4–5), 296–304.

ODOT. (2010). "Ohio Department of Transportation." <http://www.dot.state.oh.us/Pages/Home.aspx> (Apr. 28, 2010).

Ōmori, F. (1894). *On the after-shocks of earthquakes*. The University.

Padgett, J. E. (2007). "Seismic vulnerability assessment of retrofitted bridges using probabilistic methods."

Padgett, J. E., Dennemann, K., and Ghosh, J. (2010). "Risk-based seismic life-cycle cost-benefit (LCC-B) analysis for bridge retrofit assessment." *Structural Safety*, 32(3), 165–173.

Padgett, J.E., and DesRoches, R. (2009). "Retrofitted bridge fragility analysis for typical classes of multispan bridges." *Earthquake Spectra*, Earthq. Spectra (USA), 25(1), 117–41.

Padgett, Jamie E., and DesRoches, Reginald. (2007a). "Bridge Functionality Relationships for Improved Seismic Risk Assessment of Transportation Networks." *Earthquake Spectra*, 23(1), 115–130.

Padgett, Jamie E., and DesRoches, Reginald. (2007b). "Bridge Functionality Relationships for Improved Seismic Risk Assessment of Transportation Networks." *Earthquake Spectra*, 23(1), 115–130.

Padgett, Jamie E., and DesRoches, Reginald. (2008). "Methodology for the development of analytical fragility curves for retrofitted bridges." *Earthquake Engineering and Structural Dynamics*, 37(8), 1157–1174.

Padgett, Jamie Ellen, DesRoches, Reginald, and Ehlinger, R. (2010). "Experimental response modification of a four-span bridge retrofit with shape memory alloys." *Structural Control and Health Monitoring*, 17(6), 694–708.

Pantazopoulou, S. J., Bonacci, J. F., Sheikh, S., Thomas, M. D. A., and Hearn, N. (2001). "Repair of corrosion-damaged columns with FRP wraps." *Journal of Composites for Construction*, 5(1), 3–11.

Park, R., Priestley, M. J., and Gill, W. D. (1982). "Ductility of square-confined concrete columns." *Journal of the structural division*, 108(4), 929–950.

Park, Y., and Ang, A. H. -S. (1985). "Mechanistic Seismic Damage Model for Reinforced Concrete." *Journal of Structural Engineering*, 111(4), 722–739.

Park, Y.-J., Ang, Alfredo H.-S., and Wen, Yi Kwei. (1985). "Seismic Damage Analysis of Reinforced Concrete Buildings." *Journal of Structural Engineering*, 111(4), 740–757.

PEER. (2012). "PEER Strong Ground Motion Database." <http://peer.berkeley.edu/products/strong_ground_motion_db.html> (Oct. 2, 2012).

PEER. (2013). "PEER Structural Performance Database." <http://nisee.berkeley.edu/spd/> (Mar. 21, 2013).

Picard, R. R., and Cook, R. D. (1984). "Cross-validation of regression models." *Journal of the American Statistical Association*, 575–583.

Porter, K. A, Kiremidjian, A. S, and LeGrue, J. S. (2001). "Assembly-based vulnerability of buildings and its use in performance evaluation." *Earthquake Spectra*, 17(2), 291–312.

Prete, M. D., Guadagno, F. M., and Scarascia-Mugnozza, G. (1998). "Earthquake induced damage in an historic area: the September–October 1997 seismic sequence which affected Assisi, central Italy." *Bulletin of Engineering Geology and the Environment*, 57(1), 101–109.

Rathje, E. M., Stewart, J.P., Bora Baturay, M., Bray, J. D., and Bardett, J. P. (2006). "Strong Ground Motions and Damage Patterns from the 1999 Duzce Earthquake in Turkey." *Journal of Earthquake Engineering*, 10(5), 693–724.

Ravishanker, N., and Dey, D. (2002). *A first course in linear model theory*. CRC Press.

Reimann, C. (2008). *Statistical data analysis explained: applied environmental statistics with R*. John Wiley and Sons.

Rix, G. J., and Fernandez, J. A. (2004). "Earthquake Ground Motion Simulation." <www.ce.gatech.edu/research/mae_ground_motion/> (Oct. 19, 2009).

Rojahn, C., and Sharpe, R. L. (1985). *Earthquake damage evaluation data for California*. Applied Technology Council.

Rokneddin, K., Ghosh, J., Dueñas-Osorio, Leonardo, and Padgett, J. E. (2012). "Bridge retrofit prioritisation for ageing transportation networks subject to seismic hazards." *Structure and Infrastructure Engineering*, 1–17 DOI:10.1080/15732479.2011.654230

Rokneddin, K., Ghosh, J., Dueñas-Osorio, Leonardo, and Padgett, J. E. (2013). "Seismic Reliability Assessment of Aging Highway Bridge Networks with Field Instrumentation Data and Correlated Failures. II: Application." *Earthquake Spectra*, (Accepted (In Press)).

Sanchez-Silva, Mauricio, Klutke, G.-A., and Rosowsky, D. V. (2011). "Life-cycle performance of structures subject to multiple deterioration mechanisms." *Structural Safety*, 33(3), 206–217.

Seo, J., and Linzell, D. G. (2012). "Horizontally curved steel bridge seismic vulnerability assessment." *Engineering Structures*, 34, 21–32.

Shinozuka, M., Feng, M. Q, Lee, J., and Naganuma, T. (2000). "Statistical analysis of fragility curves." *Journal of Engineering Mechanics*, 126(12), 1224–1231.

Shinozuka, Masanobu, Feng, Maria Q., Kim, H.-K., and Kim, S.-H. (2000). "Nonlinear Static Procedure for Fragility Curve Development." *Journal of Engineering Mechanics*, 126(12), 1287–1295.

Shome, N., and Cornell, C. A. (1999). *Probabilistic Seismic Demand Analysis of Nonlinear Structures*. Stanford University, Stanford, California.

Silano, L. G., and Brinckerhoff, P. (1993). *Bridge inspection and rehabilitation*. Wiley-IEEE.

Simon, J., Bracci, J. M., and Gardoni, P. (2010). "Seismic response and fragility of deteriorated reinforced concrete bridges." *Journal of Structural Engineering*, 136(10), 1273–1281.

Simpson, T. W., Poplinski, J. D., Koch, P. N., and Allen, J. K. (2001). "Metamodels for Computer-based Engineering Design: Survey and recommendations." *Engineering With Computers*, 17, 129–150.

Stewart, M.G. (2004). "Spatial variability of pitting corrosion and its influence on structural fragility and reliability of RC beams in flexure." *Structural Safety*, 26(4), 453–470.

Stewart, Mark G., and Rosowsky, D. V. (1998). "Time-dependent reliability of deteriorating reinforced concrete bridge decks." *Structural Safety*, 20(1), 91–109.

Suzuki, M., Tsutsumi, T., and Irie, M. (1990). "Reliability analysis of durability/deterioration indices of reinforced concrete in a marine environment." *Corrosion of Reinforcement in Concrete*, 268–277.

Taylor, C. E., VanMarcke, E.,(2002). *Acceptable Risk Processes: Lifelines and Natural Hazards* (American Society of Civil Engineers: Technical Council on Lifeline Earthquake Engineering). ASCE Publications.

TELEATLAS. (2010). "Digital Mapping and Navigation Soultions." <http://www.teleatlas.com/index.htm>.

Thoft-Christensen, P. (1995). "Advanced bridge management systems." *Structural Engineering Review*, 7(3), 151–164.

Thoft-Christensen, P., Jensen, F. M., Middleton, C. R., and Blackmore, A. (1996). "Assessment of the reliability of concrete slab bridges." Conference or Workshop Item, , <http://publications.eng.cam.ac.uk/6361/> (Mar. 5, 2010).

TNDOT. (2010). "Tennessee Department of Transportation." <http://www.tdot.state.tn.us/construction/Average%20Unit%20Prices/aup_2009.pdf> (Apr. 28, 2010).

Transportation Research Board. (2003). *Review of Truck Characteristics as Factors in Roadway Design*. National Cooperative Highway Research Program, Washington D.C.

Trauth, M. H., Gebbers, R. (CON), and Marwan, N. (CON). (2010). *MATLAB® Recipes for Earth Sciences*. Springer.

Uji, K., Matsuoka, T., and Maruya, T. (1990). *Corrosion of Reinforcement in Concrete*. Elsevier, London.

USDOS (U.S. Department of State). (2010). "US Weather - Average Temperatures and Rainfall." <http://countrystudies.us/united-states/weather/> (Jan. 23, 2011).

USDOT. (1982). *Tolerable Movement Criteria for Highway Bridges*. U.S. Department of Transportation, Federal Highway Administration, Offices of Research and Development.

USGS. (2010). "USGS Interactive Deaggregations Maps." <http://eqint.cr.usgs.gov/deaggint/2008/index.php> (Mar. 11, 2011).

USGS. (2012). "USGS Probabilistic Hazard Curves." <http://earthquake.usgs.gov/hazards/designmaps/javacalc.php> (Apr. 3, 2012).

USGS. (2013). "USGS - U.S. Geological Survey." <http://earthquake.usgs.gov/earthquakes/map/> (May. 13, 2010).

Utsu, T., and Ogata, Y. (1995). "The centenary of the Omori formula for a decay law of aftershock activity." *Journal of Physics of the Earth*, 43(1), 1–33.

Val, D.V., Stewart, M.G., and Melchers, R.E. (2000). "Life-cycle performance of RC bridges: Probabilistic approach." *Computer-Aided Civil and Infrastructure Engineering*, 15(1), 14–25.

Val, Dimitri V., Stewart, Mark G., and Melchers, Robert E. (1998). "Effect of reinforcement corrosion on reliability of highway bridges." *Engineering Structures*, 20(11), 1010–1019.

Vapnik, V. N. (1998). *Statistical learning theory*. Wiley.

Vu, K. A. T., and Stewart, Mark G. (2000). "Structural reliability of concrete bridges including improved chloride-induced corrosion models." *Structural Safety*, 22(4), 313–333.

Wang, G. C. S., and Jain, C. L. (2003). *Regression Analysis: Modeling & Forecasting*. Institute of Business Forec.

Wang, X., Liu, Y., and Antonsson, E. K. (1999). "Fitting Functions to Data in High Dimensionsal Design Space." *ASME Design Engineering Technical Conferences, Las Vegas, NV, Paper Number DETC99/DAC-8622*.

Webster, R., and Oliver, M. A. (2008). *Geostatistics for Environmental Scientists*. John Wiley & Sons.

Wen, Y. K., and Kang, Y. J. (2001a). "Minimum Building Life-Cycle Cost Design Criteria. I: Methodology." *Journal of Structural Engineering*, 127(3), 330–337.

Wen, Y. K., and Kang, Y. J. (2001b). "Minimum Building Life-Cycle Cost Design Criteria. II: Applications." *Journal of Structural Engineering*, 127(3), 338–346.

Wen, Y. K., and Wu, C. L. (2001). "Uniform Hazard Ground Motions for Mid-America Cities." *Earthquake Spectra*, 17(2), 359–384.

Weyers, R. E., Fitch, M. G., Larsen, E. P., Al-Qadi, I. L., and Hoffman, P.C. (1994). *Concrete Bridge Protection and Rehabilitation: Chemical and Physical Techniques. Service Life Estimates*. Strategic Highway Research Program, Washington D.C., 357.

Whiting, D., Stejskal, B., and Nagi, M. (1990). *Condition of Prestressed Concrete Bridge Components: Technology Review and Field Surveys*. Federal Highway Administration, Washington.

Williams, M. S., and Sexsmith, R. G. (1997). "Seismic assessment of concrete bridges using inelastic damage analysis." *Engineering structures*, 19(3), 208–216.

Yamazaki, F., Hamada, T., Motoyama, H., and Yamauchi, H. (1999). "Earthquake damage assessment of expressway bridges in Japan." *Optimizing Post-Earthquake Lifeline System Reliability*, 361–370.

Yeo, G. L., and Cornell, C. A. (2009). "Building life-cycle cost analysis due to mainshock and aftershock occurrences." *Structural Safety*, 31(5), 396–408.

Yin, Y., and Li, Y. (2011). "Loss Estimation of Light-Frame Wood Construction Subjected to Mainshock-Aftershock Sequences." *Journal of Performance of Constructed Facilities*, 25(6), 504–513.

Yokozaki, K., Motohashi, K., Okada, K., and Tsutsumi, K. (1997). "A Rational Model to Predict the Service Life of RC Structures in Marine Environment, Forth CANMET." *ACI International Conference on Durability of Concrete*, 777–799.

Zen, K. (2005). "Corrosion and life cycle management of port structures." *Corrosion science*, 47(10), 2353–2360.